Computational reduction techniques for numerical vibro-acoustic analysis of hearing aids

Creixell Mediante, Ester

Publication date:
2018

Document Version
Publisher's PDF, also known as Version of record

Computational reduction techniques for numerical vibro-acoustic analysis of hearing aids

Ph.D. thesis by
Ester Creixell Mediante

Technical University of Denmark
2018

This thesis was submitted to the Technical University of Denmark (DTU) as partial fulfillment of the requirements for the degree of Doctor of Philosophy (Ph.D.) in Electronics and Communication. It is the product of an industrial PhD project carried out at the Acoustic Technology group in DTU and at the company Oticon A/S, with the financial support of Innovation Fund Denmark. The work was completed between January 1, 2015 and January 28, 2018 under the supervision of Associate Professor Jonas Brunskog and Professor Jakob Søndergaard Jensen from DTU, and Martin Larsen from Oticon A/S.

Title
Computational reduction techniques for numerical vibro-acoustic analysis of hearing aids

Author
Ester Creixell Mediante

Supervisors
Assoc. Prof. Jonas Brunskog
Prof. Jakob S. Jensen
Martin Larsen

Acoustic Technology
Department of Electrical Engineering
Technical University of Denmark
Kongens Lyngby, Denmark

Abstract

Numerical modelling is a key point for vibro-acoustic analysis and optimization of hearing aids. The great number of small components constituting the devices, and the strong structure-acoustic coupling of the system make it a challenge to obtain accurate and computationally efficient models. In this thesis, several challenges encountered in the process of modelling and optimizing hearing aids are addressed.

Firstly, a strategy for modelling the contacts between plastic parts for harmonic analysis is developed. Irregularities in the contact surfaces, inherent to the manufacturing process of the parts, introduce variations on the final contact points in practice, making the contact properties unknown. The suggested technique aims at characterising the contact in terms of distributed stiffness values, which are identified by means of a model updating method that matches simulation to experimental data. Secondly, the applicability of Model Order Reduction (MOR) techniques to lower the computational complexity of hearing aid vibro-acoustic models is studied. For fine frequency response calculation and optimization, which require solving the numerical model repeatedly, a computational challenge is encountered due to the large number of Degrees of Freedom (DOFs) needed to represent the complexity of the hearing aid system accurately. In this context, several MOR techniques are discussed, and an adaptive reduction method for vibro-acoustic optimization problems is developed as a main contribution. Lastly, topology optimization techniques for structure-acoustic interaction problems are investigated with the aim of evaluating their applicability to the design of hearing aid parts. The strong fluid-structure interaction between the air and some of the thin, soft parts makes it necessary to include the effects of the interface variations in the optimization, which poses a challenge due to the need of interpolating between solid and fluid elements. Two techniques are compared in this context for a 2D hearing aid suspension design problem.

Resumé

Numerisk modellering er centralt for vibro-akustisk analyse og optimering af høreapparater. På grund af det store antal små komponenter og den stærke struktur-akustiske kobling i systemet, gør det til en udfordring at opnå nøjagtige og beregningsmæssigt effektive modeller. I denne afhandling behandles flere udfordringer i modellering og optimering af høreapparater.

Først beskrives en strategi til harmonisk analyse for modellering af kontakten mellem plastdele. Uregelmæssigheder i kontaktfladerne, der er uundgåelige i fremstillingsprocessen af delene, indfører i praksis variationer på de faktiske kontaktpunkter, hvilket gør kontaktegenskaberne ukendte. Den foreslåede teknik sigter mod at karakterisere kontakten i form af distribuerede stivhedsværdier, som identificeres ved hjælp af en metode til model-opdatering, der matcher simulering til eksperimentelle data. Dernæst studeres anvendeligheden af Model Order Reduction (MOR) teknikker til at sænke beregningstiden af høreapparatets vibro-akustiske model. For en fin beregning og optimering af frekvensrespons, som kræver løsning af den numeriske model gentagne gange, opstår der en beregningsudfordring på grund af det store antal frihedsgrader, der er nødvendige for at repræsentere høreapparatssystemets kompleksitet nøjagtigt. I denne sammenhæng diskuteres flere MOR-teknikker og en adaptiv reduktionsmetode til vibro-akustiske optimeringsproblemer udvikles som hovedbidrag. Endelig undersøges topologiske optimeringsteknikker til struktur-akustiske interaktionsproblemer med det formål at evaluere deres anvendelighed til design af delene i høreapparater. Den stærke interaktion mellem luften og nogle af de tynde, bløde dele, gør det nødvendigt at inkludere virkningerne af grænsefladevariationerne i optimeringen, hvilket udgør en udfordring på grund af behovet for interpolering mellem strukturel og akustik elementer. To teknikker sammenlignes i denne sammenhæng til et designproblem i 2D af ophængningen i et høreapparat.

Acknowledgements

The past three years have been an exciting and challenging adventure in many aspects, and it would have never been possible to accomplish this Ph.D without the help and support from many people.

Firstly, I would like to thank my main supervisor, Jonas Brunskog, for his guidance and support during the course of this study. His thorough reading, thoughtful suggestions and reflective comments have been an invaluable help during the writing and correction phase of each paper, and of this thesis. My sincere thanks also goes to my company supervisor, Martin Larsen, for placing his trust in me to carry out this project, and for his priceless enthusiasm, constant support and encouragement to reach higher goals. I would also like to thank my co-supervisor, Jakob S. Jensen, who has shared his knowledge and expertise in so many fields unknown to me at the start of this study, and for the insightful discussions and ideas. A special thanks also goes to Niels Aage in that regard, for his genuine interest and eagerness to help, and to the rest of the CAMM members for listening carefully and giving interesting suggestions.

It has been a great pleasure to be part of the DTU Acoustic Technology group, a family that I gladly have seen grow during the course of this project. Special thanks to my office mates for their unconditional support and inestimable help. Likewise, I would like to thank my colleagues at Oticon for offering a welcoming, pleasant work environment.

I would also like to express my gratitude to the Noise & Vibration group at KU Leuven, for generously hosting me and being a second home in Belgium for three months. This work would have never reached the same level of maturity without their shared expertise, fruitful discussions and inspiring learning environment.

Last but not least, I would like to thank all my present and past flatmates, teammates, friends around the world and family for the invaluable moral support, fun times and inspirational conversations.

Related Publications

The papers included in this thesis are:

Paper A Creixell Mediante, E., Brunskog, J., Jensen, J. S., Larsen, M. (2018). Contact parameter identification for vibrational response variability prediction. *Applied Acoustics*, 129, 291–305. doi:10.1016/j.apacoust.2017.08.011

Paper B Creixell-Mediante, E., Jensen, J. S., Brunskog, J., Larsen, M. (2016). A Multi-Model Reduction Technique for Optimization of Coupled Structural-Acoustic Problems. *Proceedings of Inter-Noise 2016*, Hamburg, Germany.

Paper C Creixell-Mediante, E., Jensen, J. S., Brunskog, J., Larsen, M. (2016). Model reduction for optimization of structural-acoustic coupling problems. *Proceedings of ISMA 2016*, Leuven, Belgium.

Paper D Creixell-Mediante, E., Jensen, J. S., Naets, F., Brunskog, J., Larsen, M. Adaptive parametric model order reduction technique for optimization of vibro-acoustic models: Application to hearing aid design. *Journal of Sound and Vibration*, 424, 208-223. doi:10.1016/j.jsv.2018.03.013.

Report E Creixell-Mediante, E. Adaptive parametric model order reduction for vibro-acoustic problems: further applications. *Internal report.*

Paper F Creixell-Mediante, E., Jensen, J. S., Brunskog, J., Larsen, M. Topology optimization of vibro-acoustic systems with strong coupling. *Manuscript.*

On the course of the Ph.D., the following conference contributions were also published, which are not included on the thesis due to content overlap with the included publications:

- Creixell-Mediante, E., Brunskog, J., Jensen, J. S., Larsen, M. (2015). A model of mechanical contacts in hearing aids for uncertainty analysis. *Proceedings of NOVEM 2015*, Dubrovnik, Croatia.
- Creixell-Mediante, E., Jensen, J. S., Brunskog, J., Larsen, M. (2017). Reduced order modeling in topology optimization of vibro-acoustic problems. *Abstract for Acoustics'17, Boston, MA, USA. Journal of the Acoustical Society of America*, 141(5), 4035–4035. doi:10.1121/1.4989307

Contents

Chapter 1

Introduction

1.1 Motivation

The basic function of a hearing aid is to capture the sound that reaches the ear of its user and reproduce a sufficiently amplified version of it inside the impaired ear. It is therefore a main requirement for these devices to be able to deliver an as high as possible output sound level, while keeping a relatively small physical size for comfort and aesthetic reasons. A Hearing Instrument[1] (HI) must contain at least three components to accomplish its main function: a microphone, an amplifier and a loudspeaker (denominated "receiver" in the industry argot), which, given the dimensions of the instruments, sit close together inside the device. It is therefore easy to imagine that the amplified acoustic signal that is played by the receiver will to some extent be sensed by the microphone, and forwarded to the amplifier and again to the receiver, creating a loop in the signal path that amplifies certain frequency components and generates a disturbing acoustic noise. This phenomenon is known as *feedback*, and the maximum amplification that a HI can provide is limited by the level at which audible feedback occurs. The feedback signal can be measured as the electrical response of the microphone due to the receiver excitation.

[1] Hearing Instrument is a technical term for hearing aid. Both designations are used indistinctly in this thesis.

Even though modern HIs incorporate feedback cancellation systems that contribute to increase the feedback margin, coming up with a mechanical design that minimizes feedback paths can improve the final result significantly. Loudspeakers are electro-acoustic transducers that convert electrical signals into acoustic ones. This conversion is achieved by transforming the electrical signal into mechanical vibrations of some surface that in turn excites the particles of its surrounding air, generating acoustic waves. The same mechanism is employed in microphones to perform the opposite transformation, which makes both devices not only acoustic transducers but also vibration ones. It is therefore important to investigate not only acoustic but also vibration feedback paths in the design process.

Numerical modelling is a tool that can help to analyse and understand the vibro-acoustic phenomena that take place inside the hearing aid, and has slowly been introduced to the industry in the recent years. Simulation is usually combined with empirical studies; however, models can usually give a clearer picture of the performance of the instrument, since vibro-acoustic measurements are specially challenging in this field due to the small size and light weight of the devices. Moreover, applying mathematical optimization algorithms on a numerical model is a fast and flexible way of coming up with new optimized designs that minimize feedback, instead of getting into a long tedious process of trial and error using the traditional prototyping-and-measuring approach.

1.2 Goals and thesis structure

A HI is a small device composed of several parts of different natures such as transducers, electronic circuitry, plastic parts, tubes or suspensions, as illustrated in Figure 1.1, which are strongly coupled to the air that surrounds them. When these parts are put together, the location and properties of the contacts between them are often unknown and may vary across different assembled instruments, which in turn gives rise to variation in their vibro-acoustic responses. The uncertainty about contact properties arises due to manufacturing tolerances, which make the shape and surface properties of the produced parts vary slightly from the nominal design, changing the location of the contact points when these parts are put together. The contact uncertainty could be reduced by enforcing well-defined contact points in the design; however, it is required from a static mechanical design point of view to ensure a certain clearance between parts in order to account for these tolerances and prevent high stress levels. The uncertainty about contact properties is therefore difficult

Figure 1.1: Hardware of a traditional hearing aid.

to reduce, and it poses a main obstacle on the way to obtaining a numerical model that accurately represents reality. A way of characterising unknown contact properties is by means of inverse parameter identification methods, which use optimization to determine the values of the parameters of a pre-defined contact model to match data obtained empirically. This approach is discussed in Chapter 3 of this thesis, and the reader is then referred to Paper A.

The small size of the HIs make it possible to use low-frequency numerical methods such as the FEM for modelling the vibro-acoustic system up to relatively high frequencies (typically up to 10 kHz), since the mode overlap is low enough. However, the complexity of the system together with the fine meshing that is needed for obtaining accurate results at high frequencies can give rise to numerical models with a large number of Degrees Of Freedom (DOFs) that result in large algebraic systems which are computationally expensive to solve. When those models are to be used for optimization purposes, they must be solved iteratively for varying values of the design parameters according to the optimization routine of choice, which can in total require an amount of time that makes it impractical to use this strategy in the industrial product development process. One way of speeding up the computations consists in reducing the size of the algebraic system to be solved by means of Model Order Reduction (MOR) techniques. MOR consists in obtaining a reduced version of a FE model by projecting the full system into a reduced basis of vectors, chosen carefully to preserve the relevant information of the model, and therefore yielding more accurate solutions than what would be obtained by coarsening the FE mesh to obtain a similar system size. The choice and calculation of the basis vectors that can most efficiently reduce a system is highly problem-dependent, which motivates the investigation and development of a method that can be applied in a straight-forward and practical way to hearing aid optimization problems. Chapter 4 discusses MOR techniques, and the developed method is detailed in

Paper B, Paper C, Paper D and Report E.

The usual approach to optimization of HI designs consists in parametrizing some dimensions or positions of critical parts that the design engineer considers relevant, and letting the optimization algorithm find the parameter values that minimize a selected objective function the most. This approach is rather rigid, in the sense that the shape of the parts is pre-defined and cannot change during the optimization. Even though this can yield satisfactory results in many cases, allowing more freedom in the design could let the optimization algorithm produce new, more optimized shapes, different from those imagined by the design engineer. Topology optimization is a technique that was developed based on this idea, and which has been applied to a wide range of engineering problems in the last decades. In hearing aids, it could be used to improve the design of several parts, and specially of one of the most critical ones for the vibro-acoustic performance: the receiver suspension, which has the job of isolating the receiver from the rest of the HI. The suspension is usually shaped as a cylinder with thin walls made of a soft material, and it acts as a vibration isolation spring. It is exposed to high sound levels since it is directly connected to the receiver output, and its small dimensions and material properties result in a strong coupling between the structure and the air. It is therefore a key point to take the structure-acoustic interaction into account, which poses a challenge in topology optimization since the changes on the interface between the two fields must be considered in order to apply the correct boundary conditions (as opposed to the case of purely mechanical optimization, where the two fields are "structure" and "void"). An overview of topology optimization methods is given in Chapter 5 and the reader is then referred to Paper F for the discussion of its application to coupled structure-acoustic problems.

Chapter 2 contains general concepts used throughout the thesis such as the formulation of the coupled structure-acoustic problem by the Finite Element Method (FEM) and an overview of vibro-acoustic optimization methods, together with a literature review of previous work on numerical vibro-acoustic modelling of hearing aids.

Chapter 2

Structural-acoustic modelling and optimization

In this chapter, previous work on modelling and optimization of vibro-acoustics in hearing aids is reviewed, and thereafter the FEM formulation of the coupled structure-acoustic problem and optimization approach used throughout the thesis are described in detail.

2.1 Modelling of hearing aids: literature review

A few studies on vibro-acoustic modelling and optimization in the hearing aid field can be found in the literature. The most comprehensive existing study was done by Lars Friis, who studied internal feedback in hearing aids in his PhD thesis [1]. A simplified model of a hearing aid developed using mobility synthesis was firstly investigated, highlighting the difficulties of modelling sound and vibration in hearing aids and demonstrating that the interaction between the different components assembled in the device result in complicated vibration patterns with several structural resonances in the frequency range of interest (100 Hz to 10 kHz). Thereafter, a 3D model of a hearing aid was developed by combining the FEM and other techniques to model different parts in the device,

with the main contribution being the application of the theory of fuzzy structures to account for uncertainties in the dynamic coupling properties of small components [2, 3]. The simulated hearing aid vibration responses showed good agreement with measurements in general, even though some measured peaks did not appear in the model, indicating that some feedback paths were not captured. Even though the fuzzy approach proves useful for modelling uncertainties in the coupling between small components and the hearing aid shells, the contacts between the main hearing aid parts modelled in FE (Finite Element) are not discussed in the thesis. This topic is approached in the first part of the present work, in Chapter 3.

A study on the effects of viscous and thermal losses on the acoustic field in hearing aids can be found in the PhD thesis by René Christensen [4]. Viscothermal losses become relevant in HIs due to the small size of some tubes and air cavities in the device. In a more recent publication [5], purely acoustic topology optimization including losses has been presented by the same author, even though only tubes with plane wave propagation are considered for now. Other studies have been devoted to modelling of hearing aid loudspeakers (receivers) [6,7] and minimization of their nonlinear distortion, which can significantly improve the signal-to-noise ratio in the acoustic output. Viscothermal losses and transducer modelling are not investigated in this thesis, even though simplified approaches are used in the hearing aid model presented in Paper D.

Regarding optimization of vibro-acoustic response of hearing aids, only the study published in Ref. [8] can be found in the literature to the author's knowledge. In the publication, topology optimization of a hearing aid suspension is performed on a FE model of a complete hearing aid. Even though structure-acoustic interaction is considered in other parts of the model, acoustic elements are not allowed inside the topology optimization design domain in the study. Typical geometries and material properties of hearing aids suspensions often result in a strong structure-acoustic interaction, which makes it essential to consider the acoustic field and the coupling in such an optimization. For this reason, topology optimization of vibro-acoustic problems with strong coupling is investigated in the present work. Moreover, only a few discrete frequencies were considered in the optimization presented in Ref. [8]; fine frequency resolution is necessary in frequency response optimization, though, since the main peaks in the response may otherwise just be moved to non-sampled frequencies [9]. Since fine frequency resolution responses are expensive to compute due to the FE system being solved independently for each considered frequency, computational reduction techniques with application to vibro-acoustic optimization problems that can speed up such calculations are investigated in this thesis.

2.2 Finite element model of the structure-acoustic interaction problem

In this work, investigations are carried out on FE models of coupled structure-acoustic problems (except for the part on contact modelling, where a purely structural model is considered). A popular choice for the FE modelling of structural-acoustic problems in optimization is the uncoupled approach [10], which consists in solving the structural domain in vacuo first and using the results as boundary conditions to solve the acoustic domain. This is an attractive method since solving the two domains separately requires less computational effort; however, only the effect of the structure on the acoustics is taken into account, but not the effect in the opposite direction. In hearing aids, the effect of the acoustic field on the structure is specially relevant due to the small, thin and soft parts that are used; considering bi-directional coupling is therefore essential.

Several FE formulations of the coupled problem have been described in the literature, where the primary variable in the structural domain is displacement, but different primary variables for the fluid domain have been considered [11]. In the so-called one-field formulation, the acoustic domain is also described by displacement [12]. This technique introduces spurious non-zero modes, and even though this problem has been worked around by several authors [13, 14], the fact that the displacement is described by as many components as dimensions considered in the problem makes the resulting number of DOFs quite large. Therefore, a more compact formulation is desired in terms of computational efficiency [15]. Several combinations of primary variables have been used, such as velocity potential [16], a combination of velocity potential and pressure [17], a combination of displacements and pressure [18], or just pressure. The latter, introduced by Craggs [19], is known as the pressure formulation and it is the most popular choice due to its compactness, since the acoustic field is described by one single degree of freedom per node. Except in one of the methods presented in Paper F, where a mixed displacement/pressure formulation is used [20], the structure-acoustic coupled problems are described by the pressure formulation throughout this thesis.

In the following, the FE procedure to arrive to the pressure formulation is described for the coupled problem illustrated in Figure2.1. The models of the structural and the acoustic domains are first derived separately, and the coupling boundary condition is introduced at the end. For the purely structural problem discussed in Chapter 3 and Paper A, only the structural model is

used. Damping is not considered in the following procedure; in most of the problems treated in this thesis, either no damping, internal structural damping (introduced by adding an imaginary part to the Young's modulus) or Rayleigh damping (where the damping matrix is a linear combination of the stiffness and the mass FE matrices) are used, which can be easily introduced to the FE matrix system obtained at the end of this section.

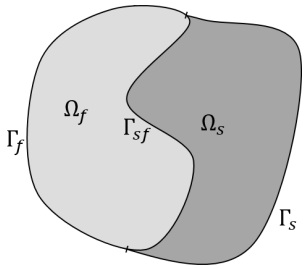

Figure 2.1: Structural and acoustic coupled domains

2.2.1 Structural model

Under the assumptions of small deformations and linear elastic material behaviour, the structures under study are modelled by the linear elasticity equation [21]. Time-harmonic linear structural analysis can be described by Newton's second law, neglecting the body force, as

$$\boldsymbol{\nabla} \cdot \boldsymbol{\sigma} = -\omega^2 \rho_s \mathbf{u} \quad \text{in } \Omega_s, \tag{2.1}$$

where $\boldsymbol{\nabla}$ is the divergence operator, $\boldsymbol{\sigma}$ is the Cauchy stress tensor, ω is the angular frequency, ρ_s is the mass density of the material and $\mathbf{u}$ is the displacement vector. In order to discretize the system, the weak form of the equilibrium equation is derived with the Galerkin method. The equation is first multiplied by an admissible set of test functions, $\mathbf{w}_s$, and integrated over the volume,

$$\int_{\Omega_s} \mathbf{w}_s^T \left(\boldsymbol{\nabla} \cdot \boldsymbol{\sigma} + \omega^2 \rho_s \mathbf{u} \right) \mathrm{dV} = 0. \tag{2.2}$$

The Neumann boundary condition

$$\boldsymbol{\sigma} \cdot \mathbf{n} = \mathbf{f} \quad \text{on } \Gamma_s, \tag{2.3}$$

where $\mathbf{f}$ is an external load applied to the structure and $\mathbf{n}$ is the normal unit vector to the structural surface, is introduced and then the Green's theorem is applied to obtain the weak form

$$-\omega^2\rho_s\int_{\Omega_s}\mathbf{w}_s^T\mathbf{u}\mathrm{dV}+\int_{\Omega_s}(\boldsymbol{\nabla}\mathbf{w}_s)^T\cdot\boldsymbol{\sigma}\mathrm{dV}=\int_{\Gamma_s}\mathbf{w}_s^T\mathbf{f}\mathrm{dV}. \tag{2.4}$$

Introducing the stress-strain constitutive matrix, $\mathbf{D}$, to relate stress and displacement, $\boldsymbol{\sigma}=\mathbf{D}\mathbf{u}$, and discretizing the weak form by introducing the shape functions $\mathbf{N}_s$, so that $\mathbf{w}_s=\mathbf{N}_s$ and $\mathbf{u}=\mathbf{N}_s\hat{\mathbf{u}}$, we obtain

$$\int_{\Omega_s}(\boldsymbol{\nabla}\mathbf{N}_s)^T\mathbf{D}\boldsymbol{\nabla}\mathbf{N}_s\mathrm{dV}\hat{\mathbf{u}}-\omega^2\rho_s\int_{\Omega_s}\mathbf{N}_s^T\mathbf{N}_s\mathrm{dV}\hat{\mathbf{u}}=\int_{\Gamma_s}\mathbf{N}_s^T\mathbf{f}\mathrm{dV}. \tag{2.5}$$

The discretized equation in matrix form becomes

$$(\mathbf{K}_s-\omega^2\mathbf{M}_s)\hat{\mathbf{u}}=\mathbf{f} \tag{2.6}$$

with

$$\mathbf{K}_s=\int_{\Omega_s}(\boldsymbol{\nabla}\mathbf{N}_s)^T\mathbf{D}\boldsymbol{\nabla}\mathbf{N}_s\mathrm{dV} \tag{2.7}$$

$$\mathbf{M}_s=\rho_s\int_{\Omega_s}\mathbf{N}_s^T\mathbf{N}_s\mathrm{dV} \tag{2.8}$$

$$\mathbf{f}=\int_{\Gamma_s}\mathbf{N}_s^T\mathbf{f}\mathrm{dV}. \tag{2.9}$$

being the stiffness and mass matrices and the force vector, respectively, and vector $\hat{\mathbf{u}}$ being the FE approximation of the displacement $\mathbf{u}$.

2.2.2 Acoustic model

Considering an inviscid, irrotational fluid that only undergoes small translations, the Helmholtz equation describes the motion of the acoustic domain in terms of the pressure [19]. For time-harmonic analysis, the wave equation in the frequency domain takes the form

$$\nabla^2 p+\frac{\omega^2}{c^2}p=0 \quad \text{in } \Omega_f, \tag{2.10}$$

where p is the acoustic pressure and c is the speed of sound in the fluid. The equation is first multiplied by a test function, $\mathbf{w}_a$, and integrated over the volume,

$$\int_{\Omega_f} \mathbf{w}_a^T \left(\nabla^2 p + \frac{\omega^2}{c^2} p \right) \mathrm{dV} = 0. \tag{2.11}$$

Introducing a "hard wall" boundary condition on the surface Γ_f,

$$\mathbf{n} \cdot \nabla p = 0 \quad \text{in } \Gamma_f, \tag{2.12}$$

with $\mathbf{n}$ being the unit vector normal to the boundary, the Green's theorem is applied to obtain the weak formulation,

$$\int_{\Omega_f} \nabla \mathbf{w}_a^T \cdot \nabla p - \mathbf{w}_a^T \frac{\omega^2}{c^2} p \ \mathrm{dV} = 0. \tag{2.13}$$

Discretizing the domain and introducing the shape functions $\mathbf{N}_a$ to describe the pressure field as $p = \mathbf{N}_a \hat{\mathbf{p}}$, where $\hat{\mathbf{p}}$ is the pressure FE approximation, and defining the test functions as $\mathbf{w}_a = \mathbf{N}_a$, we obtain

$$\int_{\Omega_f} \left(\nabla \mathbf{N}_a^T \cdot \nabla \mathbf{N}_a - \frac{\omega^2}{c^2} \mathbf{N}_a^T \mathbf{N}_a \right) \mathrm{dV} \ \hat{\mathbf{p}} = 0, \tag{2.14}$$

which can be written in matrix form as

$$(\mathbf{K}_a - \omega^2 \mathbf{M}_a) \hat{\mathbf{p}} = \mathbf{0}, \tag{2.15}$$

with

$$\mathbf{K}_a = \int_{\Omega_s} (\boldsymbol{\nabla} \mathbf{N}_a)^T \boldsymbol{\nabla} \mathbf{N}_a \mathrm{dV} \tag{2.16}$$

$$\mathbf{M}_a = \frac{1}{c^2} \int_{\Omega_f} \mathbf{N}_a^T \mathbf{N}_a \mathrm{dV} \tag{2.17}$$

being the acoustic stiffness and mass matrices.

2.2.3 Coupling

The structure-acoustic coupling can be described as a boundary condition on the fluid-structure interface, Γ_{sf}. The boundary condition for the structural domain is

$$\mathbf{n} \cdot \boldsymbol{\sigma} = p \quad \text{on } \Gamma_{sf}, \tag{2.18}$$

and for the acoustic domain,

$$\mathbf{n} \cdot \nabla p = -\omega^2 \rho_a \mathbf{n}^T \mathbf{u} \quad \text{on } \Gamma_{sf}. \tag{2.19}$$

Multiplying by the test functions and integrating to obtain the weak forms and introducing the FE approximations described above, the coupled structure-acoustic interaction problem in matrix form can be stated as

$$\left(\begin{bmatrix} \mathbf{K}_s & -\mathbf{S}^T \\ \mathbf{0} & \mathbf{K}_a \end{bmatrix} - \omega^2 \begin{bmatrix} \mathbf{M}_s & \mathbf{0} \\ \rho_a \mathbf{S} & \mathbf{M}_a \end{bmatrix} \right) \begin{bmatrix} \hat{\mathbf{u}} \\ \hat{\mathbf{p}} \end{bmatrix} = \begin{bmatrix} \mathbf{f} \\ \mathbf{0} \end{bmatrix}, \tag{2.20}$$

with the coupling matrix $\mathbf{S}$ being [15]

$$\mathbf{S} = \int_{\Gamma_{sf}} \mathbf{N}_s^T \mathbf{n} \mathbf{N}_a \mathrm{dS}. \tag{2.21}$$

For the sake of notation simplicity, $\mathbf{u}$ and $\mathbf{p}$ will be used in the rest of the thesis to denote the displacement and pressure FE approximations. In a compact form, the dynamic system equation can be written as

$$(\mathbf{K} - \omega^2 \mathbf{M})\mathbf{x} = \mathbf{f} \tag{2.22}$$

where $\mathbf{K}$ and $\mathbf{M}$ are the coupled stiffness and mass matrices, $\mathbf{x}$ is the state vector, and $\mathbf{f}$ is the external force vector.

2.3 Vibro-acoustic optimization

Optimization techniques are used throughout the work presented in this thesis. It is not within the scope of the thesis to investigate in detail or improve existing optimization algorithms or objective function formulations; therefore, well-known methods that have been widely used in the field of structural-acoustic optimization are applied. A comprehensive review on available methods can be found in Refs. [9, 10]. Structural-acoustic optimization problems can generally be classified in three categories in relation to the cost function: optimization of the vibration or acoustic response at one or more points, optimization of modal frequencies, and optimization of radiated sound power. In the current work, the two first categories are considered.

2.3.1 Optimization problem formulation

Modal frequency optimization problems can either aim at moving resonances out of a specific frequency range (for example, in structures that are excited by

harmonic or rotational forces), or at matching specific desired modal parameters. The latter case is often used in the field of modal model updating [22], where model parameters are adjusted to match experimental data, as done in the work presented in Paper A in this thesis. However, modal parameter matching can also be applied with other purposes such as in the first case presented in Paper B, where the effect of the structure-acoustic coupling on the modal frequencies of a plate is minimized. The objective function for that kind of problem is usually of the type [10]

$$g = \sum_{i=1}^{N_f} w_{f_i}(f_i - f_{opt_i})^2 + \sum_{i=1}^{N_f} w_{\eta_i}(\eta_i - \eta_{opt_i})^2 \tag{2.23}$$

where f_i and η_i are modal frequencies and damping ratios of the model, f_{opt_i} and η_{opt_i} are the targeted quantities, and w_{f_i} and w_{η_i} are weighting factors for each term that allow for assigning more relevance to certain considered modes.

For response optimization, an objective function of the type

$$g = \left(\frac{1}{\omega_{max} - \omega_{min}} \int_{\omega_{min}}^{\omega_{max}} \phi\{L_p(\omega)\} d\omega \right)^{\frac{1}{n}} \tag{2.24}$$

was suggested in [10] for sound pressure level (L_p) in dB minimization at one or more points in the model. The ϕ operator is a weighting function defined as $(L_p - L_T)^n$ for $L_p > L_T$ and 0 otherwise. In this way, only those levels above a certain threshold, L_T, are considered in the optimization. Moreover, the exponent n leads to the mean value for $n = 1$, with all levels being equally important, or to the root mean square for $n = 2$, which gives more importance to high peaks and therefore helps minimize the most problematic parts of the frequency response instead of making valleys deeper. In our work, structural vibration is minimized in most cases, and sound level is only considered in one case in Report E; however, a similar approach can be used for velocity or displacement minimization. Different variations of the following objective function are used, where the total velocity level is minimized,

$$g = 10 \log \sum_{k=1}^{K} \left| \frac{\mathbf{v}_m(\omega_k)}{v_{ref}} \right|^2 \tag{2.25}$$

where $|\mathbf{v}_m(\omega_k)|$ is the magnitude of the total velocity at the considered point, calculated as $\left| \sqrt{v_{mx}^2 + v_{my}^2 + v_{mz}^2} \right|$, v_{ref} is the reference structural velocity, k is the k-th discrete frequency line and K is the total number of frequencies. An advantage of summing the linear quantity instead of the logarithmic level in dB is that the highest values are automatically more relevant than the smaller

ones. For high frequency problems in wide-frequency ranges, a logarithmic spacing of the frequency is recommended. When insufficient frequency resolution is used, significant contributions to the objective function may be in between frequency bins causing a bias in the objective function; therefore, fine frequency resolution must be ensured [9]. Since the coupled structure-acoustic problem is solved independently for each considered frequency, evaluating such an objective function may become computationally demanding, which is the main motivation for the investigation of model reduction techniques in this thesis. This topic is approached in detail in Chapter 4.

Design variables typically include geometric and material properties, both types considered in this thesis. Design parameters require constraints in most cases in order to limit the optimization design domain, which can be introduced as lower and upper bounds. Moreover, equality or inequality constraints can be added to control other properties such as the total mass or volume, typical in thickness or topology optimization. In some cases, a problem may have several solutions, and additional requirements are made on the design variables to choose the desired outcome. For example, the minimum variation of the design variables is required in the design problem in Ref. [23], where the objective function is expressed as the variation on the design variables and the structure-acoustic quantity to be optimized is included as a constraint. A similar approach is used in Paper A, where the sum of the design variables values is maximized, and the modal frequency error is included as a constraint. Additional information can also be added to the optimization problem by means of regularization techniques when the problem is ill-posed, as done in acoustic holography applications, for example [24].

2.3.2 Optimization methods

The objective functions and constraints discussed above are nonlinear, and numerical treatment is therefore required to find a minimum. In general, it is difficult to ensure global convergence in realistic problems; however, an optimized design will in general be satisfactory enough for engineering purposes. For this reason, the most extended techniques in structural-acoustic optimization are based on sensitivity calculations and subsequent solution of approximate problems, such as in sequential linear or quadratic programming, the Method of Moving Asymptotes (MMA), the method of feasible directions or other gradient-based methods, even though they may lead to local minima in general [9]. Other techniques have also been used in the literature, such as exhaustive search (limited to low dimensionality problems) which aims at finding

a global minimum [25, 26], local and global search methods [27] and evolutionary strategies [28, 29], including genetic algorithms [27, 30–32].

In this thesis, the studies presented in Chapters 3 and 4 are done with a constrained optimization algorithm implemented in the MATLAB Optimization Toolbox [33] function *fmincon*, described in detail in Ref. [34]. For Chapter 5, two topology optimization methods are compared in Paper F, which use MMA [35] and the Bi-directional Evolutionary Structural Optimization (BESO) technique [36], also gradient-based.

Both the *fmincon* algorithm and MMA are based on mathematical programming techniques where the objective function is approximated based on its first derivatives by a simpler problem that is valid around the current optimization point. Sensitivity analysis is therefore a key point in all considered optimization methods. The simplest way to calculate the sensitivity is by approximating it by Finite Differences (FD). For an objective function $g(\boldsymbol{\mu})$, with $\boldsymbol{\mu} = [\mu_1 ... \mu_n]$ being the optimization variables, the sensitivity with respect to one variable is given by

$$\frac{\partial g}{\partial \mu_i} = \frac{g(\mu_i + \Delta\mu_i) - g(\mu_i)}{\Delta\mu_i}, \tag{2.26}$$

where $\Delta\mu_i$ should be chosen as a trade-off between giving a good local approximation and avoiding numerical noise to influence the result. FD calculations therefore require an extra objective function evaluation for each considered variable, which may become highly computationally expensive when the objective function calculation is costly. Therefore, it is desirable to obtain the sensitivities analytically when possible (i.e., for the considered objective functions, when the system matrices can be differentiated analytically with respect to the optimization variables). For an objective function of the type of eq. (2.23), direct differentiation gives the analytical gradient (see details in Chapter 3). However, other functions may not be directly differentiable, and the adjoint method can be applied in that case [37]. For linear dynamic systems with harmonic excitation described by eq. (2.22), the sensitivity of the objective function

$$g_r(\boldsymbol{\mu}) = g(\boldsymbol{\mu}, \mathbf{x}_{\Re}(\boldsymbol{\mu}), \mathbf{x}_{\Im}(\boldsymbol{\mu})) \tag{2.27}$$

can be calculated as

$$\frac{\partial g_r}{\partial \mu_i} = \frac{\partial g}{\partial \mu_i} + \Re\left\{\boldsymbol{\lambda}^H \left[\frac{\partial \mathbf{f}}{\partial \mu_i} - \frac{\partial(\mathbf{K} - \omega^2\mathbf{M})}{\partial \mu_i}\mathbf{x}\right]\right\}, \tag{2.28}$$

where ^{H} indicates the conjugate transpose, and $\boldsymbol{\lambda}$ is the adjoint vector resulting from solving the adjoint problem

$$(\mathbf{K}^H - \omega^2\mathbf{M}^H)\boldsymbol{\lambda} = \frac{\partial g}{\partial \mathbf{x}_{\Re}} + j\frac{\partial g}{\partial \mathbf{x}_{\Im}}. \tag{2.29}$$

The adjoint method is therefore not "for free" since it requires solving one extra problem; however, it is more computationally efficient than the FD approach, which requires one extra solve per optimization variable. Still, if an analytical expression for the gradient of the system matrices is not available, as in Paper C and Paper D, FD is the only applicable alternative. For topology optimization, FD is not an option in practice, since the number of optimization variables is as large as the number of elements in the design domain; therefore, the adjoint method has been applied in Paper F.

Chapter 3

Contact identification by model updating

The Finite Element Method (FEM) is a powerful numerical modelling technique that has been under development since its introduction in 1941 with the work by Hrennikoff [38] and also Courant and Robbins [39]. It has become a well-established simulation tool for many applications, one of them being vibration analysis. Despite the sophistication of methods, discrepancies are still commonly found between vibration measurement and simulation data, the main reasons being [22, 40]: (1) model structural errors, due to the difficulty in modelling material properties, joints, edges and non-linearity; (2) model parameter errors, which result from the difficulty in identifying the correct material properties or dimensions; (3) measurement errors; and (4) FE mesh discretization errors.

A main source of mismatch between experimental and simulation data in vibroacoustic analysis of hearing aids is the error introduced when modelling mechanical contacts between parts. Modelling of the dynamics of mechanical joints in assembled structures is an extensive field of study with many existing different approaches [41], mostly focused in modelling the nonlinear behaviour of the normal forces and friction between parts. However, linear models of contacts are desired for harmonic simulations; the options here consist in either bonding the two structures assuming no separation, or characterising the contact by some

stiffness and damping properties, which can be identified by model updating techniques.

Model updating methods are in fact computational routines that were developed to modify erroneous or unknown material properties in a FE model to match experimental results as closely as possible; however, they have also been applied for contact modelling purposes in the literature. Some methods for identification of joint parameters for flange, bolt or weld joints based on measured modal frequencies and modal damping ratios can be found in Refs. [42–48]. In those studies, the location of the contact is well-defined and they focus on estimating its global stiffness and damping. However, in hearing aids, the actual contact points between manufactured parts can differ significantly from the designed nominal contact areas due to irregularities introduced in the manufacturing process. A technique to determine contact properties by model updating under these conditions is developed in Paper A, and the basics of contact modelling and model updating techniques are discussed in this chapter.

3.1 Contact modelling

In this section, the types of mechanical contacts encountered in hearing aid assemblies are summarized, and the introduction of a linear contact model in a FE model is described.

3.1.1 Mechanical contacts in hearing aids

Hearing aid parts are assembled using a variety of mechanical contacts, the most used types being the screw, the snap fit, the friction contact and the pin, shown in Figure 3.1 and described in the following. The friction contact is mainly used to keep interior parts from falling out when the outer shell structure is opened, such as in the receiver support in the picture. It consists in using a layer of a material with a high friction coefficient at the sides of the part. The part is designed to fit exactly inside the shell, and the high friction prevents it from falling once it is placed. A snap fit is a joint system where the two parts to be attached present geometrically opposed shapes which fit together. The parts undergo a deformation in order to fit one into the other, and return to the original position to accomplish the fixture. The snap fit is used to fix interior parts to the shell, and also to hold the battery drawer. The screw and the pin

connection are mainly used for the purpose of assembling the top and base shell of the hearing aid.

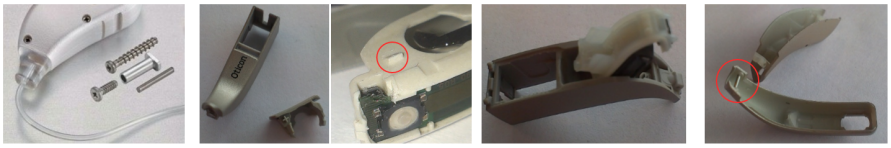

Screw Snap fit Friction Pin

Figure 3.1: Several types of mechanical contacts in hearing aids

The location of the contact for the friction type is rather well-defined compared to the pin or the snap fit connections. The contact between the pin and the plastic parts is enforced by the mechanical design; however, the plastic parts that it connects (usually the shells) are also in contact between them along an overlapping surface, where the actual contact points are highly dependent on manufacturing tolerances. Modelling of the contact in the latter scenario is the object of study of Paper A, where an assembly of two plastic parts similar to hearing aid shells with simplified geometry is used for the purpose.

3.1.2 Linear model of joint structures

Since the aim of our work is to obtain a model that can help harmonic simulation results match experimental data, rather than analysing nonlinear physical phenomena that occur at the contact, a linear lumped element model is considered. Contacts can be characterised in terms of their stiffness and damping. Contact damping is mainly induced by friction between parts and existing air micro gaps, while stiffness is mostly influenced by properties of the contact surface such as hardness, roughness and waviness [44], as well as the geometry and relative position of the parts. The latter are properties that are highly sensitive to manufacturing tolerances; therefore, in order to keep the model as simple as possible, damping is disregarded and only linear springs are considered in the case studied in Paper A. However, the method described in the following can include contact damping if an imaginary part is added to the spring constants.

For two coupled structures a and b, the mass and stiffness matrices of the assembly are built from the mass and stiffness matrices of the independent

structures and a contact spring stiffness matrix, $\mathbf{S}$, as

$$\mathbf{M} = \begin{bmatrix} \mathbf{M}_a & \mathbf{0} \\ \mathbf{0} & \mathbf{M}_b \end{bmatrix}, \tag{3.1}$$

$$\mathbf{K} = \begin{bmatrix} \mathbf{K}_a & \mathbf{0} \\ \mathbf{0} & \mathbf{K}_b \end{bmatrix} + \mathbf{S} = \tilde{\mathbf{K}} + \mathbf{S}, \tag{3.2}$$

where $\mathbf{M}_a$ and $\mathbf{K}_a$ are the system matrices of part a, $\mathbf{M}_b$ and $\mathbf{K}_b$ are the system matrices of part b and matrix $\mathbf{S}$ contains the contact spring constants, as detailed below. An illustration of the coupled model for a case with one contact spring can be seen in Figure 3.2. Structural damping is disregarded here, but could be included in a straight-forward way by adding a damping matrix to the FE models of the independent structures.

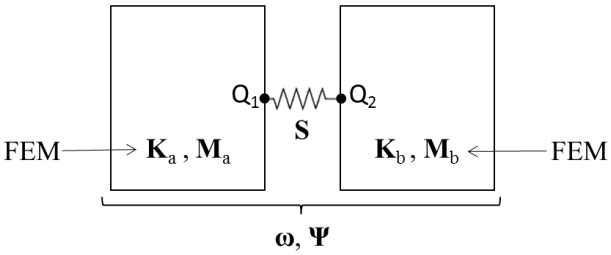

Figure 3.2: Model of two coupled structures

Matrix $\mathbf{S}$ implements two conditions between the connected degrees of freedom: equilibrium of forces and proportionality between force and displacement by Hooke's law. For one spring (with stiffness s) connecting two nodes ($Q1$ and $Q2$), this is expressed as

$$s(\mathbf{u}_{Q1} - \mathbf{u}_{Q2}) = \mathbf{f}_{Q1} = \mathbf{f}_{Q2}, \tag{3.3}$$

where $\mathbf{u}_{Q1}$ and $\mathbf{u}_{Q2}$ are the displacements of the connected DOFs, and $\mathbf{f}_{Q1}$ and $\mathbf{f}_{Q2}$ are the sum of forces acting on these nodes. Generalising for more than one contact spring, the conditions can be implemented in a matrix $\mathbf{S}$ that multiplies the displacement vector in the equation of motion,

$$\mathbf{S} = \sum_{n=1}^{N} s_n (\mathbf{1}_{Q_{an}} - \mathbf{1}_{Q_{bn}})^T (\mathbf{1}_{Q_{an}} - \mathbf{1}_{Q_{bn}}), \tag{3.4}$$

where N is the total number of contact springs, and $\mathbf{1}_{Q_{an}}$ and $\mathbf{1}_{Q_{bn}}$ are vectors with a value of 1 at Q_{an} and Q_{bn}, respectively, and zeros at the rest, where Q_{an}

and Q_{bn} are the connected degrees of freedom of part a and part b. Therefore $\mathbf{S}$ is a matrix that contains s_n at the diagonal matrix entries (Q_{an},Q_{an}) and (Q_{bn},Q_{bn}), and -s_n at the matrix entries (Q_{an},Q_{bn}) and (Q_{bn},Q_{an}).

The equation of motion under harmonic excitation of the assembled structures therefore becomes

$$\left(\left(\tilde{\mathbf{K}} + \mathbf{S}\right) - \omega^2 \mathbf{M}\right) \mathbf{u} = \mathbf{f} \tag{3.5}$$

3.2 Model updating

Model updating techniques can generally be classified in two categories: the direct methods and the penalty methods [49]. Direct methods try to update the FE model by solving a set of characteristic equations that relate it to the experimental data. For this approach, big sets of measured data are usually required, since as many equations as unknown model parameters are needed. Moreover, the FE matrices are updated directly, which can result in models that have little physical meaning. On the other hand, penalty or iterative methods consist in modifying certain model parameters connected to physical properties to minimize an error function between experimental and modelled results. Sophisticated optimization techniques can be used for finding the optimal combination of parameter values, which allows for extra flexibility and control by applying constraints and weighting factors, adjusted according to the user's criteria and confidence in the measured data and model parameters [43]. The second approach is selected in this work due to the difficulty in obtaining reliable experimental data, as discussed in the following subsection. For a full review of model updating techniques, the reader is referred to the work carried out in the nineties in Refs. [22, 49, 50], and the more recent state of the art surveys available in Refs. [40, 51].

3.2.1 Experimental data collection

With respect to the measurement data to be matched, model updating techniques can be classified into those working on the frequency response domain or the modal domain [40]; the first ones try to match Frequency Response Functions (FRFs) directly, while the second class aims at matching modal parameters, i.e. modal frequencies, modal damping ratios and/or modal vectors. Hearing aid parts are characterized by their small size and light weight, which

makes it challenging to measure vibration frequency responses by the usual methods, since excitation by hammer or shaker will influence the properties of the structure [52]; the use of non-invasive methods is therefore required. Typically, resonant frequencies and Operational Deflection Shapes (ODS) [53] of hearing aid assemblies are measured by exciting the receiver with a broadband signal (such as a frequency sweep or pseudo-random noise), and measuring the response with a laser vibrometer. When a single part is to be measured, an external acoustic excitation source is used instead.

Using this technique, the input force to the structure is not measured [54], thus FRFs are not obtained, and modal parameters cannot be calculated by the usual curve fitting methods [52]. To obtain modal parameters or cross-spectrum functions by non-invasive methods, Operational Modal Analysis (OMA) [55] could be performed by adding a second laser vibrometer to the setup described above, which would be used to capture a reference signal. The necessary equipment for such a setup was not available during the course of this study, though. Nevertheless, resonance frequencies are usually a good approximation of modal frequencies, and ODS approximate modal shapes [52], even though the influence of neighbouring modes can alter them significantly in some cases. The safest choice given the challenging measurement conditions is therefore to match model modal frequencies to measured resonant frequencies, and use the ODS to ensure that the matched frequencies correspond to the same mode. The reader is referred to Paper A for specific details on the measurement procedure.

3.2.2 Optimization problem formulation

In order to match measurement and model modal frequencies, minimizing an objective function that expresses the error between them would be the straightforward choice. However, the number of available measured modal frequencies will in general be lower than the number of model parameters, making the inverse problem ill-posed [56]. Regularization techniques can be used to alleviate this issue [47]; in our case, we chose to favour a solution that maximizes the contact stiffness, a choice motivated by the fact that the structures analysed in Paper A clearly vibrate together when measured, as observed from the mode shape plots presented therein, which indicates that the contact is strong. To implement the condition, the objective function is formulated as the inverse of the sum of all contact spring constants (eq. (3.6)), and subjected to a constraint (eq. (3.7)) that requires the error function between measurement and model modal frequencies to be below a threshold, ϵ. Additionally, the spring constants are required to be positive by a second constraint (eq. (3.8)). The resulting

optimization problem formulation is given as

$$\underset{\mathbf{p}}{\text{minimize}} \quad f(\mathbf{p}) = \frac{1}{\sum_{m=1}^{M} \mathbf{s}(\mathbf{p})} \tag{3.6}$$

$$\text{subject to } g(\mathbf{p}) = \sum_{n=1}^{N} (f_{model_n}(\mathbf{p}) - f_{meas_n})^2 < \epsilon \tag{3.7}$$

$$\mathbf{s}(\mathbf{p}) \geq \mathbf{0}, \tag{3.8}$$

where M is the number of contact springs, N is the number of considered modal frequencies, $f_{model_n}(\mathbf{s})$ is the n-th model eigenfrequency, f_{meas_n} is the n-th measured modal frequency and $\mathbf{s}(\mathbf{p})$ is the vector containing the contact spring constants, which are defined as a function of the vector of model parameters, $\mathbf{p} = [p_1, ..., p_M]$. If each spring was considered as an independent optimization variable, the problem would become difficult to handle due to the large dimensionality, and the results may be difficult to interpret. Therefore, $\mathbf{s}(\mathbf{p})$ is a function that defines dependencies between spring constants so that the number of variables is kept low and the contact is described meaningfully. Different parametrizations of the contact stiffness are discussed in Paper A.

In order to ensure that the frequencies that are subtracted in eq. (3.7) correspond to the same mode shape, a mode pairing technique can be used. The reader is referred to section 3.2.1 in Paper A for the specific details on the procedure.

3.2.2.1 Sensitivity analysis

A wide variety of optimization techniques have been used for model updating by the penalty method [51]. In the case under study, the constraint optimization problem described above can most efficiently be solved by nonlinear programming techniques, which imply iterative procedures based on the gradients of the objective function and constraints. The gradients can be approximated by finite differences, or specified analytically. The last option is preferred when possible since it requires fewer objective function evaluations and improves the computational efficiency. The gradients of eqs. (3.6) and (3.8) are calculated according to the specific parametrization functions $\mathbf{s}(\mathbf{p})$, described in Paper A. The gradient of the first constraint is discussed in the following; differentiating eq. (3.7) by the chain rule, we obtain

$$\nabla g(\mathbf{p}) = \frac{1}{4\pi^2} \sum_{n=1}^{N} \left(1 - \frac{f_{meas_n}}{f_{model_n}(\mathbf{p})}\right) \nabla \omega^2_{model_n}(\mathbf{p}), \tag{3.9}$$

where $\omega_{model_n}(\mathbf{p}) = 2\pi f_{model_n}(\mathbf{p})$ is the n-th model modal angular frequency (denoted in the following by ω_n for the sake of notation clarity), resulting from solving the eigenvalue problem

$$(\mathbf{K}(\mathbf{p}) - \omega_n^2(\mathbf{p})\mathbf{M}(\mathbf{p}))\mathbf{\Psi}_n(\mathbf{p}) = \mathbf{0}. \tag{3.10}$$

The dependency on $\mathbf{p}$ is neglected in the following for the sake of clarity in the equations. The term $\nabla\omega^2_{model_n}$ can be obtained as follows. Differentiating equation 3.10 with respect to a design parameter, p_e, and pre-multiplying it by $\mathbf{\Psi}_n^T$, gives

$$\mathbf{\Psi}_n^T \left(\frac{\partial \mathbf{K}}{\partial p_e} - \left(\frac{\partial \omega_n^2}{\partial p_e}\mathbf{M} + \omega_n^2 \frac{\partial \mathbf{M}}{\partial p_e}\right)\right) \mathbf{\Psi}_n + \mathbf{\Psi}_n^T(\mathbf{K} - \omega_n^2\mathbf{M})\frac{\partial \mathbf{\Psi}_n}{\partial p_e} = 0; \tag{3.11}$$

assuming that the eigenvectors are normalized with the mass matrix so that

$$\mathbf{\Psi}_n^T \mathbf{M} \mathbf{\Psi}_n = \mathbf{1}, \tag{3.12}$$

and matrices $\mathbf{K}$ and $\mathbf{M}$ are symmetric, implying

$$\mathbf{\Psi}_n^T(\mathbf{K} - \omega^2\mathbf{M}) = \mathbf{0}, \tag{3.13}$$

the derivative of ω_n^2 can expressed as

$$\frac{d\omega_n^2}{dp_e} = \mathbf{\Psi}_n^T \left(\frac{\partial \mathbf{K}}{\partial p_e} - \omega_n^2 \frac{\partial \mathbf{M}}{\partial p_e}\right) \mathbf{\Psi}_n. \tag{3.14}$$

Given that the design parameters only affect the stiffness matrix, and more specifically the contact stiffness matrix $\mathbf{S}$, the expression is reduced to

$$\frac{d\omega_n^2}{dp_e} = \mathbf{\Psi}_n^T \frac{\partial \mathbf{S}}{\partial p_e} \mathbf{\Psi}_n. \tag{3.15}$$

Therefore,

$$\nabla \omega^2_{model_n} = \left(\mathbf{\Psi}_n^T \frac{\partial \mathbf{S}}{\partial p_1} \mathbf{\Psi}_n, ..., \mathbf{\Psi}_n^T \frac{\partial \mathbf{S}}{\partial p_M} \mathbf{\Psi}_n\right), \tag{3.16}$$

where the terms $\frac{\partial \mathbf{S}}{\partial p_m}$ are calculated according to the parametrization functions $\mathbf{s}(\mathbf{p})$.

3.3 Contribution

In Paper A, a procedure to characterise the contact stiffness and localize the most probable contact areas between two assembled parts is presented. The contact is modelled by linear springs that connect all nodes that lie on the nominal contact area, and their stiffness constants are determined by a model updating technique that minimizes the error between measured and model modal frequencies. Since the number of contact springs is too large to consider each of their stiffness constants as an independent model parameter, the key contribution in the paper consists in the development of an efficient parametrization of the spring constant values as a function of their location. Several parametrization functions are compared for a numerical validation case, showing that the number of model parameters must be selected as a trade-off between the dimensionality of the problem and the accuracy of the results being at a desired level. A 36-parameter model based on a Fourier series approach where the Fourier coefficients are the model parameters is proposed as an outcome of the study. By identifying the contact parameters for several sets of experimental data measured under varying contact conditions, the variability of the contact between two small plastic parts due to the dis-assemblage and assemblage process is characterized.

Chapter 4

Model reduction for optimization problems

A main goal of this PhD project is to investigate how reduction techniques can be applied in hearing aid coupled structure-acoustic FE models to speed up vibro-acoustic response optimization. Together with design, control and uncertainty quantification, optimization is one of the applications that require repeated evaluations of a model for varying values of certain parameters, where parametric Model Order Reduction (pMOR) techniques become relevant [57]. Parametric model reduction is a projection-based approach to surrogate modelling, which is preferred to other available approaches such as data-fit and hierarchical models [58] when dealing with dynamic systems, since projection-based methods preserve the underlying structure of the system, allowing for the reduced version to be evolved in time or evaluated at different frequencies.

In projection-based reduction, also known as the Rayleigh-Ritz procedure, it is assumed that the response of the system can be described in terms of a set of basis vectors. For a system in $\mathbb{R}^n$ of the type introduced in Chapter 2,

$$(\mathbf{K} - \omega^2 \mathbf{M})\mathbf{x} = \mathbf{f}, \tag{4.1}$$

where $\mathbf{K}$ and $\mathbf{M} \in \mathbb{R}^{n \times n}$ are the structure-acoustic coupled stiffness and mass matrices, $\mathbf{f} \in \mathbb{R}^n$ is the external force vector, the state vector $\mathbf{x} \in \mathbb{R}^n$ can be

approximated as

$$\mathbf{x} \approx \tilde{\mathbf{x}} = \eta_1 \mathbf{v}_1 + \eta_2 \mathbf{v}_2 + \cdots + \eta_m \mathbf{v}_m = \\ = \sum_{i=1}^{m} \eta_i \mathbf{v}_i = [\mathbf{v}_1 \dots \mathbf{v}_m] \begin{bmatrix} \eta_1 \\ \vdots \\ \eta_m \end{bmatrix} = \mathbf{T}\mathbf{x}_r, \tag{4.2}$$

where $\tilde{\mathbf{x}} \in \mathbb{R}^n$ is the approximated (or reconstructed) state vector, $\mathbf{x}_r \in \mathbb{R}^m$ is the reduced state vector, $\mathbf{T} \in \mathbb{R}^{\mathbf{n}\times\mathbf{m}}$ is the transformation matrix, and $m < n$. Introducing the approximation into the equation of motion and pre-multiplying it by $\mathbf{T}^T$, the system is reduced to

$$(\underbrace{\mathbf{T}^T\mathbf{K}\mathbf{T}}_{\mathbf{K}_r} - \omega^2 \underbrace{\mathbf{T}^T\mathbf{M}\mathbf{T}}_{\mathbf{M}_r})\mathbf{x}_r = \underbrace{\mathbf{T}^T\mathbf{f}}_{\mathbf{f}_r}. \tag{4.3}$$

The full-dimensional system as expressed in eq. (4.1) will be referred to in the following as the full model, and the system in eq. (4.3), as the reduced system.

The Chapter is organized as follows. The basis vectors that form the transformation matrix $\mathbf{T}$ can be computed using different techniques, which are summarized in Section 4.1. The basis vectors will in general be sensitive to changes in the optimization variables, which motivates the introduction of pMOR techniques that avoid having to re-calculate them for each variation of the parameter values. An overview of pMOR techniques is given in Section 4.2, and error measures are discussed in Section 4.3. The author's contribution in the topic is outlined in Section 4.4.

4.1 Reduction basis construction techniques

Model Order Reduction (MOR) methods in structural dynamics have been reviewed and compared in several publications, for example in Refs. [59, 60]. In general, basis computation methods can be divided in: modal-based, Krylov subspace, balanced truncation and Proper Orthogonal Decomposition (POD). Modal methods have been used most extensively in the field of structural vibration, while Krylov subspace, modal truncation and POD have been adopted more recently from other fields such as electronics or control systems design. In the following, we summarize the most relevant techniques and give insight into their application in structure-acoustic interaction problems.

4.1.1 Modal-based reduction

Modal methods consists in using a truncated set of modal vectors as a reduction basis. The modal vectors for problem 4.1 are obtained by solving the eigenvalue problem

$$\left(\mathbf{K} - \omega_i^2 \mathbf{M}\right) \boldsymbol{\psi}_i = \mathbf{0}, \tag{4.4}$$

where ω_i and $\boldsymbol{\psi}_i$ are the modal frequency and vector corresponding to mode i. The transformation matrix $\mathbf{T}$ is then formed by concatenating the set of M lower frequency modes,

$$\mathbf{T} = \boldsymbol{\Psi}_M = [\boldsymbol{\psi}_1 \boldsymbol{\psi}_2, \ldots, \boldsymbol{\psi}_M]. \tag{4.5}$$

For purely structural problems, this yields an orthogonal vector basis that not only reduces the system but also diagonalizes matrices $\mathbf{M}$ and $\mathbf{K}$, leading to a decoupled system of equations. However, for coupled fluid-structure interaction problems, the resulting modal vectors are not mutually orthogonal due to the asymmetry of the system matrices, and the so-called left eigenvectors are also needed to decouple the system. They can be calculated by solving the eigenvalue problem

$$\left(\mathbf{K}^H - \omega_i^2 \mathbf{M}^H\right) \boldsymbol{\psi}_i^L = \mathbf{0}, \tag{4.6}$$

where the superscript ^{H} indicates the conjugate transpose matrix (or just the transposed, if the matrices are real), and $\boldsymbol{\psi}_i^L$ is the ith left eigenvector. However, a relationship between left and right eigenvectors for undamped problems was shown in Ref. [61] and extended to problems with damping matrix in Ref. [62], which avoids having to solve an extra eigenvalue problem to obtain both sets of vectors. For a system of the form of eq. (2.20), the right and left eigenvectors are related as

$$\boldsymbol{\psi}_i^L = \begin{bmatrix} \boldsymbol{\psi}_{si}^L \\ \boldsymbol{\psi}_{ai}^L \end{bmatrix} = \begin{cases} \begin{bmatrix} \boldsymbol{\psi}_{si}^R \\ \frac{1}{\omega_i^2 \rho_a} \boldsymbol{\psi}_{ai}^R \end{bmatrix}, & \omega_i \neq 0 \\ \begin{bmatrix} \mathbf{0} \\ \boldsymbol{\psi}_{ai}^R \end{bmatrix}, & \omega_i = 0 \end{cases}$$

where the subscripts s and a denote the structural and acoustic DOFs of the eigenvectors, respectively. Then, a reduced and decoupled system can be obtained by pre-multiplying the equation of motion by the left eigenvector set and projecting the response vector on the right eigenvector basis,

$$(\boldsymbol{\Psi}_M^L)^H \left(\mathbf{K} - \omega^2 \mathbf{M}\right) \boldsymbol{\Psi}_M \mathbf{x}_r = (\boldsymbol{\Psi}_M^L)^H \mathbf{f}. \tag{4.7}$$

Since solving an unsymmetric eigenvalue problem is computationally more demanding than solving a symmetric one, a method that uses the uncoupled

structural and acoustic modes was suggested in Ref. [15]; however, using modes that include information about the coupling is desirable from an accuracy point of view. The technique used in Refs. [63, 64] consists in using only the coupled right eigenvectors and orthogonalising them. The procedure splits the fluid and structural parts of the modal vectors and orthogonalises them with respect to the acoustic and structural mass matrices, respectively, since the split-field orthogonalization gives a better numerical condition of the resulting matrices [64]. Different combinations of this technique (Split Field method) and the modal reduction technique with left and right eigenvectors (Left-Right method) are described and compared in detail in Papers B and C, where it is concluded that the Field Split method is the most accurate option for the considered problems, and it is therefore used in Paper D.

An advantage of modal-based methods is that the reduction basis describes the system independently of its inputs and outputs, and can therefore be used for different excitation configurations once it is built. Moreover, the basis vectors can be calculated according to an upper frequency bound using an iterative solver, and therefore the number of vectors M does not need to be specified *a priori*. However, an upper frequency limit that ensures a good resulting accuracy may have to be much higher than the upper analysis frequency of interest, since the low frequency contribution of higher modes affects the response. The FE mesh required for such high frequency mode calculation should be much finer than the one required for the upper analysis frequency, making it highly computationally expensive to solve the eigenvalue problem, which defeats the purpose of model reduction.

Some techniques that account for the static contribution of truncated modes using information about the input force vector have been developed in the literature, such as the mode acceleration and the modal truncation augmentation methods [65]. The independence of the reduction from the input force is then lost; however, this is not an inconvenience in the type of optimization problems considered in this thesis, where the input to the system does not vary. In Paper D, a variation of the static correction technique that includes forced response vectors at several frequencies within the frequency range of analysis is used, which is shown to improve accuracy significantly. The forced responses are denominated enrichment vectors, and can also be seen as first order Krylov subspace vectors, which will be described in Section 4.1.2.

4.1.1.1 Component Mode Synthesis

Component Mode Synthesis (CMS) or substructuring techniques are a variation of the modal techniques where the global structure is divided into smaller substructures, which are reduced individually and coupled together at the interfaces. CMS was the first approach to model reduction developed in the field of structural dynamics; it was introduced in the 1960s with the Craig-Bampton method [66], which became the most popular choice in the field, even though several other approaches have been developed by other authors, see Ref. [67] for a complete review.

The CMS methods arose due to the limitations in the available computational power at that time, which did not allow for solving large FE models of large structures at once, motivating the division of the system in smaller parts. Nowadays, fast solving techniques for sparse matrix systems such as those obtained by the FEM have been developed, reducing significantly the computational cost of solving full FE models. The matrices resulting from a CMS reduction (or other projection-based reductions that do not diagonalize the system) are not sparse any more, though, and the efficient sparse solvers can therefore not be used on the reduced systems. For this reason, solving a reduced system may become more computationally expensive than solving the complete system in some cases, depending on the achieved DOF reduction rate. In CMS techniques, the substructure DOFs are divided into internal ($\mathbf{x}_i$) and boundary ($\mathbf{x}_b$) DOFs. The transformation matrix is then formed by two types of vectors: vibration modes ($\boldsymbol{\psi}$) and interface vectors ($\boldsymbol{\phi}$), so that

$$\begin{bmatrix} \mathbf{x}_b \\ \mathbf{x}_i \end{bmatrix} = [\boldsymbol{\psi} \;\; \boldsymbol{\phi}] \begin{bmatrix} \mathbf{x}_b \\ \mathbf{x}_r \end{bmatrix}, \tag{4.8}$$

where $\mathbf{x}_r$ are the reduced internal coordinates, with as many components as considered vibration modes, and the boundary DOFs $\mathbf{x}_b$ remain unchanged. The number of boundary DOFs therefore plays a key role on the achieved reduction rate; even though interface reduction techniques have been developed to improve efficiency [64,68], this makes CMS methods most applicable to structures that can be divided at small interfaces, such as the piping systems studied in Refs. [63, 64].

In Paper C, the Craig-Bampton method is described in detail and compared to a pMOR global modal reduction technique for optimization of a simplified hearing aid model. The latter option performs more efficiently in the considered cases, even though CMS also introduces an improvement in solving time compared to the full system case. CMS could still be an interesting option in the

context of optimization in cases where pMOR techniques cannot be applied, since it makes it possible to reduce all parts in a model except for that where the changes take place. However, this option has not been further investigated in this thesis.

4.1.2 Krylov subspace method

The Krylov subspace method is a rational interpolation technique based on the theory of moment-matching and Padé-type approximations [57]. This family of methods aims at approximating the input-output transfer function of a system within a given frequency range by a so-called moment expansion, where the reduced system matches the first coefficients of this expansion. The moment matching procedure is related to projections on a Krylov subspace, which provides an efficient reduction basis calculation method. The relation between Padé approximation and the Krylov subspace was first shown in Ref. [69], where a method called Padé via Lanczos was proposed. The Lanczos method is one of the most used algorithms for Krylov subspace calculation, together with the Arnoldi algorithm [70, 71].

The Krylov subspace method has been developed for first-order state-space systems of the form,

$$\begin{aligned} \mathbf{E}\dot{\mathbf{x}} &= \mathbf{A}\mathbf{x} + \mathbf{b}u \\ \mathbf{y} &= \mathbf{c}^T\mathbf{x}, \end{aligned} \tag{4.9}$$

where $\mathbf{x}$ is the state vector, $\mathbf{y}$ is the output vector, related to $\mathbf{x}$ by vector $\mathbf{c}$, $\mathbf{E}$ and $\mathbf{A}$ are the system matrices, and $\mathbf{b}u$ defines the input. The second-order system that describes the dynamics of our problem, stated in eq. (4.1), can be converted to this form; starting from its time domain expression,

$$\mathbf{M}\ddot{\mathbf{x}} + \mathbf{K}\mathbf{x} = \mathbf{f}, \tag{4.10}$$

it can be formulated into first-order state-space form by adding an additional equation, as

$$\begin{aligned} \begin{bmatrix} \mathbf{I} & \mathbf{0} \\ \mathbf{0} & \mathbf{M} \end{bmatrix} \begin{bmatrix} \dot{\mathbf{x}} \\ \ddot{\mathbf{x}} \end{bmatrix} + \begin{bmatrix} \mathbf{0} & -\mathbf{I} \\ \mathbf{K} & \mathbf{0} \end{bmatrix} \begin{bmatrix} \mathbf{x} \\ \dot{\mathbf{x}} \end{bmatrix} &= \begin{bmatrix} \mathbf{0} \\ \mathbf{f} \end{bmatrix} \\ \mathbf{y} &= \mathbf{l}^T \begin{bmatrix} \mathbf{x} \\ \dot{\mathbf{x}} \end{bmatrix}, \end{aligned} \tag{4.11}$$

with $\mathbf{l}$ being a vector that selects the response vector components that should be included in the output vector, $\mathbf{y}$.

In the frequency domain, the transfer function for eq. (4.9) is defined as

$$\mathbf{H}(\omega) = \mathbf{c}^T(j\omega\mathbf{E} - \mathbf{A})^{-1}\mathbf{b}, \tag{4.12}$$

which can be expressed in the form of a moment expansion,

$$\mathbf{H}(\omega) = \sum_{n=0}^{\infty}(-1)^n M_n(j\omega_0)(j\omega - j\omega_0)^n, \tag{4.13}$$

where ω_0 is the expansion point (or frequency) where the approximation is matched, and the moments are calculated by the Taylor expansion formula,

$$M_n(j\omega_0) = \mathbf{c}^T[j\omega_0\mathbf{E} - \mathbf{A}]^n(j\omega_0\mathbf{E} - \mathbf{A})^{-1}\mathbf{b}. \tag{4.14}$$

The goal of the Krylov subspace expansion is to find a reduction basis such that the transfer function of the reduced system matches the first k moments of the transfer function of the original system. It turns out that such reduction basis vectors are given by the Krylov subspace,

$$\mathbf{T} = \mathcal{K}_k\left((\mathbf{A} - j\omega_0\mathbf{E})^{-1}, (\mathbf{A} - j\omega_0\mathbf{E})^{-1}\mathbf{b}\right), \tag{4.15}$$

where the Krylov subspace of an arbitrary matrix $\mathbf{P}$ and vector $\mathbf{r}$ is defined as

$$\mathcal{K}_k(\mathbf{P}, \mathbf{r}) = \text{span}\left\{\mathbf{r}, \mathbf{P}\mathbf{r}, \cdots, \mathbf{P}^{k-1}\mathbf{r}\right\}. \tag{4.16}$$

For a prove of the moment matching property, see Ref. [60].

Even though the concept behind moment matching methods can appear cumbersome, the calculation of the basis vectors can be done by relatively simple algorithms, and several techniques to calculate Krylov subspace vectors efficiently can be found in the literature. Moreover, the fact that the matrices are unsymmetric for the coupled structure-acoustic problem does not pose extra challenges, and the methods can be applied straight-forwardly. In Report E, a Krylov subspace method is used to reduce a structure-acoustic coupled model of a hearing aid with surrounding air, where the Arnoldi method developed for second-order dynamic systems described in Ref. [71] is employed.

The most expensive step in the Krylov subspace computation process is the inversion of matrix $(\mathbf{A} - j\omega_0\mathbf{E})$, which is necessary to calculate the first Krylov

subspace vector. The matrix LU-decomposition is then stored and used thereafter to obtain the rest of vectors by cheap matrix-vector multiplications; increasing the order of the subspace k is therefore computationally cheap. For larger k values, the approximation holds for wider frequency ranges around the expansion point. However, several Krylov subspaces calculated at different expansion points can also be combined in one reduction basis in order to achieve an accurate reduction along a wider frequency range. Determining the optimal k value and number of expansion points is not trivial, since an *a priori* error estimator is not available. However, an algorithm that aims at automatising such choices is given in Refs. [72, 73].

4.1.3 Balanced truncation

Balanced truncation is a method that is most used in the field of systems and control. It is based on finding a so-called balanced realization, for which the states are ordered according to their contribution to the input-output behaviour, and a reduced system is obtained by discarding the states that contribute the least. The implementation of such procedure, described in detail in Ref. [60], involves the solution of two full-rank Lyapunov equations, which is computationally expensive and limits the application of this technique to systems of order $\mathcal{O}^3$ or lower. This method is therefore not further considered in this thesis, since typical FE models of hearing aids are of orders above $\mathcal{O}^5$.

4.1.4 Proper Orthogonal Decomposition

Proper Orthogonal Decomposition (POD) is a method that works in the time domain, unlike the previously discussed techniques. The concept behind it is related to principal component analysis, and it consists in building a reduction basis by assembling system response vectors calculated at several time instants (referred to as "snapshots") into a matrix, and orthogonalizing it (also eliminating vectors that contain repeated information) to avoid rank-deficiency in the resulting vector basis. Since full system solutions are required to construct the reduction basis, POD is in general less efficient than the previously discussed methods; however, an advantage of this method is that it makes no assumptions about the underlying system, and it can also be applied to nonlinear systems, for example. It was first introduced to study turbulent flows in Ref. [74], and it has been applied in a wide variety of problems ever since, being the method upon which the so-called Reduced Basis method is built [75, 76]. In the applications considered in this thesis, the methods discussed previously are better

suited since harmonic linear systems are considered; therefore, POD has not been applied in the contributed work.

4.2 Parametric Model Order Reduction

Parametric model order reduction techniques are developed with the aim of improving computational efficiency in reduction of systems with parametric dependencies, i.e. to avoid re-calculating a new reduction basis for each parameter value combination that needs to be evaluated. pMOR techniques can be used in combination with any of the reduction basis computation methods outlined in the previous section; the underlying idea consists in computing a number of local reduction basis at some sampled points of the parameter space and approximating the reduced systems at other points based on the available set of bases.

Parameter dependency can be introduced in eq. (4.1) as

$$\left(\mathbf{K}(\boldsymbol{\mu}) - \omega^2 \mathbf{M}(\boldsymbol{\mu})\right) \mathbf{x}(\boldsymbol{\mu}) = \mathbf{f}(\boldsymbol{\mu}), \tag{4.17}$$

where $\boldsymbol{\mu} = [\mu_1, \ldots, \mu_P]$ is the vector of model parameters. The parameter space is sampled at M points $\boldsymbol{\mu}_1, \ldots, \boldsymbol{\mu}_M$, where local reduction bases are computed using a reduction basis construction method of choice, yielding a set of local transformation matrices $\mathbf{T}_1, \ldots, \mathbf{T}_M$ (where $\mathbf{T}_m \equiv \mathbf{T}_{\boldsymbol{\mu}_m}$).

Based on the pMOR review paper by Benner *et al.* [57], different approaches to approximating the reduced system at non-sampled points are summarized in this section, and the choice of parameter sample points is discussed at the end.

4.2.1 Methods

4.2.1.1 Global reduction basis

The global reduction basis approach consists in assembling one single transformation matrix that includes information of all the computed local reduction bases. The most straight-forward method to construct the global transformation matrix is by concatenation of the local reduction bases,

$$\hat{\mathbf{T}} = [\mathbf{T}_1, \mathbf{T}_2, \ldots, \mathbf{T}_M]\,. \tag{4.18}$$

When using Krylov subspace methods, a more accurate way to obtain a global reduction basis would be to consider a multivariate Taylor expansion of the transfer function, $H(j\omega, \boldsymbol{\mu})$, and match moments in the parameter domain besides the frequency domain. In both cases, it is probable that the obtained global basis contains some linearly dependent vectors, leading to a rank-deficient global basis $\hat{\mathbf{T}}$. Therefore, the concatenation is usually followed by a Singular Value Decomposition (SVD) or QR decomposition that reveals the rank of the matrix and allows for elimination of the repeated components.

The matrix concatenation approach is also described in Ref. [77], where a review of pMOR techniques for structural FE models is given. A smart orthogonalization technique based on vector products linked to the kinetic and strain energy is suggested therein, described in the following. The transformation basis is required to be mass- (or stiffness-) orthonormal, i.e.

$$\mathbf{T}^T \mathbf{M} \mathbf{T} = \mathbf{I}, \tag{4.19}$$

where $\mathbf{T}$ is the orthogonalized transformation matrix, calculated as follows: the SVD of the mass matrix reduced using the rank-deficient matrix $\hat{\mathbf{T}}$ is first calculated as

$$\hat{\mathbf{T}}^T \mathbf{M} \hat{\mathbf{T}} = \mathbf{U} \boldsymbol{\Sigma} \mathbf{V}, \tag{4.20}$$

where $\boldsymbol{\Sigma}$ is a diagonal matrix containing the singular values, and $\mathbf{U}$ and $\mathbf{V}$ are unitary matrices, which are also equal and orthogonal if the decomposed matrix is symmetric, and therefore $(\mathbf{V}^{-1})^T = \mathbf{V} = \mathbf{U}$. The columns of matrix $\mathbf{U}$ corresponding to a singular value in matrix $\boldsymbol{\Sigma}$ with a value below a certain threshold are discarded, yielding the truncated matrix $\mathbf{U}_t$. Theoretically, this threshold would be zero; however, due to the numerical noise involved in real computations, a recommended value for the threshold is a multiple of the floating-point relative accuracy [78], weighted by the largest singular value and the number of vectors in $\hat{\mathbf{T}}$ (in order to penalize large reduced models [77]). Substituting $\mathbf{U}$ and $\mathbf{V}$ by $\mathbf{U}_t$ in eq. (4.20), moving the right-hand side terms to the left side and equating it to eq. (4.19), we obtain

$$\mathbf{T} = \hat{\mathbf{T}} \mathbf{U}_t \boldsymbol{\Sigma}^{-1/2}. \tag{4.21}$$

If the decomposed matrix is not symmetric, the procedure is applied equally and two (left and right) transformation matrices are obtained instead,

$$\mathbf{T}_R = \hat{\mathbf{T}} \mathbf{V}_t \boldsymbol{\Sigma}^{-1/2} \tag{4.22}$$

$$\mathbf{T}_L = \boldsymbol{\Sigma}^{-1/2} \mathbf{U}_t \hat{\mathbf{T}}. \tag{4.23}$$

The projection of the system is then done by pre-multiplying the system matrices by $\mathbf{T}_L$ and post-multiplying them by $\mathbf{T}_R$.

Besides the fact that mass-orthonormal bases are advantageous because they take scaling of different types of DOFs and distribution of structural properties into account, an advantage of this orthogonalization method is that the calculated SVD (on a matrix in $\mathbb{R}^{k\times k}$, with k being the total number of vectors in matrix $\hat{\mathbf{T}}$) is computationally cheaper than calculating the SVD of matrix $\hat{\mathbf{T}}$ (in $\mathbb{R}^{n\times k}$), since the dimensions are smaller.

The obtained transformation matrix $\mathbf{T}$ can then be used to reduce the system matrices for any parameter point using the projection approach described in eq. (4.3). The technique described up to this point is used in Papers B, C and D and Report E in this thesis, where it is referred to as Multi-Model Reduction (MMR) method.

In [57], a way to improve efficiency by avoiding the projection step of the system onto the reduction basis for each parameter point evaluation is suggested. The procedure can only be applied to system matrices with affine parametric dependence, defined for a generic system matrix, $\mathbf{A}$, as

$$\mathbf{A}(\boldsymbol{\mu}) = \mathbf{A}^0 + \sum_{i=1}^{L} f^i(\boldsymbol{\mu})\mathbf{A}^i, \tag{4.24}$$

where the scalar functions f^i determine the parametric dependency, and $\mathbf{A}^i$ for $i = 0, \ldots, L$ are parameter independent and can therefore be reduced *a priori* as $\mathbf{A}_r^i = \mathbf{T}^T\mathbf{A}^i\mathbf{T}$. The reduced system matrix for any parameter value can then be calculated without extra projection operations, as

$$\mathbf{A}_r = \mathbf{A}_r^0 + \sum_{i=1}^{L} f^i(\boldsymbol{\mu})\mathbf{A}_r^i. \tag{4.25}$$

If an affine representation does not exist, it can also be approximated as a Taylor expansion.

Another technique for global basis construction is the so-called bilinearization approach. The technique is very efficient; however, it is only applicable to systems of the form in eq. (4.9) where only matrix $\mathbf{A}$ is parameter-dependent and the parameter changes are of low rank. A great advantage of the technique is that parameter sampling is not needed, since the parameter dependency is removed and expressed as extra inputs. However, the problems studied in this thesis do not fulfil the required assumptions and the method is therefore not applied. More details can be found in [57, 79].

4.2.1.2 Interpolation of local information

Another approach to pMOR consists in interpolating information from the calculated local reduction bases at a new parameter point. An advantage of these techniques is that the resulting reduced system is smaller than when using a global reduction basis, and equal to the number of vectors contained in one local basis. A drawback is that interpolation techniques become cumbersome when multiple parameters are considered, and cases with more than 10 parameters have not been investigated [57]. A review on interpolatory MOR for frequency response calculation (i.e. interpolation on the frequency domain) in vibro-acoustic problems can be found in Ref. [80].

Three types of interpolation are possible: interpolation of reduction bases, interpolation of reduced systems, and interpolation of transfer functions. In the first approach, the local reduction bases are interpolated at the new parameter point; however, one should be careful when applying this technique, since direct interpolation can lead to bases that do not preserve desired properties. Thus, the quantity that should be interpolated is rather the underlying subspace [81]. One approach is to interpolate the subspaces corresponding to $\mathbf{T}_m$ for $m = 1, \ldots, M$ on a tangent space to a manifold of these subspaces that is chosen to preserve desired properties. Further details on the method can be found in Refs. [57, 81].

Like in the case of global reduction basis, the basis interpolation technique requires the projection of the system into the reduced basis for each parameter point, unless an affine parameter representation is available. On the other hand, the two other interpolation methods inherently avoid this issue. For reduced system interpolation, the projection is only done at the parameter points where the local bases are calculated. Thereafter, the reduced systems are interpolated directly for any other parameter point. Again, straight-forward interpolation is not recommended, and a similar approach to that used in interpolation of reduction bases can be used. One should also notice that a congruence transform of the local bases must be done prior to reduction, in order to ensure that all reduced systems are expressed in the same coordinates. Lastly, interpolation of local transfer functions is another method that can be used, which provides an input/output representation of the system but not a state-space form; however, it has been reported to introduce spurious poles in the reduced transfer function [57].

4.2.2 Parameter sampling

All described pMOR techniques are based on the assumption that a set of local reduction bases that contain enough information to represent the whole parameter space is available. The selection of points where local bases are calculated can therefore be seen as a sampling process. The number and choice of the sampled points should be such that the reduction of models corresponding to any other point in the design domain is accurate. However, the calculation of local bases is in general computationally costly, and oversampling of the parameter space should also be avoided. For low-dimensional spaces, it is possible to perform a grid or random sampling without compromising the efficiency excessively; however, as the number of parameters increases, such approaches become too time consuming.

Problem-adaptive efficient parameter sampling methods for high dimensional parametric models have been developed in the literature, the most extended technique being greedy algorithms. Recently, other adaptive techniques in the context of optimization problems that construct the reduction basis on-the-fly during the optimization loop have also been proposed. These two approaches are described in the following.

4.2.2.1 Greedy sampling

The idea behind greedy algorithms consists in adaptively sampling the design space for a specific problem in order to obtain the most efficient reduction basis. The basic algorithm can be described in two steps:

1. Given a reduction basis, find the point in the parameter space where the reduction error is highest;
2. Calculate the local reduction basis at the found point;

which are repeated until the highest reduction error in the parameter space is below a specified threshold, τ. For step 1, the reduction error can be calculated by comparing the reconstructed state vector to the full FE model state vector. However, this approach is not applicable in practice, since it would involve solving the full model at a large number of points in the design space, defeating the purpose of applying model reduction. An alternative is using cheap error estimators or residual-based error indicators, which will be discussed in Section 4.3, that allow for approximating the error in a fast way. The search of the point with highest error can then be done by a simple grid approach if the

number of parameters is low, or by solving a series of model-constraint optimization problems [82]. The optimization problems may be non-convex, and therefore global convergence is not ensured; however, even if local minima are found, the technique turns out more efficient than pure random sampling. Optimization approaches are however only useful in practice if a very cheap error estimator is available, since many queries to the error function are needed to reach convergence for every optimization problem. In Report E , a grid search greedy algorithm that uses a residual-based error indicator is applied to sample a 4-parameter space for a hearing aid model .

4.2.2.2 Adaptive sampling in optimization problems

Optimization problems differ from other applications of pMOR techniques such as system control and uncertainty quantification in that only a small part of the design domain is explored on the online phase, i.e. the path followed by the optimization algorithm. Therefore, unless the dimensionality of the problem is very small, calculating a set of local bases that represents the whole parameter space is not the most efficient approach to apply, since most of the included information will not be exploited. It is therefore desired to construct reduction bases that only contain information relevant to the optimization path. A way of achieving this goal is to start with one single local reduction basis that is accurate at the initial optimization point, and add new local bases to the current available set when necessary during the optimization.

In that direction, adaptive sampling techniques based on optimization trust-region methods have been developed recently [83–85]. They consist in solving a series of optimization problems within a trust-region determined by an available reduction error bound. The trust-region is enlarged for each consecutive optimization problem, since a local reduction basis is added for the end point of the previous optimization problem. This technique ensures that each added local basis is fully exploited; however, the required error bounds are only available for specific types of problems. Another, more straight-forward, approach that can also work with residual-based error indicators consists in calculating new local bases during the optimization loop when the reduction error indicator at a new point in the optimization path becomes too large. This idea has been applied for static structural topology optimization problems in Ref. [86], and it is used in Paper D in this thesis, where an implementation algorithm is given.

4.3 Accuracy assessment and error estimators

Model reduction techniques down-size large discrete systems in an efficient way by capturing the most relevant information and discarding less important details. En error is therefore inherently introduced in the process. Several choices must be made when applying any of the reduction techniques discussed in this chapter, i.e. the frequency limit of the included modes in modal methods, number of expansion points and order in Krylov subspace, parameter samples in pMOR techniques, etc. A reduction basis will be accurate enough when the reduction error that it introduces is below a certain required level, which will determine the choices and therefore the final size of the basis.

4.3.1 Error measures

Error measures are defined according to the quantity of interest in each application, typically being [87] modal frequencies, modal vectors, system response, effective masses or reaction forces (most useful for CMS methods, see for example [88]). The relative error for a vector of modal frequencies or for the system response vector can be calculated in terms of the 2-norm as

$$\epsilon = \frac{||\mathbf{v} - \tilde{\mathbf{v}}||_2}{||\mathbf{v}||_2} \tag{4.26}$$

for a generic vector of quantities of interest $\mathbf{v}$, with $\tilde{\mathbf{v}}$ being the approximation obtained from the reduced system. Different accuracy criteria can be required for the relative error depending on the application; typically, a 1% error requirement is used. For modal vector accuracy, the Modal Assurance Criterion (MAC)

$$MAC(x, y) = \frac{|\boldsymbol{\psi}_x^T \hat{\boldsymbol{\psi}}_y|^2}{(\boldsymbol{\psi}_x^T \boldsymbol{\psi}_x)(\hat{\boldsymbol{\psi}}_y^T \hat{\boldsymbol{\psi}}_y)}, \tag{4.27}$$

where $\boldsymbol{\psi}_x$ are the full system modal vectors and $\hat{\boldsymbol{\psi}}_y$ are the approximated modal vectors, is typically used. The MAC takes values between 0 and 1, 1 indicating linear dependency and 0 indicating orthogonality. Normally, modal vectors are considered accurate enough if a MAC value above 0.9 is obtained.

The calculation of the aforementioned error measures can be useful to check the accuracy when developing new model reduction methods; however, they cannot be used for the purpose of automatising the choices for constructing reduction bases (i.e. determining the necessary size of the basis for a specific problem)

since they require the full system solution, which we are trying to avoid with model reduction. Automatising the parameter sampling process for pMOR techniques is especially relevant, as described in Section 4.2.2, and therefore error estimators and indicators have been developed to make reduction error evaluation possible. Most application cases focus on approximating the error on the response vector, and some of the available techniques are described in the following subsection.

4.3.2 Error approximation

A priori error estimators have not been developed in the literature for the considered reduction methods to the author's knowledge; therefore, it is not possible to know the size of the reduction basis needed to achieve a given accuracy. However, iterative techniques where the error is checked *a posteriori* and the reduction basis is further enriched if needed can be applied to achieve a certain desired accuracy. Some *a posteriori* error estimators are available for systems arising from the discretization of certain types of parametrized Partial Differential Equations (PDEs) [89, 90] when the so-called Reduced Basis method is applied [75, 76]. Error estimators of this type can be computed very efficiently; however, the fact that they are limited to PDEs with certain underlying structures (i.e. parabolic PDEs [57] or affinely parametrized elliptic PDEs [90]) does not make them not applicable in the cases studied in this thesis. Error bounds are directly available for balanced truncation reduction methods [57]; however, as mentioned in section 4.1.3, balanced truncation is not suitable for reduction of large systems and it is therefore not usually applied in the field of structural dynamics.

A posteriori residual-based error indicators, on the other hand, are applicable to any type of problem and reduction method. They are based on the computation of the force residual when the reconstructed response vector is inserted into the high-dimensional system,

$$\Delta\mathbf{f} = \left(\mathbf{K} - \omega^2\mathbf{M}\right)\tilde{\mathbf{x}} - \mathbf{f}, \tag{4.28}$$

which is a relatively inexpensive step since it only requires forward matrix-vector operations. The force residual has been directly used as an error indicator in some works [84, 91]; even though it is a good indicator of how good a solution of the system the reconstructed vector is, one would aim at approximating the error measure on the quantity of interest, as expressed in eq. (4.26), when the goal is maximizing the efficiency of adaptive parameter sampling. Some techniques have been developed for Krylov subspace reduction methods [92, 93]

which make use of inherent properties of the reduction technique. A more general technique is investigated in Paper D and Report E in this thesis, which consists in finding a relationship between the force residual and the state vector error from data collected at points where the true error is available (i.e. points where a local reduction basis is calculated), based on the approach suggested in Ref. [94] for POD reduction techniques.

4.4 Contribution

Papers B, C and D, and Report E contain the work developed by the author in the field of parametric model order reduction for vibro-acoustic problems. The documents are summarized in the following.

In Paper B, several approaches to building a modal-based reduction basis for coupled fluid-structure interaction systems with unsymmetric matrices is investigated, both for single model reduction and for pMOR. The use of left and right eigenvectors versus orthogonalized right eigenvectors in the construction of the reduction basis is evaluated in terms of accuracy and efficiency, with application to a model of a plate coupled to an air column where the thickness of each element in the plate is an optimization variable (i.e. for a high-dimensional parametric space).

In Paper C, two reduction frameworks for optimization of a hearing aid model with 2 parameters are discussed. One approach consists in applying the CMS method to reduce the parts of the model that remain unchanged during the optimization, and couple the reduced substructures with the full model of the part where the optimization takes place. The other approach consists in applying a pMOR technique based on concatenation of local reduction bases to reduce the complete model, without substructuring. The results show that the pMOR technique achieves higher reduction rates and therefore yields faster calculation times of the reduced system response, which makes it a more suitable option for the considered problem. However, the time spent in building the reduction bases for each approach is not taken into account in the comparison. Even though one could expect that the CMS technique is mainly burdened by the number of DOFs in the unreduced part, it turns out that the number of interface DOFs is the main efficiency limitation factor. Applying interface-reduction techniques, this approach could be promising for cases where pMOR techniques are not applicable, for example, when changes in the parameters affect the mesh and concatenation/interpolation of local bases is not possible.

Paper D presents a pMOR sampling technique that adapts to the optimization path, with application to the hearing aid model presented in Paper C, considering 4 parameters. The main improvements with respect to Paper C are the enrichment of the modal reduction bases with response vectors to improve accuracy, the development of a residual-based error indicator suitable for the studied problem, and the introduction of an adaptive sampling algorithm for optimization problems.

In Report E , different extensions of the methods and applications presented in Papers B to D are developed. Firstly, the plate problem studied in Paper B is optimized using the adaptive pMOR (apMOR) technique developed in Paper D, showing that it is also suitable for problems with high-dimensional parameter spaces. Secondly, the hearing aid problem studied in Papers B and C is extended to include an acoustic domain surrounding the hearing aid to allow for optimization of the outside pressure. The model is optimized using the apMOR technique developed in Paper D; however, it turns out that modal-based reduction is not well-suited for the technique used to implement the Sommerfield boundary condition, and a Krylov subspace method is used to calculate the local reduction bases instead. Lastly, a greedy sampling approach is demonstrated for the calculation of a global basis valid for the 4-parameter space considered in the hearing aid model in Paper D. The pMOR and local basis construction techniques are the same as in Paper D, but an improved version of the residual-based error indicator is provided.

Chapter 5

Topology optimization

Topology optimization is a FE based design technique that was first introduced by Bendsøe and Kikuchi in 1988 [95] for mechanical problems. Since then, the method has developed in different directions and fields, including fluids, acoustics, electromagnetics, optics, etc. Topology optimization tries to answer the question of how to distribute material within a given design domain in order to optimize system performance. Compared to other structural optimization techniques, the algorithm is given almost complete freedom to come up with new structural designs, since no specific shape or placement of holes is prescribed. In this chapter, an overview of the methods available in the literature is given, and implementation details for density methods are reviewed. At the end, the contribution to the topic of Paper F included in this thesis is outlined.

5.1 Overview of methods

Topology optimization methods can be classified according to several criteria; different methods have been developed independently, giving rise to different terms arising for similar concepts in the literature sometimes. In the review paper by Sigmund and Maute [96], some of these concepts are clarified and related. A general classification can be made between gradient and non-gradient based

methods; the second approach being evaluated in Ref. [97] with the conclusion that such methods are not suited for the vast majority of topology optimization problems. Another classification can be done according to the definition of the optimization variables: in density methods, each element in the given design domain has an associated design variable, denominated density, which can vary between 0 and 1 and determines whether the element material is solid (1), void (0) or something in between; in level set methods, the interface between the solid and void domains is defined by a level set function, and it is the shape of that function that is optimized.

Furthermore, within density methods, one can distinguish between the most traditional approach where values of the design variable between 0 and 1 are allowed (continuous variable) and the optimization is solved by mathematical programming algorithms, and evolutionary approaches, where the density variable can only take the extreme values (discrete variable) and elements are added or removed according to their associated sensitivity value. The first approach has been referred to in the literature as SIMP (Simplified Isotropic Material with Penalization), even though this is actually the term for the material interpolation scheme that it uses [98], which can also be employed in evolutionary methods [96]. The distinctive characteristic between the two techniques is therefore in the design variables updating routine: mathematical programming for the first, with the Optimality Criterion (OC) and the Method of Moving Asymptotes (MMA) [35] being the most used methods, and evolutionary techniques for the second. Evolutionary topology optimization started with the so-called ESO (Evolutionary Structural Optimization) technique [99, 100], where elements could only be removed, and it was later extended to the Bi-directional approach, BESO [101]. The aforementioned classification is illustrated in Diagram 1.1. A full review of the different methods for structural vibration problems can be found in Ref. [102].

5.2 Implementation of density methods

In this thesis, we consider density methods and their application to structure-acoustic interaction problems. In this section, some challenges and techniques used in the implementation of density methods to ensure convergence to good designs are discussed; for the specifics about the application to fluid-structure coupled problems the reader is referred to Paper F.

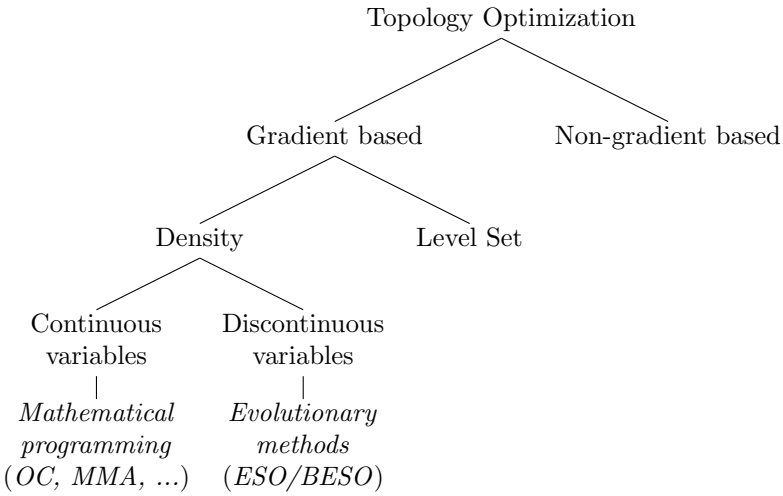

Diagram 5.1: Topology optimization methods classification

5.2.1 Interpolation schemes

Density based methods consist in defining an optimization variable (density) for each element in the design domain, which can vary between 0 and 1 allowing the element to transition between solid and void. A first question that arises in this context is how the density variable and the material properties of the element are related. In static structural problems, where the method was firstly applied, the density variable defines the value of the Young's modulus of the element material,

$$E_e = g(x_e)E_0, \tag{5.1}$$

where E_e and x_e are the Young's modulus and the density variable of element e, g is the interpolation function, and E_0 is the Young's modulus of the chosen structural material. Topology optimized designs are often plotted in black and white, where void elements are shown in white, solid elements are shown in black, and intermediate elements are shown in grey scale. Binary "black-and-white" designs are sought, and therefore it is desirable to get rid of "grey" areas. The SIMP scheme uses an interpolation function based on the power law,

$$g(x_e) = x_e^p, \tag{5.2}$$

where p is a penalization parameter, which favours binary designs (for $p > 1$). Too low values of the parameter p will yield grey designs, while too high values will cause too fast convergence to local minima; a "magic" value recommended

in Ref. [96] is $p = 3$.

The SIMP scheme has been shown to originate spurious vibration modes when applied to dynamic problems [103], due to the ratio between the mass and stiffness matrices becoming very large in the void phases. To alleviate this issue, the RAMP (Rational Approximation of Material Properties) scheme can be used instead. The RAMP interpolation function is defined as

$$g(x_e) = \frac{x_e}{1 + q(1 - x_e)}, \tag{5.3}$$

with q being the penalization parameter. In dynamics, the material density ρ is also interpolated by the density variable x (terms can get a bit confusing here); a linear function is normally used for the purpose, with

$$\rho_e = x_e \rho_0, \tag{5.4}$$

where ρ_e and x_e are the material density and the density variable of element e, and ρ_0 is the material density of the structural material. Applying penalization yields black and white designs in most cases; however, it may in some cases not be sufficient, and other techniques have been applied in the literature for the purpose, as for example in Ref. [104].

5.2.2 Filtering

It is convenient to introduce some restrictions in topology optimization problems in order to avoid designs with small features that are represented by only 1 or 2 elements, since it is well known that the FE model becomes inaccurate in such cases. Moreover, unrestricted topology optimization tends to yield designs with checkerboard patterns [105], where black and white elements alternate next to each other. Length-scale filtering and gradient or perimeter control are tools that help avoiding these issues and obtaining mesh-independent designs.

Filtering techniques are the most extended approach, with the sensitivity filter developed by Sigmund [106] being the most widely used. Sensitivity filtering consists in modifying an element sensitivity with the average of the sensitivities of the neighbouring elements within a radius r_{min}, which determines the desired length-scale of the final design. The new sensitivity of an element e for an objective function c is defined as follows,

$$\frac{\hat{\partial c}}{\partial x_e} = \frac{1}{\max(\gamma, x_e) \sum_{i \in N_e} H_{ei}} \sum_{i \in N_e} H_{ei} x_i \frac{\partial c}{\partial x_i} \tag{5.5}$$

where γ is a small value (i.e. $\approx 10^{-3}$) to avoid division by 0, N_e is the set of elements i for which the center-to-center distance to element e ($\Delta(e,i)$) is smaller than the filter radius r_{min}, and H_{ei} is a weighting function defined as

$$\max(0, r_{min} - \Delta(e,i)). \tag{5.6}$$

Modifying the sensitivities implies that a different objective function is actually being optimized; however, the sensitivity filter has been implemented in many academic and commercial codes, and the many applications where it has been shown to work has proven the value of the concept.

As an alternative, it is possible to filter the density variable, as

$$\hat{x_e} = \frac{1}{\sum_{i \in N_e} H_{ei}} \sum_{i \in N_e} H_{ei} x_i, \tag{5.7}$$

and correct the sensitivities accordingly by means of the chain rule. Both filtering approaches have the problem of introducing grey areas at the solid-void interface, an effect that can be mitigated by applying more sophisticated strategies that include projection of the grey scales [96].

5.2.3 Density updating

As discussed in Section 5.1, the main difference between the classical density approach and the evolutionary is the optimization variables updating strategy, forced by the fact that evolutionary methods use discrete variables instead of continuous. When continuous variables are used, the problems can be solved by efficient, well-proven mathematical programming techniques such as those introduced in Chapter 2, which also allow for the addition of global constraints in a straight-forward way [96]. The ESO/BESO approach, on the other hand, has been criticized for failing in certain situations due to the heuristic nature of the discrete variable updating scheme [107]. However,it is a popular choice due to its ease of use [108], and it has also been applied successfully to a wide variety of problems in its improved version [109] (described in Paper F), which addresses a lot of the reported critical arguments. Some challenges remain, mostly related to convergence and definition of the optimization stopping criterion [96], which in its best version simply evaluates the change in the mean value of the objective function in the last few iterations.

5.3 Contribution

In Paper F, the application of topology optimization methods to vibro-acoustic problems with strong structure-acoustic interaction is discussed. A main challenge arises when formulating the interpolation due to the elements changing between solid and air (instead of void), which are not only two different materials, but two different physics governed by different equations. Accounting for the changes in the fluid-structure interface becomes especially relevant in strongly coupled problems, where the influence of one medium onto the other is relevant in both directions. The performance of two density based methods that have been presented in the literature is evaluated for different degrees of coupling strength in a hearing aid suspension design problem.

Chapter 6

Summary and conclusions

Different challenges encountered in vibro-acoustic modelling and optimization of hearing aids have been investigated in this thesis. The study has been divided into three topics: contact modelling, model reduction and topology optimization, and the research has been presented in five scientific papers and a report. The main results and conclusions are summarized in this chapter, and directions for future work are discussed.

Modelling of contacts between small plastic parts for harmonic analysis has been investigated, and a contact identification technique based on model updating has been developed in Paper A. The technique adjusts the contact parameters for the model to match experimental data, being a few measured resonance frequencies and deflection shapes. A main challenge in contact modelling in hearing aids is that the location of the contact points between parts is often unknown due to surface irregularities introduced in the manufacturing process; the main contribution of the paper compared to other existing techniques is the modelling of the contact as distributed linear springs, which allows for extracting information about the location of the contact from the results. It has been shown that the number of model parameters should be chosen as a trade-off between the accuracy of the results being at a desired level and the dimensionality of the problem not giving rise to trivial solutions of the model updating optimization problem; therefore, the spring stiffness values are not

considered as independent optimization variables, but they are parametrized according to their location in an efficient way by a Fourier decomposition approach, with the Fourier coefficients becoming the optimization variables. The developed technique has been applied successfully for contact identification of a simple test structure inspired on hearing aid shells, for which the variability on the vibration response due to changes in the contact resulting from disassembly and assembly of the parts has also been evaluated.

Model reduction has been investigated in Papers B-D and Report E. Two approaches to modal-based model reduction for coupled structure-acoustic problems have been compared in Papers B and C; the first method uses left and right modal vectors to form the reduction basis (Left-Right method) and the second one uses a set of right eigenvectors where the acoustic and structural fields are separated and orthogonalized (Split Field method). As a conclusion, the Field Split method yields a better accuracy in some cases, and the Left-Right method yields smaller reduced systems which are faster to solve. The difference in solving time is however not critical, and it is therefore more recommendable to use the Field Split method when possible. In Paper C, a parametric Model Order Reduction (pMOR) technique and a Component Mode Synthesis (CMS) based approach are compared for vibro-acoustic optimization of a simplified hearing aid model, where the pMOR technique is shown to perform more efficiently. The same technique is made adaptive in Paper D by developing a reduction error estimator that allows for monitoring the accuracy of the reduced system during the optimization and updating the reduction basis on-the-fly. Applying the apMOR technique for the optimization of the response of a simplified hearing aid model with fine frequency resolution, the time required for the optimization is 20 times shorter than when using the full model. In Report E, the apMOR technique is demonstrated to also be efficient for a plate optimization with a large number of parameters and for global reduction basis construction by a greedy algorithm; moreover, a modification where the reduction basis is formed by Krylov subspace vectors is shown to perform better than modal-based reduction when the model includes exterior acoustics.

Topology optimization of vibro-acoustic problems has been investigated in Paper F, with focus on hearing aid suspension design. The study has shown that the structure-acoustic coupling between the suspension and the surrounding air becomes strong due to the used geometry and material properties, which makes it essential to consider the changes in the fluid-structure interface during the optimization. Two topology optimization methods have been compared; the first one uses a mixed displacement/pressure formulation that allows elements to vary between solid and air gradually while being governed by the same equa-

tions (Mixed-MMA), and the second is based on an evolutionary optimization technique where intermediate elements are not allowed and the classical segregated displacement/pressure formulation is used (Segregated-BESO). Both methods achieve optimized designs when the coupling is weak or when the required volume changes are small; however, the Segregated-BESO method is challenged for strongly coupled problems when a significant volume reduction is demanded, due to the fact that the sensitivity calculation is done by assuming that removed solid elements become void instead of air, which hinders convergence to good designs. The Mixed-MMA method, on the other hand, shows smooth convergence in all cases; still, the obtained final designs contain some intermediate elements, and projection to binary values can worsen the achieved performance significantly in some cases. Even though the Mixed-MMA method performs better, the Segregated-BESO technique is an attractive choice for industrial applications due to its ease of implementation and direct interpretation of the results; therefore, it could be a promising choice after further research and improvement.

6.1 Directions for future work

Regarding contact modelling, several aspects of the method proposed in Paper A could be further investigated. One of the weak points of the technique is that the inverse problem becomes ill-posed for an increasing number of contact model parameters, and even though the dimensionality is kept as low as possible by describing the geometrical contact stiffness distribution as a truncated Fourier series, the number of parameters needed to obtain an accurate result still yields a problem with several solutions. In this context, the solution with the highest total stiffness is chosen, motivated by the assumption that a strong contact exists since the measured vibration patterns show that the assembled structures vibrate together. The hypothesis that the chosen solution yields realistic results could be validated by comparing the obtained contact stiffness values with the real contact locations, which could perhaps be retrieved by Computed Tomography scanning. Furthermore, the applicability of regularization techniques to solve the encountered ill-posed problem may be investigated.

In relation to the application of the method to realistic structures, the Fourier decomposition approach proposed in the paper should be generalized in order for it to be applicable to more complicated geometries. Moreover, sources of mismatch between model and measurement data other than the contact model parameters (due to difficulties in accurately modelling complex geometries or

material properties) become more significant for real structures, and the way to prevent them from biasing the identified contact properties should be investigated. From a more general point of view, the mechanical design of contacts in hearing aids could be improved by better defining specific contact points between parts, which would both ease the modelling task and reduce variation in the vibration responses across serially produced devices.

With respect to model reduction for hearing aid optimization problems, it would be interesting to extend the apMOR technique suggested in Paper D to be made applicable to models with frequency-dependent material properties. This could be achieved by considering frequency as an extra parameter and computing several frequency-local reduction bases that would then be combined into a global one. Furthermore, the technique could be improved by making the selection of sampled frequencies automatic, which could be achieved by applying a greedy sampling technique as the one presented in Report E, with the frequency being the sampled parameter. The same approach could be applied for sampling the frequencies where enrichment vectors are calculated (or expansion points in the Krylov subspace case) in the frequency-independent case, which would make the method fully automatic.

A limitation of pMOR techniques is that re-meshing is not allowed during the optimization, since the reduction bases computed for different parameter values should be expressed in the same DOFs for them to be concatenated or interpolated. When major shape/size/position changes take place during the optimization, the FE mesh may have to be modified to represent the new design accurately; in such cases, the CMS approach investigated in Paper C could be applied, since the part of the model where the changes take place can be left unreduced. However, further investigation on the applicability of interface reduction techniques to hearing aid models is required, since Paper C showed that interface DOFs add a significant computational burden to the CMS reduced system.

Concerning topology optimization for coupled structure-acoustic problems, the two methods compared in Paper F could be enhanced. On the one hand, the application of extra measures to improve convergence to binary designs for the Mixed-MMA method should be investigated in order to obtain more realistic results. On the other hand, it would be interesting to study the possibility of considering the air domain in the sensitivity calculation for the Segregated-BESO method without changing the underlying segregated formulation, which has advantages such as a lower number of DOFs (compared to the mixed formulation) and a realistic representation of the fluid-structure interface. In addition,

investigation of high frequency optimization (above the first resonance) is necessary in order to account for the whole frequency range of interest in hearing aid suspension design problems. Eventually, the application of model reduction techniques for topology optimization problems should be investigated to make fine frequency resolution response optimization of realistic models with higher number of DOFs practically possible.

Bibliography

[1] L. Friis, Investigation of internal feedback in hearing aids, Ph.D. thesis.

[2] L. Friis, M. Ohlrich, Vibration modeling of structural fuzzy with continuous boundary, Journal of the Acoustical Society of America 123 (2) (2008) 718–728.

[3] L. Friis, M. Ohlrich, Simple vibration modeling of structural fuzzy with continuous boundary by including two-dimensional spatial memory, Journal of the Acoustical Society of America 124 (1) (2008) 192–202.

[4] R. Christensen, Acoustic modeling of hearing aid components, Ph.D. thesis (2010).

[5] R. Christensen, Topology optimization of thermoviscous acoustics in tubes and slits with hearing aid applications, Comsol Conference 2017.

[6] J. Jensen, Nonlinear distortion mechanisms and efficiency of balanced-armature loudspeakers, Ph.D. thesis (2014).

[7] B. R. Varanda, Characterization of the dominant structural vibration of hearing aid receivers: towards the moderation of mechanical feedback in hearing aids, Ph.D. thesis (2015).

[8] M. B. Sondergaard, C. B. W. Pedersen, Applied topology optimization of vibro-acoustic hearing instrument models, Journal of Sound and Vibration 333 (3) (2014) 683–692.

[9] S. Marburg, M. Shepherd, S. A. Hambric, Structural-acoustic optimization, Engineering Vibroacoustic Analysis: Methods and Applications (2014) 268–304.

[10] S. Marburg, Developments in structural-acoustic optimization for passive noise control, Archives of Computational Methods in Engineering 9 (4) (2002) 291–370.

[11] G. Everstine, Finite element formulations of structural acoustics problems, Computers and Structures 65 (3) (1997) 307–321.

[12] L. Kiefling, G. C. Feng, Fluid-structure finite element vibrational analysis, AIAA Journal 14 (2) (1976) 199–203.

[13] A. Bermudez, R. Rodriguez, Finite-element computation of the vibration modes of a fluid-solid system, Computer Methods in Applied Mechanics and Engineering 119 (3-4) (1994) 355–370.

[14] K. Bathe, Finite element procedures, Prentice-Hall, 1996.

[15] P. Davidsson, Structure-acoustic analysis; finite element modelling and reduction methods, Ph.D. thesis (2004).

[16] G. Everstine, A symmetric potential formulation for fluid-structure interaction, Journal of Sound and Vibration 79 (1) (1981) 157–160.

[17] H. Morand, R. Ohayon, Substructure variational analysis of the vibrations of coupled fluid-structure systems; finite element results, International Journal of Numerical Methods in Engineering 14 (5) (1979) 741–755.

[18] X. Wang, K. Bathe, Displacement/pressure based mixed finite element formulations for acoustic fluid–structure interaction problems, International Journal for Numerical Methods in Engineering 40 (11) (1997) 2001–2017.

[19] A. Craggs, The transient response of a coupled plate-acoustic system using plate and acoustic finite elements, Journal of Sound and Vibration 15 (4) (1971) 509–28, 509–528.

[20] O. Sigmund, P. M. Clausen, Topology optimization using a mixed formulation: An alternative way to solve pressure load problems, Computer Methods in Applied Mechanics and Engineering 196 (13-16) (2007) 1874–1889.

[21] O. A. Bauchau, J. I. Craig, Basic equations of linear elasticity, Springer Netherlands, Dordrecht, 2009, pp. 3–51.

[22] M. Friswell, J. Mottershead, Finite element model updating in structural dynamics, Vol. 38, Kluwer Academic Publishers, Dordrecht Boston London, 1995.

[23] C. Pal, I. Hagiwara, Dynamic analysis of a coupled structural-acoustic problem - simultaneous multimodal reduction of vehicle interior noise

level by combined optimization, Finite Elements in Analysis and Design 14 (2-3) (1993) 225–234.

[24] E. G. Williams, Regularization methods for near-field acoustical holography, Journal of the Acoustical Society of America 110 (4) (2001) 1976–1988.

[25] C. Soize, J. Michelucci, Structural shape parametric optimization for an internal structural-acoustic problem, Aerospace Science and Technology 4 (4) (2000) 263–275.

[26] S. Marburg, H. Hardtke, Shape optimization of a vehicle hat-shelf - improving acoustic properties for different load cases by maximizing first eigenfrequency, Computers and Structures 79 (20-21) (2001) 1943–1957.

[27] P. Hajela, Nongradient methods in multidisciplinary design optimization - status and potential, Journal of Aircraft 36 (1) (1999) 255–265.

[28] M. Montemurro, Y. Koutsawa, S. Belouettar, A. Vincenti, P. Vannucci, Design of damping properties of hybrid laminates through a global optimisation strategy, Composite Structures 94 (11) (2012) 3309–3320.

[29] W. M. Vicente, R. Picelli, R. Pavanello, Y. M. Xie, Topology optimization of frequency responses of fluid-structure interaction systems, Finite Elements in Analysis and Design 98 (2015) 1–13.

[30] A. Keane, Passive vibration control via unusual geometries - the application of genetic algorithm optimization to structural design, Journal of Sound and Vibration 185 (3) (1995) 441–453.

[31] A. Ratle, A. Berry, Use of genetic algorithms for the vibroacoustic optimization of a plate carrying point-masses, Journal of the Acoustical Society of America 104 (6) (1998) 3385–3397.

[32] M. H. Shojaeifard, R. Talebitooti, A. Yadollahi, Optimization of sound transmission through laminated composite cylindrical shells by using a genetic algorithm, Mechanics of Composite Materials 47 (4) (2011) 481–494.

[33] MATLAB optimization toolbox user's guide R2015b, MathWorks, Natick, MA, 2015.

[34] R. H. Byrd, M. E. Hribar, J. Nocedal, An interior point algorithm for large-scale nonlinear programming, SIAM Journal on Optimization 9 (4) (1999) 877–900.

[35] K. Svanberg, The method of moving asymptotes - a new method for structural optimization, International Journal for Numerical Methods in Engineering 24 (2) (1987) 359–373.

[36] X. Huang, Y. M. Xie, Convergent and mesh-independent solutions for the bi-directional evolutionary structural optimization method, Finite Elements in Analysis and Design 43 (14) (2007) 1039–1049.

[37] M. P. Bendsøe, O. Sigmund, Topology Optimization - Theory, Methods, and Applications, Springer Verlag, 2003.

[38] A. Hrennikoff, Solution of problems of elasticity by the framework method, Journal of Applied Mechanics 8 (1941) A169–A175.

[39] R. H. Courant, R., What is mathematics?, Oxford University Press, 1941.

[40] T. Marwala, Finite-element-model Updating Using Computional Intelligence Techniques, Springer London, 2010.

[41] S. Bograd, P. Reuss, A. Schmidt, L. Gaul, M. Mayer, Modeling the dynamics of mechanical joints, Mechanical Systems and Signal Processing 25 (8) (2011) 2801–2826.

[42] Z. Ling-mi, G. Qin-tao, Identification of the mechanical joint parameters with model uncertainty, Chinese Journal of Aeronautics 18 (1) (2005) 47–52.

[43] W. L. Li, A new method for structural model updating and joint stiffness identification, Mechanical Systems and Signal Processing 16 (Part 1) (2002) 155–168.

[44] M. Hanss, S. Oexl, L. Gaul, Identification of a bolted-joint model with fuzzy parameters loaded normal to the contact interface, Mechanics Research Communications 29 (2-3) (2002) 177–187.

[45] J. Dos Santos, B. Mace, Modelling Uncertainty in Mechanical Joint Parameters using Component Modal and Fuzzy Approaches, Springer Netherlands, 2006, pp. 302–302.

[46] C. Ehrlich, A. Schmidt, L. Gaul, Reduced thin-layer elements for modeling the nonlinear transfer behavior of bolted joints of automotive engine structures, Archive of Applied Mechanics 86 (1-2) (2016) 59–64.

[47] H. Jalali, Linear contact interface parameter identification using dynamic characteristic equation, Mechanical Systems and Signal Processing 66-67 (2016) 111–119.

[48] F. Adel, S. Shokrollahi, M. Jamal-Omidi, H. Ahmadian, A model updating method for hybrid composite/aluminum bolted joints using modal

test data, Journal of Sound and Vibration 396 (Supplement C) (2017) 172 – 185.

[49] J. Mottershead, M. Friswell, Model updating in structural dynamics - a survey, Journal of Sound and Vibration 167 (2) (1993) 347–375.

[50] M. Imregun, W. Visser, A review of model updating techniques, The Shock and vibration digest 23 (1) (1991) 9–20.

[51] S. Sehgal, H. Kumar, Structural dynamic model updating techniques: A state of the art review, Archives of Computational Methods in Engineering 23 (3) (2016) 515–533.

[52] A. Brandt, Noise and Vibration Analysis, John Wiley & Sons Ltd, 2011.

[53] O. Dossing, Structural stroboscopy - measurement of operational deflection shapes, Sound and Vibration 22 (8) (1988) 18–26, 18–26.

[54] S. Jin, P. Pai, Locating structural defects using operational deflection shapes, Journal of Intelligent Material Systems and Structures 11 (8) (2000) 613–630.

[55] R. Brincker, C. E. Ventura, Introduction to Operational Modal Analysis, Wiley Blackwell, 2015.

[56] A. Nobari, D. Ewins, On the effectiveness of using only eigenvalues in structural model updating problems, Shock and Vibration 1 (4) (1994) 339–348.

[57] P. Benner, S. Gugercin, K. Willcox, A survey of projection-based model reduction methods for parametric dynamical systems, SIAM Review 57 (4) (2015) 483–531.

[58] M. S. Eldred, D. M. Dunlavy, Formulations for surrogate-based optimization with data fit, multifidelity, and reduced-order models, Collection of Technical Papers - 11th Aiaa/issmo Multidisciplinary Analysis and Optimization Conference 4 (2006) 2450–2469.

[59] P. Koutsovasilis, M. Beitelschmidt, Comparison of model reduction techniques for large mechanical systems, Multibody System Dynamics 20 (2) (2008) 111–128.

[60] B. Besselink, U. Tabak, A. Lutowska, N. van de Wouw, H. Nijmeijer, D. Rixen, M. Hochstenbach, W. Schilders, A comparison of model reduction techniques from structural dynamics, numerical mathematics and systems and control, Journal of Sound and Vibration 332 (19) (2013) 4403 – 4422.

[61] Z. Ma, I. Hagiwara, Sensitivity analysis methods for coupled acoustic-structural systems Part I. Modal sensitivities, AIAA Journal 29 (11) (1991) 1787–1795.

[62] W. D. Zhu, J. M. Liu, Y. F. Xu, H. Q. Ying, A modal test method based on vibro-acoustical reciprocity, Conference Proceedings of the Society for Experimental Mechanics Series 45 (7) (2014) 495–509.

[63] M. Maess, L. Gaul, Substructuring and model reduction of pipe components interacting with acoustic fluids, Mechanical Systems and Signal Processing 20 (1) (2006) 45–64.

[64] J. Herrmann, M. Maess, L. Gaul, Substructuring including interface reduction for the efficient vibro-acoustic simulation of fluid-filled piping systems, Mechanical Systems and Signal Processing 24 (1) (2010) 153–163.

[65] D. Rixen, Generalized mode acceleration methods and modal truncation augmentation, Collection of Technical Papers - AIAA/ASME/ASCE/AHS/ASC Structures, Structural Dynamics and Materials Conference 2 (2001) 884–894.

[66] R. R. Craig, M. C. C. Bampton, Coupling of substructures for dynamic analyses, AIAA Journal 6 (7) (1968) 1313–1319.

[67] R. R. Craig, Coupling of substructures for dynamic analyses: an overview, Collection of Technical Papers - AIAA/ASME/ASCE/AHS/ASC Structures, Structural Dynamics and Materials Conference 5 (2000) 3–14.

[68] S. Donders, B. Pluymers, P. Ragnarsson, R. Hadjit, W. Desmet, The wave-based substructuring approach for the efficient description of interface dynamics in substructuring, Journal of Sound and Vibration 329 (8) (2010) 1062–1080.

[69] P. Feldmann, R. Freund, Efficient linear circuit analysis by pade approximation via the lanczos process, European Design Automation Conference - Proceedings (1994) 170–175.

[70] A. Odabasioglu, M. Celik, L. T. Pileggi, Prima: Passive reduced-order interconnect macromodeling algorithm, IEEE/ACM International Conference on Computer-aided Design, Digest of Technical Papers (1997) 58–65.

[71] Z. Bai, Y. Su, Dimension reduction of large-scale second-order dynamical systems via a second-order Arnoldi method, SIAM Journal on Scientific Computing 26 (5) (2005) 1692–1709.

[72] S. Gugercin, A. C. Antoulas, C. Beattie, H-2 model reduction for large-scale linear dynamical systems, SIAM Journal on Matrix Analysis and Applications 30 (2) (2008) 609–638.

[73] X. Xie, H. Zheng, S. Jonckheere, A. van de Walle, B. Pluymers, W. Desmet, Adaptive model reduction technique for large-scale dynamical systems with frequency-dependent damping, Computer Methods in Applied Mechanics and Engineering 332 (2018) 363–381.

[74] J. Lumley, The structures of inhomogeneous turbulent flow, Atmospheric Turbulence and Radio Wave Propagation (1967) 166–178.

[75] G. Rozza, An introduction to reduced basis method for parametrized pdes, Series on Advances in Mathematics for Applied Sciences 82 (2010) 508–519.

[76] A. Quarteroni, G. Rozza, A. Manzoni, Certified reduced basis approximation for parametrized partial differential equations and applications, Journal of Mathematics in Industry 1 (1) (2011) 1–49.

[77] E. Balmès, Parametric families of reduced finite element models. Theory and applications, Mechanical Systems and Signal Processing 8 (8) (1994) 381–394.

[78] G. Golub, C. van Loan, Matrix computations, The Johns Hopkins University Press, 1996.

[79] U. Baur, C. Beattie, P. Benner, Mapping parameters across system boundaries: Parameterized model reduction with low rank variability in dynamics, Proceedings in Applied Mathematics and Mechanics 14 (1) (2014) 19–22, 19–22.

[80] U. Hetmaniuk, R. Tezaur, C. Farhat, Review and assessment of interpolatory model order reduction methods for frequency response structural dynamics and acoustics problems, International Journal for Numerical Methods in Engineering 90 (13) (2012) 1636–1662.

[81] D. Amsallem, C. Farhat, Interpolation method for adapting reduced-order models and application to aeroelasticity, AIAA Journal 46 (7) (2008) 1803–1813.

[82] T. Bui-Thanh, K. Willcox, O. Ghattas, Model reduction for large-scale systems with high-dimensional parametric input space, SIAM Journal on Scientific Computing 30 (6) (2008) 3270–3288.

[83] Y. Yue, K. Meerbergen, Accelerating optimization of parametric linear systems by model order reduction, SIAM Journal on Optimization 23 (2) (2013) 1344–1370.

[84] M. J. Zahr, C. Farhat, Progressive construction of a parametric reduced-order model for pde-constrained optimization, International Journal for Numerical Methods in Engineering 102 (5) (2015) 1111–1135.

[85] P. Benner, E. Sachs, S. Volkwein, Model Order Reduction for PDE Constrained Optimization, in Trends in PDE Constrained Optimization, Springer International Publishing, 2014, pp. 303–326.

[86] C. Gogu, Improving the efficiency of large scale topology optimization through on-the-fly reduced order model construction, International Journal for Numerical Methods in Engineering 101 (4) (2015) 281–304.

[87] G. J. Claessens, J. J. Wijker, The accuracy of reduced component models, European Space Agency, (Special Publication) (386) (1996) 533–547.

[88] L. Cortes, J. M. Mencik, S. Meo, Interpolatory model reduction for component mode synthesis analysis of structures involving substructures with frequency-dependent parameters, Proceedings of ISMA 2016 - International Conference on Noise and Vibration Engineering (2016) 3463–3477.

[89] K. Veroy, C. Prud'Homme, D. V. Rovas, A. T. Patera, A posteriori error bounds for reduced-basis approximation of parametrized noncoercive and nonlinear elliptic partial differential equations, 16th AIAA Computational Fluid Dynamics Conference.

[90] G. Rozza, D. B. P. Huynh, A. T. Patera, Reduced basis approximation and a posteriori error estimation for affinely parametrized elliptic coercive partial differential equations, Archives of Computational Methods in Engineering 15 (3) (2007) 1–47.

[91] U. Hetmaniuk, R. Tezaur, C. Farhat, An adaptive scheme for a class of interpolatory model reduction methods for frequency response problems, International Journal for Numerical Methods in Engineering 93 (10) (2013) 1109–1124.

[92] D. Amsallem, U. Hetmaniuk, A posteriori error estimators for linear reduced-order models using Krylov-based integrators, International Journal for Numerical Methods in Engineering 102 (5) (2015) 1238–1261.

[93] P. Heres, Robust and efficient Krylov subspace methods for model order reduction, Ph.D. thesis (2008).

[94] A. Paul-Dubois-Taine, D. Amsallem, An adaptive and efficient greedy procedure for the optimal training of parametric reduced-order models, International Journal for Numerical Methods in Engineering 102 (5) (2015) 1262–1292.

[95] M. P. Bendsøe, N. Kikuchi, Generating optimal topologies in structural design using a homogenization method, Computer Methods in Applied Mechanics and Engineering 71 (2) (1988) 197–224.

[96] O. Sigmund, K. Maute, Topology optimization approaches, Structural and Multidisciplinary Optimization 48 (6) (2013) 1031–1055.

[97] O. Sigmund, On the usefulness of non-gradient approaches in topology optimization, Structural and Multidisciplinary Optimization 43 (5) (2011) 589–596.

[98] P. Bendsø e, M., Optimal shape design as a material distribution problem, Structural Optimization 1 (4) (1989) 193–202.

[99] C. Mattheck, S. Burkhardt, A new method of structural shape optimization based on biological growth, International Journal of Fatigue 12 (3) (1990) 185–190.

[100] Y. Xie, G. Steven, A simple evolutionary procedure for structural optimization, Computers and Structures 49 (5) (1993) 885–896.

[101] V. Young, O. Querin, G. Steven, Y. Xie, 3D and multiple load case Bi-directional Evolutionary Structural Optimization (BESO), Structural Optimization 18 (2-3) (1999) 183–192.

[102] S. Zargham, T. A. Ward, R. Ramli, I. A. Badruddin, Topology optimization: a review for structural designs under vibration problems, Structural and Multidisciplinary Optimization 53 (6) (2016) 1157–1177.

[103] N. L. Pedersen, Maximization of eigenvalues using topology optimization, Structural and Multidisciplinary Optimization 20 (1) (2000) 2–11.

[104] J. S. Jensen, O. Sigmund, Topology optimization of photonic crystal structures: a high-bandwidth low-loss T-junction waveguide, Journal of the Optical Society of America B 22 (6) (2005) 1191–1198.

[105] O. Sigmund, J. Petersson, Numerical instabilities in topology optimization: A survey on procedures dealing with checkerboards, mesh-dependencies and local minima, Structural Optimization 16 (1) (1998) 68–75.

[106] O. Sigmund, On the design of compliant mechanisms using topology optimization, Mechanics of Structures and Machines 25 (4) (1997) 493–524.

[107] M. Zhou, G. I. Rozvany, On the validity of ESO type methods in topology optimization, Structural and Multidisciplinary Optimization 21 (1) (2001) 80–83.

[108] J. Rong, Y. Xie, X. Yang, Q. Liang, Topology optimization of structures under dynamic response constraints, Journal of Sound and Vibration 234 (2) (2000) 177–189.

[109] X. Huang, Y. Xie, A further review of ESO type methods for topology optimization, Structural and Multidisciplinary Optimization 41 (5) (2010) 671–683.

Included papers

Paper A

Contact parameter identification for vibrational response variability prediction

Applied Acoustics 129 (2018) 291–305

Contents lists available at ScienceDirect

Applied Acoustics

journal homepage: www.elsevier.com/locate/apacoust

Contact parameter identification for vibrational response variability prediction ☆

Ester Creixell-Mediante [a,b,*], Jonas Brunskog [a], Jakob S. Jensen [a], Martin Larsen [b]

[a] Acoustic Technology, Department of Electrical Engineering, Technical University of Denmark, Ørsteds Plads 352, 2800 Kgs. Lyngby, Denmark
[b] Oticon A/S, Kongebakken 9, 9765 Smørum, Denmark

ARTICLE INFO

Article history:
Received 22 March 2017
Received in revised form 28 July 2017
Accepted 14 August 2017

Keywords:
Contact modeling
Model updating
Vibrations
Structural acoustics
Linear modeling

ABSTRACT

Variability in the dynamic response of assembled structures can arise due to variations in the contact conditions between the parts that conform them. Contact conditions are difficult to model accurately due to randomness in physical properties such as contact surface, load distribution or geometric details. Those properties can vary for a given structure due to the assembly and disassembly process, and also across nominally equal items that are produced in series. This work focuses on modeling the contact between small light-weight plastic pieces such as those used in the hearing aid industry, where the vibrational behavior of the structures within the hearing frequency range is critical for the performance of the devices. A procedure to localize the most probable contact areas and determine the most sensitive contact points with respect to variations in the modes of vibration of the assembled plastic parts is presented. The procedure uses a gradient-based optimization strategy that updates the stiffness constants of a number of contact spring elements to match experimental data. By identifying the contact parameters for several sets of experimental data measured under varying contact conditions, the variability of the contact parameters can be characterized.

1. Introduction

Variability in the vibrational response of nominally identical devices is a well known problem that affects several industries with serial production. Studies on this variability have been published in the literature for generic products [1], and for specific industries, such as guitar manufacturing [2] and automotive vehicles [3]. This problem is also a matter of concern in the hearing aid industry, where controlling the vibrational response of the devices is critical, as unpredicted vibration transmission paths can become relevant causes of mechanical feedback between the loudspeaker and the microphones. As described in Ref. [4], smaller designs of hearing aids are desired from an aesthetic and practical point of view, while high amplification levels are required for performance. The strong acoustic-mechanical interaction results in complicated dynamic behavior and large sensitivity to structural details and variations [5], therefore predicting the variability of the vibrational response is a key point in obtaining a reliable model of acoustic-mechanical feedback paths, and to design products that will perform as desired.

The variability is observed in most complex systems that are composed of several parts, which suggests that the variation is partly generated when these parts are put together. In the hearing aid industry, each device is formed by multiple parts, such as those shown in Fig. 1, which gives rise to high variability in the vibrational response of nominally equal devices produced in series. Variability on the physical properties of the contact surface such as hardness, roughness and waviness, as well as the geometry and the material properties [6] have a strong influence on the coupling conditions, and hence on the transmission properties at the contact, and results in the observed variability in the vibrational responses of the structures. Those properties are also affected by the process of assembly and disassembly of the parts, due to small changes in the relative position and erosion effects. A simple experiment where the response of the two assembled plastic pieces shown in Fig. 4 is measured five times with the parts being dissassembled and assembled back between measurements (the conditions of the experiment are given in detail in Section 2), presents the vibrational responses shown in Fig. 2 (where the curves have been separated by 10 dB for a clearer visualization but would

☆ Part of this work was presented at NOVEM2015, Dubrovnik, Croatia.

* Corresponding author at: Acoustic Technology, Department of Electrical Engineering, Technical University of Denmark, Ørsteds Plads 352, 2800 Kgs. Lyngby, Denmark.

E-mail addresses: emed@oticon.com (E. Creixell-Mediante), jbr@elektro.dtu.dk (J. Brunskog), json@elektro.dtu.dk (J.S. Jensen), mnla@oticon.com (M. Larsen).

http://dx.doi.org/10.1016/j.apacoust.2017.08.011
0003-682X/

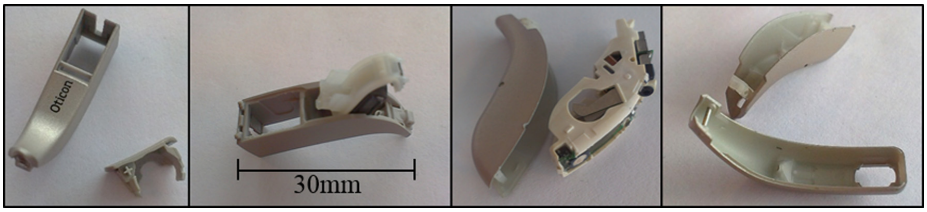

Fig. 1. Several hearing aid parts.

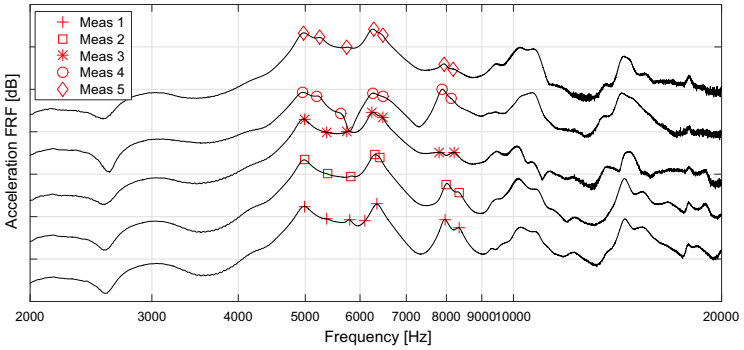

Fig. 2. Vibrational responses of the same assembly of plastic pieces with small contact changes due to disassembly and reassembly. The curves have been separated by a 10 dB offset for better visualization. The red marks indicate resonant frequencies, identified as described in Section 2. (For interpretation of the references to colour in this figure legend, the reader is referred to the web version of this article.)

otherwise be on top of each other at the lower frequency range). The variation across measurements of five of the identified modal frequencies is shown in Fig. 3(b). When comparing to the variation due to measurement uncertainty (i.e. re-measuring the structure without disassembling), shown in Fig. 3(a), it is clear that the variation due to the disassembling and reassembling process is significant.

Studies of the uncertainty problem in large scale built-up structures have suggested the use of statistical energy methods for response prediction, given the probabilistic nature of the problem [1]. Statistical energy methods [7] are shown to be adequate for modeling the response at frequencies where the mode overlap is sufficiently high, which are also the frequency ranges where the variability due to contact uncertainties is most significant for large structures [8]. The variability problem in the hearing aid industry arises within the most critical frequency range; the audible frequency span. Here, the small light-weight structures that compose the devices often present their fundamental modes of vibration, which makes statistical energy methods unapplicable. An alternative is running a number of computations of deterministic Finite Element (FE) models for randomized parameters (Monte-Carlo simulations), for which the probability distributions must be esti-

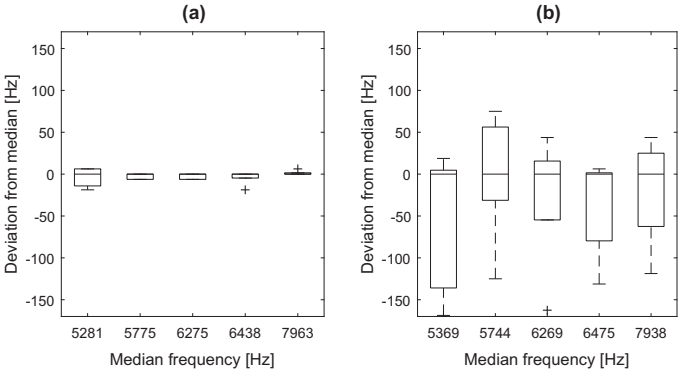

Fig. 3. Variations in resonant frequencies across five measurements of the assembly in Fig. 4 for (a) unchanged contact condition and (b) varying contact condition. On each box, the central mark is the median, the edges of the box are the 25th and 75th percentiles, the whiskers extend to the most extreme datapoints the algorithm considers to be not outliers, and the outliers are plotted individually.

mated in advanced. Monte-Carlo simulations are usually demanding in terms of computational costs that scale with the number of considered parameters; moreover, collecting data for probability modeling of all relevant uncertain parameters can be challenging when they are not directly measurable [1] and complex inverse stochastic identification methods may be required [9]. In order to make these studies practically possible for contact variability characterization in hearing aids, the present work focuses on developing a contact model that describes the contact conditions with a reduced set of parameters and a technique to identify them so that their probability distributions can be easily estimated.

Since the physical properties of the contact are not directly observable, an inverse problem approach is used to identify the contact parameters. Some of the studies on contact parameter identification that can be found in the literature try to estimate stiffness and damping parameters of the contact directly from experimental Frequency Response Functions (FRFs) of the structure [10–13]. However, this technique is based on the inversion of those FRFs, which requires precise and low noise experimental data; this can be challenging to obtain for small light-weight structures such as hearing aid parts, since the usual excitation methods like impact hammer or shaker would either affect the results or not be practically possible. Other methods are based on estimation of the contact conditions by updating a Finite Element model to match experimentally obtained modal parameters, which requires less precise measurements. Experimental mode shapes can be challenging to obtain though, due to inaccessibility to some surfaces of the structures. Modal frequencies, on the other hand, are easier to estimate accurately, and it is therefore desirable to develop a method based only on them.

Some methods for identification of joint parameters for flange, bolt or weld joints based on measured modal frequencies and modal damping ratios can be found in Refs. [6,14–17]. In those studies, the location of the contact is well-defined and they focus on estimating its stiffness and damping, which makes this problem significantly different from the present one, where the actual contact points between manufactured parts can differ significantly from the designed nominal contact areas. The purpose here is not to model the physical phenomena that act at the contact and are responsible for keeping the parts together, such as normal forces and sliding resistance, but to obtain a simple linear contact model that can be used for simulation of the harmonic vibration response of assemblies. Therefore, the obtained spring stiffness values do not have a direct physical meaning, but are an indicator of which areas contain more contact points than others. A similar goal on interface damping modeling was pursued in the approach suggested in Ref. [18].

The present study focuses on developing a method that identifies the stiffness parameters of the contact but also localizes the most probable contact areas while keeping the required experimental data collection process at a practical level. The contact parameters are identified by a gradient-based optimization technique that updates the model to match measured data, which are the modal frequencies of a set of modes of vibration of the assembly. The contact parameters are estimated for several experimental data sets corresponding to the assembly under different contact conditions, and based on this information, the parameters that vary the most can be identified and selected for Monte-Carlo simulation studies in the future.

2. Experimental study

The uncertainty of the contact conditions is one of the main challenges for vibro-acoustic modeling of hearing aids. However, there are other sources of uncertainty that can introduce deviations between model and measured results, the most relevant being approximations in the material models and simplification of complicated geometric details. In order to focus on the contact uncertainty problem, the test structure shown in Fig. 4 is studied in this paper. The parts are inspired by hearing aid shells, however, they present a simpler geometry, without curvatures and interior details, and are made of a plastic material without fibres, Grilamid TR55. This eases the finite element model of the independent parts fitting with experimental data, isolating the contact as main source of uncertainty. Hearing aid shells are usually held together by a pin, which has not been included here in order to reduce the number of components implied in the study (the pieces are instead held together by the forces acting at the contact).

Evaluating the changes on the measured modal frequencies of the presented assembly due to disassembling and reassembling its parts is the object of this study. Two different experiments are conducted in order to evaluate the significance of these changes with respect to variability caused by measurement uncertainty. The vibrational response of the assembly is measured five times in each experiment; in experiment 1, the assembly remains assembled but it is dismounted and mounted on the measurement setup between measurements, and in experiment 2, the parts are disjoined and joined back between each measurement. A similar design of experiments was used by R. Craik et al. for evaluating the effect of workmanship on sound transmission through building elements [19,20].

Obtaining accurate modal data from experiments can be challenging for small light-weight structures, since excitation by impact hammer or shaker would influence the measurement results. The used measurement set-up is a trade-off between practicality and accuracy of the obtained data. The structure is hung from a light wire as shown in Fig. 5(a), which emulates free boundary conditions, inside an acoustic box that contains loudspeakers on 5 walls and one glass door, shown in Fig. 5(b). A periodic chirp in which sinusoidal signals are emitted at all FFT lines between 1 kHz and 20 kHz with a resolution of 6.25 Hz is used as excitation signal, which is reproduced simultaneously by the 5 loudspeakers, exciting the structure by acoustic waves coming from several directions. For each measurement, the velocity frequency response is measured with a laser vibrometer sequentially at 312 points on the 4 main outer surfaces of the structure and averaged. For each measured surface, the structure is mounted so that the laser beam is projected perpendicularly on it, and for each measurement point, the response is the result of 15 complex averages. The electrical input voltage to the loudspeakers is used as a reference, which allows to obtain the structural deflection shapes, shown for one of the measurements in Fig. 8(a).

The five vibrational responses obtained for experiment 2 are shown in Fig. 2. The resonant frequencies marked in red have been identified from the peaks in both the averaged curves and single-point measurements, since some weak resonances can only be detected at a few measurement points. The spread of the resonance frequencies for each experiment is plotted in Fig. 3, which shows variations in resonance frequencies up to 40 Hz for experiment 1, and up to 150 Hz for experiment 2. Thus, resonance frequencies vary almost four times more in experiment 2 than in experiment 1, clearly indicating that the changes in the contact that are produced when the pieces are disassembled and assembled back affect the resulting resonance frequencies significantly.

3. Methodology

The method suggested here characterizes the contact conditions of the assembled structure from the observation of its modal frequencies. In Section 3.1, the modeling of the assembly by the

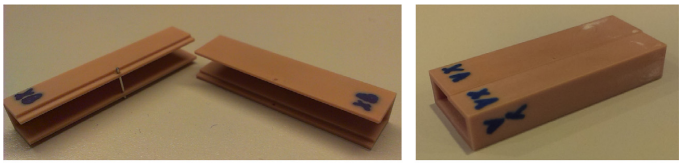

(a) (b)

Fig. 4. Manufactured test structure, with outer dimensions of the assembly of 5 mm × 12 mm × 30 mm and a thickness of 1 mm. (a) Separate parts. (b) Assembled parts.

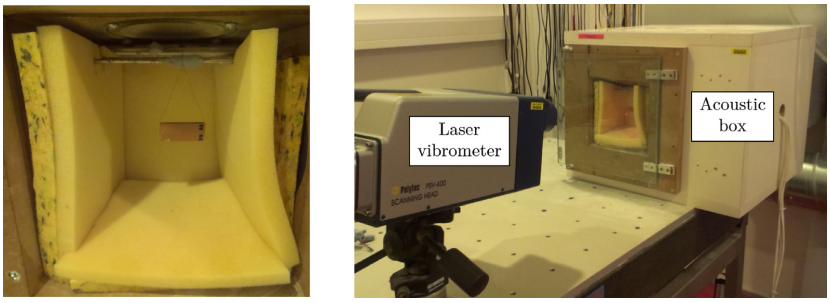

Fig. 5. (a) Mounting of the structure for measurement. (b) Measurement setup.

Finite Element Method (FEM) with the contact being described by springs is described. Section 3.2 describes the identification of the contact spring constants, which is done by a model updating technique based on a gradient-based optimization method that minimizes the difference between measured and model modal frequencies of the assembly.

3.1. Model of coupled structures

For assemblies of lightly damped structures such as the considered parts, the variability in the vibrational response is mainly observed as shifts in the natural frequencies. These are primarily dominated by the stiffness; therefore, only linear springs are considered for the contact model, and the damping at the contact and material damping of the parts are neglected in this study.

The Finite Element (FE) mesh for the assembly presented in Fig. 4 is shown in Fig. 6, with all elements being 20-node hexahedra (with midside nodes). The model of the disconnected parts has been done in the commercial software ANSYS®Workbench and ANSYS®Mechanical, Release 15.0, and the necessary mesh size has been determined by a convergence study of the modal frequencies within the frequency range of interest (i.e. up to 8 kHz) with respect to element size, which has resulted in 10260 nodes and 30780 degrees of freedom.

Since the material properties can vary in reality with respect to the information provided by the manufacturer, the material properties of Grilamid TR55 have been tuned by matching modelled and experimental modal frequencies and mode shapes for a beam structure made of this material, measured following the same procedure described in Section 2, yielding the material data listed in Table 1. The E-modulus for bending and torsional modes presented a difference of around 10%, however, the material model used in the FE model is isotropic, and therefore an average value has been selected. This assumption together with geometric tolerances and measurement uncertainties results in small deviations between measurement and simulation for the parts under study, as listed in Table 2. It is worth mentioning that these deviations are smaller but in the same order of magnitude as the deviations due to changes in the contact observed in the measurements (Fig. 3). However, since this is an error that is introduced constantly in all simulations, the variations on the obtained contact parameters for the different measurement results will still be meaningful.

The contact springs connect those nodes from the two parts that share the same coordinates at the contact surface, which are shown in Fig. 6(a). Fig. 6(b) shows in detail the mesh at the contact surfaces, and how the springs are virtually placed. There are 674 nodes at the contact surfaces, which, with three springs per node (one for each degree of freedom), yields 2022 contact springs.

3.1.1. Formulation of the contact problem

The FE formulation of the free vibration problem takes the form

$$\mathbf{M}\ddot{\mathbf{x}}(t) + \mathbf{K}\mathbf{x}(t) = \mathbf{0}, \tag{1}$$

where $\mathbf{M}$ and $\mathbf{K}$ are the mass and stiffness matrices, respectively, and $\mathbf{x}$ is a vector containing the nodal displacements. By assuming harmonic displacement, $\mathbf{x}(t) = \psi e^{i\omega t}$, we obtain the eigenvalue problem

$$(\mathbf{K} - \omega^2\mathbf{M})\psi = \mathbf{0}, \tag{2}$$

where ψ is the mode shape and ω is the natural frequency.

For two coupled structures a and b, the mass and stiffness matrices of the assembly are built from the mass and stiffness matrices of the independent structures and a contact spring stiffness matrix $\mathbf{S}$ as

$$\mathbf{M} = \begin{bmatrix} \mathbf{M}_a & \mathbf{0} \\ \mathbf{0} & \mathbf{M}_b \end{bmatrix}, \tag{3}$$

$$\mathbf{K} = \begin{bmatrix} \mathbf{K}_a & \mathbf{0} \\ \mathbf{0} & \mathbf{K}_b \end{bmatrix} + \mathbf{S} = \tilde{\mathbf{K}} + \mathbf{S}, \tag{4}$$

where $\mathbf{M}_a$ and $\mathbf{K}_a$ are the system matrices of part a, $\mathbf{M}_b$ and $\mathbf{K}_b$ are the system matrices of part b and matrix $\mathbf{S}$ contains the contact spring constants and is discussed in details in the following. An

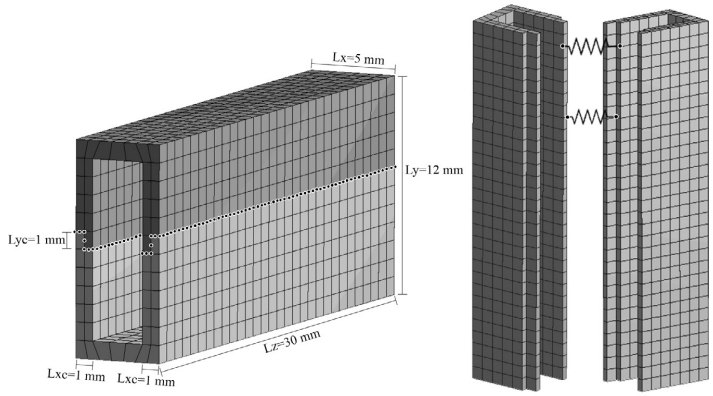

Fig. 6. FE mesh and contact nodes (black dots). (a) Nodes on the contact surface, and dimensions of the structure. (b) Illustration of springs placement for an example where two springs connect two node pairs.

Table 1
Material properties of Grilamid TR55.

Property	Value
E-modulus	$1.94 \cdot 10^9$ Pa
Poisson's ratio	0.38
Density	1040 kg/m^3

illustration of the model for a case with one contact spring can be seen in Fig. 7.

Matrix **S** implements two conditions between the connected degrees of freedom: equilibrium of forces and proportionality between force and displacement by Hooke's law. For one spring (s) connecting two nodes ($Q1$ and $Q2$), this is expressed as

$$s(\mathbf{x}_{Q1} - \mathbf{x}_{Q2}) = \mathbf{f}_{Q1} = \mathbf{f}_{Q2}, \tag{5}$$

where $\mathbf{x}_{Q1}$ and $\mathbf{x}_{Q2}$ are the displacements of the connected DOFs, and $\mathbf{f}_{Q1}$ and $\mathbf{f}_{Q2}$ are the sum of forces acting on these nodes. This can be extended to more than one contact spring and expressed in a matrix form as

$$\mathbf{S} = \sum_{n=1}^{N} s_n (\mathbf{1}_{Qan} - \mathbf{1}_{Qbn})^T (\mathbf{1}_{Qan} - \mathbf{1}_{Qbn}) \tag{6}$$

where N is the total number of contact springs, and $\mathbf{1}_{Qan}$ and $\mathbf{1}_{Qbn}$ are vectors with a value of 1 at Qan and Qbn, respectively, and zeros at the rest, where Qan and Qbn are the connected degrees of freedom of part a and part b. Therefore **S** is a matrix that contains s_n at the diagonal matrix entries (Qan, Qan) and (Qbn, Qbn),X and -s_n at the matrix entries (Qan, Qbn) and (Qbn, Qan).

Introducing this in Eq. (1), we obtain

$$\mathbf{M}\ddot{\mathbf{x}}(t) + \left(\tilde{\mathbf{K}} + \mathbf{S}\right)\mathbf{x}(t) = \mathbf{0}. \tag{7}$$

For the structure in Fig. 6, matrix **S** contains 2022 parameters s_n, for which the values are determined by the model updating technique described in Section 3.2.

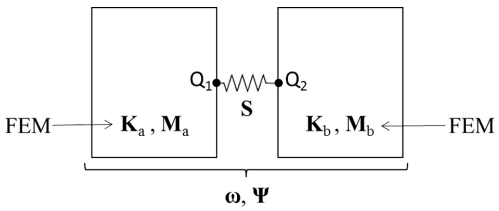

Fig. 7. Model of two coupled structures.

3.2. Model updating

Model updating techniques consist in minimizing an error function between experimental and modelled results. Any existing optimization technique can be used for the purpose, which allows for constraints and weighting factors that can be adjusted according to the user's criteria and confidence in the measured data [15]. The model updating technique used here to identify the contact parameters minimizes the difference between model eigenfrequencies and the modal frequencies of the structure obtained experimentally.

3.2.1. Optimization problem formulation

The minimization of the least squares distance between measurement and model modal frequencies is formulated here as a constraint in the optimization problem, where ϵ is chosen so that the differences at the final point are comparable to those observed between measurement and simulation of the disconnected parts. Since the number of optimization variables will in general be larger than the number of modal frequencies that are considered, the problem becomes underdetermined. In this case, the structures clearly vibrate together when measured, as observed from the mode shape plots; therefore, we can assume that a strong contact

Table 2
Deviations between model and measurement of the single parts for the first five modal frequencies.

	$f_{model_n} - f_{meas_n}$ (Hz)				
	f_1	f_2	f_3	f_4	f_5
Part 1	−36.4 (1.2%)	−12.4 (0.3%)	−49.3 (0.8%)	25.1 (0.4%)	−19.2 (0.2%)
Part 2	−12.2 (0.4%)	−7.5 (0.2%)	−20.4 (0.5%)	22.6 (0.5%)	8.3 (0.1%)

exists, which motivates the choice of the solution that will maximize the stiffness at the contact. This extra requirement is formulated in the optimization problem by minimizing the inverse of the sum of all contact spring constants, which means that the contact stiffness is maximized. Additionally, the springs are required to be positive,

$$\underset{\mathbf{p}}{\text{minimize}} f(\mathbf{p}) = \frac{1}{\sum_{m=1}^{M} \mathbf{s}(\mathbf{p})} \tag{8}$$

$$\text{subject to } g(\mathbf{p}) = \sum_{n=1}^{N} (f_{model_n}(\mathbf{p}) - f_{meas_n})^2 < \epsilon \tag{9}$$

$$\mathbf{s}(\mathbf{p}) \geqslant \mathbf{0}. \tag{10}$$

M is the number of contact springs, N is the number of considered modal frequencies, $f_{model_n}(\mathbf{s})$ is the n-th model eigenfrequency, f_{meas_n} is the n-th measured modal frequency and $\mathbf{s}$ is the vector containing the contact spring constants. If each spring was considered as an independent optimization variable, the problem would become difficult to handle due to the large dimensionality, and the results may be difficult to interpret. Therefore, a parametrization of the spring constants that defines dependencies between them is introduced so that the number of variables is kept low and the contact is described meaningfully. The contact parameters are indicated here as vector $\mathbf{p}$, and different approaches to how to define them will be discussed in Section 4.

Large variations of the contact parameters can result in mode switching (changes on the order of appearance of the modes in the model), which requires the introduction of a pairing technique in order to ensure that the compared natural frequencies at each summation term in Eq. (9) (i.e. for each value of n) correspond to the same mode shape. For that purpose, the cross-orthogonality check (XOC) is calculated between the model eigenvectors ($\mathbf{\Psi}_{model}$) and the measurement eigenvectors ($\mathbf{\Psi}_{meas}$), as [21]

$$\mathbf{XOC} = \mathbf{\Psi}_{model}\mathbf{M}\mathbf{\Psi}_{meas}, \tag{11}$$

which is bounded between 0 and 1 when the eigenvectors are normalized with the mass matrix so that

$$\psi_i^T \mathbf{M} \psi_i = 1. \tag{12}$$

Those modes with a XOC value close to one will be identified as the same mode. Even though the Modal Assurance Criterion (MAC) is more commonly used for mode shape matching between measurements and simulations [21], the XOC gives more extreme values (closer to 0 or 1) than the MAC [22], which makes it preferable for this application where the purpose is to identify matching modes rather than to evaluate the degree of resemblance between measured and simulated mode shapes.

The fact that modal vector matching is included also allows for using only those experimental modes which the user is more confident with or interested in, since only modes from the model that correspond to the selected target experimental data can be selected. Therefore, closely spaced modes from which the modal parameters are difficult to retrieve, or modal shapes that cannot be measured accurately due to practical limitations do not need to be included in the optimization.

Calculating the XOC directly between measured and modelled data can be cumbersome, since the FE mesh should be sampled at the measurement grid points and the data can be in different formats. In the experiments, the order of appearance of the modes does not vary across measurements, therefore, a reference modal matrix is calculated using the numerical model, which will be used for controlling the mode switching during the model-updating. To generate the reference modal matrix, a model where the contact spring constants $\mathbf{s}$ are set to a chosen value is used. The value should be such that five of the resulting modal vectors from the model can be clearly identified with the first five measured modal shapes, which is achieved by setting the stiffness value of all the springs to 5000 N/m. The selected modal shapes, shown in Fig. 8 (b), are then grouped into a reference modal matrix. Since these mode shapes are an approximation of the measured ones, the threshold value of the XOC for which two vectors are recognised as the same mode shape is set to 0.5. In the event that not all of the five modes are recognized for a certain parameter point during the optimization, that point will be rejected.

3.2.2. Optimization algorithm

The minimization problem is solved by means of a gradient-based constrained optimization algorithm implemented in the MATLAB Optimization Toolbox function *fmincon* [23]. It is an implementation of an Interior Point Algorithm, which is currently considered one of the most powerful algorithms for large-scale nonlinear programming [24] (a detailed description of this method can be found in Ref. [25]).

The gradient of the first constraint is derived from Eq. (9) as

$$\nabla g(\mathbf{p}) = \frac{1}{4\pi^2} \sum_{n=1}^{N} \left(1 - \frac{f_{meas_n}}{f_{model_n}(\mathbf{p})}\right) \nabla \omega_{model_n}^2(\mathbf{p}) \tag{13}$$

with

$$\nabla \omega_{model_n}^2(\mathbf{p}) = \left(\psi_n(\mathbf{p})^T \frac{\partial \mathbf{S}}{\partial p_1} \psi_n(\mathbf{p}), \ldots, \psi_n(\mathbf{p})^T \frac{\partial \mathbf{S}}{\partial p_M} \psi_n(\mathbf{p})\right), \tag{14}$$

where ω_{model_n} is the n-th simulated modal angular frequency, $\mathbf{p} = [p_1, \ldots, p_M]$ is the vector of optimization parameters, and the terms $\frac{\partial \mathbf{S}}{\partial p_m}$ are calculated according to the parametrizations that will be discussed in Section 4. The gradient of the objective function in Eq. (8) is

$$\nabla f(\mathbf{p}) = -\sum_{m=1}^{M} \frac{\partial \mathbf{s}(\mathbf{p})}{\partial p_m}, \tag{15}$$

where $\mathbf{s}$ is the vector of spring stiffnesses and M is the total number of parameters. The Hessians are approximated by a quasi-Newton method. The algorithm stops when the size of the step or the change of the objective function between iterations are below a specified tolerance, in this case 10^{-10}. An overview of the optimization procedure is shown in Fig. 9.

4. Results and discussion

The purpose of this study is to model the contact between the two parts for each of the five measurement results of the two conducted experiments. Identification of the areas of the nominal contact surface that present the most probable contact points in each case and characterization of how these areas vary due to the disassembling and assembling process are the sought outcomes. The contact parameters identified for each of the measurement results are unique to the tested configuration, and therefore the results are not applicable to different geometries or boundary conditions, but allows for studying the variability of the vibration response due to the changes in the contact for the assembly conditions under study. Although this variability on the vibrational response has already been measured, for more complex models such as for a full hearing aid assembly, one could be interested in looking at the variability of the vibration response at other points that are difficult to measure or at other quantities such as acoustic pressure, for which the model would then be used.

A main challenge in the contact identification process is to choose a parametrization that yields an accurate result (i.e. a good match between measured and simulated modal frequencies) with a reduced number of parameters. For this purpose, three different

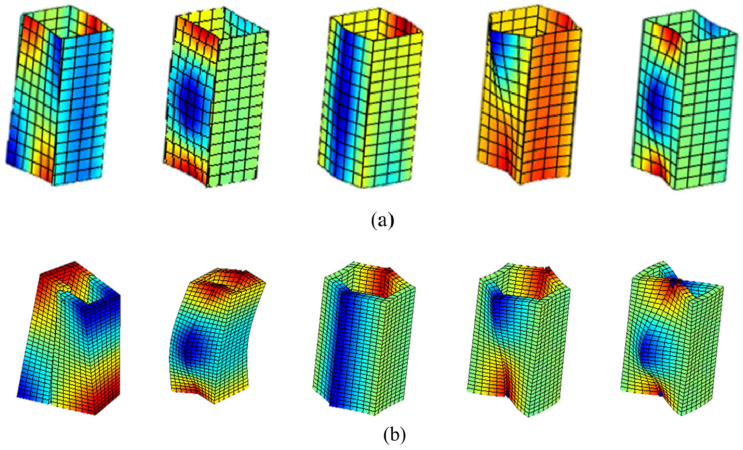

Fig. 8. (a) Measured deflection shapes of assembled structure. (b) Simulated mode shapes corresponding to the measured deflection shapes.

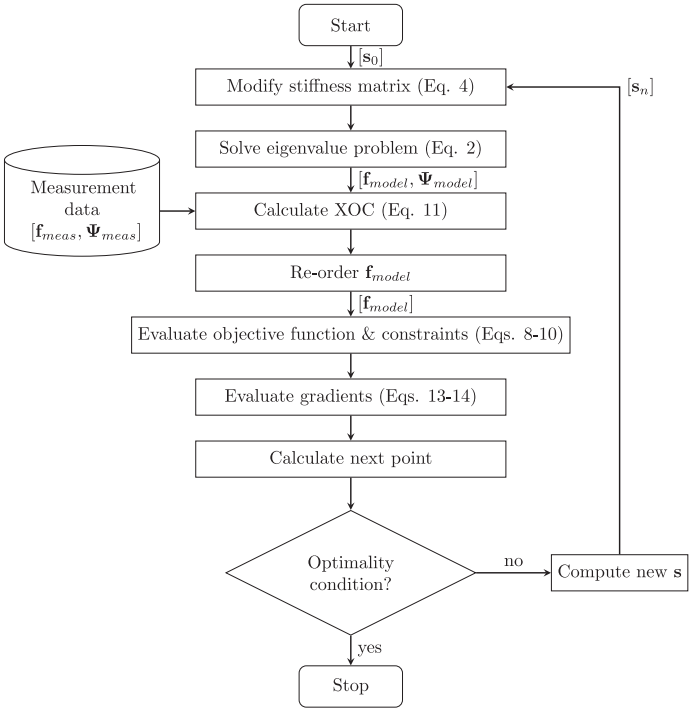

Fig. 9. Flow diagram of the optimization algorithm.

parametrizations of the contact, with different degrees of complexity, are compared for a numerical validation case in Section 4.1. Firstly, a quite straight-forward division of the contact springs in three groups is done, which gives an initial idea of the location of the contact. Then, a description of the contact based on a Fourier decomposition is introduced, in order to obtain a finer representation of the variations at the contact surfaces. One parametrization is then selected according to the outcome of the numerical test and used for studying the real contact of the structure, based on the collected experimental data, in Section 4.2.

4.1. Numerical validation with a known contact condition

In order to define an appropriate parametrization of the contact, a numerical test case with known contact conditions is set up, to which different parametrization approaches are applied and

compared. An arbitrary known contact condition is numerically imposed in the model by bonding some of the contact nodes with constraint equations and letting the rest free; the resulting modal frequencies are then used as "measured data" for the inverse identification procedure. The contact spring values resulting from the nonlinear optimization are then compared to the originally bonded contact points to evaluate how the solution reflects the real contact conditions.

Fig. 10 shows the mesh of the nominal contact surface. In red are shown the nodes where the constraint equations are defined, i.e. the nodes of the bottom part and the top part with the same coordinates to which a no separation condition has been imposed. The nodes shown in blue are left free, i.e. part A and part B can move independently at those locations. This could represent a realistic situation where only some areas of the nominal contact surface are actually in contact, due to surface irregularities. As can be seen in the figure, the number of constrained nodes on the upper level of the contact area (with respect to Y) is higher than for the lower and middle levels; with respect to the X direction, the number of nodes on each side is similar, and with respect to the Z direction, the concentration is slightly higher towards the extremes than at the center. The resulting spring stiffness spatial distribution is expected to reflect these characteristics.

The modal frequencies of the assembly under the imposed contact condition that correspond to the mode shapes shown in Fig. 8 are listed in Table 3. They are used as the vector of measured frequencies f_{meas} for the minimization problem in Eqs. (8)–(10), which will be solved using different parametrizations in the following.

4.1.1. 3-parameter model

The first parametrization consists in dividing the contact springs in three groups with respect to the Y axis, as shown in Fig. 11. Three model parameters are therefore considered (P_1, P_2 and P_3), being the stiffness constants of the contact springs in each group. The spring constants of the 3 directional springs at each node are considered equal.

As a result of the optimization problem, the parameter values listed in Table 4 are obtained. P_1 is significantly higher than P_2 and P_3, which shows that the resulting contact model correlates well with the real contact conditions, since the upper area of the contact is the one with the most bonded points.

The value of the objective function at the final optimization point and the individual differences between the target modal frequencies (Table 3) and the modal frequencies at the solution point are listed in Table 5. The deviations are relatively small; however, their absolute values are in the same order of magnitude as the deviations due to the contact variation shown in Fig. 3, which we intend to model. Therefore, a parametrization with a larger number of variables is introduced in the next section in order to obtain more accurate results. Moreover, no details of the contact location with respect to the X or Z direction can be identified with this parametrization. Therefore, the new parametrization should allow variations in these directions too.

Table 3
Modal frequencies of the numerical validation model (Hz).

f_1	f_2	f_3	f_4	f_5
5960.7	6764.3	7640.1	8173.8	9487.8

4.1.2. 12-parameter model

The 3-parameter model divided the contact springs with respect to their Y coordinate only. In order to capture contact variations in other directions, divisions of the springs with respect to the X or the Z directions should be added, which would multiply quickly the number of parameters. In order to obtain size-optimal models, a parametrization based on a truncated Fourier series with the coefficients as design variables is introduced instead.

The spring stiffness values are described by a spatial Fourier decomposition, where each spring constant is calculated according to the coordinates of its nodes, as

$$\begin{aligned} s_{xyz} = {} & P_1 + P_2 \sin\left(\frac{\mathbf{x}\pi}{L_x}\right) + P_3 \cos\left(\frac{5\mathbf{x}\pi}{L_x}\right) + P_4 \sin\left(\frac{10\mathbf{x}\pi}{L_x}\right) + P_5 \cos\left(\frac{15\mathbf{x}\pi}{L_x}\right) \\ & + P_6 \sin\left(\frac{\mathbf{y}\pi}{L_{yc}}\right) + P_7 \cos\left(\frac{\mathbf{y}\pi}{L_{yc}}\right) + P_8 \sin\left(\frac{\mathbf{z}\pi}{L_z}\right) + P_9 \sin\left(\frac{2\mathbf{z}\pi}{L_z}\right) \\ & + P_{10} \sin\left(\frac{3\mathbf{z}\pi}{L_z}\right) + P_{11} \sin\left(\frac{4\mathbf{z}\pi}{L_z}\right) + P_{12} \sin\left(\frac{5\mathbf{z}\pi}{L_z}\right) \end{aligned} \tag{16}$$

where the dimensions L_x, L_{yc} and L_z are defined as in Fig. 6, and $\mathbf{x}, \mathbf{y}$ and $\mathbf{z}$ are the vectors of coordinates of the nodes where the springs are placed, contained in the domain $\mathbf{x} \in [-2.5, -1.5] \cup [1.5, 2.5]$ mm, $\mathbf{y} \in [-1, 0]$ mm and $\mathbf{z} \in [0, 30]$, according to the dimensions of the specimen. P_1 to P_{12} are the coefficients of the Fourier series (and the design parameters). The choice of the Fourier decomposition components can be better understood by looking at the illustration in Fig. 12. Two components have been included for the parametrization with respect to the Y direction, with parameters P_6 and P_7, which combined can model the same variations as for the 3-parameter model in Section 4.1.1. The solid part of the $P_2 - P_5$ curves in Fig. 12 indicate the parts of the X components within the contact surfaces domain. P_2 is introduced to capture asymmetry in the contact conditions, and P_3 to P_5 introduce $\frac{1}{2}, 1$ and $1\frac{1}{2}$ sinusoidal cycle variations on each side. Finally, the $P_8 - P_{12}$ components are included in order to detect variations in the Z direction.

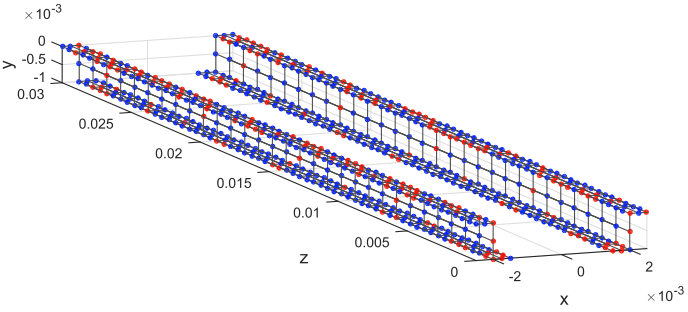

Fig. 10. Numerically imposed contact conditions for validation. Red nodes: bonded contact. Blue nodes: no contact. (For interpretation of the references to colour in this figure legend, the reader is referred to the web version of this article.)

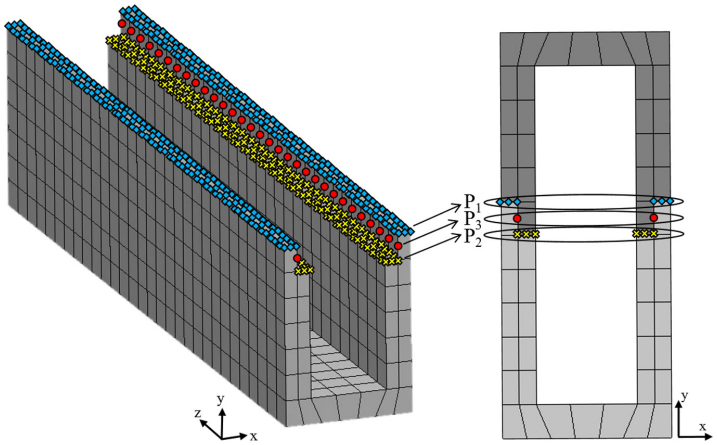

Fig. 11. Grouped contact nodes where the connecting springs share the same stiffness constant. Diamonds: P_1, Crosses: P_2, Circles: P_3.

Table 4
Fitted parameter values for the numerical validation with the 3-parameter model (N/m).

P_1	P_2	P_3
123×10^5	3.17×10^4	1.58×10^4

The spring constants for the 3 directional springs at each node are also assumed equal here.

The resulting differences between the individual target and simulated modal frequencies at the solution point are listed in Table 6. The modal frequencies deviations are below 0.25%, showing that the result is more accurate than for the 3-parameter model.

The resulting contact spring constants are shown in Fig. 13, where the color of the dots indicates the stiffness value of each spring according to its location. The stiffness is higher at the upper part of the contact with respect to the Y direction and towards the extremes with respect to the Z direction, which correlates well with the distribution of the constraint nodes in Fig. 10. It is clear that very local behaviour cannot be captured with this approach, since the Fourier components are defined globally. Therefore, the areas with the most contact points dominate the resulting values of the Fourier coefficients. This is the reason why, in this case, the variations in the Z direction reflect well the distribution of the contact nodes on the upper contact surface, but for the middle level (Y=-0.5), they do not represent the contact nodes in Fig. 10, which are uniformly distributed along the Z axis. In order to capture such local details, more Fourier components could be added to the parametrization.

4.1.3. 3D 12-parameter model

In the previous parametrizations, the 3 directional springs at each node were assumed equal. However, since the physical phenomena that occur on the normal and tangential directions at the contact surfaces are different, it might be relevant to consider separately the X, Y and Z directional springs. By describing each of the 3 directions with the 12-parameter model introduced in the previous section, a 36-parameter contact model is obtained.

As a result, $g(\mathbf{p})$ takes a value of 6×10^{-19} at the final point, which means that the deviations between modelled and target modal frequencies effectively vanish. The obtained spring constants for each direction are shown in Figs. 14–16, which shows that, in general, the stiffness at the upper contact surface is higher, correlating well with the previous results and the enforced contact conditions. This difference between the upper and lower contact surfaces is very clear for the Y-directional springs (Fig. 19), while for the X-directional and Z-directional ones (Figs. 18 and 20) the main stiffness variations occur in the X direction, with the stiffness being higher at those nodes that belong to the vertical contact surface (perpendicular to X) than for the rest. This tendency could also be seen for the 12-parameter model, but becomes more obvious here, and could be related to the fact that the upper part of the contact (where most contact points are placed) presents more contact points at the inner part than the outer part.

Since the artificial contact was created by bonding interface nodes from the two parts, the relative displacement between the linked nodes is constrained in the three DOFs. Intuitively, this should result in no difference between the three dimensional spring constants at each node. However, the exact contact configuration cannot be precisely represented by a model which has a low number of parameters compared to the total number of contact springs; therefore, the model finds the best approximation to reality, given the selected Fourier components. As a conclusion, the introduction of different variables for the 3 dimensional springs allows for modeling the most relevant contact locations for each direction separately, which improves the resulting accuracy. Moreover, in real contact conditions, the differences on the directional spring stiffness values may actually represent physical

Table 5
Individual frequency differences and objective function value at the model updating resulting point for the 3-parameter model.

$f_{model_n} - f_{meas_n}$ (Hz)					$g(\mathbf{p})$
f_1	f_2	f_3	f_4	f_5	
−24 (0.4%)	14 (0.21%)	60 (0.79%)	−76 (0.93%)	13 (0.15%)	1.05×10^4

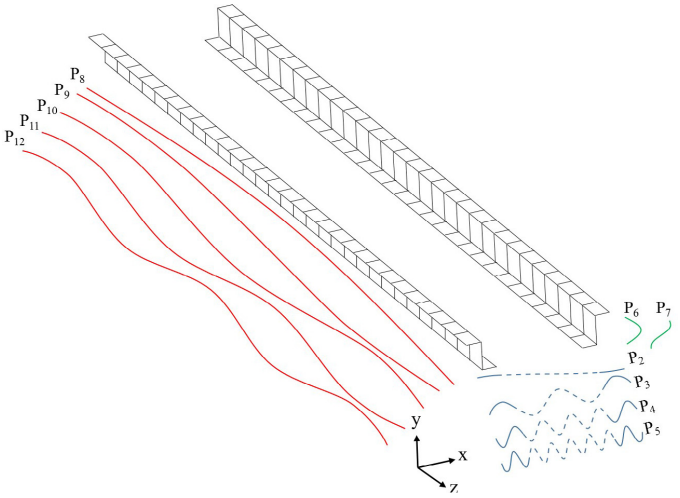

Fig. 12. Fourier expansion components of the 12 parameter model.

Table 6
Individual frequency differences and objective function value at the model updating resulting point for the 12-parameter model.

$f_{model_n} - f_{meas_n}$ (Hz)					$g(\mathbf{p})$
f_1	f_2	f_3	f_4	f_5	
−14 (0.25%)	14 (0.21%)	5 (0.07%)	−3 (0.04%)	−4 (0.04%)	4.94×10^2

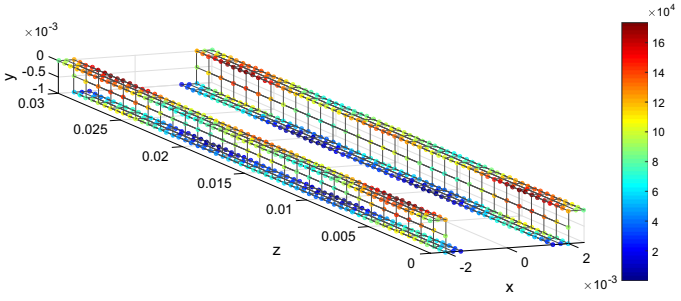

Fig. 13. Spring constant values (N/m).

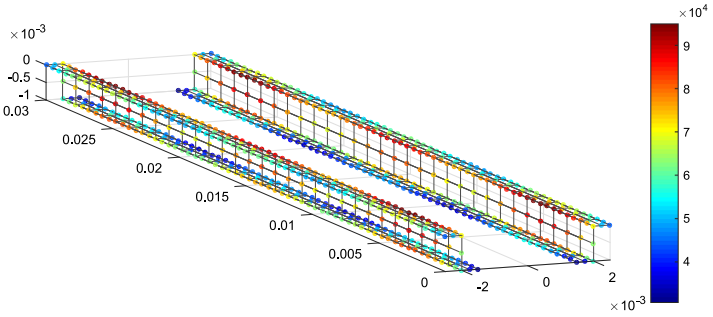

Fig. 14. X directional spring constants (N/m).

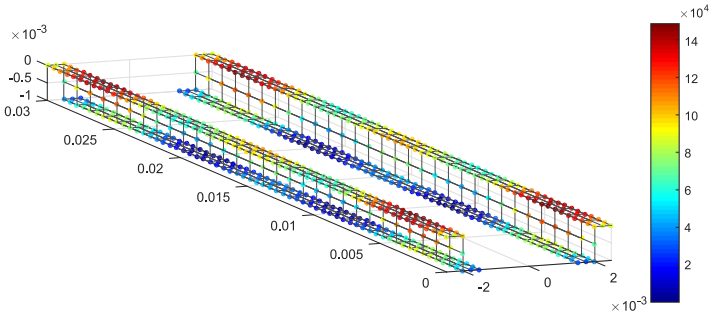

Fig. 15. Y directional spring constants (N/m).

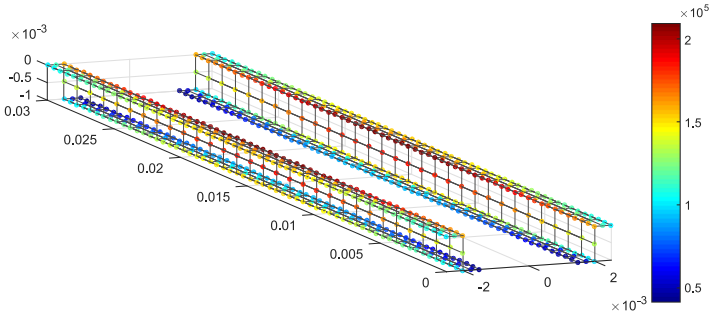

Fig. 16. Z directional spring constants (N/m).

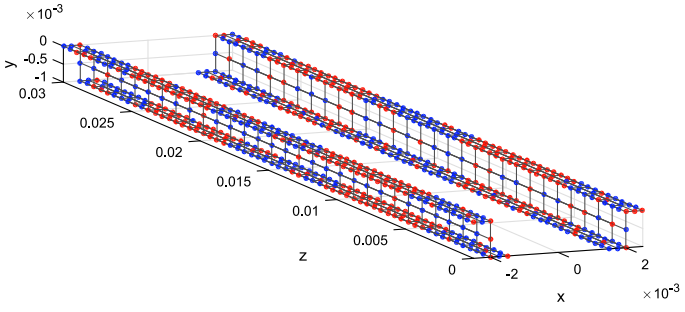

Fig. 17. Numerically imposed contact conditions for validation case 2. Red nodes: bonded contact. Blue nodes: no contact. (For interpretation of the references to colour in this figure legend, the reader is referred to the web version of this article.)

features at the contact surface, since irregularities can lock the relative displacement between contact points differently in different directions.

In order to further validate the method, a new numerical case where the contact configuration is actually possible to model accurately with the suggested model is shown here, so that the results can be directly related to the numerically enforced contact points. The constraint equations are now distributed as shown in Fig. 17, where the constrained nodes are concentrated around two areas with respect to the *Z* direction, and the variations with respect to the *X* and *Y* directions are not significant. The choice of these areas is done so that the contact can be modelled directly with the *P*10 component in Fig. 12. The results of the inverse identification procedure are shown in Figs. 18–20, where the contact stiffness is now almost identical for the three dimensional springs and presents a high value at those areas where the contact nodes were concentrated, showing that the method is able to identify the bonded location successfully.

Higher order Fourier components could be added in order to capture more local details of the contact location; however, there is a limit to the number of variables that can be considered in the optimization before the number of local minima becomes too large and yields trivial solutions. For this reason, a model such as the one proposed here which is able to describe the most contributing contact areas while keeping the number of parameters at an acceptable level is a good compromise. This

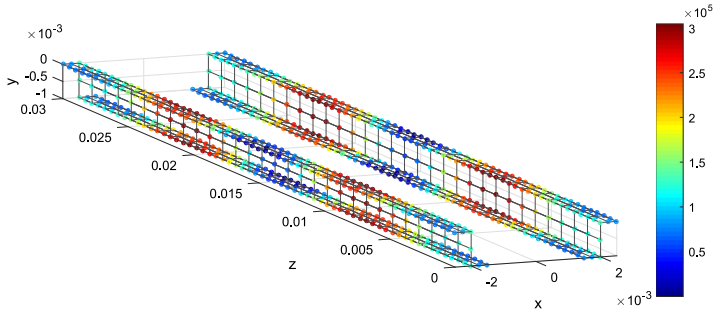

Fig. 18. X directional spring constants (N/m) for validation case 2.

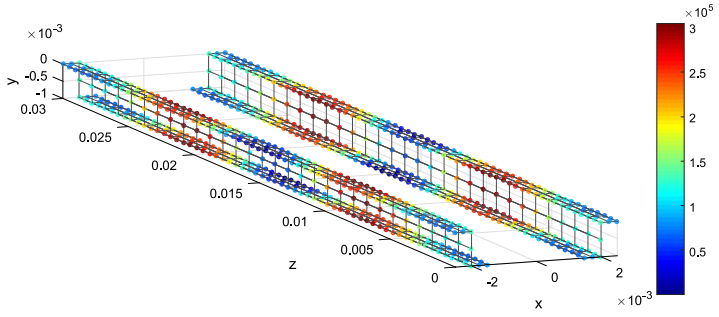

Fig. 19. Y directional spring constants (N/m) for validation case 2.

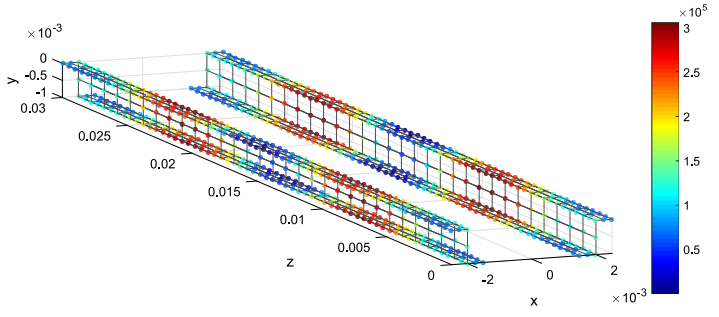

Fig. 20. Z directional spring constants (N/m) for validation case 2.

parametrization is therefore selected for modeling the experimental results.

4.2. Experimental results fitting

The five measured modal frequency sets of each of the two experiments, for which the spread was shown in Fig. 3, are now fitted with the 3D 12-parameter contact model, yielding the spread of the resulting model parameters shown in Figs. 21–23. The variations of the parameter values are larger for experiment 2 than for experiment 1, which correlates well with the spread of the measured data, showing that the selected parameters are sensitive to the variations of the modal frequencies. The mean values of the parameters are similar between experiment 1 and experiment 2, which indicates that the locations of the contact points do not vary drastically when dismounting and mounting the two parts, but only small changes take place.

The contact spring constants for one of the fitted measurement results are shown in Figs. 24–26. The results for the *X*-directional springs clearly show that the lower surface of the contact area presents the most relevant contact points, with the spring constants being very low at the rest of the points. For the *Y*-directional springs, the stiffness shows large oscillations along the *Z* axis, which indicates that the most relevant contact points are concentrated around two areas. Regarding the *Z*-directional springs, the most relevant contact points are identified at the upper surface and at the center with respect to the *Z* axis, which is surprisingly different from the results in the *X* and *Y* directions. The different

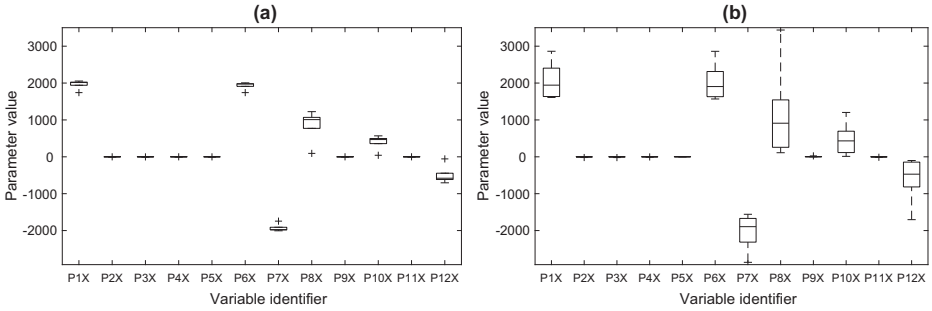

Fig. 21. X-direction model parameters distribution. (a) experiment 1 and (b) experiment 2. On each box, the central mark is the median, the edges of the box are the 25th and 75th percentiles, the whiskers extend to the most extreme datapoints and the outliers are plotted individually.

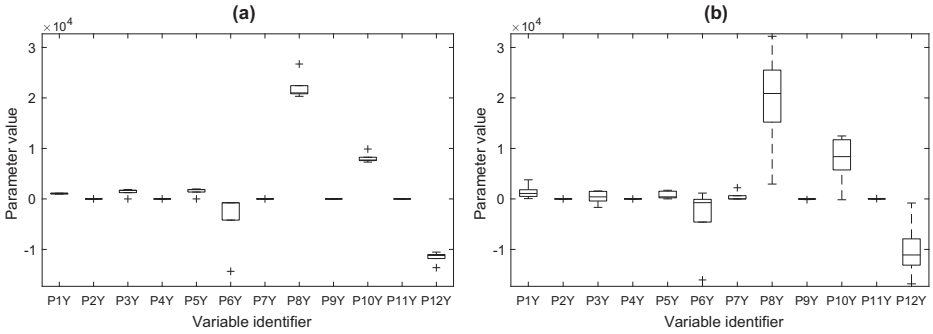

Fig. 22. Y-direction model parameters distribution. (a) experiment 1 and (b) experiment 2. On each box, the central mark is the median, the edges of the box are the 25th and 75th percentiles, the whiskers extend to the most extreme datapoints and the outliers are plotted individually.

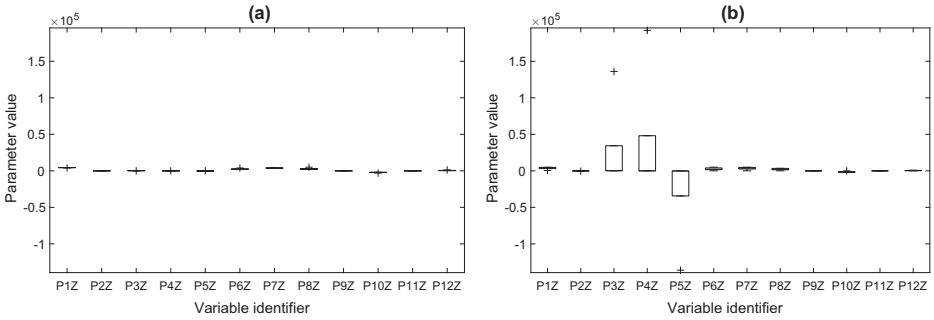

Fig. 23. Z-direction model parameters distribution. (a) experiment 1 and (b) experiment 2. On each box, the central mark is the median, the edges of the box are the 25th and 75th percentiles, the whiskers extend to the most extreme datapoints and the outliers are plotted individually.

behavior might be related to the fact that the *Z* directional springs are tangential to all considered surfaces, while the *X* and *Y* directional springs are normal to the surface in some areas, and tangential in others, therefore, they represent different kinds of contact forces.

The median and maximum values of the constraint function $g(\mathbf{p})$ and the deviations between the target and modelled modal frequencies at the solution points of the optimizations for the 10 measurement results are shown in Table 7. The deviations on the modal frequencies are within the same range than the deviations observed between the measured and modelled modal frequencies of the independent parts (Table 2), which were associated to sources of error such as simplifications of the material models and geometric details or measurement uncertainty. Therefore, the contact model yields a result as accurate as possible in this context.

4.3. Discussion

The final goal of our work is to be able to characterise the variability of the vibration response of built-up structures due to contact uncertainty. With the method presented here, the contact

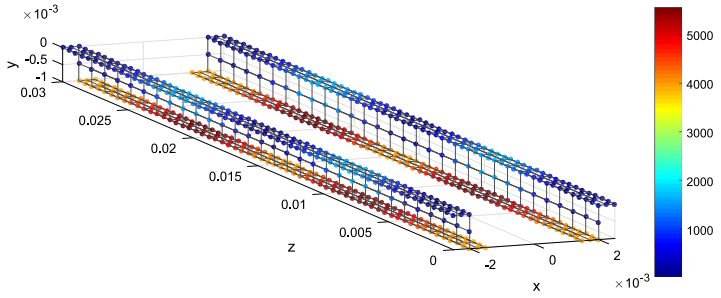

Fig. 24. X directional spring constants for one of the fitted measurement results.

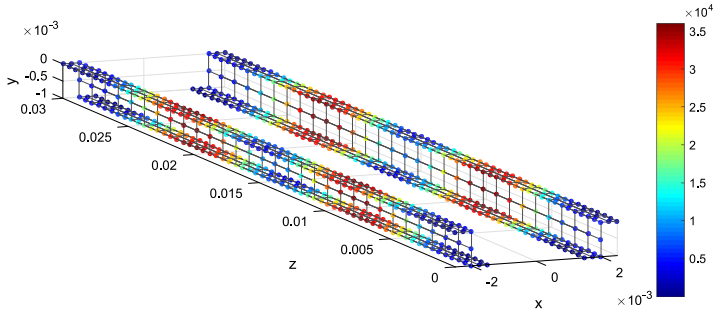

Fig. 25. Y directional spring constants for one of the fitted measurement results.

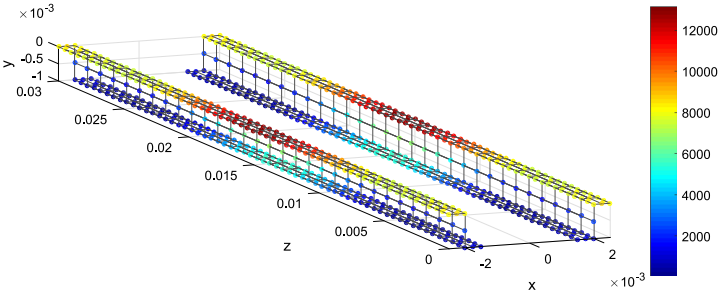

Fig. 26. Z directional spring constants for one of the fitted measurement results.

Table 7
Median and maximum values of the individual frequency differences and the objective function values for the 10 fitted measurements with the 3D 12-parameter model.

	$f_{model_n} - f_{meas_n}$ (Hz)					$g(p)$
	f_1	f_2	f_3	f_4	f_5	
Md	−2.5(0.04%)	−1.5(0.02%)	−40.7(0.66%)	34.9(0.55%)	10.7(0.13%)	3.00×10^3
Max	−0.9(0.01%)	−10(0.17%)	−34.5(0.56%)	47.5(0.75%)	12.4(0.15%)	5.05×10^3

conditions can be estimated from measurement data that is relatively easy to obtain. Therefore, if the contact parameters are estimated for a sufficiently large sample of cases (for example, a number of serially produced hearing aid parts), their probability distributions can be extracted and used, for example, in Monte-Carlo simulation studies to predict the vibration response variability.

Variability in the contact conditions can originate serious problems if it is not controlled, since resonance frequencies can come close to each other resulting in an unexpected increase of the vibration transmission at certain frequency ranges due to mode overlap. Those cases could also be studied using the suggested contact model by setting up an optimization problem that minimizes the differences between specific modal frequencies when the

model parameters are constrained within their previously estimated bounds. The model could also be used to find optimal contact points, which could then be enforced by including features on the contact surfaces; in this way, the variability would be reduced and the response optimized at the same time. For example, the contact points for which the distance between modal frequencies is maximized could be found by formulating the corresponding optimization problem.

5. Conclusions

In the present paper, the variability of the contact conditions between two small plastic parts due to the dis-assemblage and assemblage process has been studied. A methodology for identifying the most relevant contact areas based on an inverse problem formulation has been developed, where the contact conditions are estimated from measured modal frequencies of the assembled structure. The contact is modelled by means of linear springs, for which the stiffness constants are identified. Several parametrizations of the contact springs have been compared for a numerical validation case, showing that the number of parameters must be selected as a trade-off between the dimensionality of the problem and the accuracy of the results being at a desired level. A 36-parameter model based on a Fourier decomposition of the spring constants value according to their position and direction has been found to fulfil these requirements, and selected for modeling the contact conditions of the real assembly. The experimental study has shown that the variability of the modal frequencies due to the dis-assemblage and assemblage process is significant in comparison to the variability due to measurement uncertainty. The outcome of the contact conditions identification procedure also yields a significant variation of the contact parameters, but shows that the main contact areas remain the same throughout the different measured cases, and the changes on the contact conditions due to the dis-assemblage and assemblage process are small.

Acknowledgments

The authors would like to thank the Innovation Fond Denmark and the Oticon Foundation for their financial support.

References

[1] Plunt J. Generic limitations of vibro-acoustic prediction methods for product noise. In: Proceedings of inter-noise 96 - the 1996 international congress on noise control engineering, Liverpool, Books 1-6, INST ACOUSTICS; 1996, p. 3047–52.
[2] Pate A, Le Carrou J-L, Fabre B. Modal parameter variability in industrial electric guitar making: manufacturing process, wood variability, and lutherie decisions. Appl Acoust 2015;96():118–31. http://dx.doi.org/10.1016/j.apacoust.2015.03.023.
[3] Kompella MS, Bernhard RJ. Variation of structural-acoustic characteristics of automotive vehicles. Noise Control Eng J 1996;44(2):93–9.
[4] Friis L. Investigation of internal feedback in hearing aids [Ph.D. thesis]. Technical University of Denmark; 2009.
[5] Sondergaard MB, Pedersen CBW. Applied topology optimization of vibro-acoustic hearing instrument models. J Sound Vib 2014;333(3):683–92. http://dx.doi.org/10.1016/j.jsv.2013.09.029.
[6] Hanss M, Oexl S, Gaul L. Identification of a bolted-joint model with fuzzy parameters loaded normal to the contact interface. Mech Res Commun 2002;29(2–3):177–87. http://dx.doi.org/10.1016/S0093-6413(02)00245-8.
[7] Lyon RH, DeJong RG. Theory and application of statistical energy analysis. Newton, MA: Butterworth-Heinemann; 1995.
[8] Le Bot A, Cotoni V. Validity diagrams of statistical energy analysis. J Sound Vib 2010;329(2):221–35. http://dx.doi.org/10.1016/j.jsv.2009.09.008.
[9] Sepahvand K, Marburg S. Identification of composite uncertain material parameters from experimental modal data. Probab Eng Mech 2014;37:148–53. http://dx.doi.org/10.1016/j.probengmech.2014.06.008.
[10] Tsai JS, Chou YF. The identification of dynamic characteristics of a single bolt joint. J Sound Vib 1988;125(3):487–502. http://dx.doi.org/10.1016/0022-460X(88)90256-8.
[11] Hwang HY. Identification techniques of structure connection parameters using frequency response functions. J Sound Vib 1998;212(3):469–79. http://dx.doi.org/10.1006/jsvi.1997.1433.
[12] Yang TC, Fan SH, Lin CS. Joint stiffness identification using FRF measurements. Comput Struct 2003;81(28–29):2549–56. http://dx.doi.org/10.1016/S0045-7949(03)00328-6.
[13] Čelič D, Boltežar M. Identification of the dynamic properties of joints using frequency-response functions. J Sound Vib 2008;317(1–2):158–74. http://dx.doi.org/10.1016/j.jsv.2008.03.009.
[14] Ling-mi Z, Qin-tao G. Identification of the mechanical joint parameters with model uncertainty. Chin J Aeronaut 2005;18(1):47–52. http://dx.doi.org/10.1016/s1000-9361(11)60281-1.
[15] Li WL. A new method for structural model updating and joint stiffness identification. Mech Syst Signal Process 2002;16(1):155–68.
[16] Dos Santos J, Mace B. Modelling uncertainty in mechanical joint parameters using component modal and fuzzy approaches. In: Proceedings of III European conference on computational mechanics. Netherlands: Springer; 2006. http://dx.doi.org/10.1007/1-4020-5370-3_302. p. 302–302.
[17] Ehrlich C, Schmidt A, Gaul L. Reduced thin-layer elements for modeling the nonlinear transfer behavior of bolted joints of automotive engine structures. Arch Appl Mech 2016;86(1–2):59–64. http://dx.doi.org/10.1007/s00419-015-1109-1.
[18] Dovstam K, Goransson P, Gartmeier O. On linear modeling of interface damping in vibrating structures. J Sound Vib 2012;331(19):4299–312. http://dx.doi.org/10.1016/j.jsv.2012.03.036.
[19] Craik RJM, Steel JA. Effect of workmanship on sound transmission through buildings. Part 1. Airborne sound. Appl Acoust 1989;27(1):57–63. http://dx.doi.org/10.1016/0003-682X(89)90045-5.
[20] Craik RJM, Evans D. The effect of workmanship on sound-transmission through buildings. Part 2. Structure-borne sound. Appl Acoust 1989;27(2):137–45. http://dx.doi.org/10.1016/0003-682X(89)90006-6.
[21] Allemang RJ. The modal assurance criterion – twenty years of use and abuse. Sound Vib 2003;37(8):14–21.
[22] Zang C, Ma S, Friswell MI. Finite element model updating of an assembled aero-engine casing. Conf Proc Soc Exp Mech Ser 2013;5:199–212. http://dx.doi.org/10.1007/978-1-4614-6564-5_20.
[23] MATLAB optimization toolbox user's guide R2015b, MathWorks, Natick, MA; 2015.
[24] Nocedal J, Wright SJ. Numerical optimization. New York: Springer; 2006.
[25] Byrd RH, Hribar ME, Nocedal J. An interior point algorithm for large-scale nonlinear programming. Siam J Optim 1999;9(4):877–900. http://dx.doi.org/10.1137/S1052623497325107.

Paper B

A Multi-Model Reduction Technique for Optimization of Coupled Structural-Acoustic Problems

inter.noise
HAMBURG 2016

A Multi-Model Reduction Technique for Optimization of Coupled Structural-Acoustic Problems

Ester CREIXELL-MEDIANTE[1*,2]; Jakob Søndergaard JENSEN[2*]; Jonas BRUNSKOG[2] ; Martin LARSEN[1]

[1] Oticon A/S, Denmark

[2] Acoustic Technology, Department of Electrical Engineering, Danmarks Tekniske Universitet (DTU), Denmark

ABSTRACT

Finite Element models of structural-acoustic coupled systems can become very large for complex structures with multiple connected parts. Optimization of the performance of the structure based on harmonic analysis of the system requires solving the coupled problem iteratively and for several frequencies, which can become highly time consuming. Several modal-based model reduction techniques for structure-acoustic interaction problems have been developed in the literature. The unsymmetric nature of the pressure-displacement formulation of the problem poses the question of how the reduction modal base should be formed, given that the modal vectors are not orthogonal due to the asymmetry of the system matrices. In this paper, a multi-model reduction (MMR) technique for structure-acoustic interaction problems is developed. In MMR, the reduction base is formed with the modal vectors of a family of models that sample the design domain of the optimization parameters. The orthogonalization of the resulting reduction base is therefore a key point in the method. The use of the different reduction approaches found in the literature for developing an efficient and robust MMR technique is investigated. Several methods are compared in terms of accuracy and size of the reduced systems for optimization of simple models.

Keywords: Model Reduction, Optimization, Structure-acoustic interaction

1. INTRODUCTION

Significant computational challenges are encountered when solving numerical problems that require iterative and/or repeated calculations of large complex models. In our investigations, we focus on the challenges encountered in the field of hearing aids, which are devices composed of a large number of small parts with complex dynamic and acoustical behavior. Numerical vibro-acoustic analysis of hearing aids is essential for the study of problems such as feedback, which is currently the main gain limiting factor of the hearing devices, and requires fine resolution frequency calculations. Tasks such as uncertainty analysis by means of Monte-Carlo methods, or parametric and topology optimization, require solving the system repeatedly for a large number of variations of different parameters. Therefore, the time required for solving the numerical problem at each iteration becomes a critical factor.

Recently, a topology optimization study including structure-acoustic interaction was performed on a part of a hearing instrument [1]. To facilitate the study, some restrictions on the design freedom were imposed and the performance was evaluated and optimized for a limited number of frequencies. The effects of such simplifications are difficult to control; therefore, there is a need to develop computational reduction techniques that make performing these processes with the required level of accuracy practically possible.

[1]email: emed@oticon.com

[2]email: json@elektro.dtu.dk

Reduction of Finite Element (FE) models of hearing aids is quite an unexplored field. The main challenges of modelling sound and vibrations in hearing aids have been discussed in Ref. [2], where a complete model of a hearing aid was developed for the purpose of studying the feedback paths. A pragmatic 3-D model was suggested, which uses the FE method combined with other methods including structural fuzzy [3] (describing regions with large uncertainty), lumped elements, two-port acoustical networks and measured data. These methods describe some of the parts of the hearing aid in a more efficient way than a pure FE model. However, when a high accuracy is required, the details of complex geometries need to be included in the model, which requires pure FE modeling that results in large matrices.

Model reduction techniques have been described in the literature and applied in several fields. The Component Mode Synthesis (CMS) methods have been widely used for reducing large complex structural problems. They are based on decomposing big structures into several substructures, which are then described by a number of modes, and linked together by shared degrees of freedom [4, 5]. The method has also been extended to describe problems with structure-acoustic interaction by several authors, who have taken different approaches when constructing the reduction base. One approach is using the uncoupled structural and acoustic modes, which, for problems with weak coupling, can be efficiently applied. However, for problems with strong interaction, a large amount of modes would be required in order to obtain an accurate reduced model, as described in Ref. [6]. Methods that use coupled modes for the reduction have also been developed. A drawback of those methods is that solving the coupled eigenvalue problem requires higher computational effort due to the unsymmetric nature of the matrices when the pressure-displacement formulation is used. However, the coupled modal vectors can better describe the system, and smaller reduction bases can be obtained. The asymmetry of the matrices also implies that the modal vectors do not form an orthogonal base, which is a basic requirement for forming a vector base. This issue can be solved by using both left and right eigenvectors [7], or by applying orthogonalization techniques [8].

In CMS methods, the interface degrees of freedom between substructures need to be kept in the reduced set of coordinates. This makes them not suitable for structures where it is challenging to find small interfaces to split the model, such as fully coupled structural-acoustic models that include exterior acoustic domains. Even though interface reduction methods have been developed, such as in Refs. [9, 10], avoiding the interfaces would be desirable. In many cases, the available computational power is sufficient to allow for solving the full model eigenvalue problem, which provides the global modal vectors. Those can be used as a reduction base for the system matrices, allowing for the calculation of fine resolution frequency responses at a reduced computational cost. However, for optimization purposes, the reduction base should be re-calculated at each iteration (unless the sensitivity of the modal vectors to the optimization variables is low enough, as assumed in Refs. [11, 12]), which would still be highly time-consuming.

The Multi-Model Reduction (MMR) technique consists in constructing a reduction base with modal vectors from a family of models, formed by sampling the design domain of the optimization parameters. The sampling should be fine enough so that the design points that are not sampled are approximated accurately enough, therefore the efficiency of this method depends on how many different models need to be included in the reduction base. This technique has been described for structural problems in Ref. [13], where the need of orthogonalizing the reduction base is highlighted. Since some modal vectors from different sampled models can be very similar, the linearly dependent vectors would originate ill-conditioning otherwise. When using MMR for coupled problems, the fact that the modal vectors resulting from the unsymmetric matrix systems are inherently not orthogonal needs to be taken into account on top of that.

This paper discusses how to adapt the MMR technique for coupled problems and reviews different approaches to form a numerically stable reduction base. In section 2, the different approaches are described, and in section 3, the efficiency of the different suggested methods is compared for the optimization of a simple model of a plate coupled to an air column.

2. METHODS

In this section, different approaches to reducing a coupled structure-acoustic interaction problem are described. For an undamped system, the pressure-displacement formulation yields the coupled eigenvalue problem

$$\left(\begin{bmatrix} [\mathbf{K}_s] & -[\mathbf{S}]^T \\ \mathbf{0} & [\mathbf{K}_a] \end{bmatrix} - \omega_i^2 \begin{bmatrix} [\mathbf{M}_s] & [\mathbf{0}] \\ \rho_a[\mathbf{S}] & [\mathbf{M}_a] \end{bmatrix} \right) \begin{Bmatrix} \{\boldsymbol{\psi}_{sR}^i\} \\ \{\boldsymbol{\psi}_{aR}^i\} \end{Bmatrix} = \begin{Bmatrix} \{\mathbf{0}\} \\ \{\mathbf{0}\} \end{Bmatrix} \tag{1}$$

where $[\mathbf{K}_s]$ and $[\mathbf{M}_s]$ are the structural stiffness and mass matrices, $[\mathbf{K}_a]$ and $[\mathbf{M}_a]$ are the acoustic stiffness and mass matrices, $[\mathbf{S}]$ is the coupling matrix, ρ_a is the density of the acoustic medium, ω_i is the i-th modal angular frequency, $\{\boldsymbol{\psi}_{sR}^i\}$ is the structural displacement part of the i-th right modal vector and $\{\boldsymbol{\psi}_{aR}^i\}$ is the acoustic pressure part of the i-th right modal vector.

For the sake of notation clarity in the following sections, let us introduce $[\mathbf{M}]$ and $[\mathbf{K}]$ as the coupled mass and stiffness matrices, $\{\boldsymbol{\psi}_R^i\}$ as the i-th complete right eigenvector and $\{\boldsymbol{\psi}_L^i\}$ as the i-th complete left eigenvector, the latter being the result from solving the eigenvalue problem

$$([\mathbf{K}]^T - \omega_i^2[\mathbf{M}]^T)\{\boldsymbol{\psi}_L^i\} = \{\mathbf{0}\}. \tag{2}$$

It becomes clear that a disadvantage of using both left and right eigenvectors in the reduction is that two eigenvalue problems must be solved in order to construct the base. However, according to Refs. [14] and [7], the left eigenvectors can be calculated from the right eigenvectors as

$$\{\boldsymbol{\psi}_L^i\} = (\{\boldsymbol{\psi}_{sR}^i\}^T, \frac{1}{\omega_i^2}\{\boldsymbol{\psi}_{aR}^i\}^T), \tag{3}$$

which avoids the extra computational effort.

Moreover, let us define the truncated modal matrices as $[\boldsymbol{\psi}_L] = [\{\boldsymbol{\psi}_L^1\} \ldots \{\boldsymbol{\psi}_L^N\}]$, $[\boldsymbol{\psi}_R] = [\{\boldsymbol{\psi}_R^1\} \ldots \{\boldsymbol{\psi}_R^N\}]$, $[\boldsymbol{\psi}_{aL}] = [\{\boldsymbol{\psi}_{aL}^1\} \ldots \{\boldsymbol{\psi}_{aL}^N\}]$, $[\boldsymbol{\psi}_{sL}] = [\{\boldsymbol{\psi}_{sL}^1\} \ldots \{\boldsymbol{\psi}_{sL}^N\}]$, $[\boldsymbol{\psi}_{aR}] = [\{\boldsymbol{\psi}_{aR}^1\} \ldots \{\boldsymbol{\psi}_{aR}^N\}]$ and $[\boldsymbol{\psi}_{sR}] = [\{\boldsymbol{\psi}_{sR}^1\} \ldots \{\boldsymbol{\psi}_{sR}^N\}]$, where N is the number of modes included in the modal matrix.

In section 2.1, different approaches to reduction bases for the coupled system are described, and in section 2.2 those methods are extended to form multi-model reduction bases.

2.1 Single Model Reduction

The right eigenvectors from unsymmetric eigenvalue problems are not orthogonal, which makes them not suitable as a reduction base. However, the left and right eigenvectors form an orthogonal base with respect to the unsymmetric mass matrix, $[\boldsymbol{\psi}_L][\mathbf{M}][\boldsymbol{\psi}_R] = [\mathbf{I}]$; therefore, they can be used together to reduce the system. Another option consists in orthogonalizing the set of right eigenvectors, as done in Ref. [8], where the acoustic and structural parts of the coupled eigenvectors are separated and orthogonalized with respect to the acoustic and structural mass matrices respectively. From these two basic approaches, 6 reduction methods have been designed in order to compare and determine the most efficient and accurate reduction technique for the cases at hand.

In the following, $[\mathbf{T}_L]$ is the left reduction matrix, and $[\mathbf{T}_R]$ is the right reduction matrix, meaning that the reduced system matrices are calculated as

$$[\mathbf{M}_{red}] = [\mathbf{T}_L][\mathbf{M}][\mathbf{T}_R] \tag{4}$$
$$[\mathbf{K}_{red}] = [\mathbf{T}_L][\mathbf{K}][\mathbf{T}_R]. \tag{5}$$

The six methods are summarized in the following.

1. Method 1: Using only the right eigenvectors for both left and right reduction matrices,

$$[\mathbf{T}_L] = [\boldsymbol{\psi}_R] \tag{6}$$
$$[\mathbf{T}_R] = [\boldsymbol{\psi}_R]. \tag{7}$$

2. Method 2: Using only the left eigenvectors for both left and right reduction matrices,

$$[\mathbf{T}_L] = [\boldsymbol{\psi}_L] \tag{8}$$
$$[\mathbf{T}_R] = [\boldsymbol{\psi}_L]. \tag{9}$$

3. Method 3: Using the right eigenvectors for the right reduction matrix, and the left eigenvectors for the left reduction matrix,

$$[\mathbf{T}_L] = [\boldsymbol{\psi}_L] \tag{10}$$
$$[\mathbf{T}_R] = [\boldsymbol{\psi}_R]. \tag{11}$$

4. Method 4: Using only right eigenvectors, separating the fields and orthogonalizing. The matrices are formed by orthogonalizing the acoustic and structural parts of the right eigenvectors with the acoustic and structural mass matrices respectively, so that

$$[\mathbf{T}_{aL}]^T[\mathbf{M}_a][\mathbf{T}_{aR}] = [\mathbf{I}] \tag{12}$$
$$[\mathbf{T}_{sL}]^T[\mathbf{M}_s][\mathbf{T}_{sR}] = [\mathbf{I}], \tag{13}$$

   and including them separately in the reduction matrices

$$[\mathbf{T}_L] = \begin{bmatrix} [\mathbf{T}_{sL}] & [\mathbf{0}] \\ [\mathbf{0}] & [\mathbf{T}_{aL}] \end{bmatrix} \tag{14}$$
$$[\mathbf{T}_R] = \begin{bmatrix} [\mathbf{T}_{sR}] & [\mathbf{0}] \\ [\mathbf{0}] & [\mathbf{T}_{aR}] \end{bmatrix}. \tag{15}$$

   In this way, the structure of the complete unsymmetric problem in eq. (1) is preserved in the reduced problem, but the base is not orthogonal with respect to the total mass or stiffness matrices.

   Due to the separation of the two domains, some vectors can be very similar, and those must be removed from the base to avoid ill-conditioning. The detection of collinear vectors is done before the orthogonalization by performing a Singular Value Decomposition (SVD) of the matrices $[\boldsymbol{\psi}_{aR}]^T[\mathbf{M}_a][\boldsymbol{\psi}_{aR}]$ and $[\boldsymbol{\psi}_{sR}]^T[\mathbf{M}_s][\boldsymbol{\psi}_{sR}]$, and keeping those vectors for which the singular values are below a selected tolerance. A recommended value [15] is $tol = \epsilon\sigma_1 n$, where ϵ is the floating-point relative accuracy, σ_1 is the biggest singular value and n is the length of the diagonal of the matrix. Since the SVD has already been calculated, the obtained matrices can be used for orthogonalizing the base. The process for orthogonalizing $[\boldsymbol{\psi}_{aR}]$ is described in the following. The SVD is calculated, yielding

$$[\boldsymbol{\psi}_{aR}]^T[\mathbf{M}_a][\boldsymbol{\psi}_{aR}] = [\mathbf{U}][\boldsymbol{\Sigma}][\mathbf{V}]^T, \tag{16}$$

where $[\mathbf{\Sigma}]$ is the matrix with the singular values on its diagonal, and $[\mathbf{U}]$ and $[\mathbf{V}]$ are unitary matrices. Then,

$$[\mathbf{T}_{aR}] = [\boldsymbol{\psi}_{aR}][\mathbf{V}]^{-T}[\mathbf{\Sigma}]^{-1/2} \tag{17}$$

$$[\mathbf{T}_{aL}] = [\mathbf{\Sigma}]^{-1/2}[\mathbf{U}]^{-1}[\boldsymbol{\psi}_{aR}]^{T} \tag{18}$$

are orthogonal bases. Moreover, since $[\mathbf{U}]$ and $[\mathbf{V}]$ are also orthogonal matrices, $[\mathbf{U}]^{-1} = [\mathbf{U}]^{T}$ and $[\mathbf{V}]^{-T} = [\mathbf{V}]$, which avoids matrix inversions in the calculation. The same procedure is followed to obtain $[\mathbf{T}_{sL}]$ and $[\mathbf{T}_{sR}]$, but using $[\boldsymbol{\psi}_{sR}]$ in eqs. (17-18).

5. Method 5: Using only left eigenvectors, separating the fields and orthogonalizing. The procedure is as in Method 4, but using the left eigenvectors, $[\boldsymbol{\psi}_{aL}]$ and $[\boldsymbol{\psi}_{sL}]$, in eqs. (17-18).

6. Method 6: Using both left and right eigenvectors, separating the fields and orthogonalizing. This method combines features from methods 3, 4 and 5 by forming two bases with right and left eigenvectors where the structural and acoustical parts of the vectors are separated,

$$[\hat{\boldsymbol{\psi}}_{L}] = \begin{bmatrix} [\boldsymbol{\psi}_{sL}] & [\mathbf{0}] \\ [\mathbf{0}] & [\boldsymbol{\psi}_{aL}] \end{bmatrix} \tag{19}$$

$$[\hat{\boldsymbol{\psi}}_{R}] = \begin{bmatrix} [\boldsymbol{\psi}_{sR}] & [\mathbf{0}] \\ [\mathbf{0}] & [\boldsymbol{\psi}_{aR}] \end{bmatrix}, \tag{20}$$

and then orthogonalizing them with respect to the full coupled mass matrix, so that

$$[\mathbf{T}_{L}][\mathbf{M}][\mathbf{T}_{R}] = [\mathbf{I}]. \tag{21}$$

The orthogonalization is done by following the same procedure as described for Method 4, but using $[\hat{\boldsymbol{\psi}}_{L}]$ in eq. (17) and $[\hat{\boldsymbol{\psi}}_{R}]$ in eq. (18). Therefore, in this case the reduction base is orthogonal with respect to the total mass matrix.

Since methods 1 and 2 use a non-orthogonal base, inaccurate results are expected due to ill-conditioning of the reduced matrices. To avoid that, in methods 4 and 5 an orthogonalization step is introduced, which is applied to the acoustic and structural parts independently. This should enhance the results, since the independent fields can present very similar shapes across vectors; however, the downside of the method is that the initial reduction base contains twice as many vectors due to the splitting of the fields, and even though the final size depends on the number of vectors that are eliminated in the orthogonalization procedure, the reduced matrices will be larger and therefore more time consuming to solve. Method 3 uses the left and right eigenvectors, which are orthogonal with respect to the mass matrix, and should therefore form a complete expansion base that reduces the system accurately without increasing the size of the problem. However, there might be a benefit from separating the acoustic and structural fields due to the large scaling differences between the pressure values of the acoustic field and the displacement values of the structural field; therefore, in Method 6, this concept is introduced on top of the Method 3 approach. The performance of the different methods is evaluated in section 3.1.

2.2 Multi-Model Reduction

In order to use these reduction methods in optimization procedures, the reduction base would have to be calculated at each iteration, since the modal vectors will change when the values of the optimization parameters vary. However, this would be highly time consuming, and it is desirable to pre-construct the reduction base

outside the optimization loop. If the modal vectors are not highly sensitive to the optimization parameters, a reduction base could be formed with the modes of the initial model and used throughout the optimization; however, this is often not the case. Then, a reduction base can be formed with the modal vector matrices from several models where the design domain of the optimization parameters have been sampled.

The six methods described in section 2.1 should be modified by substituting the single-model modal matrices $[\boldsymbol{\psi}_L]$ and $[\boldsymbol{\psi}_R]$ by the multi-model modal matrices, formed as

$$[[\boldsymbol{\psi}_L]_1\,[\boldsymbol{\psi}_L]_2 \ldots [\boldsymbol{\psi}_L]_M] \tag{22}$$

$$[[\boldsymbol{\psi}_R]_1\,[\boldsymbol{\psi}_R]_2 \ldots [\boldsymbol{\psi}_R]_M]\,, \tag{23}$$

where $[\boldsymbol{\psi}_{L/R}]_j$ is the modal matrix of the j-th model and M is the total number of models included in the base. Since some of the modal vectors from different models will be very similar, an orthogonalization step must be added to methods 1, 2 and 3 (since methods 4, 5 and 6 already included one). The orthogonalization for methods 1, 2 and 3 is done following the procedure described for Method 4, but orthogonalizing the multi-model modal matrices with respect to the total mass matrix.

The number of models that need to be included and the sampling criteria of the design domain will be model-dependent. In section 3.2, the procedure to form an efficient base for the optimization of a plate model is discussed.

3. RESULTS

A model of a plate coupled to an air column is considered for testing the methods. The dimensions of the plate are $L_x = 4$ cm, $L_y = 3$ cm, and the objective is to optimize its thickness, which can vary between 10^{-5} m and 10^{-2} m. The air column is $Lz = 5$ cm high, and its walls are rigid, except for the side that is coupled to the plate. The frequency range of interest is between 100 Hz and 10 kHz. L_x is discretized with 20 elements, L_y is discretized with 16 elements and L_z is discretized with 25 elements, which means that the acoustic elements are hexahedra of 2x1.9x2 mm. The plate elements are formulated with 3 DOFs per node (one displacement and two rotations), and the acoustic elements are formulated with 1 DOF per node, and using linear shape functions, with the total number of DOFs resulting in 10353.

In section 3.1, the 6 methods introduced in section 2.1 are tested for 18 plate models where the thickness of each of the elements in the plate is defined by a random number between the aforementioned limits. In section 3.2, the efficiency of the methods introduced in section 2.2 is evaluated for the same 18 models, and the number of models that are needed to form an accurate base for the optimization of the plate is determined. The selected reduction bases are then used for the optimization of the plate thickness, and the results are shown and compared to full-model optimization results in section 3.3.

The accuracy of the methods is evaluated in terms of the modal frequencies, the modal vectors and the pressure frequency response at a point of the acoustic column. The error between the modal frequencies from the full system and the reduced system is evaluated as

$$f_{err} = \max_{n=1:N} \frac{|\,\mathbf{f}_{\mathbf{n_{Full}}} - \mathbf{f}_{\mathbf{n_{Red}}}\,|}{\mathbf{f}_{\mathbf{n_{Full}}}} \cdot 100, \tag{24}$$

where N is the highest modal frequency below the upper limit of 10 kHz. The modal vectors accuracy is evaluated by calculating the Modal Assurance Criterion (MAC) between the modal vectors resulting from the full and the reduced systems. The MAC matrix between two generic vector matrices $[\boldsymbol{\phi}]_A$ and $[\boldsymbol{\phi}]_B$ is calculated as

$$[\mathbf{MAC}](i,j) = \frac{|\,\{\boldsymbol{\phi}\}_{Ai}^T \{\boldsymbol{\phi}\}_{Bj}\,|^2}{(\{\boldsymbol{\phi}\}_{Ai}^T \{\boldsymbol{\phi}\}_{Ai})(\{\boldsymbol{\phi}\}_{Bj}^T \{\boldsymbol{\phi}\}_{Bj})} \tag{25}$$

for each vector pair ($i, j = 1 : N$). The MAC is bounded between 0 and 1, 1 indicating linearly dependent vectors, and 0 indicating orthogonal vectors. The minimum diagonal value of the MAC matrix of all modes below 10 kHz is used as accuracy indicator,

$$v_{acc} = \min_{n=1:N} [\mathbf{MAC}](n, n). \tag{26}$$

The accuracy of the pressure frequency response at a point at the upper corner of the acoustic domain when the plate is excited by a perpendicular point force at its central point is evaluated as the mean Sound Pressure Level (SPL) error in dB between the results of the full system and the reduced system. When the frequency response is sampled logarithmically at K points between 100 Hz and 10 kHz, the error is calculated as

$$\overline{\Delta L_p} = \frac{1}{K} \sum_{k=1}^{K} 20 \log \left(\frac{\mid p_{red}(k) \mid}{\mid p_{full}(k) \mid} \right). \tag{27}$$

where k is the k-th frequency line, and K is the total number of frequencies included in the analysis.

3.1 Single Model Reduction

The accuracy of the six methods has been evaluated for 18 plate models, where the thickness of each plate element is defined by a random number between the given limits (10^{-5} m and 10^{-2} m). The variation along 4 orders of magnitude is selected in order to test the effects of having a wide design space. The abrupt changes of thickness between neighbouring elements will have an effect on the acoustic domain which is not taken into account here, since this is not relevant for the purpose of testing the efficiency of the reduction methods. All modes under a given frequency limit are included in the reduction base. In this case, the limit has been varied between 10 kHz and 20 kHz, but no benefit of extending the frequency range above the upper considered frequency (10 kHz) can be seen in the results. Figure 1 shows the spread of the accuracy of each method for the 18 models, in terms of modal frequencies, modal vectors and SPL, calculated as in eqs. (24-27), versus the computational time required for solving the reduced eigenvalue problem and calculating the frequency response at 300 frequency lines. As a reference, using the full system, that calculation takes about 2 min.

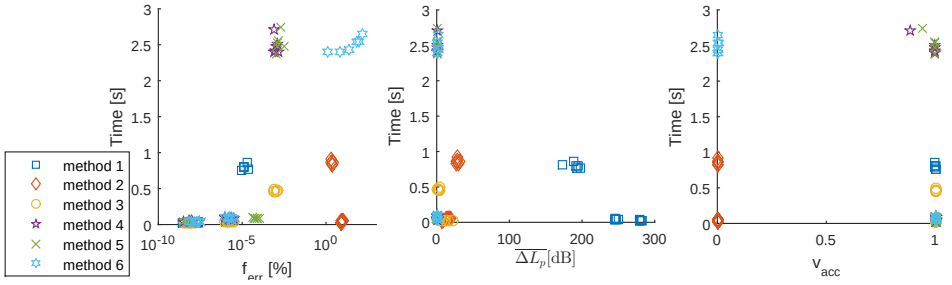

Figure 1: Accuracy and time consumption of solving the single-model reduced system with the 6 methods for 18 different thickness conditions of the plate.

The results show that Method 2 presents poor accuracy in terms of modal frequencies and vectors, and Method 1 shows the worst accuracy in terms of the frequency response. Method 3 is the least time consuming overall, and shows good accuracy in terms of modal frequencies and vectors, but presents significant SPL errors for some of the samples. Methods 4 and 5 present the best accuracy overall, however, they are more time consuming than the rest. Regarding Method 6, the accuracy is poor in terms of modal vectors for some

of the samples, and it is as time consuming as methods 4 and 5.

Looking at the calculated frequency responses for Method 3, it can be seen that the amplitude is correct around the peaks, and the errors arise around the antiresonances, which indicates that the errors may be due to a poor approximation of the phase shifts between modes. The choice of the best method for each application should be a compromise between required accuracy (where Methods 4 or 5 are best) and speed (where Method 3 is best).

3.2 Multi-Model Reduction

In order to construct a reduction base that can be used to optimize the plate, several models where the domain of the optimization parameters is sampled should be included. The thickness of each plate element is a parameter to be optimized, therefore there are 16x20=320 optimization parameters. Due to the large number of variables, a random sampling of the design space is used. Given that the parameter domain varies through 4 orders of magnitude (10^{-5} mm to 10^{-2} mm), and the modal parameters are more sensitive to relative than linear changes of the design variables, the models for the reduction base are calculated as vectors of random numbers drawn from the uniform distributions

$$\text{Model}\,1 : \mathbf{t} \sim U([0, 10^{-2}]) \tag{28}$$

$$\text{Model}\,2 : \mathbf{t} \sim U([0, 10^{-3}]) \tag{29}$$

$$\text{Model}\,3 : \mathbf{t} \sim U([0, 10^{-4}]) \tag{30}$$

$$\text{Model}\,4 : \mathbf{t} \sim U([0, 10^{-5}]). \tag{31}$$

For higher number of models, the sequence is repeated (i.e. Model 5 is generated as Model 1, etc.). For each model, all modes below 10 kHz are included in the reduction base. In order to determine the number of models necessary for each of the 6 available methods to obtain an accurate reduced system, three criteria are considered,

$$f_{err} < 1\% \tag{32}$$

$$v_{acc} > 0.9 \tag{33}$$

$$\overline{\Delta L_p} < 1\,\text{dB}, \tag{34}$$

which are evaluated at the 18 different design points that were used in section 3.1. The results for the 6 methods have been analysed for a number of models ranging between 1 and 20. Methods 1 and 2 do not reach the required accuracy for any of the tested number of models, therefore, they will not be considered further. For methods 4, 5 and 6, 8 models are sufficient to fulfil the requirements at all tested points, and for Method 3, 20 models yield good accuracy for most of the points, but low MAC values for a few points. Adding more models does not improve the results in terms of the MAC and increases the calculation times, therefore the 20 model option is selected as the most efficient for Method 3.

Figure 2 shows the spread of the results when 20 models are used for Method 3, and 8 models are used for Methods 4, 5 and 6. It can be seen that Method 3 is still faster than methods 4 and 5, even if more models are included in the base. However, Method 6 presents solving times on the same range as Method 3, and a good accuracy for all points; therefore, this seems to be the most efficient option regarding both accuracy and speed.

It should be noticed that the results between the single-model and the multi-model reduction experiments show quite different tendencies for Method 6, which was not working well for single-model reduction, but is the most efficient method for multi-model reduction. This indicates that the method benefits from having a wider initial sample of vectors to create an orthogonal base.

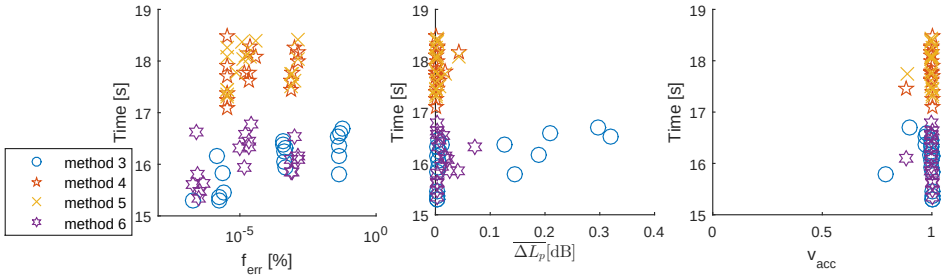

Figure 2: Accuracy and time consumption of solving the multi-model reduced system with the 6 methods for 18 different thickness conditions of the plate.

3.3 Optimization of a plate

In this section, the thickness of the plate elements is optimized for two different objectives with the full and the selected MMR reduced models, and the results are compared.

3.3.1 Optimization of modal frequencies

As a starting point, a plate with a constant thickness of 0.1 mm is considered. The structure-acoustic interaction in this case is strong, which means that the modal frequencies for the uncoupled and the coupled system are quite different. The optimization problem consists in modifying the thickness of the plate so that the modal frequencies below 10 kHz are the same as for the uncoupled plate of 0.1 mm of thickness. In other words, the influence of the acoustic domain in terms of modal frequencies should be removed.

The objective function is defined as

$$g(\mathbf{t}) = \sum_{i=1}^{N} \left(\omega_c^i(\mathbf{t})^2 - {\omega_u^i}^2 \right)^2 \tag{35}$$

where $\mathbf{t}$ is the vector of thicknesses of the elements, N is the number of modal frequencies below 10 kHz, ω_c^i is the i-th modal frequency of the coupled plate and ω_u^i is the i-th modal frequency of the uncoupled plate with 0.1 mm thickness. The gradient of the objective function is

$$\frac{dg(\mathbf{t})}{dt_j} = 2 \left(\omega_c^i(\mathbf{t})^2 - {\omega_u^i}^2 \right) [\boldsymbol{\psi}_L(\mathbf{t})]^T \frac{\partial [\mathbf{S}(\mathbf{t})]}{\partial t_j} [\boldsymbol{\psi}_R(\mathbf{t})], \tag{36}$$

where t_j is the thickness of the j-th element, and

$$\frac{\partial [\mathbf{S}(\mathbf{t})]}{\partial t_j} = \left(\frac{\partial [\mathbf{K}(\mathbf{t})]}{\partial t_j} - \omega_c^i(\mathbf{t})^2 \frac{\partial [\mathbf{M}(\mathbf{t})]}{\partial t_j} \right). \tag{37}$$

Therefore, it is required from the reduced model that the modal frequencies and the left and right modal vectors are accurately calculated.

The constrained optimization algorithm implemented in the Matlab Optimization Toolbox [16] function *fmincon* is used for the optimization (a detailed description of this method can be found in Ref. [17]). The analytical expression of the gradient is supplied, and the Hessian is approximated by a quasi-Newton method.

Each objective function evaluation takes on average 5.2 s when using the full system, 3.4 s for the system reduced with Method 3, 3.8 s with Method 4 and 3.5 s with Method 6. The resulting thickness designs when using the full system, and the reduction methods 3, 4 and 6 are shown in Figure 3. It can be seen that the

designs resemble much each other, and the mean errors between the results of the reduced methods and the full system are $1.76 \cdot 10^{-5}$ for Method 3, $1.27 \cdot 10^{-5}$ for Method 4 and $1.72 \cdot 10^{-5}$ for Method 6, which shows that the accuracy of the three methods is in the same range.

3.3.2 Optimization of compliance

In this case, the compliance of the system is to be maximized when the plate is excited by a unitary point force on its central point and the sum off all thicknesses is constrained below 0.05 mm. The objective function is

$$g(\mathbf{t}) = \sum_{k=1}^{K} \mid \mathbf{u}(k,\mathbf{t})^T \mathbf{f} \mid \tag{38}$$

where $\mathbf{u}$ is the vector of displacements and pressures, $\mathbf{f}$ is the input force vector, $\mathbf{t}$ is the vector of thicknesses, k is the k-th frequency line and K is the total number of frequencies included in the optimization, in this case, 100 frequency lines sampled logarithmically between 100 Hz and 10 kHz. The gradient can be calculated as

$$\frac{dg(\mathbf{t})}{dt_j} = \sum_{k=1}^{K} -\text{sgn}(\mathbf{u}(k,\mathbf{t})^T \mathbf{f}) \mathbf{u}(k,\mathbf{t})^T \frac{\partial[\mathbf{S}(k,\mathbf{t})]}{\partial t_j} \mathbf{u}(k,\mathbf{t}) \tag{39}$$

with

$$\frac{\partial[\mathbf{S}(k,\mathbf{t})]}{\partial t_j} = \left(\frac{\partial[\mathbf{K}(\mathbf{t})]}{\partial t_j} - \omega_k(\mathbf{t})^2 \frac{\partial[\mathbf{M}(\mathbf{t})]}{\partial t_j} \right). \tag{40}$$

Therefore, in this case the accuracy of the displacement values is the main requirement from the reduced systems.

Each objective function evaluation takes on average 50 s when using the full system, 6.7 s for the system reduced with Method 3, 7.5 s with Method 4 and 7 s with Method 6. Figure 4 shows the designs obtained with the full and the reduced systems. The designs show larger differences than in the case of optimization of modal frequencies. This is due to the fact that the accuracy of the displacement vectors is lower than the accuracy of the modal frequencies, and even though the error is small, the deviations propagate through the optimization steps and result in significant differences in the result. However, there are many solutions to this optimization problem; therefore, the small deviations on the sensitivities lead to different results, which are not necessarily wrong. In this case, the four designs are quite different, but yield a similar final value of the compliance. If the objective function had a unique minimum, all methods would probably converge towards the same point eventually.

4. CONCLUSIONS

In this paper, several model reduction methods have been compared for a model of a plate coupled to an air column. For single-model reduction, using left and right modal vectors has been found to be the fastest approach. However, using only one kind of modal vectors and separating the acoustic and structural fields in the reduction base has shown a better accuracy. When combining both approaches, a poorer performance has been achieved. On the other hand, for multi-model reduction, the combined approach has performed more efficiently than the rest of the methods. All methods have been found to be accurate enough when optimizing the thickness of a plate to match certain modal frequencies. When optimizing the compliance, different designs have been reached by the different methods due to small deviations of the displacement vector leading to different paths in the optimization process. However, all designs are optimized for a reduced compliance; therefore, the results would be usable in any case. The multi-model reduction approach has been shown to be efficient for the presented cases, where the calculation time of the optimizations is dramatically reduced when using the reduced systems.

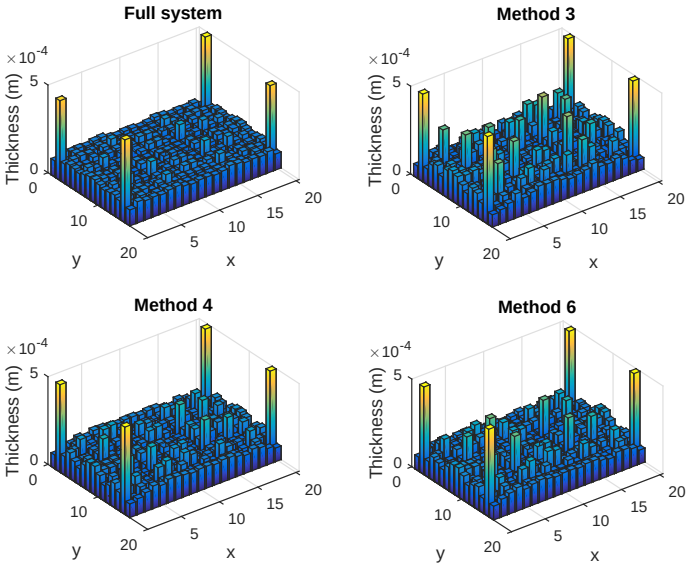

Figure 3: Thickness designs obtained with the full system and the three reduction methods for the optimization of modal frequencies.

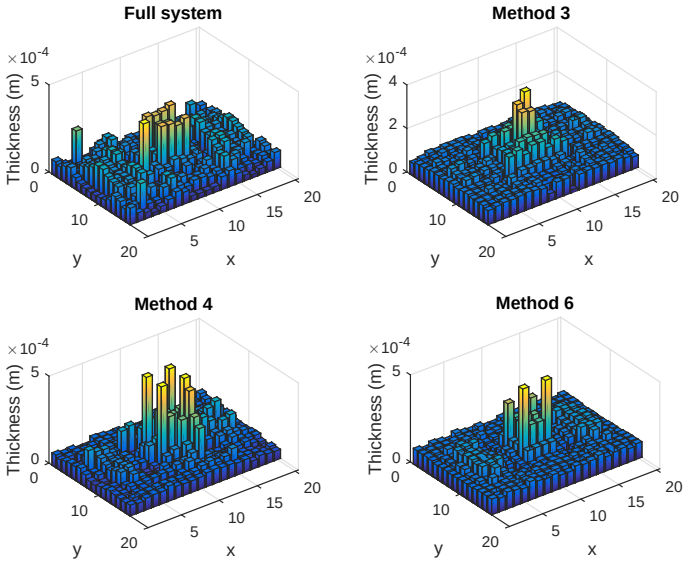

Figure 4: Thickness designs obtained with the full system and the three reduction methods for the optimization of the compliance.

REFERENCES

[1] M. B. Sondergaard and C. B. W. Pedersen. Applied topology optimization of vibro-acoustic hearing instrument models. *Journal of Sound and Vibration*, 333(3):683–692, 2014.

[2] L. Friis. *Investigation of internal feedback in hearing aids*. PhD thesis, Technical University of Denmark, 2009.

[3] L. Friis and Mogens Ohlrich. Vibration modeling of structural fuzzy with continuous boundary. *Journal of the Acoustical Society of America*, 123(2):718–728, 2008.

[4] R. R. Craig and M. C. C. Bampton. Coupling of substructures for dynamic analyses. *AIAA Journal*, 6(7):1313–1319, 1968.

[5] R. R. Craig. Coupling of substructures for dynamic analyses: an overview. *Collection of Technical Papers - AIAA/ASME/ASCE/AHS/ASC Structures, Structural Dynamics and Materials Conference*, 5:3–14, 2000.

[6] P. Davidsson and G. Sandberg. A reduction method for structure-acoustic and poroelastic-acoustic problems using interface-dependent lanczos vectors. *Computer Methods in Applied Mechanics and Engineering*, 195(17-18):1933–1945, 2006.

[7] M. Stammberger and H. Voss. Automated multi-level substructuring for a fluid-solid vibration problem. *Numerical Mathematics and Advanced Applications*, pages 563–570, 2008.

[8] M. Maess and L. Gaul. Substructuring and model reduction of pipe components interacting with acoustic fluids. *Mechanical Systems and Signal Processing*, 20(1):45–64, 2006.

[9] S. Donders, B. Pluymers, P. Ragnarsson, R. Hadjit, and W. Desmet. The wave-based substructuring approach for the efficient description of interface dynamics in substructuring. *Journal of Sound and Vibration*, 329(8):1062–1080, 2010.

[10] J. Herrmann, M. Maess, and L. Gaul. Substructuring including interface reduction for the efficient vibro-acoustic simulation of fluid-filled piping systems. *Mechanical Systems and Signal Processing*, 24(1):153–163, 2010.

[11] C. Pal and I. Hagiwara. Dynamic analysis of a coupled structural-acoustic problem - simultaneous multimodal reduction of vehicle interior noise level by combined optimization. *Finite Elements in Analysis and Design*, 14(2-3):225–234, 1993.

[12] L. Hermans and M. Brughmans. Enabling vibro-acoustic optimization in a superelement environment: A case study. *Proceedings of the International Modal Analysis Conference and Exhibit*, 2:1146–1152, 2000.

[13] E. Balmès. Parametric families of reduced finite element models. theory and applications. *Mechanical Systems and Signal Processing*, 8(8):381–394, 1994.

[14] Z. Ma. Development of a new mode-superposition technique for modal frequency response analysis of coupled acoustic-structural systems. *Finite Elements in Analysis and Design*, 14(2-3):209–223, 1993.

[15] G.H. Golub and C.F. van Loan. *Matrix computations*. The Johns Hopkins University Press, 1996.

[16] *MATLAB optimization toolbox user's guide R2015b*. MathWorks, Natick, MA, 2015.

[17] Richard H. Byrd, Mary E. Hribar, and Jorge Nocedal. An interior point algorithm for large-scale nonlinear programming. *Siam Journal on Optimization*, 9(4):877–900, April 1999.

Paper C

Model reduction for optimization of structural-acoustic coupling problems

Model reduction for optimization of structural-acoustic coupling problems

E. Creixell-Mediante [1,2], **J. S. Jensen** [1], **J. Brunskog** [1], **M. Larsen** [2]
[1] Danmarks Tekniske Universitet (DTU), Acoustic Technology, Department of Electrical Engineering, Ørsteds Plads 352, 2800, Kgs. Lyngby, Denmark
e-mail: **ecrme@elektro.dtu.dk**

[2] Oticon A/S,
Kongebakken 9, 9765 Smørum, Denmark

Abstract
Fully coupled structural-acoustic models of complex systems, such as those used in the hearing aid field, may have several hundreds of thousands of nodes. When there is a strong structure-acoustic interaction, performing optimization on one part requires the complete model to be taken into account, which becomes highly time consuming since many iterations may be required. The use of model reduction techniques to speed up the computations is studied in this work. The Component Mode Synthesis (CMS) method and the Multi-Model Reduction (MMR) method are adapted for problems with structure-acoustic coupling, for which two different approaches to constructing a modal reduction base are discussed. The efficiency and accuracy of the CMS and the MMR methods are strongly model-dependent; in this paper, they are compared for two optimization problems in the hearing aid context, where the MMR technique is found to be the most efficient, speeding up the optimizations up to 6 times compared to the full model.

1 Introduction

Simulation is gaining relevance in industrial design procedures, which have evolved from a purely prototyping and testing approach to a context where numerical simulation is used from the early phases. Obtaining reliable models is a key point for the design process to be efficient, and as more and more accuracy is required, the complexity of the models increases. This is the case in the hearing aid field, where the high number of small parts that form the devices and the strong structure-acoustic interaction require models with a high number of degrees of freedom in order to capture the physical behaviour accurately.

There is an interest in the industry to perform tasks such as optimization or uncertainty analysis, where the numerical model must be solved iteratively for numerous combinations of the studied parameters. Performing optimization on one part requires the complete model to be taken into account when there is a strong acoustic-mechanical interaction, since the multiple vibrational and acoustic transmission paths between parts have a significant influence; therefore, these processes can become very time consuming. Recently, a topology optimization study including structure-acoustic interaction was performed on a part of a hearing instrument [1]. However, some simplifications in terms of frequency resolution and detail of the model were done to ease the process, for which the effects are difficult to control. Thus, in order to make it practically possible to perform optimization on accurate models, reliable and efficient reduction techniques need to be developed.

Substructuring is a widely used approach for the reduction of Finite Element (FE) models, which consists in dividing the model of the complete structure into substructures, obtaining reduced order models of each sub-

structure and coupling them at the interface Degrees Of Freedom (DOFs). The Component Mode Synthesis (CMS) method [2,3] is a substructuring technique that has been widely used in the context of large problems that require too high computational effort to be solved as a whole. This technique could also be beneficial for optimization purposes, where the part to be optimized would be left as a detailed FE model which would be updated at each iteration, and coupled with the rest of the model, reduced in one unchanging substructure. The reduction of the substructure is done by a transformation matrix that is constructed with vibration modes and interface-dependent static modes, the latter making the size of the reduced models strongly dependent on the number of interface DOFs. It is worth noticing that the reduced matrices become full due to the transformation of coordinates, while the full FE models present sparse matrices that can be solved more efficiently with high-performance sparse solvers; therefore, the ratio between the interface and the total DOFs must be sufficiently small for the operation to yield a reduction in calculation time. The efficiency of the reduction is therefore strongly model-dependent. Interface reduction methods have been developed to tackle this issue, as described in Refs. [4, 5], which consist in applying a modal-based reduction on the interface DOFs in a similar way as for the interior DOFs.

An alternative is reducing the complete system with a transformation matrix constructed only with vibration modes, eliminating the need for interface-dependent modes and for keeping full FE model parts. The size of the reduced matrices would then be equal to the number of modes included in the transformation matrix, and can be used for frequency response calculation at a large number of frequencies in a very short time. However, when varying parameter values, the modal base must be re-calculated, which implies solving the eigenvalue problem to obtain the new modes of vibration at each iteration in an optimization context (unless the modal vectors are not sensitive to changes in the optimization parameters, as assumed in Refs. [6] and [7]). This would still be too time-consuming, and it is therefore desirable to construct a reduction base that can reduce the model accurately for any parameter value, which gives rise to the Multi-Model Reduction (MMR) approach. Here, the transformation matrix is formed with vibration modes from a family of models with varying values of the parameters [8], which sample the parameter domain finely enough for the reduction base to describe the model accurately at any design point. The size of the reduced system will depend on the number of models that need to be included in the base; thus, the efficiency of the MMR method is also strongly model-dependent.

Both suggested methods include vibration modes in their transformation matrix. For structural problems, the modal vectors are orthogonal, which makes them suitable as a transformation base. However, for coupled structural-acoustic problems, the system matrices become unsymmetric due to the coupling terms when the pressure-displacement formulation is used, which yields non-orthogonal modal vectors. Therefore, those cannot be directly included in the transformation matrix. One approach to obtaining an orthogonal base is using the uncoupled modes, which can be efficient for problems with weak coupling, but becomes inefficient when the structure-acoustic interaction is strong, as a large amount of modes should be included in the reduction base [9]. Since the coupled eigenvectors can better describe the system, it is desirable to use them to obtain smaller reduction bases. One option consists in building two transformation matrices with the left modal vectors and the right modal vectors, since the two combined sets are orthogonal with respect to the system matrices [10]. Another approach consists in orthogonalizing the set of right eigenvectors, where the acoustic and structural fields of the vectors can be separated and orthogonalized with respect to the acoustic and structural mass matrices, respectively, in order to improve the numerical stability of the base [11].

In this paper, the CMS and the MMR methods are adapted for problems with structure-acoustic interaction by using the two different approaches to forming modal bases. The methods are described in Section 2, and in Section 3 the different techniques are compared in terms of efficiency and accuracy for optimization of different hearing parts in a simplified hearing aid model.

2 Reduction bases for coupled problems

The model reduction procedure for the Component Mode Synthesis method and the Multi-Model Reduction method, adapted for problems with structure-acoustic interaction, is described here. In Section 2.1, two different approaches to forming the modal bases are described, and in Sections 2.2 and 2.3 the procedure to include them in the CMS and the MMR methods is shown.

2.1 Modal bases for coupled problems

For an undamped system, the FE pressure-displacement formulation yields the coupled eigenvalue problem

$$\left(\begin{bmatrix} [\mathbf{K}_s] & -[\mathbf{S}]^T \\ \mathbf{0} & [\mathbf{K}_a] \end{bmatrix} - \omega_i^2 \begin{bmatrix} [\mathbf{M}_s] & [\mathbf{0}] \\ \rho_a[\mathbf{S}] & [\mathbf{M}_a] \end{bmatrix} \right) \begin{Bmatrix} \{\boldsymbol{\psi}_{sR}^i\} \\ \{\boldsymbol{\psi}_{aR}^i\} \end{Bmatrix} = \begin{Bmatrix} \{\mathbf{0}\} \\ \{\mathbf{0}\} \end{Bmatrix} \tag{1}$$

where $[\mathbf{K}_s]$ and $[\mathbf{M}_s]$ are the structural stiffness and mass matrices, $[\mathbf{K}_a]$ and $[\mathbf{M}_a]$ are the acoustic stiffness and mass matrices, $[\mathbf{S}]$ is the coupling matrix, ρ_a is the density of the acoustic medium, ω_i is the i-th modal angular frequency, $\{\boldsymbol{\psi}_{sR}^i\}$ is the structural displacement part of the i-th right modal vector and $\{\boldsymbol{\psi}_{aR}^i\}$ is the acoustic pressure part of the i-th right modal vector.

For the sake of notation clarity in the following sections, let us introduce $[\mathbf{M}]$ and $[\mathbf{K}]$ as the coupled mass and stiffness matrices, $\{\boldsymbol{\psi}_R^i\}$ as the i-th complete right eigenvector and $\{\boldsymbol{\psi}_L^i\}$ as the i-th complete left eigenvector, the latter being the result from solving the transposed eigenvalue problem,

$$([\mathbf{K}]^T - \omega_i^2[\mathbf{M}]^T)\{\boldsymbol{\psi}_L^i\} = \{\mathbf{0}\}. \tag{2}$$

Moreover, let us define the truncated modal matrices as $[\boldsymbol{\psi}_L] = [\{\boldsymbol{\psi}_L^1\} \dots \{\boldsymbol{\psi}_L^N\}]$, $[\boldsymbol{\psi}_R] = [\{\boldsymbol{\psi}_R^1\} \dots \{\boldsymbol{\psi}_R^N\}]$, $[\boldsymbol{\psi}_{aL}] = [\{\boldsymbol{\psi}_{aL}^1\} \dots \{\boldsymbol{\psi}_{aL}^N\}]$, $[\boldsymbol{\psi}_{sL}] = [\{\boldsymbol{\psi}_{sL}^1\} \dots \{\boldsymbol{\psi}_{sL}^N\}]$, $[\boldsymbol{\psi}_{aR}] = [\{\boldsymbol{\psi}_{aR}^1\} \dots \{\boldsymbol{\psi}_{aR}^N\}]$ and $[\boldsymbol{\psi}_{sR}] = [\{\boldsymbol{\psi}_{sR}^1\} \dots \{\boldsymbol{\psi}_{sR}^N\}]$, where N is the number of modes included in the modal matrix.

The right eigenvectors from unsymmetric eigenvalue problems are not orthogonal, which makes them unsuitable as a reduction base. However, the left and right eigenvectors form an orthogonal base with respect to the unsymmetric mass matrix, $[\boldsymbol{\psi}_L][\mathbf{M}][\boldsymbol{\psi}_R] = [\mathbf{I}]$; therefore, they can be used together to reduce the system. Another option consists in orthogonalizing the set of right eigenvectors, as done in ref. [11], where the acoustic and structural parts of the coupled eigenvectors are separated and orthogonalized with respect to the acoustic and structural mass matrices, respectively. The two modal base construction methods are described in detail in the following, where $[\boldsymbol{\Phi}_L]$ refers to the left reduction base, and $[\boldsymbol{\Phi}_R]$ to the right reduction base, meaning that the reduced system matrices would be calculated as

$$[\mathbf{M}_{red}] = [\boldsymbol{\Phi}_L][\mathbf{M}][\boldsymbol{\Phi}_R] \tag{3}$$

$$[\mathbf{K}_{red}] = [\boldsymbol{\Phi}_L][\mathbf{K}][\boldsymbol{\Phi}_R]. \tag{4}$$

2.1.1 Left-Right Method

Here, the right eigenvectors are used for the right reduction matrix, and the left eigenvectors for the left reduction matrix,

$$[\boldsymbol{\Phi}_L] = [\boldsymbol{\psi}_L] \tag{5}$$

$$[\boldsymbol{\Phi}_R] = [\boldsymbol{\psi}_R]. \tag{6}$$

Consequently, the reduced mass matrix in eq. (3) becomes the identity matrix and the reduced stiffness matrix becomes a diagonal matrix with the eigenvalues at the diagonal. The size of the reduced matrices equals the number of vectors included in the base.

2.1.2 Split Field Method

The matrices are formed by separating the acoustic and structural parts of the coupled right eigenvectors and orthogonalizing them with respect to the acoustic and structural mass matrices, respectively. The reason for separating the fields is that the independent fields can be very similar across some of the modal vectors, and those linear dependencies can be better detected when orthogonalizing them with respect to their mass matrices, since they present large magnitude differences between the structural and the acoustic case. The modal matrices are orthogonalized so that

$$[\hat{\boldsymbol{\psi}}_{aR}]^T[\mathbf{M}_a][\hat{\boldsymbol{\psi}}_{aR}] = [\mathbf{I}] \tag{7}$$

$$[\hat{\boldsymbol{\psi}}_{sR}]^T[\mathbf{M}_s][\hat{\boldsymbol{\psi}}_{sR}] = [\mathbf{I}], \tag{8}$$

where the $\hat{}$ symbol indicates that the matrix has been orthogonalized following the procedure described in Appendix A, and grouping them in the transformation matrices,

$$[\boldsymbol{\Phi}_L] = [\boldsymbol{\Phi}_R] = \begin{bmatrix} [\hat{\boldsymbol{\psi}}_{sR}] & [\mathbf{0}] \\ [\mathbf{0}] & [\hat{\boldsymbol{\psi}}_{aR}] \end{bmatrix}. \tag{9}$$

In this way, the structure of the complete unsymmetric problem in eq. (1) is preserved in the reduced problem, but the base is not orthogonal with respect to the total mass or stiffness matrices.

Even though the vectors used in the Left-Right Method form a complete base, orthogonalizing the independent fields might yield more numerically stable results due to the detection of collinearities in the independent fields. The downside of the Split Field Method is that the initial reduction base contains twice as many vectors due to the splitting of the fields, and even though the final size depends on the number of vectors that are eliminated in the orthogonalization procedure, the reduced matrices will be larger and therefore more time consuming to solve.

2.2 Component Mode Synthesis

The Component Mode Synthesis Method consists in dividing the structure into several substructures, reducing them, and coupling the reduced parts by their interface DOFs. The reduction base must contain vibration modes and coupling modes, which can be of different kinds, as summarized in ref. [3]. In this study, the Craig-Bampton method [2] is considered, and adapted for structure-acoustic coupling cases by calculating the modal bases according to Section 2.1. The reduction and coupling of substructures is done following the classical procedure, summarized in this section.

The Craig-Bampton transformation matrix includes vibration modes of the substructures with fixed interface DOFs, and coupling modes calculated as a static reduction, $[\boldsymbol{\Theta}] = [-\mathbf{K_{ii}} \backslash \mathbf{K_{ib}}]$, where i are interior DOFs and b are boundary (interface) DOFs. For coupled problems, two transformation matrices are formed, as

$$[\mathbf{T}_L] = \begin{bmatrix} [\boldsymbol{\Phi}_L] & [\boldsymbol{\Theta}] \\ [\mathbf{0}] & [\mathbf{I}] \end{bmatrix} \tag{10}$$

$$[\mathbf{T}_R] = \begin{bmatrix} [\mathbf{\Phi}_R] & [\mathbf{\Theta}] \\ [\mathbf{0}] & [\mathbf{I}] \end{bmatrix}. \tag{11}$$

$[\mathbf{\Phi}_L]$ and $[\mathbf{\Phi}_R]$ can be calculated using the Left-Right Method or the Split Field Method, using substructure fixed-interface modal vectors as the initial modal matrices $[\boldsymbol{\psi}_L]$ and $[\boldsymbol{\psi}_R]$ or $[\boldsymbol{\psi}_{Ra}]$ and $[\boldsymbol{\psi}_{Rs}]$.

The displacement coordinates, $\mathbf{x}$, are then reduced to a set of generalized coordinates, $\mathbf{u}$, as

$$\left\{ \begin{array}{c} \mathbf{x_i} \\ \mathbf{x_b} \end{array} \right\} = \begin{bmatrix} [\mathbf{\Phi}_R] & [\mathbf{\Theta}] \\ [\mathbf{0}] & [\mathbf{I}] \end{bmatrix} \left\{ \begin{array}{c} \mathbf{u_i} \\ \mathbf{u_b} \end{array} \right\}, \tag{12}$$

where the boundary DOFs remain unchanged, so $\mathbf{u_b} = \mathbf{x_b}$, and $\mathbf{u_i}$ are the modal coordinates. Substituting this transformation into the equation of motion and pre-multiplying it by $[\mathbf{T}_L]^T$, the problem in eq. (1) is reduced to

$$([\mathbf{T}_L]^T[\mathbf{K}][\mathbf{T}_R] - \omega^2[\mathbf{T}_L]^T[\mathbf{M}][\mathbf{T}_R])\{\mathbf{u}\} = [\mathbf{T}_L]^T\{\mathbf{f}\}. \tag{13}$$

where the reduced mass and stiffness matrices can also be split into interior DOFs (corresponding to modal coordinates) and boundary DOFs,

$$[\mathbf{M_r}] = [\mathbf{T}_L]^T[\mathbf{M}][\mathbf{T}_R] = \begin{bmatrix} [\mathbf{M}_{r_{ii}}] & [\mathbf{M}_{r_{ib}}] \\ [\mathbf{M}_{r_{bi}}] & [\mathbf{M}_{r_{bb}}] \end{bmatrix} \tag{14}$$

$$[\mathbf{K_r}] = [\mathbf{T}_L]^T[\mathbf{K}][\mathbf{T}_R] = \begin{bmatrix} [\mathbf{K}_{r_{ii}}] & [\mathbf{K}_{rib}] \\ [\mathbf{K}_{r_{bi}}] & [\mathbf{K}_{r_{bb}}] \end{bmatrix}. \tag{15}$$

The coupling of substructures enforces displacement continuity at the boundary, namely $\mathbf{x_b^i} = \mathbf{x_b^j}$ for two substructures i and j. For the case of one reduced substructure (1) coupled to one unreduced substructure (2), the total mass and stiffness matrices become

$$[\mathbf{M_{CMS}}] = \begin{bmatrix} [\mathbf{M}^1_{r_{ii}}] & [\mathbf{0}] & [\mathbf{M}^1_{r_{ib}}] \\ [\mathbf{0}] & [\mathbf{M}^2_{ii}] & [\mathbf{M}^2_{ib}] \\ [\mathbf{M}^1_{r_{bi}}] & [\mathbf{M}^2_{bi}] & [\mathbf{M}^1_{r_{bb}}] + [\mathbf{M}^2_{bb}] \end{bmatrix} \tag{16}$$

$$[\mathbf{K_{CMS}}] = \begin{bmatrix} [\mathbf{K}^1_{r_{ii}}] & [\mathbf{0}] & [\mathbf{K}^1_{r_{ib}}] \\ [\mathbf{0}] & [\mathbf{K}^2_{ii}] & [\mathbf{K}^2_{ib}] \\ [\mathbf{K}^1_{r_{bi}}] & [\mathbf{K}^2_{bi}] & [\mathbf{K}^1_{r_{bb}}] + [\mathbf{K}^2_{bb}] \end{bmatrix}. \tag{17}$$

Therefore, the size of the reduced matrices equals the size of the unreduced substructure matrices plus the number of vibration modes included in the reduction. The matrices of the reduced substructure become full due to the reduction process, while the FE matrices of the unreduced system are sparse. Since pure FE models can be solved very efficiently by optimized sparse solvers, the reduced system must be significantly smaller in order to achieve a reduction in solving time.

2.3 Multi-Model Reduction

The Multi-Model Reduction technique consists in reducing the whole model with global vibration modes. Since the parts affected by the parameters are included in the reduction, the modal vectors will vary across the design domain, and the reduction base of the initial model will not be valid for all design points. It would be highly time consuming to re-compute the base at each point, therefore, it is desirable to construct

a transformation matrix that is valid throughout the design domain. The MMR technique consists in building a reduction base with the modal vector matrices from several models, where the design domain of the parameters has been sampled, and assuming that the reduction will be accurate enough at the points that are not included in the base. Constructing this reduction base requires solving the full problem at a number design points, which should be significantly lower than the number of function evaluations required in the parameter study for the reduction to be efficient.

The modal base construction methods described in Section 2.1 can be used here by substituting the single-model modal matrices by the multi-model modal matrices. For the Left-Right Method,

$$[\boldsymbol{\Psi}_L] = [[\boldsymbol{\psi}_L]_1\,[\boldsymbol{\psi}_L]_2 \ldots [\boldsymbol{\psi}_L]_M] \tag{18}$$

$$[\boldsymbol{\Psi}_R] = [[\boldsymbol{\psi}_R]_1\,[\boldsymbol{\psi}_R]_2 \ldots [\boldsymbol{\psi}_R]_M]\,, \tag{19}$$

and for the Field Split Method

$$[\boldsymbol{\Psi}_{aR}] = [[\boldsymbol{\psi}_{aR}]_1\,[\boldsymbol{\psi}_{aR}]_2 \ldots [\boldsymbol{\psi}_{aR}]_M] \tag{20}$$

$$[\boldsymbol{\Psi}_{sR}] = [[\boldsymbol{\psi}_{sR}]_1\,[\boldsymbol{\psi}_{sR}]_2 \ldots [\boldsymbol{\psi}_{sR}]_M]\,, \tag{21}$$

where M is the total number of models included in the base. Since some of the modal vectors from different models will be very similar, an orthogonalization step must be added to the Left-Right Method (the Field Split Method already includes this step). The orthogonalization is done following the procedure described in Appendix A, but orthogonalizing the multi-model modal matrices with respect to the total mass matrix. Therefore, the transformation matrices for the Left-Right Method become

$$[\mathbf{T}_L] = [\hat{\boldsymbol{\Psi}}_L] \tag{22}$$

$$[\mathbf{T}_R] = [\hat{\boldsymbol{\Psi}}_R] \tag{23}$$

and for the Field Split Method,

$$[\mathbf{T}_L] = [\mathbf{T}_R] = \begin{bmatrix} [\hat{\boldsymbol{\Psi}}_{sR}] & [\mathbf{0}] \\ [\mathbf{0}] & [\hat{\boldsymbol{\Psi}}_{aR}] \end{bmatrix}, \tag{24}$$

which reduce the system matrices as

$$[\mathbf{M}_{\mathbf{MMR}}] = [\mathbf{T}_L]^T[\mathbf{M}][\mathbf{T}_R] \tag{25}$$

$$[\mathbf{K}_{\mathbf{MMR}}] = [\mathbf{T}_L]^T[\mathbf{K}][\mathbf{T}_R]. \tag{26}$$

The number of models that need to be included in the base will be model-dependent. The procedure of eliminating linearly dependent modes and determining which models to include in the base is not a trivial matter and has a strong influence on the accuracy of the results. The procedure used in this work is described in appendix A and section 3. The final size of the reduced matrices will be the number of models included in the reduction base times the number of modes per model, and with the number of modes eliminated at the orthogonalization phase subtracted. The reduced matrices also become full in this case, therefore, the method will only be efficient if the number of modes included in the base is significantly lower than the total number of DOFs of the full system.

3 Optimization of hearing aid parts

A simplified model of a Hearing Instrument (HI), shown in Figure 1, is considered. The lower part of the tube is fixed, and a unitary volume velocity is applied at the excitation point, simulating the receiver excitation. The Young's modulus and thickness of the tube and the suspension are to be optimized for minimizing the displacement in the X direction at the microphone position. After a convergence check, the mesh of the complete model is formed by 23166 elements and 39673 nodes, resulting in a total of 90803 DOFs, and the nominal material properties are listed in Table 1. The meshing and formulation of the stiffness and mass matrices is done in ANSYS, and the matrices are imported into MATLAB, where the mode calculation, reduction and optimization are done.

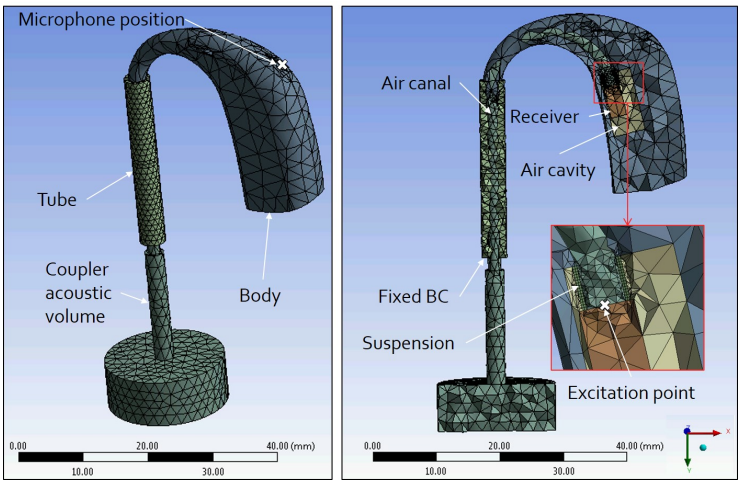

Figure 1: Simplified hearing aid model

	Density [kg/m^3]	E-modulus [Pa]	Poisson ratio
Body	1040	$2 \cdot 10^9$	0.4
Tube	1300	$1 \cdot 10^8$	0.4
Receiver	7850	$2 \cdot 10^{11}$	0.3
Suspension	1100	$6 \cdot 10^6$	0.49

Table 1: Nominal material properties of the HI

The displacement is to be minimized between 100 Hz and 10 kHz, and the objective function is formulated as the sum of the displacement over the frequency range, in dB, as a function of the Young's modulus (E) and the thickness (t) of the part being optimized,

$$g(E,t) = 10 \log \left(\sum_{k=1}^{K} \mathbf{x_d^2}(E,t) \right) \tag{27}$$

where $\mathbf{x_d}$ is the displacement in the X direction at the microphone position, in mm, k is the k-th discrete frequency line and K is the total number of frequencies in the response, in this case, 25 logarithmically sampled frequencies. The constrained optimization algorithm implemented in the MATLAB Optimization Toolbox [12] function *fmincon* is used for the optimization (a detailed description of this method can be

found in ref. [13]), and the gradient is calculated using finite differences.

In Sections 3.1 and 3.2 the optimization of the tube and the optimization of the suspension, respectively, are described. For each case, the model is reduced using CMS and MMR in combination with the Left-Right Method and the Split Field Method, and the accuracy of the reduced models is evaluated by comparing the results to the full system in terms of the modal frequencies, the modal vectors and the displacement frequency response at the microphone position. The error in the modal frequencies is evaluated as

$$f_{err} = \max_{n=1:N} \frac{\mid \mathbf{f_{n_{Full}}} - \mathbf{f_{n_{Red}}} \mid}{\mathbf{f_{n_{Full}}}} \cdot 100(\%), \tag{28}$$

where N is the number of modal frequencies below the upper limit of 10 kHz. The modal vectors accuracy is evaluated by calculating the Modal Assurance Criterion (MAC) between the modal vectors from the full and the reduced systems. Since the MAC is bounded between 0 and 1, 1 indicating linearly dependent vectors, and 0 indicating orthogonal vectors, the minimum diagonal value of the MAC matrix of all modes below 10 kHz is used as accuracy indicator,

$$v_{acc} = \min_{n=1:N} [\mathbf{MAC}](n,n). \tag{29}$$

The accuracy of the displacement frequency response is evaluated as the mean error in dB between the results of the full system and the reduced system. When the frequency response is sampled logarithmically at K points between 100 Hz and 10 kHz, the error is calculated as

$$\overline{\Delta L_x} = \frac{1}{K} \sum_{k=1}^{K} 20 \log \left(\frac{\mid \mathbf{x_{red}}(k) \mid}{\mid \mathbf{x_{full}}(k) \mid} \right) (dB), \tag{30}$$

where k is the k-th frequency line.

For each studied case, the most efficient technique is chosen for the optimization, and the results are compared to the full system optimization results.

3.1 Tube

The Young's modulus and thickness of the PVC tube are optimized in this section within the design space specified in Table 2.

	Lower bound	Upper bound	Nominal value
E modulus [Pa]	10^8	10^9	10^8
Thickness [mm]	1	1.8	1

Table 2: Design space of the tube properties

3.1.1 Comparison of reduced models

For the CMS reduction, the model is divided into two substructures by a cut on the hook part of the body, as shown in Figure 2, which yields 141 boundary DOFs (structural and acoustic). The part that contains the PVC tube is left unreduced (21886 DOFs), and the upper part is reduced using 200 vibration modes. The reduced and the unreduced substructures are coupled as indicated in eqs. (16) and (17). The accuracy of the reduction when using the Left-Right Method and the Split Field Method for the modal base is assessed according to eqs. (28) - (30), and the results are compared in Table 3, where the time required for the frequency

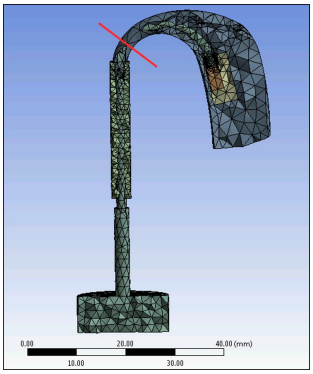

Figure 2: Division of the HI in two substructures for the CMS reduction

response calculation at 25 frequencies is also shown.

For the Multi-Model Reduction approach, the reduction base is formed by adding models to it until certain accuracy criteria are fulfilled. The included models sample the design domain of the optimization parameters, starting by the extreme values and refining the sample gradually. The accuracy of the reduction base is evaluated at 25 points, generated by assigning random values of the design parameters within their design domain. When the worst case error measures out of the 25 points fulfil the following criteria, the number of models included in the base is considered sufficient,

$$f_{err} < 1\% \tag{31}$$

$$v_{acc} > 0.9 \tag{32}$$

$$\overline{\Delta L_x} < 2\,\mathrm{dB}. \tag{33}$$

In this case, including 4 models with the 4 combinations of extreme values of the design space is sufficient to fulfil the criteria for both the Left-Right Method and the Field Split Method. The accuracy results and frequency response calculation time are shown in Table 3.

Reduction Technique	Component Mode Synthesis		Multi-Model Reduction		Full model
Modal Base Type	Left-Right	Field Split	Left-Right	Field Split	-
f_{err} (%)	0.5	0.009	0.09	0.09	-
v_{ac}	0.4	1	0.91	0.91	-
$\overline{\Delta L_x}$ (dB)	3.6	0	1.9	1.22	-
Time (s)	42	43	3.7	4.6	330

Table 3: Comparison of accuracy and frequency response calculation time between the models reduced for tube optimization and the full model

Both the CMS and the MMR methods achieve remarkable time reductions compared to the full model frequency response calculation. The MMR method presents the same accuracy when the modal base is built with the Left-Right Method or the Split Field method. When combined with the Left-Right approach (MMR-LR), it is 10 times faster than the CMS methods and 100 times faster than the full model, which makes it the most efficient option. The CMS combined with the Field Split Method is slightly more accurate overall, however, when the CMS is combined with the Left-Right Method, it does not fulfill the accuracy requirements in eqs. (31) - (33), showing that the choice of the modal base type does have an impact in this case.

3.1.2 Optimization results

The optimization of the tube parameters with the most efficient reduced model (MMR-LR) yields a value for the E modulus of the tube of $2.8 \cdot 10^8$ Pa and a thickness of 1.77 mm, which present a very slight deviation (3%) to the results obtained with the full model, showing that the reduction is accurate throughout the optimization. The optimization took 50 minutes with the reduced system and 6 hours with the full system, a speed-up that is not directly proportional to the harmonic response calculation speed-up (100 times) because the process of building the matrices and importing them into MATLAB at each function evaluation is common for the reduced and the full model. The resulting displacement frequency response at the microphone position can be seen in Figure 3, compared to the frequency response when the nominal values of the tube parameters are used. The total reduction in the objective function value is of 4.8 dB.

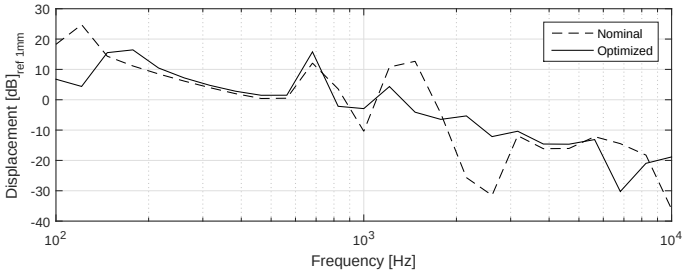

Figure 3: Displacement frequency responses for the optimized and nominal values of the tube properties, sampled at 25 frequencies

The frequency resolution of the optimized curve is quite poor; thus, it could be that the peaks of the response have just been moved to unsampled frequencies. Performing the optimization for a larger number of frequencies with the full model would be too time consuming; however, once the reduction has been shown to yield accurate results for the tested case, it can be used trustfully for an optimization with higher resolution. Optimizing the frequency response logarithmically sampled at 300 frequencies yields a value for the E modulus of the tube of $8.4 \cdot 10^8$ Pa and a thickness of 1.8 mm, and the nominal and optimized frequency responses can be seen in Figure 4.

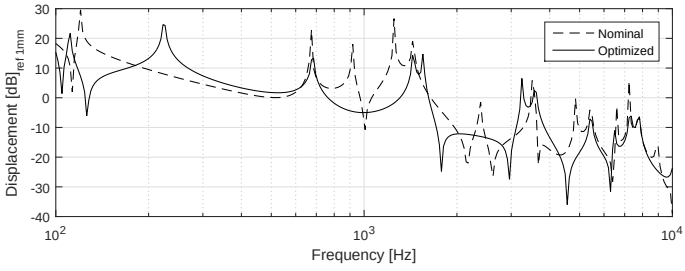

Figure 4: Displacement frequency responses for the optimized and nominal values of the tube properties, sampled at 300 frequencies

3.2 Suspension

In this section, the same procedure is followed for the optimization of the Young's modulus and thickness of the suspension within the design space specified in Table 4.

	Lower bound	Upper bound	Nominal value
E modulus [Pa]	10^6	10^8	$6 \cdot 10^6$
Thickness [mm]	0.175	0.2	0.2

Table 4: Design space of the suspension parameters

3.2.1 Comparison of reduced models

For the CMS, the model is divided into two parts by cutting the suspension and its surrounding elements into a spherical substructure, as shown in Figure 5, which in this case yields 440 boundary DOFs. The part that contains the suspension is left unreduced (49393 DOFs), and the outer part is reduced using 100 vibration modes. Even though the unreduced part includes only the suspension and the closest neighbouring elements, a fine mesh is required in order to model this sensitive region in an accurate way, therefore, it contains more than half of the DOFs of the total system. The model is reduced following the same procedure as for the tube. The Multi-Model Reduction base is formed following the same criteria as for the tube, which in this case results in including 5 models in the base.

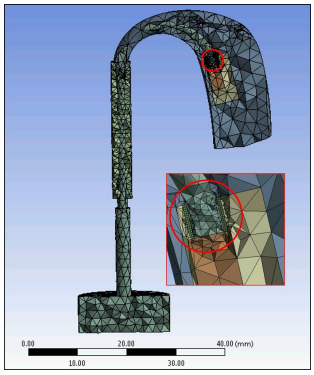

Figure 5: Division of the HI in two substructures for the CMS reduction

Reduction Technique	Component Mode Synthesis		Multi-Model Reduction		Full model
Modal Base Type	Left-Right	Field Split	Left-Right	Field Split	-
f_{err} (%)	0.1	0.1	0.1	0.1	-
v_{ac}	0.1	0.1	1	1	-
$\overline{\Delta L_x}$ (dB)	0.2	0.2	1	1	-
Time (s)	223	235	7.7	12.6	330

Table 5: Comparison of accuracy and frequency response calculation time between the models reduced for suspension optimization and the full model

The comparison of the accuracy results and time consumption in Table 5 shows that the time reduction achieved with CMS is not as significant here as for the tube case, due to the unreduced part containing more

than half of the DOFs of the full system. The accuracy of the modal vectors is poor for CMS independently of the chosen modal base type, but the modal frequencies and frequency response accuracy is good for both, which indicates that the poor MAC value is probably due to mode switching of modes that are close in frequency. The MMR combined with the Left-Right Method (MMR-LR) is the most efficient approach.

3.2.2 Optimization results

The optimization of the suspension parameters yields a Young's modulus value of $7.4 \cdot 10^6$ Pa and a thickness of 0.188 mm with the MMR-LR reduced model, with a deviation of 2% compared to the result obtained with the full system. The objective function value is reduced by 4.2 dB and the optimized displacement frequency response is shown in Figure 6, compared to the nominal frequency response.

The total time of the optimization is reduced from 3.7 hours to 40 minutes. This reaffirms the accuracy and efficiency of the reduced model, showing that it is the best approach for optimization speed-up in the considered cases.

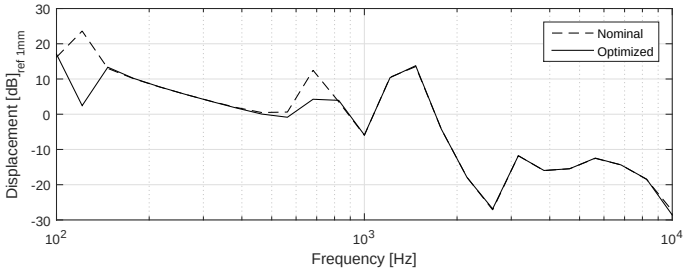

Figure 6: Displacement frequency responses for the optimized and nominal values of the suspension properties, sampled at 25 frequencies

As for the case of the tube optimization, the poor frequency resolution can yield optimized values that do not correspond to real minimized frequency responses. Optimizing the frequency response sampled at 300 frequencies with the reduced model yields the result shown in Figure 7, with an optimized value for the Young's modulus of $1.2 \cdot 10^6$ Pa and a thickness of 0.191 mm.

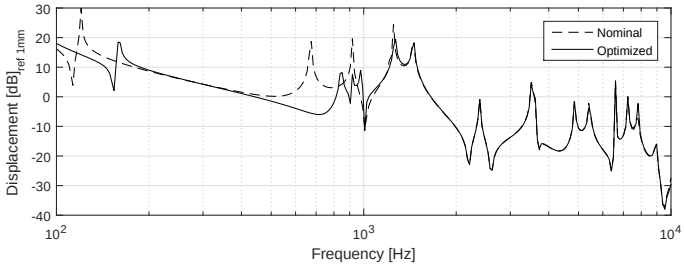

Figure 7: Displacement frequency responses for the optimized and nominal values of the suspension properties, sampled at 300 frequencies

4 Discussion

For the MMR technique, both modal base types have yielded the same accuracy in the results. However, for the CMS reduction, the Split Field modal base yields more accurate results than the Left-Right type for the tube case, showing that the latter method is less numerically stable in some cases.

The MMR technique is faster than the CMS technique for both tested cases. A drawback of the MMR technique is that the mesh must remain unchanged between the different models, therefore, it is not valid for optimization of parameters that would require re-meshing at each iteration. In this case, the thickness of the tube and the suspension has been varied by displacing their outer nodes, which limits the design space, as for large variations some elements should be added or removed. In the case where the position of a part should be optimized, re-meshing would also be required, and the model could not be reduced using MMR. In those cases, the CMS technique could be used for the reduction, if the boundary nodes are fixed, and the mesh modifications affect only the interior DOFs of the unreduced part. Therefore, the speed-up introduced by this method can also be useful for certain optimization problems.

5 Conclusions

In this work, two reduction methods and two approaches to building modal bases for problems with structure-acoustic coupling have been compared for the optimization of the Young's modulus and the thickness of two parts of a model of a hearing aid. The Multi-Model Reduction technique has been found to be more efficient than the Component Mode Synthesis method, showing a better accuracy and time reduction for the two tested cases. In terms of the modal base types, the Left-Right method has been found to be fastest due to its reduction base being smaller; however, the Split Field method presents a higher accuracy in some cases. Overall, the MMR-LR, being up to 100 times faster than the full model for frequency response calculation, is recommended as the most efficient technique.

References

[1] M. B. Sondergaard, C. B. W. Pedersen, *Applied topology optimization of vibro-acoustic hearing instrument models*, Journal of Sound and Vibration, vol. 333, no. 3, (2014), pp. 683–692.

[2] R. R. Craig, M. C. C. Bampton, *Coupling of substructures for dynamic analyses*, AIAA Journal, vol. 6, no. 7, (1968), pp. 1313–1319.

[3] R. R. Craig, *Coupling of substructures for dynamic analyses: an overview*, in *Collection of Technical Papers - AIAA/ASME/ASCE/AHS/ASC Structures, Structural Dynamics and Materials Conference*, vol. 5, AAIA, (2000), pp. 3–14.

[4] S. Donders, B. Pluymers, P. Ragnarsson, R. Hadjit, W. Desmet, *The wave-based substructuring approach for the efficient description of interface dynamics in substructuring*, Journal of Sound and Vibration, vol. 329, no. 8, (2010), pp. 1062–1080.

[5] J. Herrmann, M. Maess, L. Gaul, *Substructuring including interface reduction for the efficient vibro-acoustic simulation of fluid-filled piping systems*, Mechanical Systems and Signal Processing, vol. 24, no. 1, (2010), pp. 153–163.

[6] C. Pal, I. Hagiwara, *Dynamic analysis of a coupled structural-acoustic problem - simultaneous multi-modal reduction of vehicle interior noise level by combined optimization*, Finite Elements in Analysis and Design, vol. 14, no. 2-3, (1993), pp. 225–234.

[7] L. Hermans, M. Brughmans, *Enabling vibro-acoustic optimization in a superelement environment: A case study*, in *Proceedings of the International Modal Analysis Conference and Exhibit*, vol. 2, SEM, (2000), pp. 1146–1152.

[8] E. Balmès, *Parametric families of reduced finite element models. theory and applications*, Mechanical Systems and Signal Processing, vol. 8, no. 8, (1994), pp. 381–394.

[9] P. Davidsson, G. Sandberg, *A reduction method for structure-acoustic and poroelastic-acoustic problems using interface-dependent lanczos vectors*, Computer Methods in Applied Mechanics and Engineering, vol. 195, no. 17-18, (2006), pp. 1933–1945.

[10] M. Stammberger, H. Voss, *Automated multi-level substructuring for a fluid-solid vibration problem*, Numerical Mathematics and Advanced Applications, (2008), pp. 563–570.

[11] M. Maess, L. Gaul, *Substructuring and model reduction of pipe components interacting with acoustic fluids*, Mechanical Systems and Signal Processing, vol. 20, no. 1, (2006), pp. 45–64.

[12] *MATLAB optimization toolbox user's guide R2015b*, MathWorks, Natick, MA (2015).

[13] R. H. Byrd, M. E. Hribar, J. Nocedal, *An interior point algorithm for large-scale nonlinear programming*, Siam Journal on Optimization, vol. 9, no. 4, (1999), pp. 877–900.

[14] G. Golub, C. van Loan, *Matrix computations*, The Johns Hopkins University Press (1996), ISBN 0801854148, 9780801854149.

Appendix A Orthogonalization procedure

This Appendix describes the orthogonalization procedure used throughout this work for a generic case where $[\mathbf{T}_L]$ and $[\mathbf{T}_R]$ are orthogonalized so that

$$[\hat{\mathbf{T}}_L]^T[\mathbf{M}][\hat{\mathbf{T}}_R] = [\mathbf{I}]. \tag{34}$$

Some of the vectors in the initial matrices $[\mathbf{T}_L]$ and $[\mathbf{T}_R]$ can be almost identical, and must be removed in order to avoid ill-conditioning. The detection of very collinear vectors is done by performing a Singular Value Decomposition (SVD) of the matrices, as

$$[\mathbf{T}_L]^T[\mathbf{M}][\mathbf{T}_R] = [\mathbf{U}][\mathbf{\Sigma}][\mathbf{V}]^T, \tag{35}$$

where $[\mathbf{\Sigma}]$ is the matrix with the singular values on its diagonal, and $[\mathbf{U}]$ and $[\mathbf{V}]$ are unitary matrices. Those vectors for which the singular values are below a selected tolerance are then eliminated. A recommended value for the tolerance is a multiple of the floating-point relative accuracy [14], which can be weighted by the largest singular value and the size of the reduction base in order to penalize large reduced models [8].

Since the SVD has already been calculated, the obtained matrices are used for orthogonalizing the rest of the vectors, as

$$[\hat{\mathbf{T}}_R] = [\mathbf{T}_R][\mathbf{V}]^{-T}[\mathbf{\Sigma}]^{-1/2} \tag{36}$$

$$[\hat{\mathbf{T}}_L] = [\mathbf{\Sigma}]^{-1/2}[\mathbf{U}]^{-1}[\mathbf{T}_L]^T. \tag{37}$$

Since $[\mathbf{U}]$ and $[\mathbf{V}]$ are also orthogonal matrices, $[\mathbf{U}]^{-1} = [\mathbf{U}]^T$ and $[\mathbf{V}]^{-T} = [\mathbf{V}]$, which avoids matrix inversions in the calculation.

If $[\mathbf{M}]$ is symmetric and $[\mathbf{T}] = [\mathbf{T}_L] = [\mathbf{T}_R]$, then $[\mathbf{V}] = [\mathbf{U}]^T$, and therefore $[\hat{\mathbf{T}}] = [\hat{\mathbf{T}}_R] = [\hat{\mathbf{T}}_L]$.

Paper D

Adaptive parametric model order reduction technique for optimization of vibro-acoustic models: Application to hearing aid design

Journal of Sound and Vibration 424 (2018) 208–223

Contents lists available at ScienceDirect

Journal of Sound and Vibration

journal homepage: www.elsevier.com/locate/jsvi

Adaptive parametric model order reduction technique for optimization of vibro-acoustic models: Application to hearing aid design☆

Ester Creixell-Mediante [a,b,*], Jakob S. Jensen [a], Frank Naets [c,d], Jonas Brunskog [a], Martin Larsen [b]

[a] Acoustic Technology, Department of Electrical Engineering, Technical University of Denmark, Ørsteds Plads 352, 2800 Kgs. Lyngby, Denmark
[b] Oticon A/S, Kongebakken 9, 9765 Smørum, Denmark
[c] Department of Mechanical Engineering, KU Leuven, Celestijnenlaan 300B, B-3001 Heverlee, Leuven, Belgium
[d] Fellow of Flanders Make, Belgium

ARTICLE INFO

Article history:
Received 7 August 2017
Revised 13 December 2017
Accepted 13 March 2018
Available online XXX

Keywords:
Model reduction
Optimization
Structure-acoustic interaction

ABSTRACT

Finite Element (FE) models of complex structural-acoustic coupled systems can require a large number of degrees of freedom in order to capture their physical behaviour. This is the case in the hearing aid field, where acoustic-mechanical feedback paths are a key factor in the overall system performance and modelling them accurately requires a precise description of the strong interaction between the light-weight parts and the internal and surrounding air over a wide frequency range. Parametric optimization of the FE model can be used to reduce the vibroacoustic feedback in a device during the design phase; however, it requires solving the model iteratively for multiple frequencies at different parameter values, which becomes highly time consuming when the system is large. Parametric Model Order Reduction (pMOR) techniques aim at reducing the computational cost associated with each analysis by projecting the full system into a reduced space. A drawback of most of the existing techniques is that the vector basis of the reduced space is built at an offline phase where the full system must be solved for a large sample of parameter values, which can also become highly time consuming. In this work, we present an adaptive pMOR technique where the construction of the projection basis is embedded in the optimization process and requires fewer full system analyses, while the accuracy of the reduced system is monitored by a cheap error indicator. The performance of the proposed method is evaluated for a 4-parameter optimization of a frequency response for a hearing aid model, evaluated at 300 frequencies, where the objective function evaluations become more than one order of magnitude faster than for the full system.

1. Introduction

Simulation is gaining relevance in industrial design procedures, which have evolved from a purely prototyping and testing approach to a context where numerical simulation is used from the early phases. Obtaining reliable models is a key point in the

☆ Part of this work was presented in Internoise 2016 and ISMA 2016.

* Corresponding author. Oticon A/S, Kongebakken 9, 9765 Smørum, Denmark.
E-mail addresses: emed@oticon.com (E. Creixell-Mediante), json@elektro.dtu.dk (J.S. Jensen), frank.naets@kuleuven.be (F. Naets), jbr@elektro.dtu.dk (J. Brunskog), mnla@oticon.com (M. Larsen).

https://doi.org/10.1016/j.jsv.2018.03.013
0022-460X/

design process, and as more and more accuracy is required, the complexity of the models increases. In the field of hearing aids, numerical vibro-acoustic analysis is essential for the study of problems such as feedback; currently the main gain limiting factor of the hearing devices. The high number of small parts that conform them, the strong structure-acoustic interaction between those parts and the internal air volume require models with a large number of Degrees Of Freedom (DOFs) in order to capture the physical behaviour accurately. Therefore, significant computational challenges are encountered when solving problems that require iterative and/or repeated solutions of the numerical model. Tasks such as uncertainty analysis by means of Monte-Carlo methods, or parametric and topology optimization, require solving the system of model equations repeatedly for a large number of variations of different parameters. Therefore, the time required for solving the numerical problem at each iteration becomes a critical factor. In the present work, we develop an adaptive model order reduction technique and apply it to a hearing aid design problem.

In a recent paper [1], topology optimization of a part of a hearing instrument including structure-acoustic interaction was performed. Optimizing one part of the device requires the complete assembly to be taken into account when there is a strong acoustic-mechanical interaction, since the multiple vibrational and acoustic transmission paths between parts have a significant influence on the system performance. To facilitate the study, the performance was evaluated and optimized for a limited number of frequencies; therefore, the effects at the rest of the frequency range were not controlled. This highlights the need to develop computational reduction techniques that allow optimization to be carried out with a higher level of accuracy and frequency resolution.

Model order reduction techniques have been described in the literature and applied in several fields [2–4]. The earliest research on the topic deals with structural dynamics problems, with the Component Mode Synthesis (CMS) method being developed in the 1960s [5,6]. When modal-based methods were to be extended to problems with structure-acoustic interaction, different approaches were developed to construct the reduction basis. Since solving the coupled eigenvalue problem requires higher computational effort due to the asymmetric nature of the matrices when the pressure-displacement formulation is used, one suggested approach [7] consisted in using the uncoupled structural and acoustic modes, which is an efficient solution for problems with a weak structure-acoustic coupling. However, for problems with strong interaction, a large amount of modes are required in order to obtain an accurate reduced model [8], making it a poorly efficient technique. With the recent improvements on eigenvalue solvers and computational power, solving the asymmetric problem has become less challenging; therefore, the coupled modal vectors, that better describe true behaviour of the system, can now be used in practice. Another issue that arises from the asymmetry of the matrices is that the modal vectors do not form an orthogonal basis, which has been addressed in the literature in two ways: by using both left and right eigenvectors [9,10], or by applying orthogonalization techniques on the right eigenvectors [11]. The two approaches have been compared by the authors in Ref. [12], which showed that the second approach is more suited to the present problem, and is therefore employed in this work.

In CMS, the model is divided in substructures, which are reduced internally while the interface DOFs are kept unmodified. Even though interface reduction methods have been developed [13,14], this method is most efficient for systems that can be divided at low-dimensional interfaces, such as the pipes studied in Ref. [11], but it can be difficult to efficiently substructure systems that consist of complex 3D parts, as in hearing aid models. Despite the cost of solving the full eigenvalue problem, it turns out that a more efficient technique [15] consists in reducing the complete structure in terms of the global modal vectors, since fine resolution frequency response calculations can then be done at a very low computational cost on the reduced system. Therefore, this approach is selected in our work.

For parametric optimization purposes, a new modal reduction basis would have to be calculated for each variation of the parameter values when using the suggested approach (unless the modal vectors are not sensitive to the parameters, as assumed in Refs. [16,17]). This would still be faster than calculating the full system frequency response if the number of considered frequencies is large; however, parametric Model Order Reduction (pMOR) techniques have been developed to make this process even more efficient. The Multi-Model Reduction (MMR) technique is one of the most straight-forward pMOR methods, which consists in constructing a global reduction basis that is valid for any value of the parameters within a given design domain by concatenating the modal vectors calculated at several points in the parameter space in a global reduction matrix [4,18]. The number of included points should be sufficient to ensure that the reduction error at any point in the domain is below a required level. The resulting global vector matrix is then orthogonalized, since some modal vectors calculated at different sampled points can be linearly dependent, and they would otherwise result in ill-conditioning. When using MMR for coupled problems, the fact that the modal vectors resulting from the asymmetric matrix system are inherently not orthogonal should also be taken into account.

The MMR technique is usually applied in an offline-online fashion, where the reduction basis is constructed first (offline) and used for very fast function evaluation during the optimization (online). A drawback of this approach is that the offline phase can become very costly for an increasing number of parameters, since (a) the full model eigenvalue problem must be solved for each point that is included in the basis, and (b) the full model solution must be calculated at a representative sample of non-included points to evaluate the reduction error and ensure accuracy. To avoid problem (b), error bounds or error estimators that are cheaper to compute can be used instead of the true error [19]. Tight error bounds can be found for specific types of partial differential equations [20]; however, we will use a residual-based error indicator in this work, since they can be applied for any kind of problem and have already been successfully used in frequency response calculation problems [21].

A key point for reducing the computational time due to problem (a) is minimizing the number of points that need to be included in the basis. Greedy algorithms have been suggested for this purpose [22–25]; they consist in iteratively finding the point of the domain where the reduction error is maximal and adding it to the basis, until the maximum error is below some requirement. These methods are most efficient for applications like uncertainty characterization studies or system control, where most of the parameter domain is evaluated in the online phase. However, for optimization problems, only a small part of this domain is actually explored, and the efforts made for accurately representing points that will not be evaluated during the optimization are unnecessary. To exploit this feature, an adaptive reduced order basis construction approach that breaks the offline-online framework is proposed in this work. Previous works in this direction can be found in Refs. [26,27], where a method based on trust-region optimization is suggested; however, those approaches require solving a series of optimization problems bounded by an error estimator, which only results in an efficiency improvement when a very cheap error bound is available. Since we choose to use a residual-based error indicator, this approach does not lead to an efficient framework in the considered case. A more straight-forward basis updating methodology is therefore developed in this work. The suggested approach consists in updating the reduced order basis during the course of the optimization by evaluating the error indicator at each objective function calculation and adding the current point if it drops below a selected threshold. A similar approach is used in Ref. [28] for static structural topology optimization problems.

The main contributions by the authors are the extension of the MMR technique to vibroacoustic modal reduction bases, the development of a state vector error indicator adequate for such bases, and the algorithm for adaptively updating the reduced order basis during the optimization. This article is organized as follows. In Section 2, the hearing aid study case model and optimization problem that will be used for testing the algorithm suggested in this paper are presented. In Section 3, the details of the proposed adaptive pMOR optimization technique are described. In Section 4, the performance of the method is evaluated for the proposed case, and Section 5 summarizes the conclusions. All numerical tests were performed on a regular desktop computer (Intel Core i7-4790 k, 4 GHz CPU and 32 GB of RAM memory).

2. Test case: hearing aid design optimization problem

A main objective during the design phase of a hearing aid is the minimization of feedback paths, i.e. the acoustic and vibratory isolation of the microphones (which capture the outer acoustic signal, but are also sensitive to vibration) from the receiver (the loudspeaker that emits the sound into the ear, which also introduces structural vibration) to avoid signal loops. Even though powerful Digital Signal Processing (DSP) feedback cancellation algorithms are implemented in most hearing instruments, a design that maximizes the isolation between the transducers from a physical point of view is a key aspect for the final performance of the product. This motivates the use of FE models for frequency response optimization of the hearing aid. The models can however become very large, since the maximum frequency of interest goes up to 10 kHz, requiring a highly refined mesh especially for parts with soft materials and for the air volumes. Moreover, the frequency resolution of the optimized response should be fine enough to capture the complex behaviour of the system, requiring solutions for a high number of frequencies. These factors make the vibroacoustic response calculation highly time consuming and its optimization practically impossible, which triggers the need for the application of model order reduction techniques.

2.1. Problem statement

Hearing aids are formed by a large number of small parts connected to each other. One of the most critical components in the design is the receiver (loudspeaker) suspension, since its main role is the isolation of the receiver from the rest of the system. The tube that brings the sound from the receiver output to the ear is also a potential source of feedback, since it interacts strongly with the inner air due to its soft material and thin dimensions. In this study, we consider the optimization of the Young's modulus and thickness of these two parts to minimize the vibration velocity at the microphone position over the usual frequency range of interest in hearing aid design: between 100 Hz and 10 kHz.

A simplified model of a Behind The Ear (BTE) hearing aid, shown in Fig. 1, is built for this purpose. The parts that play a main role in the vibro-acoustic response are included, being the suspension, the tube and the receiver (simplified as a steel block), and the remaining components are modelled as a single solid body. The acoustic domain consists of a hard-walled acoustic volume, the coupler that simulates the acoustic impedance of the ear, an air canal that connects it to the receiver output through the tube and the suspension, and a small air cavity surrounding the receiver and the suspension. For the sake of simplicity and since the specific purpose of this study is evaluating the performance of the suggested model order reduction method, the air that surrounds the hearing aid and the transducer models of the receiver and the microphones are not included in the calculation. However, the acoustic and vibratory excitation signals are obtained from a lumped element model of the receiver, and applied as a frequency-dependent particle velocity and two directional forces, shown in Fig. 2, at a point on the surface between the receiver and the air canal.

2.2. Model set-up and optimization problem

The model has been set up in ANSYS® Academic Research Release 17.1, and the ANSYS® acoustic extension v171.4. Even

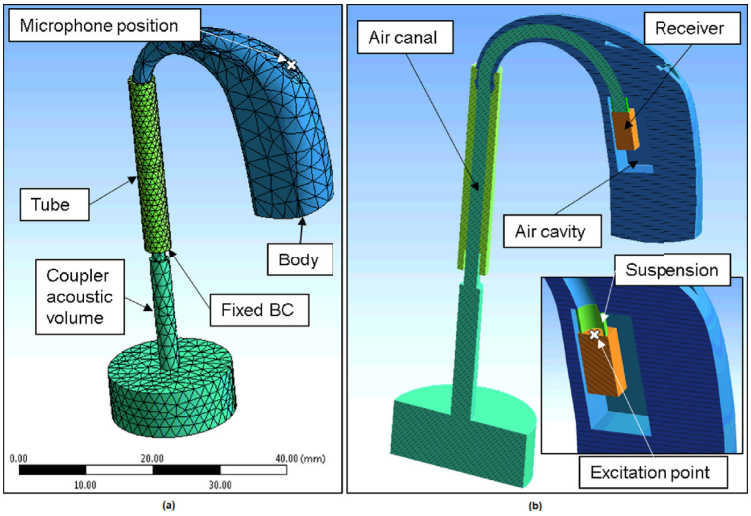

Fig. 1. Considered hearing aid model. (a) View of the model from outside, without outer air. (b) View of the vertically sliced model with zoomed view of the suspension and its surrounding area.

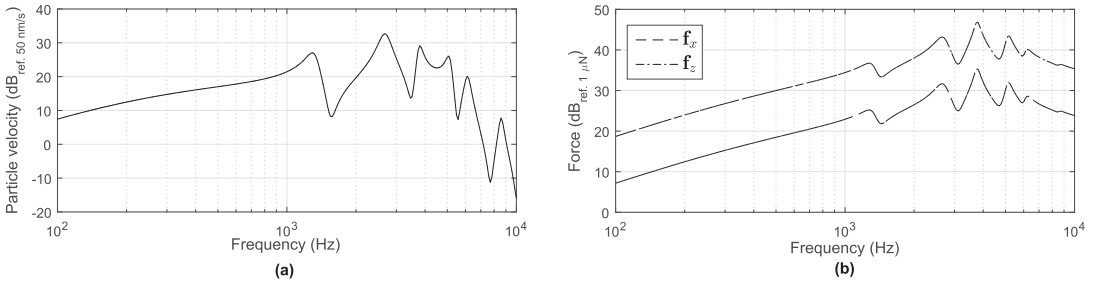

Fig. 2. Particle velocity (a) and forces (b) obtained from the receiver lumped element model.

though the maximum frequency of interest is 10 kHz, modal extraction will be performed with the model up to 12 kHz for model reduction purposes, as will be explained in the next section; therefore, the size of the mesh of the complete model has been determined by a convergence study of the eigenfrequencies of the system up to 12 kHz, resulting in 90821 DOFs, where the suspension requires the finest mesh in order to capture its rich modal behaviour. The nominal material properties for each part can be seen in Table 1.

In hearing aids, thermo-viscous losses become important in thin tubes and small cavities. They are usually modelled by a Boundary Layer Impedance (BLI) model [29], implemented in the ANSYS® FLUID elements (FLUID220 and FLUID221 are used in the model), which is frequency-dependent. Since losses in the air canal have an effect on the velocity response at the microphone position in the presented model, as shown by the solid and dashed lines in Fig. 3, it is important to include them to avoid optimizing a non-realistic peaky curve. However, reducing a system with frequency-dependent properties is significantly more cumbersome than a frequency-independent one. Therefore, a simplified version of the loss model is applied here, where the BLI effect is only calculated at 1000 Hz and added as a constant matrix to the system along the full frequency range. The resulting response is shown by the dotted line in Fig. 3, which is almost on top of the solid line. Even though the response is not exactly

Table 1
Nominal material properties of the hearing aid.

	Density (ρ) [kg/m^3]	Young's modulus (E) [Pa]	Poisson ratio (σ)	Damping coefficient (ν)[%]
Body	1040	$2 \cdot 10^9$	0.4	0
Tube	1300	$1 \cdot 10^8$	0.4	0.2
Receiver	7850	$2 \cdot 10^{11}$	0.3	0
Suspension	1100	$6 \cdot 10^6$	0.49	0.1

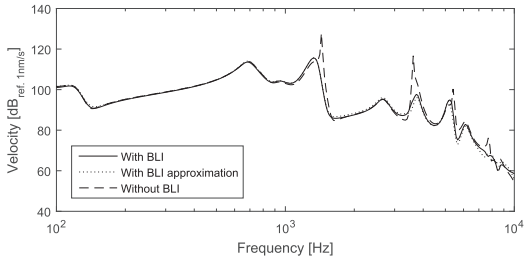

Fig. 3. Comparison of the total velocity at the microphone position when applying BLI, the frequency-independent BLI approximation, and no losses.

Table 2
Parameter design space.

	Lower bound $\boldsymbol{\mu}_l$	Upper bound $\boldsymbol{\mu}_u$	Initial value $\boldsymbol{\mu}_0$
Tube E modulus [Pa]	$9 \cdot 10^7$	10^9	10^8
Tube thickness [mm]	0.96	1.4	1
Suspension E modulus [Pa]	10^6	10^8	$6 \cdot 10^6$
Suspension thickness [mm]	0.175	0.225	0.2

the same, we hypothesize that using this approximation during the optimization will lead in practice to a result that is also close to optimal when the full BLI model is applied. This hypothesis will be validated in Section 4, where the results are presented.

When the pressure-displacement formulation is used, the equation of motion in the frequency domain of the complete system under harmonic excitation takes the form

$$\left(\begin{bmatrix} \mathbf{K}_s & -\mathbf{S}^T \\ \mathbf{0} & \mathbf{K}_a \end{bmatrix} - \omega^2 \begin{bmatrix} \mathbf{M}_s & \mathbf{0} \\ \rho_a \mathbf{S} & \mathbf{M}_a \end{bmatrix} \right) \begin{Bmatrix} \mathbf{x}_s \\ \mathbf{p}_a \end{Bmatrix} = \begin{Bmatrix} \mathbf{f}_s \\ \mathbf{f}_a \end{Bmatrix}, \tag{1}$$

where $\mathbf{K}_s$ and $\mathbf{M}_s$ are the structural stiffness and mass matrices, $\mathbf{K}_a$ and $\mathbf{M}_a$ are the acoustic stiffness and mass matrices, $\mathbf{S}$ is the fluid-structure interaction coupling matrix, ρ_a is the density of the acoustic medium, ω is the frequency, $\mathbf{x}_s$ is the vector of structural displacements, $\mathbf{p}_a$ is the vector of acoustic pressures, $\mathbf{f}_s$ is the vector of external structural forces and $\mathbf{f}_a$ is the vector of external acoustic excitations. In this model, the damping matrix vanishes since only hysteretic material damping is considered, which is included as the imaginary part to the structural stiffness matrix, $\mathbf{K}_s$, and the terms associated with the BLI are included as a constant matrix added to the stiffness matrix, $\mathbf{K}_a$.

The optimization problem we consider in this work can be formulated as

$$\begin{aligned} &\underset{\boldsymbol{\mu}}{\text{minimize}} \quad g(\boldsymbol{\mu}) = 10 \log \sum_{k=1}^{K} \left| \frac{\mathbf{v}_m(\boldsymbol{\mu}, k)}{v_{ref}} \right|^2 \\ &\text{subject to} \quad \boldsymbol{\mu}_l \geq \boldsymbol{\mu} \geq \boldsymbol{\mu}_u, \end{aligned} \tag{2}$$

where $|\mathbf{v}_m(\boldsymbol{\mu}, k)|$ is the magnitude of the total velocity at a node on the microphone position, calculated as $\left| \sqrt{v_{mx}^2 + v_{my}^2 + v_{mz}^2} \right|$, v_{ref} is the reference structural velocity, k is the k-th discrete frequency line and K is the total number of frequencies (300 frequencies logarithmically distributed between 100 Hz and 10 kHz in this case). The vector $\boldsymbol{\mu}$ contains the four considered optimization parameters: the Young's moduli and the thicknesses of the tube and the suspension:

$$\boldsymbol{\mu} = \begin{bmatrix} E_t \\ E_s \\ t_t \\ t_s \end{bmatrix}, \tag{3}$$

which can vary within the lower and upper bounds, $\boldsymbol{\mu}_l$ and $\boldsymbol{\mu}_u$, specified in Table 2.

The thickness modification is done by moving all the nodes on the outer surface of the tube or the suspension, respectively, in the direction normal to the surface. The upper and lower bounds are therefore determined by the amount of deformation that can be applied before the mesh becomes too distorted.

Table 3
Objective function evaluation computational times for the full system.

	Building matrices in ANSYS® and importing into MATLAB®	Solving eq. (1) @ 300 freq. lines	Total
Time [s]	255	8500	8755 (2.4 h)

2.3. Optimization framework with full model

The optimization is performed in MATLAB®, using a constrained optimization algorithm implemented in the MATLAB® Optimization Toolbox [30] function *fmincon* (a detailed description of this method can be found in Ref. [31]) and the gradient is calculated using finite differences. Therefore, at each optimization iteration, the objective function in Eq. (2) must be evaluated at least 5 times: for the current point and for the calculation of each component of the gradient. For each function evaluation, MATLAB® interfaces with ANSYS® to update the design parameters and command building the new system matrices, which are then read into MATLAB®, where the system in Eq. (1) is reduced and solved for the different frequency lines, as will be explained in the following sections, and the objective function value is calculated. The algorithm stops the optimization when the size of the step or the variation of the objective function between two consecutive iterations is below a specified tolerance.

If the full system in Eq. (1) is solved without reduction, the computational time required for a single objective function evaluation is around 2.4 h, which is spent in different steps as detailed in Table 3. Even though a significant amount of time is spent in the communication between softwares, the largest burden is clearly on the response calculation, which is proportional to the number of considered frequencies. The proposed model order reduction technique focuses on reducing the time spent at that step.

3. Adaptive model order reduction method for parametric optimization

In this chapter, the proposed framework for optimization using reduced order modelling is described. A model order reduction technique for vibroacoustic problems is developed in Section 3.1, and the procedure to make it adaptive for parametric optimization problems is described in Section 3.2.

3.1. Modal-based reduction for structural-acoustic coupling problems

A projection-based approach to Model Order Reduction (MOR) [4] is adopted in this work. In this approach the state vector $\mathbf{x} \in \mathbb{R}^n$ is approximated by a lower rank basis $\mathbf{T} \in \mathbb{R}^{\mathbf{n\times m}}$:

$$\mathbf{x} \approx \mathbf{T}\mathbf{x}_r, \tag{4}$$

where $\mathbf{x}_r \in \mathbb{R}^m$ is the reduced state vector, and $m < n$.

In this work we employ a Galerkin projection such that for a generalized dynamic stiffness matrix and external load, the reduced equations of motion in the frequency domain can be written as:

$$\mathbf{T}^T\mathbf{D}\mathbf{T}\mathbf{x}_r = \mathbf{T}^T\mathbf{f}, \tag{5}$$

or

$$\mathbf{D}_r\mathbf{x}_r = \mathbf{f}_r, \tag{6}$$

where $\mathbf{D}_r \in \mathbb{R}^{m\times m}$ is the reduced generalized dynamic stiffness matrix. The construction of matrix $\mathbf{T}$ is discussed in the following.

Modal vectors have been widely used in model reduction of structural problems, since they form an orthogonal set which is easy to truncate according to their modal frequency and the maximum frequency of interest in the analysis. They are good descriptors of the system dynamics and have a clear physical interpretation, which have made them a popular choice also in the field of vibro-acoustics. In this section, the challenges encountered to obtain an efficient and accurate modal basis for vibroacoustic problems, and more specifically for the hearing aid problem introduced in Section 2, are discussed.

The coupled eigenvalue problem must be solved to obtain the modal vectors. For the problem stated in Eq. (1), it takes the following form:

$$\left(\underbrace{\begin{bmatrix} \mathbf{K}_s & -\mathbf{S}^T \\ \mathbf{0} & \mathbf{K}_a \end{bmatrix}}_{\mathbf{K}} - \lambda_i^2 \underbrace{\begin{bmatrix} \mathbf{M}_s & \mathbf{0} \\ \rho_a\mathbf{S} & \mathbf{M}_a \end{bmatrix}}_{\mathbf{M}} \right) \begin{Bmatrix} \boldsymbol{\psi}_s^i \\ \boldsymbol{\psi}_a^i \end{Bmatrix} = \begin{Bmatrix} \mathbf{0} \\ \mathbf{0} \end{Bmatrix}, \tag{7}$$

where $\{\boldsymbol{\psi}_s^i\}$ is the structural displacement part of the i-th modal vector, $\{\boldsymbol{\psi}_a^i\}$ is the acoustic pressure part of the i-th modal vector, and λ_i is the i-th eigenvalue given by $\lambda_i = \omega_i + j\delta_i$, δ_i/ω_i being the modal damping ratio, and ω_i the damped modal angular frequency. Note that these modal vectors are representing the full coupled system, and are not the uncoupled modal

vectors as used in Ref. [7]. Since only those modes with a frequency below a required threshold, ω_t, are needed for the reduction, the truncated structural and acoustic modal matrices, $\boldsymbol{\Psi}_s = [\boldsymbol{\psi}_s^1, \dots, \boldsymbol{\psi}_s^N]$ and $\boldsymbol{\Psi}_a = [\boldsymbol{\psi}_a^1, \dots, \boldsymbol{\psi}_a^N]$ with $\omega_N < \omega_t$, can be obtained most efficiently by solving the eigenvalue problem with an iterative algorithm that stops after obtaining all modes below the selected frequency, such as the "Unsymmetric Method" used by the ANSYS® software [32].

Unlike for the purely structural case, the system matrices $\mathbf{M}$ and $\mathbf{K}$ are unsymmetric due to the coupling terms. This results in the right eigenvectors not being mutually orthogonal, which makes them not directly suitable as a reduced order basis. Based on the results of previous investigations by the authors [12], the proposed approach consists in separating the acoustic and structural fields from the coupled modal vectors and orthogonalizing them with respect to the acoustic and structural mass matrices respectively, so that

$$\widehat{\boldsymbol{\Psi}}_a^T \mathbf{M}_a \widehat{\boldsymbol{\Psi}}_a = \mathbf{I} \tag{8}$$

$$\widehat{\boldsymbol{\Psi}}_s^T \mathbf{M}_s \widehat{\boldsymbol{\Psi}}_s = \mathbf{I}, \tag{9}$$

where $\widehat{(\cdot)}$ indicates that the matrix has been orthogonalized. The orthogonalization procedure is detailed in the following for matrix $\widehat{\boldsymbol{\Psi}}_a$, and is valid for all matrix orthogonalizations indicated in this paper with $\widehat{(\cdot)}$.

Due to splitting the modal vectors into their acoustic and structural fields, the partial modal matrices $\boldsymbol{\Psi}_a$ and $\boldsymbol{\Psi}_s$ can contain linearly dependent vectors, which must be removed from the basis to avoid ill-conditioning. The vector products linked to the kinetic and strain energy are a good measure of independence [18], therefore we choose to construct a basis that is mass orthonormal here. This is done by performing a Singular Value Decomposition (SVD) of the mass-weighted vector product,

$$\boldsymbol{\Psi}_a^T \mathbf{M}_a \boldsymbol{\Psi}_a = \mathbf{U} \boldsymbol{\Sigma} \mathbf{V}^T, \tag{10}$$

where $\boldsymbol{\Sigma}$ is a diagonal matrix with the singular values on its diagonal and $\mathbf{U}$ and $\mathbf{V}$ are unitary matrices, which are also equal and orthogonal since the decomposed matrix is symmetric, and therefore $(\mathbf{V}^{-1})^T = \mathbf{V} = \mathbf{U}$. For eliminating the linearly dependent basis vectors, the columns of matrix $\mathbf{U}$ for which the singular value is below a certain threshold are discarded, yielding the truncated matrix $\mathbf{U}_t$. Theoretically, this threshold would be zero; however, due to the numerical noise involved in real computations, a recommended value for the threshold is a multiple of the floating-point relative accuracy [33], weighted by the largest singular value and the number of vectors in $\boldsymbol{\Psi}_a$ (in order to penalize large reduced models [18]). Substituting $\mathbf{U}$ by $\mathbf{U}_t$ in Eq. (10), moving the right-hand side terms to the left side and equating it to Eq. (8), we obtain

$$\widehat{\boldsymbol{\Psi}}_a = \boldsymbol{\Psi}_a \mathbf{U}_t \boldsymbol{\Sigma}^{-1/2}. \tag{11}$$

The resulting orthogonalized modal matrices are then grouped to form the reduction basis as

$$\mathbf{T} = \begin{bmatrix} \widehat{\boldsymbol{\Psi}}_s & \mathbf{0} \\ \mathbf{0} & \widehat{\boldsymbol{\Psi}}_a \end{bmatrix}. \tag{12}$$

For the hearing aid model described in Section 2 with the nominal parameter values, calculating the eigenmodes up to 12 kHz in ANSYS® takes 160 s and yields a reduction basis with 94 vectors. The error introduced by the reduction can be quantified by comparing the solution of the full system to the reconstructed solution of the reduced system. In terms of the 2-norm, the relative reduction error on the state response vector as a function of frequency is

$$\epsilon(\omega) = \frac{\|\mathbf{x}(\omega) - \widetilde{\mathbf{x}}(\omega)\|_2}{\|\mathbf{x}(\omega)\|_2}, \tag{13}$$

which is shown by the grey line ("no enrichment") in Fig. 4 for the reduction with modes below 12 kHz. The 1% error line is also shown, since it is commonly used as a pragmatic maximum reduction error level allowed to ensure accuracy. The relative error is above this line for frequencies above 2 kHz; therefore, the current reduction basis is not accurate enough for the system under study.

An efficient way to improve the accuracy of the reduced order model consists in enriching the reduction basis by including information about the external excitation [34]. The basis can be enriched with a static response, or with several dynamic responses calculated at selected frequencies. For a given frequency ω_k, an enrichment vector $\mathbf{x}_k$ is obtained by solving the full model at that frequency,

$$\mathbf{x}_k = \left(\mathbf{K} - \omega_k^2 \mathbf{M}\right)^{-1} \mathbf{f}(\omega_k). \tag{14}$$

The obtained set of enrichment vectors is not necessarily orthogonal; therefore, the same procedure as for the modal vectors is applied. The acoustic and structural parts of the response vectors are grouped separately in $\mathbf{X}_a$ and $\mathbf{X}_s$, which are orthogonalized following the technique described above to obtain $\widehat{\mathbf{X}}_a$ and $\widehat{\mathbf{X}}_s$. Then, the final reduced order basis is formed by concatenating them with the orthogonalized modal matrices, as

$$\mathbf{T} = \begin{bmatrix} \begin{bmatrix} \widehat{\boldsymbol{\Psi}}_s & \widehat{\mathbf{X}}_s \end{bmatrix} & \mathbf{0} \\ \mathbf{0} & \begin{bmatrix} \widehat{\boldsymbol{\Psi}}_a & \widehat{\mathbf{X}}_a \end{bmatrix} \end{bmatrix}. \tag{15}$$

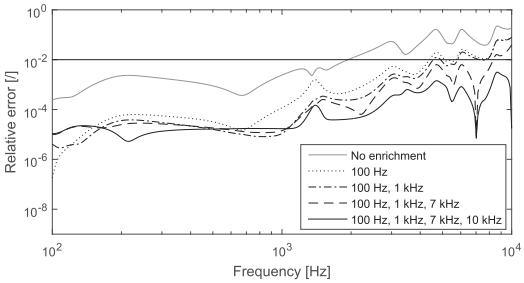

Fig. 4. Reduction error for increasingly enriched reduction bases.

Table 4
Reduction basis construction computational times.

	Solving eigenvalue problem in ANSYS® and importing vectors into MATLAB®	Calculating enrichment vectors	Orthogonalizing matrices	Total
Time [s]	322	114	0.5	436.5 (7.3 min)

When enriching the previously calculated modal basis with dynamic responses, we find that 4 enrichment vectors calculated at 100 Hz, 1 kHz, 7 kHz and 10 kHz are needed for the error to be below the desired level, as shown in Fig. 4. This yields a reduced order basis with 102 basis vectors, only 8 more than for the original modal basis, consisting of 94. The time required for solving this reduced system at 300 frequencies is 9 s, which is 945 times shorter than the full system solution time, which took 8500 s (Table 3).

The construction of the reduction basis consists therefore of three main steps: solving the eigenvalue problem to obtain the modes up to 12 kHz, calculating 4 enrichment vectors, and orthogonalizing the resulting matrices to form $\mathbf{T}$. The time required for each step is detailed in Table 4, and adds up to 7.3 min. If the 9 s required for solving the reduced system and the 255 s required to obtain the matrices from ANSYS® (according to Table 3) are added to that, a total of 11.7 min are needed for a single objective function evaluation, which is 12 times faster than the 2.4 h required when using the full system.

3.2. Parametric model order reduction by adaptive basis construction

The approach described so far does not take into account the parametric dependency of the model. The reduced order basis could be re-computed for each combination of parameter values that needs to be evaluated during the optimization process, which has been shown to be 12 times more efficient than using the full model. However, this approach would still be relatively time consuming compared to what can be achieved when using parametric Model Order Reduction (pMOR) techniques. Typically, pMOR methods consist in constructing a reduction basis "offline" (i.e. before the optimization) that is accurate throughout the parameter design domain, and the basis is then used throughout the optimization to reduce the system matrices, avoiding to solve the full system during the "online" phase [35].

The pMOR technique selected in this work consists in sampling the parameter design space and forming a global reduction basis by concatenating the basis vectors calculated at the different sample points. In the classical approach, the reduction basis should be formed by sampling the parametric space finely enough so that the obtained global basis introduces a reduction error below a required threshold throughout the full design domain. To ensure that, the error must be evaluated at a representative set of non sampled points, and new points must be added to the basis until the requirement is fulfilled [18]. This can become highly time consuming due to two factors: (1) the full model needs to be solved in order to calculate the error, which is computationally expensive, and (2) a large number of points must be added to the basis in order to represent the whole parameter space.

In this section, issues (1) and (2) are addressed. Firstly, a cheap pragmatic error indicator is presented. Secondly, a technique to reduce the number of points that need to be included in the reduction basis is introduced. The proposed approach exploits the fact that, during the optimization, a specific path within the design domain will be followed, and therefore only a small part of it will actually be evaluated. Consequently, there is no need to represent accurately the complete design domain, but only those areas that will actually be explored, as illustrated in Fig. 5.

3.2.1. Error indicator

Many *a posteriori* error indicators are based on the computation of the norm of residuals associated with the full model. The norm of the force residual can be computed relatively cheaply by inserting the reconstructed state vector into the full system

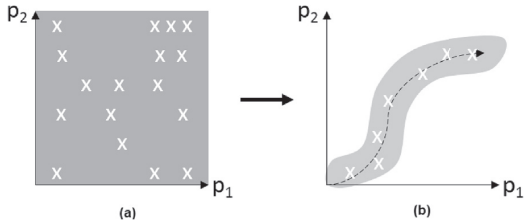

Fig. 5. Traditional parameter sampling for reduction basis construction (a) and new adaptive approach (b) for an example with 2 parameters. The white crosses indicate points on the parameter space that are included in the reduction basis, and the dashed line represents the path followed during the optimization. The grey area indicates the parameter space where the reduction is accurate in each case.

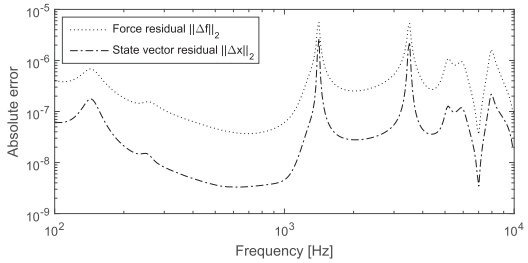

Fig. 6. Comparison of the force residual and the state vector residual.

equation of motion, i.e.

$$\Delta\mathbf{f} = \left(\mathbf{K} - \omega^2\mathbf{M}\right)\widetilde{\mathbf{x}} - \mathbf{f}. \tag{16}$$

The force residual has been directly used as an error indicator in the literature [21,27]. It measures how good of a solution to the system the reconstructed response is; however, we are concerned about how much the reconstructed response deviates from the full model response; therefore, we search for an estimate of the relative state vector error, as expressed in Eq. (13). In the literature, most suggested approaches to approximating this error from the norm of the force residual are mainly concerned with reduction methods based on Proper Orthogonal Decomposition (POD). POD consists in building the reduction basis from "snapshots" of the state vector at different parameter points, where the full system must be solved. The true error can directly be obtained at those points since the full system solution is available, and it is used in Ref. [24] to create a linear model between the norm of the force residual, $\|\Delta\mathbf{f}\|_2$, and the norm of the state vector residual, $\|\Delta\mathbf{x}\|_2 = \|\mathbf{x} - \widetilde{\mathbf{x}}\|_2$, which is then used to estimate the error at other points.

For modal-based reduction, the full system response is not calculated when building the reduction basis; therefore, this approach cannot be directly used. However, the idea of finding a relationship between the residual on the dynamic force balance and the state error may still be feasible. In practice, we observed that when the ROM is sufficiently accurate, there is close to a constant offset between the force residual and state vector error over the frequency range of interest, which is demonstrated in Fig. 6. Therefore, as a pragmatic approximation, this offset could be calculated at one single frequency, f_0, and used to roughly approximate the state vector residual at the rest of the frequency range by multiplying it by the force residual,

$$k = \frac{\|\Delta\mathbf{x}(f_0)\|_2}{\|\Delta\mathbf{f}(f_0)\|_2}, \tag{17}$$

$$\|\Delta\mathbf{x}(\omega)\|_2 \approx k\|\Delta\mathbf{f}(\omega)\|_2. \tag{18}$$

Then, the relative error can be estimated as

$$\epsilon_{ind}(\omega) = \frac{k\|\Delta\mathbf{f}(\omega)\|_2}{\|\widetilde{\mathbf{x}}(\omega)\|_2} \approx \epsilon(\omega) = \frac{\|\Delta\mathbf{x}(\omega)\|_2}{\|\mathbf{x}(\omega)\|_2}. \tag{19}$$

The resulting estimated error, when f_0 is chosen at 5 kHz, is shown in Fig. 7 in comparison to the true error. The curves are almost on top of each other in most of the frequency range, which shows that the indicator approximates well the sought error. If f_0 was chosen to be one of the frequencies at which the reduction basis enrichment vectors are calculated, $\mathbf{x}(f_0)$ would directly be available when calculating factor k for a point that is included in the reduction basis, which could reduce computational costs. However, the error can drop to very small values at those frequencies (as observed for example in Fig. 4), which makes the ratio between the residuals at those frequencies not representative of the overall offset. Therefore, it is a better choice to select an

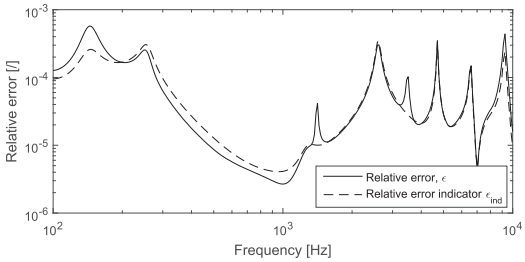

Fig. 7. Comparison of the state vector true relative error and the error indicator.

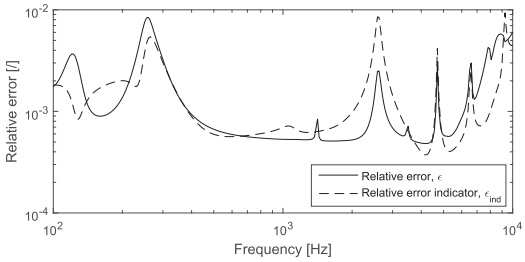

Fig. 8. Comparison of the state vector true relative error and the error indicator at a point further from the points included in the basis.

f_0 far from the enrichment frequencies. Still, it is clear that the error indicator accuracy depends on the choice of f_0; moreover, the estimate deviates further from the true error when evaluating points that are far from the points included in the reduction basis, as in the case shown in Fig. 8. There is therefore an uncertainty about the accuracy of the error indicator which must be taken into account. This is done by requiring a low value of the error indicator for a reduced model to be considered accurate enough; for example, allowing 0.5% as maximum value instead of the usual 1%. This solution proves effective in practice, as will be further discussed in Section 4.

Even though the computation of the error indicator is cheap compared to solving the full system, the time required for the calculation is not negligible. The two most time-consuming steps are the calculation of $\mathbf{x}(f_0)$ for obtaining factor k and the calculation of the force residual, $\Delta\mathbf{f}(\omega)$, for a large number of frequencies. In the considered problem, the first step requires 29 s and the second step 74 s; this shows that checking the accuracy of the response still takes longer than the frequency response calculation itself, which took 9 s for the reduced system obtained in Section 3.1. The time consumption of each step in the calculations is further detailed in Section 4.

3.2.2. Adaptive parametric model order reduction basis updating and optimization framework

A parameter space sampling method for the reduction basis construction that breaks the traditional offline-online approach is suggested here. The fact that only a specific path within the design domain is explored during the optimization is exploited to construct an efficient reduction basis that does not include information of the unexplored parts. Adaptive approaches for pMOR have been previously proposed by e.g. Zahr et al. [27]; however, they consist in solving a series of optimization problems in between which the reduction basis is updated, while the algorithm suggested here embeds an *on-the-fly* basis updating routine into the optimization loop. The method works as follows:

- An initial reduction basis is calculated for the initial parameter set as shown in Section 3.1.
- During the optimization, a new parameter point is added to the global reduced order basis if the accuracy falls below a required level, which is checked by means of the suggested error indicator.

For the addition of a new point m to a reduction basis containing $m-1$ points, the global reduced order basis is obtained as follows. Maintaining the same philosophy as for the single-point reduction basis, the acoustic and structural modal matrices of each point included in the basis are concatenated separately, as

$$\boldsymbol{\Theta}_a = \left[\boldsymbol{\Psi}_a^1 \boldsymbol{\Psi}_a^2 \ \dots \ \boldsymbol{\Psi}_a^{m-1} \boldsymbol{\Psi}_a^m\right] \tag{20}$$

$$\boldsymbol{\Theta}_s = \left[\boldsymbol{\Psi}_s^1 \boldsymbol{\Psi}_s^2 \ \dots \ \boldsymbol{\Psi}_s^{m-1} \boldsymbol{\Psi}_s^m\right]. \tag{21}$$

The orthogonalization is then done on these global matrices, which reduces their size significantly in practice, since many modal vectors calculated for different parameter values are (close to) linearly dependent and therefore eliminated. The same approach is taken to obtain the global enrichment vector matrices,

$$\mathbf{Y}_a = \left[\mathbf{X}_a^1 \mathbf{X}_a^2 \ \dots \ \mathbf{X}_a^{m-1} \mathbf{X}_a^m\right] \tag{22}$$

$$\mathbf{Y}_s = \left[\mathbf{X}_s^1 \mathbf{X}_s^2 \ \dots \ \mathbf{X}_s^{m-1} \mathbf{X}_s^m\right], \tag{23}$$

and the global reduction basis is then formed by concatenating the orthagonalized global modal and enrichment matrices,

$$\mathbf{T} = \begin{bmatrix} \left[\widehat{\boldsymbol{\Theta}}_s \ \widehat{\mathbf{Y}}_s\right] & [\mathbf{0}] \\ [\mathbf{0}] & \left[\widehat{\boldsymbol{\Theta}}_a \ \widehat{\mathbf{Y}}_a\right] \end{bmatrix}. \tag{24}$$

Algorithm 1 describes the procedure for one objective function evaluation using the suggested adaptive reduction scheme. Firstly, the system is reduced with the current reduction basis and the response is calculated. The accuracy of the solution is checked by calculating the error indicator as in Eq. (19) and detecting if its value is below a specified threshold, τ. If the error indicator is above the threshold, the current point is added to the reduction basis, which means that the modal vectors are obtained from ANSYS®, the enrichment components are calculated, and both sets are added to the global transformation matrix as specified in Eqs. (20)–(24). The non-orthogonalized modal and enrichment matrices, Y_a, Y_s, Θ_a and Θ_s, are stored so that the orthogonalization is always done with respect to the mass matrices at the last added parameter point. Since the memory required for storing the matrices and the computational cost of orthogonalizing them grows with their size, a limitation (M) to the number of points that the reduction basis can contain is set. If the basis already contains M points when a new one is to be added, the first point in the basis is discarded, since it is assumed to be the furthest and therefore least relevant to the current point.

Algorithm 1: Objective function evaluation with apMOR

```
[g, T] = ReducedObjectiveFunction(μ, T, τ, M, ω);
Input  : Design parameters μ, current reduced order basis T, reduction tolerance τ, maximum
         number of sample points in basis M, frequency lines ω
Output: Goal function g, updated reduced order basis T
Get model matrices K, M from ANSYS for design parameters μ;
Perform model reduction: K_r = T^T K T, M_r = T^T M T;
Solve the reduced system (K_r − ω^2 M_r) x_r = f_r and obtain the reconstructed vector as x̃ = T x_r for
  all frequency lines in ω;
Evaluate error indicator ε_ind using Eqs. (17)-(19);
if ε_ind ≥ τ then
    if M sample points in T then
        Remove first point from global bases: Θ_a := [Ψ_a^2 ... Ψ_a^M], Θ_s := [Ψ_s^2 ... Ψ_s^M], Y_a := [X_a^2 ... X_a^M],
          Y_s := [X_s^2 ... X_s^M];
    end
    Calculate enriched modal basis Ψ_a^m, Ψ_s^m, X_a^m, X_s^m for parameters μ;
    Set up new global bases, orthogonalize them and update T according to Eqs. (20)-(24);
    Perform model reduction: K_r = T^T K T, M_r = T^T M T;
    Solve the reduced system (K_r − ω^2 M_r) x_r = f_r and obtain the reconstructed vector as x̃ = T x_r
      for all frequency lines in ω;
end
Evaluate objective function g from Eq. (2);
```

The proposed adaptive parametric Model Order Reduction (apMOR) technique can be used in combination with any existing optimization algorithm. In this work, the gradient-based constrained optimization algorithm implemented in the MATLAB Optimization Toolbox function *fmincon* [30] is used, with the gradient being calculated by Finite Differences (FD). At each iteration of the optimization routine, Algorithm 1 is called several times since several objective function evaluations are required for gradient calculation and decision of the next parameter point.

4. Application results

The results obtained for the optimization problem introduced in Section 2 using the suggested apMOR method are discussed here. The thickness and E-modulus of both the tube and the suspension are optimized within the given design space in order to minimize the total velocity at the microphone position over a frequency range between 100 Hz and 10 kHz, when the receiver excites the system with the signals shown in Fig. 2.

Table 5
Computational time spent at different objective function evaluation steps and total minimum, average and maximum time per evaluation, calculated depending on the required steps at each evaluation according to the Algorithm 1.

	Building matrices in ANSYS® and importing into MATLAB®	Reducing system and solving @ 300 freq. lines (min. - max.)	Calculating k factor [eq. (17)]	Evaluating $\Delta\mathbf{f}$ [eq. (16)] and ϵ_{est} [eq. (19)]	Adding point to basis (Table 4)	Total (min. - avg. - max.)
Time [s]	255	9–44	29	73	436.5	337 - 438 - 983 (5.6 - 7.3 - 16.4 min)

4.1. Considerations on the optimization setup

Given that the gradient of the objective function is calculated by FD, at least 5 objective function evaluations are needed at each iteration of the optimization algorithm. Since the accuracy of the reduced system is checked at each objective function evaluation, it is crucial to make the calculation of the error indicator as efficient as possible. As mentioned in Section 3.2.1, updating factor k is relatively time consuming since it requires solving the full system at one frequency. Based on the assumption that the value of k only experiences large variations when the reduction basis is modified or when the parameter values vary significantly, the approach taken here to speed up the process consists in updating k only when a new point is added to the basis and at the start of each *fmincon* iteration. For the rest of objective function evaluations, ϵ_{est} is calculated using the last updated k value and only the force residual needs to be computed, which saves 29 s per evaluation.

The maximum number of points allowed in the reduction basis, M, and the threshold on the error indicator for which the reduction is considered accurate, τ, must be specified beforehand. The first parameter is set here to 5, which has been selected as a trade-off between accuracy and the computational cost required for orthogonalization of the basis. Regarding parameter τ, a value of $5 \cdot 10^{-3}$ (0.5%) is chosen, which is more restrictive than the 1% threshold that would be recommended if the true error was being evaluated instead of an error indicator, and also leaves a small margin with respect to the maximum error at the initial point, shown in Fig. 4, which was $3 \cdot 10^{-3}$. In general, the error decreases when increasing the number of points included in the reduction basis; therefore, it should always be below this threshold when a new point is added.

4.2. Optimization results

The optimization reached convergence after 12 iterations of the *fmincon* algorithm, which required 63 objective function evaluations. During the process, 7 points of the parameter space were added to the reduction basis besides the initial point, which adds up to 8 points in total, and therefore the 3 first points were removed from it during the process to fulfill the selected 5 point limitation. In total, the optimization process took 7 h and 40 min; if the full system had been used, 153 h would have been needed for 63 function evaluations, given that each one takes 2.4 h as shown in Table 3. Therefore, the suggested method speeds up the optimization by a factor of 20.

The time required for a function evaluation with the reduced system varies according to the steps needed and size of the reduced system at each point. The times required for each step are detailed in Table 5, where the minimum total time is given for an evaluation where factor k is not calculated and no new point is added to the basis, and the total maximum is for an

Table 6
Final parameter values.

	$\boldsymbol{\mu}_{out}$
Tube E modulus [Pa]	$1.8 \cdot 10^8$
Tube thickness [mm]	0.973
Suspension E modulus [Pa]	$1 \cdot 10^6$
Suspension thickness [mm]	0.175

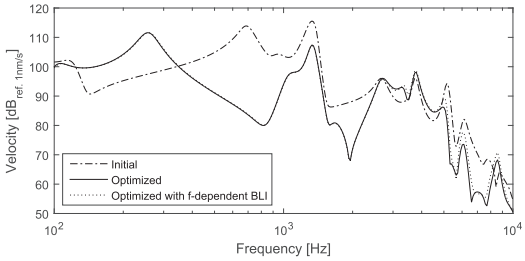

Fig. 9. Total velocity at the microphone position at the initial and final points of the optimization.

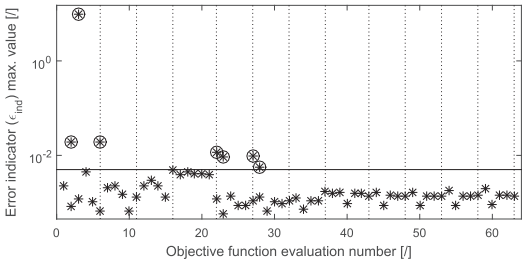

Fig. 10. Evolution of the maximum value of the error indicator vs. objective function evaluations. Simple asterisks: error estimate at the end of the objective function evaluation. Circled asterisks: error estimate before reduction basis update at parameter points that are added to the basis.

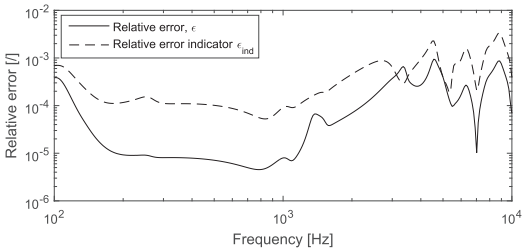

Fig. 11. Comparison of the state vector true relative error and the error indicator at the final point.

evaluation where a new point is added (and therefore the response and error indicator are calculated twice). For the upper bound, the function evaluation is 9 times faster than for the full system, which shows that even in the worst case scenario a significant speed-up is achieved.

The total reduction on the objective function value was of 3.4 dB, which was reached for the parameter values in Table 6. The suspension parameters experienced the largest changes with respect to the initial point, while the tube parameters varied very slightly. The initial and final curves of the total velocity at the microphone position are shown in Fig. 9, where it can be observed that the first peak has been shifted down in frequency as a result of the decrease on the suspension Young's modulus. The peak at 1330 Hz (originated by a peak on the excitation signals) cannot be shifted but is attenuated due to the lower mode overlap resulting from the shift of the first peak. The dotted curve in Fig. 9 shows the velocity curve calculated with frequency dependent losses for the optimized parameters in order to verify that the frequency independent BLI approximation used in the optimization yields realistic results. The differences with respect to the solid curve are small and occur mainly at very low velocity levels, which confirms that the introduced approximation yields meaningful results.

The evolution of the error indicator maximum value with respect to the objective function evaluations is shown in Fig. 10, where the dotted vertical lines indicate the start of a new iteration. The evaluations where the error is above the required threshold τ (indicated by the solid horizontal line) present two values, the circled asterisk being the error before adding the current point to the reduction basis, and the simple asterisk indicating the error after the update. At the function evaluation number 23, the fifth basis update takes place, which means that the basis is now formed by 6 points in total. Therefore, the initial point is removed from it, and the value marked by the simple asterisk is the error after addition of the new point and removal of the first point, which is kept below the required threshold. The same procedure is followed at the function evaluations 27 and 28, keeping the total number of points in the basis at 5. The error estimate at the final point is shown in Fig. 11 in comparison

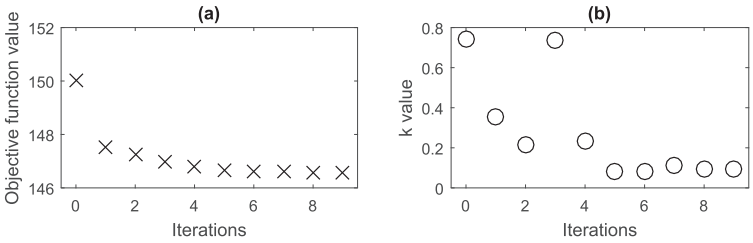

Fig. 12. (a) Evolution of the objective function. (b) Parameter k during the optimization.

with the true error, where it can be seen that the shapes are slightly different, but the values oscillate within the same range.

The objective function and parameter k values at each iteration are shown in Fig. 12(a) and (b). The objective function value experiences its largest change at iteration 1, and it decreases slowly thereafter. Therefore, the largest parameter changes occur at the beginning of the optimization, which explains that the first basis updates take place during iterations 0 and 1, and, after a few updates in iterations 4 and 5, the reduction basis remains unchanged at the second half of the optimization, as shown in Fig. 10. The k value, which is only updated when a point is added or removed from the basis and at the start of each iteration, presents the largest variations within the first 6 iterations, which also correlates with the fact that the reduction basis is being updated in those. Even though it is recalculated at each iteration thereafter, the variations are very small from iteration 7, confirming that it does not change significantly when the parameter variations are small. The fact that no basis updates are needed after iteration 5 makes the final part of the optimization very fast, corroborating that the suggested method is specially powerful for gradient-based optimization problems, where the final steps require many function evaluations around the last point in order to detect convergence.

4.3. Discussion

Even though frequency dependency is not considered in the suggested modal-based reduction approach, visco-thermal losses have been considered by applying a frequency independent approximation that has been shown not to introduce a significant error to the optimization results in the studied case. However, it would be interesting to include other frequency dependent properties that are relevant in the field of hearing aids as well as in others, such as material data or transducer models, for which the suggested method could be extended by considering frequency as an extra parameter, as for example in Refs. [36,37]. Moreover, modelling the air that surrounds the hearing aid would also be desired in order to optimize for the acoustic pressure outside; in that case, calculating the modes can become computationally time consuming since it is challenging to calculate only those modal vectors that are necessary for model reduction in an infinite acoustic domain [38]. Therefore, other techniques such as rational interpolation methods [4] could be a better choice for obtaining a reliable reduction basis, as done in Ref. [39].

The error indicator has been developed as a trade-off between accuracy and computational cost. The accuracy could have been improved by calculating the k factor at several frequencies and taking an average, or by updating it at each objective function evaluation; however, the extra computational time that this would require is not worthwhile in practice, since it has been shown that the true error at the final point is well below the required level, and therefore the used approximation fulfills the purpose for which the error indicator was intended.

Regarding the suggested adaptive parameter sampling algorithm, it is worth noting that the traditional offline-online approach might be more efficient for other applications of parametrized models such as system control, where the speed of the reduced system evaluations during the online phase is crucial, and justifies having a long offline phase where an accurate global basis is obtained. However, in the context of optimization and related applications such as model updating and inverse problems, the reduction basis will rarely be re-used, and the most important factor is the total time that the optimization takes, including reduction basis construction.

To confirm that the suggested approach is more efficient for the discussed case, an approximation of the time that would be required with the offline-online approach can be done from the previous work by the authors presented in Ref. [15], where a simpler version of the hearing aid model presented here was optimized for 2 parameters. In order to build the global reduction basis offline, 4 parameter points were needed, corresponding to the combination of all the extreme values. From that, it can be extrapolated that at least 16 points would be needed when considering 4 parameters as in the current work, for which the reduction basis would take 2 h to be built considering the times given in Table 4. According to Table 6, reducing the system and solving it takes 44 s for a reduction basis with 5 points; from that, we can approximate that it would take about 140 s for a basis with 16 points. Adding the time spent on interfacing with ANSYS®, the online phase would then take about 7 h assuming that 63 objective function evaluations would be needed as well. The complete process would take 9 h, which is longer than the time required by the suggested apMOR technique (7.6 h). Moreover, the time that should be spent in checking the reduction error during the offline phase has not been included in this approximation, which would make the time difference significantly larger in reality.

5. Conclusions

An adaptive algorithm for parametric Model Order Reduction (pMOR) basis construction in optimization problems that updates the reduction basis automatically along the optimization loop avoiding previous parameter space sampling has been presented. The method relies on a newly developed residual-based error indicator to ensure a selected accuracy of the reduction basis at all evaluated points. An enriched modal-based reduction method has been developed, which overcomes the orthogonalization issues that arise from the non-symmetric nature of the vibroacoustic system matrices when the pressure-displacement formulation is used. The performance is demonstrated for a classical optimization problem from the hearing aid field where the feedback between the loudspeaker and the microphone is to be minimized within a wide frequency range (100 Hz–10 kHz), where the objective function evaluation requires fine resolution frequency response calculation. The suggested method is shown to be efficient in such context, since the average objective function evaluation time is 20 times shorter than if using the full

model. Further validation of the proposed methodology by means of experimental measurements of the optimized solution is left as future work.

Acknowledgments

The authors would like to thank the Innovation Fond Denmark and the Oticon Foundation for their financial support.

References

[1] M.B. Sondergaard, C.B.W. Pedersen, Applied topology optimization of vibro-acoustic hearing instrument models, J. Sound Vib. 333 (3) (2014) 683–692, https://doi.org/10.1016/j.jsv.2013.09.029.
[2] B. Besselink, U. Tabak, A. Lutowska, N. van de Wouw, H. Nijmeijer, D. Rixen, M. Hochstenbach, W. Schilders, A comparison of model reduction techniques from structural dynamics, numerical mathematics and systems and control, J. Sound Vib. 332 (19) (2013) 4403–4422, https://doi.org/10.1016/j.jsv.2013.03.025, http://www.sciencedirect.com/science/article/pii/S0022460X1300285X.
[3] P. Koutsovasilis, M. Beitelschmidt, Comparison of model reduction techniques for large mechanical systems, Multibody Syst. Dyn. 20 (2) (2008) 111–128, https://doi.org/10.1007/s11044-008-9116-4.
[4] P. Benner, S. Gugercin, K. Willcox, A survey of projection-based model reduction methods for parametric dynamical systems, SIAM Rev. 57 (4) (2015) 483–531, https://doi.org/10.1137/130932715.
[5] R.R. Craig, M.C.C. Bampton, Coupling of substructures for dynamic analyses, AIAA J. 6 (7) (1968) 1313–1319.
[6] R.R. Craig, Coupling of substructures for dynamic analyses: an overview, in: Collection of Technical Papers - AIAA/ASME/ASCE/AHS/ASC Structures, Structural Dynamics and Materials Conference, vol. 5, 2000, pp. 3–14.
[7] J. Wolf, Modal synthesis for combined structural-acoustic systems, AIAA J. 15 (5) (1977) 743–745, https://doi.org/10.2514/3.60685.
[8] P. Davidsson, G. Sandberg, A reduction method for structure-acoustic and poroelastic-acoustic problems using interface-dependent lanczos vectors, Comput. Meth. Appl. Mech. Eng. 195 (17–18) (2006) 1933–1945, https://doi.org/10.1016/j.cma.2005.02.024.
[9] Z. Ma, I. Hagiwara, Improved mode-superposition technique for modal frequency-response analysis of coupled acoustic-structural systems, AIAA J. 29 (10) (1991) 1720–1726, https://doi.org/10.2514/3.10795.
[10] M. Stammberger, H. Voss, Automated multi-level substructuring for a fluid-solid vibration problem, Numerical Mathematics and Advanced Applications, 2008, pp. 563–570.
[11] M. Maess, L. Gaul, Substructuring and model reduction of pipe components interacting with acoustic fluids, Mech. Syst. Signal Process. 20 (1) (2006) 45–64, https://doi.org/10.1016/j.ymssp.2005.02.008.
[12] E. Creixell-Mediante, J.S. Jensen, J. Brunskog, M. Larsen, A multi-model reduction technique for optimization of coupled structural-acoustic problems, in: Proceedings of Inter-noise 2016, 2016, pp. 7601–7612.
[13] S. Donders, B. Pluymers, P. Ragnarsson, R. Hadjit, W. Desmet, The wave-based substructuring approach for the efficient description of interface dynamics in substructuring, J. Sound Vib. 329 (8) (2010) 1062–1080, https://doi.org/10.1016/j.jsv.2009.10.022.
[14] J. Herrmann, M. Maess, L. Gaul, Substructuring including interface reduction for the efficient vibro-acoustic simulation of fluid-filled piping systems, Mech. Syst. Signal Process. 24 (1) (2010) 153–163, https://doi.org/10.1016/j.ymssp.2009.05.003.
[15] E. Creixell-Mediante, J.S. Jensen, J. Brunskog, M. Larsen, Model reduction for optimization of structural-acoustic coupling problems, Proceedings of Isma 2016.
[16] C. Pal, I. Hagiwara, Dynamic analysis of a coupled structural-acoustic problem - simultaneous multimodal reduction of vehicle interior noise level by combined optimization, Finite Elem. Anal. Des. 14 (2–3) (1993) 225–234, https://doi.org/10.1016/0168-874x(93)90022-i.
[17] L. Hermans, M. Brughmans, Enabling vibro-acoustic optimization in a superelement environment: A case study, in: Proceedings of the International Modal Analysis Conference and Exhibit, vol. 2, 2000, pp. 1146–1152.
[18] E. Balmès, Parametric families of reduced finite element models. theory and applications, Mech. Syst. Signal Process. 8 (8) (1994) 381–394, https://doi.org/10.1006/mssp.1996.0027.
[19] M. Drohmann, K. Carlberg, The romes method for statistical modeling of reduced-order-model error, SIAM/ASA J. Uncertain. Quantif. 3 (1) (2015) 116–145, https://doi.org/10.1137/140969841.
[20] A. Quarteroni, G. Rozza, A. Manzoni, Certified reduced basis approximation for parametrized partial differential equations and applications, J. Math. Ind. 1 (1) (2011) 1–49, https://doi.org/10.1186/2190-5983-1-3.
[21] U. Hetmaniuk, R. Tezaur, C. Farhat, An adaptive scheme for a class of interpolatory model reduction methods for frequency response problems, Int. J. Numer. Meth. Eng. 93 (10) (2013) 1109–1124, https://doi.org/10.1002/nme.4436.
[22] G. Rozza, An introduction to reduced basis method for parametrized pdes, Ser. Adv. Math. Appl. Sci. 82 (2010) 508–519.
[23] A. Manzoni, A. Quarteroni, G. Rozza, Computational reduction for parametrized pdes: strategies and applications, Milan J. Math. 80 (2) (2012) 283–309, https://doi.org/10.1007/s00032-012-0182-y.
[24] A. Paul-Dubois-Taine, D. Amsallem, An adaptive and efficient greedy procedure for the optimal training of parametric reduced-order models, Int. J. Numer. Meth. Eng. 102 (5) (2015) 1262–1292, https://doi.org/10.1002/nme.4759.
[25] T. Bui-Thanh, K. Willcox, O. Ghattas, Model reduction for large-scale systems with high-dimensional parametric input space, SIAM J. Sci. Comput. 30 (6) (2008) 3270–3288, https://doi.org/10.1137/070694855.
[26] Y. Yue, K. Meerbergen, Accelerating optimization of parametric linear systems by model order reduction, SIAM J. Optim. 23 (2) (2013) 1344–1370, https://doi.org/10.1137/120869171.
[27] M.J. Zahr, C. Farhat, Progressive construction of a parametric reduced-order model for pde-constrained optimization, Int. J. Numer. Meth. Eng. 102 (5) (2015) 1111–1135, https://doi.org/10.1002/nme.4770.
[28] C. Gogu, Improving the efficiency of large scale topology optimization through on-the-fly reduced order model construction, Int. J. Numer. Meth. Eng. 101 (4) (2015) 281–304, https://doi.org/10.1002/nme.4797.
[29] R. Bossart, N. Joly, M. Bruneau, Hybrid numerical and analytical solutions for acoustic boundary problems in thermo-viscous fluids, J. Sound Vib. 263 (1) (2003) 69–84.
[30] MATLAB Optimization Toolbox User's Guide R2015b, MathWorks, Natick, MA, 2015.
[31] R.H. Byrd, M.E. Hribar, J. Nocedal, An interior point algorithm for large-scale nonlinear programming, SIAM J. Optim. 9 (4) (1999) 877–900, https://doi.org/10.1137/S1052623497325107.
[32] ANSYS, Inc., ANSYS Academic Research, Release 17.1, Help System, Theory Reference.
[33] G. Golub, C. van Loan, Matrix Computations, The Johns Hopkins University Press, 1996.
[34] D.J. Rixen, Generalized mode acceleration methods and modal truncation augmentation, 19th AIAA Applied Aerodynamics Conference.
[35] P. Benner, S. Gugercin, K. Willcox, A survey of model reduction methods for parametric systems, Max Planck Institute Magdeburg Preprint MPIMD/13–14, available from http://www.mpi-magdeburg.mpg.de/preprints/.
[36] Z.S. Chen, G. Hofstetter, H.A. Mang, A 3d boundary element method for determination of acoustic eigenfrequencies considering admittance boundary conditions, J. Comput. Acoust. 1 (4) (1993) 455–468, https://doi.org/10.1142/S0218396X93000238.
[37] H. Peters, N. Kessissoglou, S. Marburg, Modal decomposition of exterior acoustic-structure interaction problems with model order reduction, J. Acoust. Soc. Am. 135 (5) (2014) 2706–2717, https://doi.org/10.1121/1.4869086.

[38] L. Moheit, S. Marburg, Infinite elements and their influence on normal and radiation modes in exterior acoustics, J. Comput. Acoust. 25 (04) (2017) 1650020, https://doi.org/10.1142/S0218396X1650020X.
[39] A. van de Walle, Y. Shiozawa, H. Matsuda, W. Desmet, Model order reduction for the transient vibro-acoustic simulation of acoustic guitars, in: Proceedings of Isma2016 International Conference on Noise and Vibration Engineering and Usd2016 International Conference on Uncertainty in Structural Dynamics, 2016, pp. 4007–4017.

Report E

Adaptive parametric model order reduction for vibro-acoustic problems: further applications

Adaptive parametric model order reduction for vibro-acoustic problems: further applications

Ester Creixell-Mediante

Contents

---

1. Introduction

This report presents three applications of the adaptive parametric Model Order Reduction (apMOR) technique presented by the author in Paper D of the PhD thesis in which this report is included. The first application consists in the optimization of the dynamic compliance of a plate coupled to an air column, where the thickness of each of the elements in the plate is a design variable. The problem can be seen as a kind of topology optimization, as done in Ref. [1], and it is analyzed here in order to study the possibility of applying the developed technique to high-dimensional parametric problems. The second application is an extension of the hearing aid optimization problem presented in Paper D, where the air that surrounds the hearing aid is added to the model and the exterior pressure at the microphone position is minimized. Due to the approach used for modelling the Sommerfield condition of the exterior air, the modal-based reduction basis used in Paper D becomes inaccurate in this case, and a rational interpolation method is used to obtain the reduction basis instead. Lastly, a variation of the apMOR technique suitable for uncertainty evaluation by Monte Carlo methods is developed and tested on the hearing aid model presented in Paper D. The technique differs from the one developed for optimization in that a global reduction basis that is accurate throughout the whole parameter domain is sought, since Monte Carlo methods draw random samples of the uncertain parameters. For an efficient reduction basis construction, a greedy algorithm combined with the error indicator developed in Paper D is used. The three applications are presented in sections 2, 3 and 4 of this report.

2. Plate thickness optimization

In this section, the plate thickness optimization problem presented in Ref. [2] (or Paper B of the thesis) is solved using the apMOR technique presented in Paper D. In Paper B, the strategy employed for reduction of the problem consisted in creating a global reduction basis that was accurate in the whole design domain previous to starting the optimization, while the adaptive technique proposed in Paper D builds an efficient reduction basis adaptively during the optimization. Another difference is that the modal-based reduction basis is enriched with response vectors in the technique developed in Paper D, while it was purely formed by modal vectors in Paper B. Moreover, structural damping is added to the plate model in the present study, in order to avoid infinite amplitude values on the peaks of the vibration response that is minimized. For these reasons, the results obtained here cannot be directly compared to those from Paper B; however, since solving the unreduced system is less costly than in the case studied in Paper D, it is possible here to optimize the plate both with the reduced and the full system and compare the total time spent.

2.1. Problem statement

A model of a small plate coupled to an air column is considered here. The dimensions of the plate are $L_x = 40$ mm and $L_y = 30$ mm, and the objective is to optimize the thickness of each of its elements, which is allowed to vary between 0.01 mm and 10 mm. The material of the plate has a density of 1040 kg/m^3, a Young's modulus of $2 \cdot 10^9$ Pa, Poisson's ratio of 0.4 and Rayleigh damping coefficients $\alpha = 0.5$ and $\beta = 5 \cdot 10^{-6}$. The air column is $Lz = 50$ mm high, and its walls are rigid, except for the side that is coupled to the plate. The small dimensions make the modal density low up to 10 kHz, as is also typically the case for hearing aid parts; therefore, it is appropriate to simulate the response up to such frequencies with a FE model. L_x, L_y and L_z are discretized with 20, 16 and 25 elements respectively, yielding acoustic hexahedral elements of 2x1.9x2 mm. The plate elements are formulated with 3 DOFs per node (one displacement and two rotations), and the acoustic elements are formulated with 1 DOF per node, being the pressure, and using linear shape functions, with the total number of DOFs resulting in 10353.

The optimization problem consists in minimizing the dynamic compliance of the system when the plate is excited by a unitary perpendicular point force on its central point. The system is governed by the equation of motion,

$$\mathbf{S}\mathbf{x} = \mathbf{f}, \tag{1}$$

where $\mathbf{x}$ is the state vector, including displacements and pressures, $\mathbf{f}$ is the input force vector and $\mathbf{S}$ is the system matrix,

$$\mathbf{S} = \left(\mathbf{K} + j\omega_k \mathbf{C} - \omega^2 \mathbf{M}\right), \tag{2}$$

where $\mathbf{K}$, $\mathbf{C}$ and $\mathbf{M}$ are the structure-acoustic stiffness, damping and mass matrices, including coupling. The optimization problem is formulated as,

$$\underset{\mathbf{t}}{\text{minimize}} \qquad g(\mathbf{t}) = \sum_{k=1}^{K} \mid \mathbf{f}^T \mathbf{x}(k, \mathbf{t}) \mid \tag{3}$$

$$\text{subject to} \qquad V(\mathbf{t}) \leq c \tag{4}$$

$$10^{-5} \geq \mathbf{t} \geq 10^{-2},$$

where $\mathbf{t}$ is the vector of design variables (plate element thicknesses), K is the total number of frequencies considered in the optimization and k is the k-th considered frequency. 300 frequency lines logarithmically distributed between 100 Hz and 10 kHz are considered here, since this is the typical frequency range of interest in hearing aid simulations. The problem is constrained by the total volume $V(\mathbf{t})$ of the plate being

below a limit c, in this case set to 200 mm^3. When the optimization is done with reduction, the reconstructed state vector $\tilde{\mathbf{x}}$ is used for the calculation of $g(\mathbf{t})$ instead of $\mathbf{x}$ (see Paper D for further details on the reduction and calculation of the reconstructed vector).

Unlike for the model in Paper D, where the gradient had to be approximated by finite differences due to the difficulty in obtaining an analytical expression for it, the gradient can be calculated analytically here since there is an explicit dependency between the structural mass and stiffness element matrices and the thickness of the elements. By the adjoint method [3], the sensitivity analysis is done as

$$\frac{dg}{dt_e} = -\sum_{k=1}^{K} \Re\left(\boldsymbol{\lambda}^T \frac{\partial \mathbf{S}(k)}{\partial t_j}\mathbf{x}(k)\right) \tag{5}$$

where $\boldsymbol{\lambda}$ can be obtained by solving the adjoint problem,

$$\mathbf{S}^H(k)\boldsymbol{\lambda} = \left(\frac{\partial g}{\partial \mathbf{x}_\Re} + j\frac{\partial g}{\partial \mathbf{x}_\Im}\right) = \left(\frac{\mathbf{f}^T\mathbf{x}_\Re\mathbf{f} + j\mathbf{f}^T\mathbf{x}_\Im\mathbf{f}}{g}\right) = \frac{\mathbf{f}^T\mathbf{x}\mathbf{f}}{g}, \tag{6}$$

with the superscript ^{H} denoting the conjugate transpose, $\mathbf{x}_\Re$ and $\mathbf{x}_\Im$ being the real and imaginary parts of the state vector $\mathbf{x}$, and assuming that $\mathbf{f}$ is real. For purely structural systems, the adjoint problem does not need to be solved for compliance problems, since $\mathbf{S}(k)$ is symmetric and $\boldsymbol{\lambda}$ becomes a multiple of $\mathbf{x}$. This assumption was wrongly applied in the plate study in Paper B; however, for the coupled problem, which has unsymmetric matrices, this additional problem must be solved.

Just like for the original problem, the adjoint problem can be reduced by projection of the transposed system matrices on the reduction basis, yielding

$$\left((\mathbf{K}^H)_r + j\omega(\mathbf{C}^H)_r - \omega^2(\mathbf{M}^H)_r\right)\boldsymbol{\lambda}_r = \frac{\mathbf{f}^T\tilde{\mathbf{x}}}{g}\mathbf{f}_r. \tag{7}$$

The reconstructed adjoint $\tilde{\boldsymbol{\lambda}}$ and state $\tilde{\mathbf{x}}$ vectors are then used in the sensitivity calculation in eq. (5) when the optimization is done with reduction.

In topology optimization, sensitivities are spatially filtered in order to obtain mesh-independent designs. In the current study, we apply the filtering scheme proposed in [4] with a radius of 6 elements in order to obtain smooth designs.

2.2. Reduction basis construction

The reduction basis is constructed as described in Paper D. All modal vectors below 12 kHz are included, and the modal basis is enriched with three response vectors calculated at 5 kHz, 8 kHz and 10 kHz. The optimization starts with a plate with constant thickness and a volume equal to the constraint of 200 mm^3. Given that the design domain of the element thicknesses comprises 4 orders of magnitude (10^{-5} to 10^{-2}), the modal content can vary more significantly than in the hearing aid case studied in Paper D. Therefore, the initial reduction basis is constructed with the vectors calculated both at the initial optimization point and at the lower bound (constant thickness of 10^{-5}), since the number of modes below 12 kHz is highest for the smallest thickness and therefore a lot of information is added to the reduction basis by including that point.

2.3. Optimization results

The optimization problem is solved both with the full system and the apMOR technique. The results for both methods are summarized in Table 1, and the optimized frequency responses and plate designs are

	Number of function evaluations	Total time (hours)	Time per iteration (mins)	Final objective function value
Full system	48	9	11.25	0.314
Reduced system	42	1	1.43	0.318

Table 1: Results of the optimization of the plate for the full system and the adaptively reduced system.

shown in Figures 1 and 2. The objective function value at the initial point is of 3.203, and it is reduced to 10% at the end of the optimization with both approaches; even though, the obtained designs are similar but not identical. The optimized designs are much smoother and symmetric than those that were obtained in Paper B, which is due to both the addition of damping to the plate model and the spatial sensitivity filtering. The reduction basis is updated a total of 8 times during the optimization, and the total optimization time is 9 times shorter when using the apMOR technique compared to solving the full system, which demonstrates that highly dimensional parametric problems can also benefit from the suggested apMOR technique.

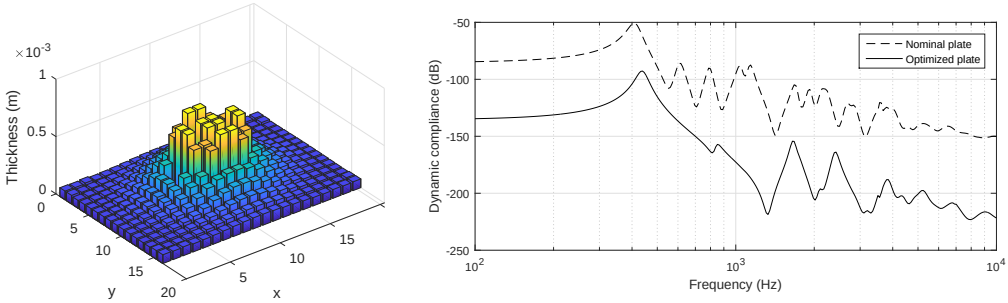

Figure 1: Results for the optimization with full system. (Left) Final plate design. (Right) Dynamic compliance for the nominal plate and the optimized plate

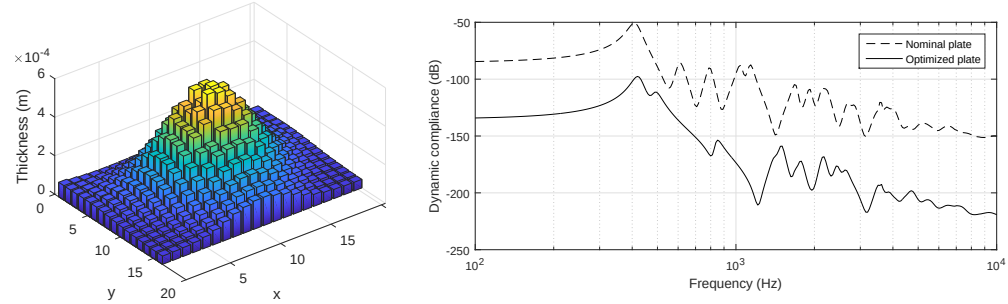

Figure 2: Results for the optimization with adaptively reduced system. (Left) Final plate design. (Right) Dynamic compliance for the nominal plate and the optimized plate

3. Optimization of a hearing aid model with surrounding air

In Paper D, the proposed apMOR technique is applied to the optimization of a hearing aid model, where the vibration at the microphone position due to the loudspeaker excitation is minimized. The air that surrounds the hearing aid is not modeled in that case, since its influence on the vibration level at the microphone position is not significant. However, it would be interesting to include the acoustic pressure at the microphone position in the minimization problem, and in this way minimize both structural and acoustic feedback paths. To do so, it is necessary to model the air that surrounds the hearing aid.

In an exterior acoustics problem, the pressure waves must satisfy the Sommerfield radiation condition. Since the model of the hearing aid is done in ANSYS, the technique that the software provides to implement this condition is used. It consists in truncating the outer air domain and introducing a second-order absorbing element on the outer surface of the truncated air domain. For a 3-D acoustic analysis, the absorbing boundary must be a spherical enclosure. Further details on the implementation of the absorbing elements can be found in the ANSYS theory reference [5]. The hearing aid model with outer air, shown in Figure 3, has 156732 DOFs (1.7 times the number of DOFs in the model without outer air). All dimensions and material properties are described in Paper D, and the outer air sphere has a radius of 30mm.

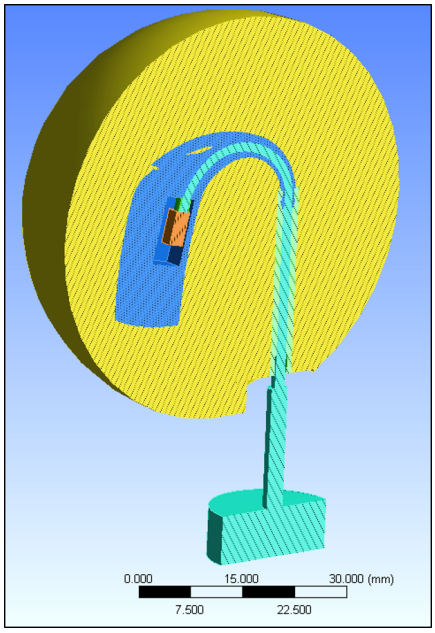

Figure 3: Considered hearing aid model with surrounding air sphere

3.1. Reduction basis construction

Using the enriched modal-based reduction approach described in Paper D, which includes all modes below 12 kHz and 4 enrichment response vectors at 100 Hz, 1 kHz, 7 kHz and 10 kHz, the relative error at an acoustic DOF on the microphone position is above 0.01 (1%) at most of the frequency range, as shown in Figure 4. A reduction basis of these characteristics was sufficient for approximating the structural vibration

response with an error below 1%, as shown in Paper D; therefore, the reason for a worse result here may come from inaccuracies in the calculation of the outer air modes in ANSYS when the mentioned absorbing boundary condition is used.

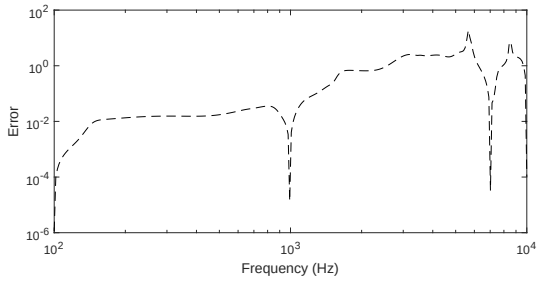

Figure 4: Error on a pressure DOF at the microphone position with modal-based reduction

Exterior acoustics modes can be accurately calculated when the Sommerfield condition is implemented with other techniques such as infinite elements, and can be used for efficient calculation of sound power and acoustic radiation from structures [6]. However, since infinite elements are not available in ANSYS, a solution to circumvent the modal calculation problem is switching to a non modal-based reduction basis approach. Krylov subspace projection methods are suitable for problems with one excitation case, and could therefore be a good alternative. They are based on moment-matching of the frequency response at certain expansion points (i.e. certain frequencies), and the basis vectors can be efficiently calculated using a second-order Arnoldi method [7].

Using a Krylov subspace reduction basis with 3 expansion points (1 kHz, 5 kHz and 8 kHz) and order 60, the obtained error at the pressure DOF on the microphone position, shown in Figure 5, is now below 1% for the whole frequency range. The reduction basis has in this case 211 vectors, and the time required for solving the reduced system at 300 frequencies is 17 seconds, which is twice the time that was required with the reduction basis used in Paper D.

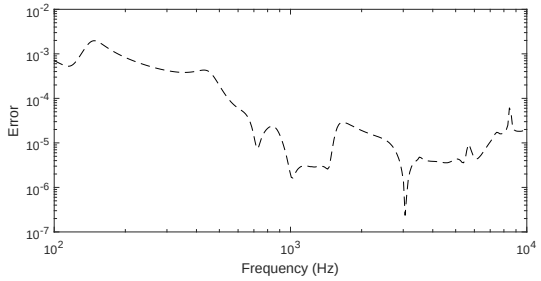

Figure 5: Error on a pressure DOF at the microphone position with Krylov-based reduction

3.2. Optimization problem: minimization of vibration and acoustic pressure

The objective of the optimization is to minimize both the velocity and the acoustic pressure at the microphone position due to the receiver excitation. The objective function is formulated as the sum in dB

of the velocity level and the sound pressure level at one node on the microphone position,

$$\begin{aligned} \underset{\boldsymbol{\mu}}{\text{minimize}} \;\; & g(\boldsymbol{\mu}) = 10\log\sum_{k=1}^{K}\left|\frac{\mathbf{v}_m(\boldsymbol{\mu},k)}{v_{ref}}\right|^2 + 10\log\sum_{k=1}^{K}\left|\frac{\mathbf{p}_m(\boldsymbol{\mu},k)}{p_{ref}}\right|^2 \\ \text{subject to} \;\; & \boldsymbol{\mu}_l \geq \boldsymbol{\mu} \geq \boldsymbol{\mu}_u, \end{aligned} \tag{8}$$

where $|\mathbf{v}_m(\boldsymbol{\mu},k)|$ is the magnitude of the total velocity at the selected node on the microphone position, calculated as $\left|\sqrt{v_{mx}^2+v_{my}^2+v_{mz}^2}\right|$, v_{ref} is the reference structural velocity of 1 nm/s, $|\mathbf{p}_m(\boldsymbol{\mu},k)|$ is the magnitude of the pressure at the same node, p_{ref} is the reference pressure of 20 μPa, k is the k-th discrete frequency line and K is the total number of frequencies (300 frequencies logarithmically distributed between 100 Hz and 10 kHz in this case). The vector $\boldsymbol{\mu}$ contains the four considered optimization parameters: the Young's moduli and the thicknesses of the tube and the suspension, which can vary within the bounds specified in Paper D.

3.3. Optimization results

Running the optimization with the apMOR algorithm given in Paper D, 15 hours, 50 function evaluations and 24 basis updates are needed to reach convergence. At the final point, the Krylov basis had 1590 vectors. The times spent on each step of one objective function evaluation are shown in Table 2, compared to the times that were needed in the case presented in Paper D. The mean total time is 2.3 times longer here, which is not only due to the bigger size of the reduced basis, but also because the number of basis updates is much larger (24 vs. 7). The reason for such an increment in the number of basis updates for a similar number of objective function evaluations is that the reduction error was evaluated here only for the pressure DOF that is targeted by the optimization, which is more sensitive than the average model response error that was used in Paper D. However, one function evaluation with the full system takes 4.9 hours, and therefore the mean reduced system function evaluation time is still 17.5 times shorter.

Time [s]	Building matrices in ANSYS® and importing into MATLAB®	Reducing system and solving @ 300 freq. lines (min. - max.)	Calculating k factor	Evaluating $\Delta\mathbf{f}$ and ϵ_{est}	Adding point to basis	Total (min. - avg. - max.)
Modal (No outer air)	255	9 - 44	29	73	436.5	337 - 438 - 983 (5.6 - 7.3 - 16.4 mins)
Krylov (With outer air)	255	13 - 192	61	100	424	429 - 1008 - 1385 (7.15 - 17 - 23 mins)

Table 2: Computational time spent at different objective function evaluation steps and total minimum, average and maximum time per evaluation, calculated depending on the required steps at each evaluation according to the Algorithm 1 in Paper D.

The initial and optimized vibration and pressure frequency responses are shown in Figures 6 and 7. The results are very similar to those obtained in Paper D, which shows that reducing the vibration at the microphone position also reduces the acoustic pressure at that point.

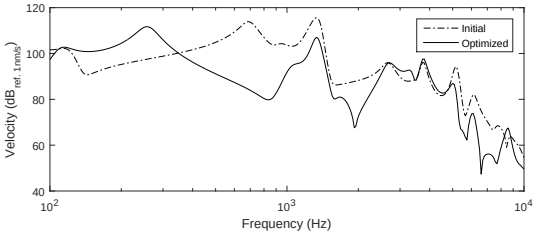

Figure 6: Initial and optimized velocity at the microphone position

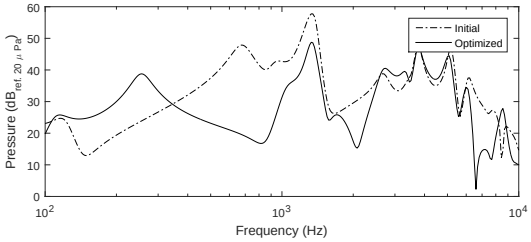

Figure 7: Initial and optimized pressure at the microphone position

4. Efficient reduction basis construction for uncertainty evaluation

Another application that can benefit from parametric model order reduction is uncertainty analysis, where the variability of the response of a system due to uncertainties in the input parameters is evaluated. Monte Carlo methods are often used, which consist in evaluating the system response for large numbers of combinations of design parameters generated randomly; solving the system such a large number of times becomes expensive, and model reduction can be applied to speed up the process.

Unlike in optimization problems, the whole parameter domain is explored in this application and the system must be solved a large number of times. Therefore, it is more efficient to use an offline-online approach, where a reduction basis that represents the whole parameter space accurately is constructed beforehand (offline), and only the reduced system is used during the Monte Carlo simulation (online).

The construction of the reduction basis can be done most efficiently by means of a greedy algorithm. The general idea of greedy algorithms is to iteratively find those points in the design domain for which the reduction error is largest and add them to the reduction basis. A cheap error indicator is needed in order to make this process efficient. In the simplest implementation of the method, a grid of points in the parameter space is pre-selected, where the error indicator is evaluated and the point with highest error is added to the basis at each iteration of the algorithm, until the error at all points in the grid is below a certain threshold. Since the error is only evaluated in the pre-defined grid, it might be that the resulting basis is not accurate enough at other points. Some authors have suggested adaptive approaches for finding the points where the error is worst, based on surrogate models of the error [8] or by solving an optimization problem that maximizes the error within the parameter domain [9].

The error indicator developed in Paper D can be used in combination with a greedy algorithm for reduction basis construction. For the hearing aid model presented in Paper D, calculating the error indicator is significantly faster than evaluating the real error; however, it is still relatively time consuming since it

requires 1) building the system matrices, 2) importing them from ANSYS, 3) solving the full system at one frequency to obtain factor k and 4) evaluating the force residual. The adaptive approaches mentioned above require the evaluation of the error indicator at many points, and can become too time consuming with the available error indicator. The simpler approach that uses a pre-defined grid is therefore chosen here. In the following, the procedure to build the reduction basis is described, and the technique is tested for the hearing aid model presented in Paper D, considering the same 4 parameters and the same enriched modal reduction basis approach.

4.1. Reduction basis construction

The proposed greedy sampling technique is described in the following. A grid of points is defined, and an initial reduction basis is computed. At each iteration of the greedy algorithm, the grid point with the largest reduction error must be added to the basis; however, in order to avoid evaluating the error estimator for all grid points at each iteration, the parameter points that are furthest from those already added in the reduction basis are evaluated first. When a point with an error value above a selected threshold, τ, is found, it is added to the reduction basis, and the iteration is finalized. The proposed algorithm works as follows:

1. Select one or more initial points of the grid arbitrarily, calculate the enriched modal basis vectors and form the initial global reduction basis.
2. Find the point of the grid furthest to the points already added in the basis.
3. Evaluate the error indicator at the point. If the estimated error is above the requested tolerance, τ, add the point to the global reduction basis. If the error indicator is below τ, find the next furthest point and repeat the process until a point is added to the basis, or all points in the grid have been checked.
4. If a model has been added to the basis in step 3, repeat 2 and 3. Otherwise, the algorithm is finished.

The error indicator proposed in Paper D is calculated as

$$\epsilon_{ind}(\omega) = \frac{k||\Delta\mathbf{f}(\omega)||_2}{||\tilde{\mathbf{x}}(\omega)||_2} \tag{9}$$

where $||\Delta\mathbf{f}(\omega)||_2$ is the norm of the force residual, $||\tilde{\mathbf{x}}(\omega)||_2$ is the norm of the reconstructed state vector, ω is the angular frequency and k is a scaling factor calculated as

$$k = \frac{||\Delta\mathbf{x}(f_0)||_2}{||\Delta\mathbf{f}(f_0)||_2} \tag{10}$$

where f_0 is a selected frequency within the frequency range of interest.

Since calculating the scaling factor k requires solving the full system at frequency f_0 to obtain $||\Delta\mathbf{x}(f_0)||_2$, in Paper D, the k value is only updated when a new point is added to the basis, in order to speed up process. The most recent value of k is then used in subsequent error indicator evaluations, since it is assumed that the value of k does not vary significantly when the parameter values experience small variations. However, this cannot be assumed in the current application, where the subsequent parameter samples are selected as far as possible from the last added point. Therefore, we use a different approach where $||\Delta\mathbf{x}(f_0)||_2$ is still only calculated when a new point is added to the reduction basis, and the technique suggested in Ref. [8] is used to estimate k in subsequent evaluations. The technique is based on a linear model that uses the information from all points where $||\Delta\mathbf{x}(f_0)||_2$ has been calculated. The model is a simplification of the statistical methods suggested in Ref. [10] for approximating the relation between error indicators and real errors. The chosen approach suggests that there is a linear dependency between the logarithms of the norms of the force residual and the state vector residual, i.e.

$$\log(||\Delta\mathbf{x}||_2) \approx \gamma \log(||\Delta\mathbf{f}||_2) + \beta, \tag{11}$$

where γ and β are the linear model parameters, which can be estimated by curve fitting using all calculated values of $||\Delta\mathbf{x}(f_0, \boldsymbol{\mu})||_2$ and corresponding $||\Delta\mathbf{f}(f_0, \boldsymbol{\mu})||_2$, with $\boldsymbol{\mu}$ being the parameter vector. k can then be estimated at other points using only the force residual, as

$$k \approx \frac{(||\Delta\mathbf{f}(f_0, \boldsymbol{\mu})||_2)^{\gamma} + e^{\beta}}{||\Delta\mathbf{f}(f_0, \boldsymbol{\mu})||_2}. \tag{12}$$

4.2. Reduction basis for a hearing aid model

The suggested procedure is tested with the hearing aid model introduced in Paper D. The evaluation grid is created by sampling each parameter at 3 equidistant points, which results in $3^4 = 81$ grid points. The initial reduction basis is formed with the reduction vectors calculated at two parameter points corresponding to all parameters upper bounds and lower bounds. We require that the relative error at all points is below 1% with the resulting reduction basis; in order to account for possible underestimations of the error indicator, τ is set to a value of 0.1%.

The greedy algorithm execution results in 8 parameter points added to the initial 2, which gives a final reduction basis formed by 766 vectors. Figure 8 shows the samples and fitted linear model between the logarithm of the residuals calculated for the 8 points added to the reduction basis, which confirms that the assumed linear relationship is fulfilled. The true error for the resulting reduction basis has been calculated at the 81 grid points, which has yielded values well below 1% at all points, as shown in Figure 9. Therefore, the accuracy requirement is fulfilled by the obtained reduction basis.

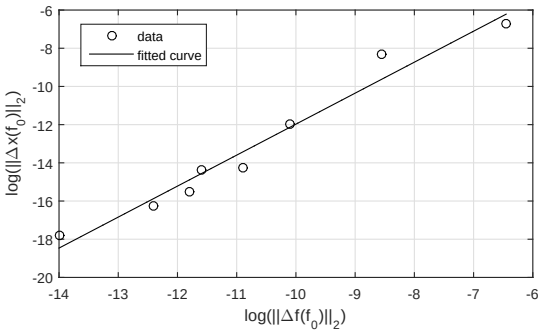

Figure 8: Logarithms of state vector residual vs. force residual and fitted linear model

Figure 9 (left) also shows the error indicator values for the 81 evaluated points, calculated with the k factor resulting from the linear fit, where it can be seen that the indicator presents values below the true error in all cases. As shown in Paper D, the error may be underestimated by the indicator due to the fact that factor k is calculated for one only frequency. In the present case, the linear model fit used to calculate k can also provide confidence intervals for the γ and β parameters, which makes it possible to use a β value corresponding to a higher confidence interval, and obtain a more conservative value of the error indicator that lowers the chances of underestimation. The error indicator values when the k factor is calculated with a β corresponding to the 80% confidence interval is shown in Figure 9 (right). The error indicator is now much closer to the true error, and it only underestimates the true error slightly at very few points.

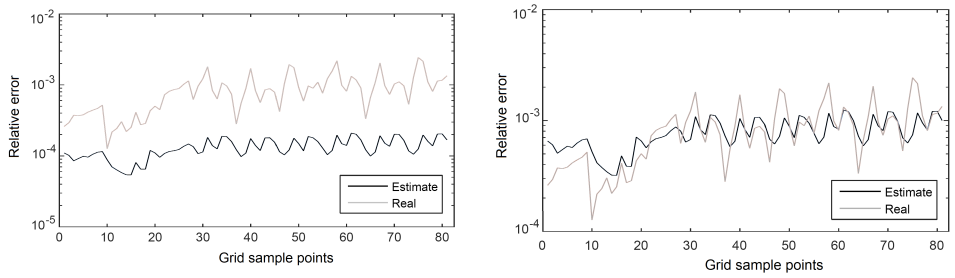

Figure 9: (left) Maximum value of the error indicator compared to the actual relative error at the 81 grid points. (right) Maximum value of the error indicator when the 80% confidence interval for β is used compared to the actual relative error at the 81 grid points

References

[1] W. Akl, A. El-Sabbagh, K. Al-Mitani, A. Baz, Topology optimization of a plate coupled with acoustic cavity, International Journal of Solids and Structures 46 (10) (2009) 2060–2074. doi:10.1016/j.ijsolstr.2008.05.034.

[2] E. Creixell-Mediante, J. S. Jensen, J. Brunskog, M. Larsen, A multi-model reduction technique for optimization of coupled structural-acoustic problems, Proceedings of Inter-noise 2016 (2016) 7601–7612.

[3] M. P. Bendsøe, O. Sigmund, Topology Optimization - Theory, Methods, and Applications, Springer Verlag, 2003.

[4] O. Sigmund, T. U. of Denmark, DTU, On the design of compliant mechanisms using topology optimization, Vol. 535, 1996.

[5] ANSYS, Inc., ANSYS Academic Research, Release 17.1, Help System, Theory Reference.

[6] L. Moheit, S. Marburg, Infinite elements and their influence on normal and radiation modes in exterior acoustics, Journal of Computational Acoustics 25 (04) (2017) 1650020. doi:10.1142/S0218396X1650020X.

[7] Z. Bai, Y. Su, Dimension reduction of large-scale second-order dynamical systems via a second-order arnoldi method, Siam Journal on Scientific Computing 26 (5) (2005) 1692–1709. doi:10.1137/040605552.

[8] A. Paul-Dubois-Taine, D. Amsallem, An adaptive and efficient greedy procedure for the optimal training of parametric reduced-order models, International Journal for Numerical Methods in Engineering 102 (5) (2015) 1262–1292. doi:10.1002/nme.4759.

[9] T. Bui-thanh, K. Willcox, O. Ghattas, Model reduction for large-scale systems with high-dimensional parametric input spacedoi:10.1.1.145.7923.

[10] M. Drohmann, K. Carlberg, The romes method for statistical modeling of reduced-order-model error, Siam/asa Journal on Uncertainty Quantification 3 (1) (2015) 116–45, 116–145. doi:10.1137/140969841.

Paper F

Topology optimization of vibro-acoustic systems with strong coupling

Topology optimization of vibro-acoustic systems with strong coupling. ☆

Ester Creixell-Mediante[a,b,*], Jakob S. Jensen[a], Jonas Brunskog[a], Martin Larsen[b]

[a] *Acoustic Technology, Department of Electrical Engineering, Technical University of Denmark, Ørsteds Plads 352, 2800 Kgs. Lyngby, Denmark*
[b] *Oticon A/S, Kongebakken 9, 9765 Smørum, Denmark*

Abstract

Topology optimization is a powerful, versatile tool that has been applied successfully in many engineering fields. In vibro-acoustic design problems, the fact that the interface between the solid and the acoustic domains varies during the optimization poses an extra challenge for the sensitivity calculation. In this paper, two topology optimization methods for structure-acoustic interaction problems that have been proposed in the literature are compared in the context of hearing aid suspension design, a system where the structural-acoustic coupling is strong due to the suspension shape and material properties. The first method, referred to as "Mixed-MMA", uses a mixed formulation of the fluid-structure interaction problem where both the structural and the acoustic domains are governed by the same equations and present displacement and pressure primary variables. This allows for converting solid elements into fluid ones, and vice-versa, by varying their material properties, which can be done in a smooth way by allowing intermediate elements during the optimization. The second method, referred to as "Segregated-BESO", uses the more conventional formulation of the problem where the solid and the acoustic domains are described by different equations and primary variables; therefore, the fluid-structure interface must be well-defined at all stages, and an optimization strategy that uses discrete variables is used. A drawback of the second method is that the sensitivities cannot be calculated accurately, since an interpolation scheme between solid and acoustic elements is not available; however, attractive features are the ease of implementation in commercial FE softwares and the compactness of the segregated formulation. The performance of the two methods is evaluated on a 2D suspension design problem for different degrees of the structure-acoustic coupling strength, which shows that the Segregated-BESO method is challenged due to the sensitivity errors when the coupling is strong.

Keywords: Topology optimization, vibro-acoustics, fluid-structure interaction

1. Introduction

Numerical structural optimization is gaining relevance in industrial design procedures, which have evolved from a purely prototyping and testing approach to a context where simulation tools are used from the early phases to come up with optimal designs. In the field of hearing aids, the main design challenge from a vibro-acoustic point of view is the minimization of feedback, which is the main gain limiting factor of the hearing instruments. Parametric optimization is already used in the design process, where geometric or material parameters are adjusted to minimize feedback paths. However, the design of critical parts such as the receiver suspension (which has the function of isolating the loudspeaker from the rest of the hearing

☆ Part of this article has been submitted to the NOVEM 2018 conference
* Corresponding author
Email addresses: emed@oticon.com (Ester Creixell-Mediante), json@elektro.dtu.dk (Jakob S. Jensen), jbr@elektro.dtu.dk (Jonas Brunskog), mnla@oticon.com (Martin Larsen)

instrument) is still a challenge; in this respect, there could be a benefit from using optimization techniques that allow for more design freedom, such as topology optimization.

Topology optimization has been applied successfully to a wide variety of problems since its introduction by Bendsøe and Kikuchi in 1988 [1]. In a recent paper [2], topology optimization of a suspension of a hearing instrument was performed; however, even though structure-acoustic interaction was considered in other parts of the model, the elements inside the design domain could only vary between solid and void. The geometric and material properties of the suspension often result in a strong structure-acoustic interaction with the surrounding air, which makes it essential to consider the acoustic field in such an optimization. Only a few studies in the literature concern topology optimization where the structure-acoustic interface is modified [3–11], which have arisen mainly within the past decade. The challenge in applying density-based topology optimization in structure-acoustic interaction problems lies in the fact that the governing equations on the two considered media (solid material and air) are different and have different primary variables (pressure for air and displacement for solid, when using the standard Eulerian pressure formulation [12]), which poses the question of how to formulate the interpolation between the two. Topology optimization with the level set method, as done in Ref. [8], is an alternative to circumvent the problem, since the interface is defined inherently in the method. Pros and cons of the level-set method for purely structural problems are discussed in Ref. [13], which can be expected to hold for structure-acoustic interaction problems.

Dühring *et al.* [5] presented a method that considers pure acoustic design, which allows for modelling the whole domain with the Helmholtz equation, with the solid material being either reflecting of absorbing. The method is shown to be useful for optimization of rooms or acoustic barriers; however, it does not apply to vibro-acoustic problems. In Refs. [4, 14], topology optimization of coupled problems using a mixed displacement and pressure formulation is presented. In the mixed formulation, the whole domain is governed by the same equations, with the same primary variables (pressure and displacement), and the structural and acoustic domains can be described simultaneously by varying the shear and bulk moduli. The method was also used by Kook *et al.* [11] for the design of periodic microstructures. A drawback of the mixed formulation compared to the segregated displacement/pressure formulation is that the size of the system is larger due to the additional primary variables. Moreover, designs with intermediate elements (elements with material properties that are between the solid and the fluid ones) are allowed during the optimization, which represent the Fluid-Structure Interaction (FSI) in a non-physical way.

The series of papers recently published by Vicente *et al.* [9, 10] describes a topology optimization methodology based on the Bi-directional Evolutionary Structural Optimization (BESO) method applied to fluid-structure interaction problems. BESO is a discrete optimization technique, i.e. intermediate elements are not allowed during the optimization; therefore, the FSI is well-defined at all stages, which allows for calculating the system response using the segregated displacement/pressure formulation. However, an interpolation scheme between solid and fluid elements is not available due to the two media presenting different primary variables, which means that the sensitivity analysis cannot account for solid elements changing to fluid, and vice-versa. Instead, the sensitivities are calculated only on the structural domain based on an interpolation between solid and void, as done in purely structural problems. Even though the method does not address the fluid-structure interpolation matter, optimized vibro-acoustic response results are obtained in the examples given in the papers, which indicates that the approach can still be useful in some cases in practice. The method has some clear advantages from a practical point of view, such as the implementation simplicity of the BESO updating routine [15] and the fact that there is no need to implement solid/fluid intermediate elements with increased number of primary variables. Therefore, the method would be relatively easy to get implemented in commercial Finite Element (FE) softwares, which makes it an attractive option from an industrial point of view, since that could allow for direct integration with the currently used simulation tools and optimization of complicated geometries.

In this work, the applicability of the aforementioned mixed formulation and BESO-based techniques (referred to as "Mixed-MMA" and "Segregated-BESO", respectively, in this paper) for hearing aid suspension

design is investigated. The techniques are described in detail in Section 2, and a 2-dimensional simplified model of a suspension is used as a case study in Section 3, where the material properties are varied to achieve different degrees of structure-acoustic coupling strength, and the optimization performance of the two methodologies in each case is studied. As an outcome, the found limitations of the techniques are outlined and future research lines are suggested.

2. Methodology

In this section, the topology optimization problem formulation for vibration minimization is given, and the two topology optimization techniques applied in this work are described.

2.1. Problem formulation

We consider a coupled structure-acoustic FE model where vibration or pressure levels at one or more Degrees of Freedom (DOFs) are to be minimized by modifying elements comprised in a given design domain. Assuming time-harmonic excitation, the equation of motion in the frequency domain takes the form,

$$(\mathbf{K} - \omega^2 \mathbf{M})\mathbf{d} = \mathbf{f} \tag{1}$$

where $\mathbf{K}$ and $\mathbf{M}$ are the coupled stiffness and mass matrices, ω is the angular frequency, $\mathbf{d}$ is the response vector of displacements and pressures, and $\mathbf{f}$ is the vector of structural forces and acoustic excitations. The formulation of the system matrices is described in the subsections below for each of the two considered methods, yielding the forms in Eqs. (10) and (15). A damping matrix is not considered here, since only internal structural damping is used in this work, which is modelled as an imaginary part of the stiffness matrix.

The objective function can be formulated as

$$\phi = \mathbf{l}^T \mathbf{d}^2, \tag{2}$$

where $\mathbf{l}$ is a vector with ones at the DOFs where the response should be minimized (objective function domain) and zeros at the rest, and $\mathbf{d}$ is the pressure/displacement response vector. If several frequencies should be considered in the optimization, the objective function could be formulated as the sum of several response vectors calculated at each of the frequencies. The sensitivity with respect to the design variables can be calculated by the adjoint method [16] as

$$\frac{\partial \phi}{\partial x_e} = \Re \left\{ \boldsymbol{\lambda}^H \left(\frac{\partial \mathbf{K}}{\partial x_e} - \omega^2 \frac{\partial \mathbf{M}}{\partial x_e} \right) \mathbf{d} \right\}, \tag{3}$$

where x_e is the design variable corresponding to the element e, the superscript ^{H} indicates the conjugate transpose, and the adjoint vector $\boldsymbol{\lambda}$ is calculated by solving the adjoint equation,

$$\left(\mathbf{K}^H - \omega^2 \mathbf{M}^H\right) \boldsymbol{\lambda} = -2\mathbf{l}^T \mathbf{d}. \tag{4}$$

The differentiation of matrices $\mathbf{K}$ and $\mathbf{M}$ is done according to the used interpolation scheme for the material properties, given in the subsections below for each of the two considered formulations.

2.2. Topology optimization methods

In the following, the two topology optimization methods for vibro-acoustic problems considered in this work are described. The first method, suggested in Ref. [4], uses a mixed displacement/pressure ($\mathbf{u}/p$) formulation of the structure-acoustic interaction problem combined with the standard density approach to topology optimization. The second method, based on Ref. [10], uses the classical segregated $\mathbf{u}/p$ formulation

of the coupled problem combined with an evolutionary topology optimization technique.

The two topology optimization methods are density and gradient-based. Topology optimization problems are usually non-linear and require iterative techniques to be solved; in gradient-based methods, the value of the design variables for the next iteration is calculated using their sensitivity information, which is usually more efficient than using non-gradient methods as discussed, in Ref. [17]. In density methods, a design variable that can vary between 0 and 1 is assigned to each element within the design domain; for vibro-acoustic problems, a value of 0 indicates that the element medium is air, and a value of 1 indicates solid. The design variables may be continuous, if they can take values between 0 and 1 during the optimization, or discrete, if only the extreme values are allowed [13], which is one of the differences between the two considered methods.

2.2.1. Continuous design variables and mixed $\mathbf{u}/p$ *formulation, "Mixed-MMA"*

Methods that use discrete variables tend to exhibit difficulties in converging efficiently to optimized designs in a stable manner [13], which motivates the choice of continuous variables when possible. In order to allow for intermediate elements, the structure-acoustic interaction problem is formulated here using a mixed formulation where the solid and fluid fields are governed by the same equations [4].

Assuming time-harmonic excitation, the formulation can be obtained by starting from the linear elasticity equilibrium equation neglecting the body forces,

$$\sigma_{ij,j} = -\omega^2 \rho u_i \quad \text{in } \Omega, \tag{5}$$

where the Einstein's summation convention is used, the subscript $()_{,j}$ is short for $\frac{\partial()}{\partial x_j}$, σ_{ij} is the symmetric stress tensor, ω is the angular frequency, ρ is the material density and u_i is the displacement. Considering the boundary conditions

$$n_i \sigma_{ij} = T_i \quad \text{on } \Gamma_T, \tag{6}$$

$$u_i = u_i^* \quad \text{on } \Gamma_u, \tag{7}$$

where n_i is the surface normal and T_i is the prescribed displacement on the boundary Γ_T; the pressure relationship to the volumetric strain,

$$p = -K\varepsilon_v, \tag{8}$$

where p is the pressure, K is the bulk modulus and ε is the volumetric strain; and the definition of σ_{ij}

$$\sigma_{ij} = K\varepsilon_v \delta_{ij} + 2Ge_{ij}, \tag{9}$$

with G being the shear modulus, we can follow the procedure in Ref. [14] to write the system in a FE matrix form, as

$$\left(\underbrace{\begin{bmatrix} \mathbf{K}_{uu} & \mathbf{K}_{up} \\ \mathbf{K}_{up}^T & \mathbf{K}_{pp} \end{bmatrix}}_{\mathbf{K}} - \omega^2 \underbrace{\begin{bmatrix} \mathbf{M}_{uu} & \mathbf{0} \\ \mathbf{0} & \mathbf{0} \end{bmatrix}}_{\mathbf{M}} \right) \underbrace{\begin{Bmatrix} \mathbf{u} \\ \mathbf{p} \end{Bmatrix}}_{\mathbf{d}} = \underbrace{\begin{Bmatrix} \mathbf{f}_u \\ \mathbf{f}_p \end{Bmatrix}}_{\mathbf{f}}, \tag{10}$$

where $\mathbf{u}$ and $\mathbf{p}$ are the displacement and pressure vectors, and $\mathbf{K}_{uu}$, $\mathbf{K}_{pp}$, $\mathbf{M}_{uu}$, $\mathbf{K}_{up}$, $\mathbf{f}_u$ and $\mathbf{f}_p$ are the stiffness matrices for displacement and pressure, the mass matrix, the coupling matrix, the external structural force vector and the external vector of acoustic excitations, respectively.

It has been demonstrated that by varying the shear modulus G and the bulk modulus K, the acoustic domain and the structural domain can be described simultaneously [18, 19]. The bulk and shear moduli for 2D plane stress are defined in terms of the Young's modulus (E) and the Poisson's ratio (ν) as follows

$$K = \frac{E}{2(1-\nu)}, \; G = \frac{E}{2(1+\nu)}. \tag{11}$$

The three involved material properties, ρ, K and G, can be used to change the elements between solid ($\rho = \rho_s$, $K = K_s$, $G = G_s$) and air ($\rho = \rho_a$, $K = K_a$, $G = G_a = 0$). A RAMP (Rational Approximation of Material Properties) interpolation scheme is used for that purpose, where the material properties are defined as a function of the element deign variable, $x_e \epsilon [0, 1]$, as

$$K(x_e) = K_s \frac{x_e}{1 + (1 - x_e)n} + K_a \left(1 - \frac{x_e}{1 + (1 - x_e)n}\right) \tag{12}$$

$$G(x_e) = G_s \frac{x_e}{1 + (1 - x_e)n} \tag{13}$$

$$\rho(x_e) = \rho_s x_e + \rho_a \left(1 - x_e\right), \tag{14}$$

where n denotes the penalty factor, which is used to improve the convergence to 0-1 solutions, and it is usually given a value between 3 and 6. The matrices in Eq. (10) are assembled element-wise, with the element matrices that form $\mathbf{K}_{uu}$, $\mathbf{K}_{pp}$ and $\mathbf{M}_{uu}$ being proportional to $G(x_e)$, $1/K(x_e)$ and $\rho(x_e)$, respectively.

The optimization problem is solved using the Method of Moving Asymptotes (MMA) [20], the most standard gradient-based method used in topology optimization, and the sensitivity filtering scheme proposed in [21] is used to obtain mesh-independent designs. This method will be referred to as the "Mixed-MMA" method in the rest of this paper.

2.2.2. Discrete design variables and segregated $\mathbf{u}/p$ *formulation, "Segregated-BESO"*

The segregated $\mathbf{u}/p$ formulation is the most standard way of modeling coupled structure-acoustic systems. The total size of the system is smaller than with other formulations, since the acoustic response is modeled with a single primary variable, the pressure p, while the structural response is described by the displacement vector, $\mathbf{u}$.

The procedure to obtain the FE matrix form of the coupled system equations starting from the Helmholtz equation for the acoustic domain and the linear elasticity equation for the structural domain has been described in many books and papers, such as in Ref. [22]. The equation of motion in the frequency domain of the complete system under harmonic excitation takes the form

$$\left(\underbrace{\begin{bmatrix} \mathbf{K}_s & -\mathbf{S}^T \\ \mathbf{0} & \mathbf{K}_a \end{bmatrix}}_{\mathbf{K}} - \omega^2 \underbrace{\begin{bmatrix} \mathbf{M}_s & \mathbf{0} \\ \rho_a \mathbf{S} & \mathbf{M}_a \end{bmatrix}}_{\mathbf{M}} \right) \underbrace{\begin{Bmatrix} \mathbf{u} \\ \mathbf{p} \end{Bmatrix}}_{\mathbf{d}} = \underbrace{\begin{Bmatrix} \mathbf{f}_s \\ \mathbf{f}_a \end{Bmatrix}}_{\mathbf{f}}, \tag{15}$$

where $\mathbf{K}_s$ and $\mathbf{M}_s$ are the structural stiffness and mass matrices, $\mathbf{K}_a$ and $\mathbf{M}_a$ are the acoustic stiffness and mass matrices, $\mathbf{S}$ is the fluid-structure interaction coupling matrix, ρ_a is the density of the acoustic medium, ω is the frequency, $\mathbf{u}$ is the vector of structural displacements, $\mathbf{p}$ is the vector of acoustic pressures, $\mathbf{f}_s$ is the vector of external structural forces and $\mathbf{f}_a$ is the vector of external acoustic excitations. It is worth noting that the $\mathbf{u}$ vector is only defined at the nodes in the structural domain and the $\mathbf{p}$ vector is only defined at the nodes in the acoustic domain here, while they are both defined on the two domains for the mixed formulation in eq. (10). The size of the matrices is therefore smaller for the segregated formulation.

Even though discrete design variables are used for the topology optimization, an interpolation scheme is necessary in order to calculate the element sensitivities. Since the primary variables are different in the two domains, it is not possible to interpolate between solid and fluid elements. Instead, the sensitivities are calculated as in a purely structural optimization, where the material properties are interpolated between solid and void. In vibration problems, the RAMP interpolation is usually applied to avoid spurious modes appearing at areas with low density values [23]; however, this is not a problem here, since elements with

zero-valued design variable are replaced by air. Therefore, the classical SIMP (Simplified Isotropic Material with Penalization) interpolation scheme [24], or power-law approach, can be used. The interpolated material properties are the material density (ρ) and the Young's modulus (E),

$$\rho(x_e) = x_e \rho_s \tag{16}$$

$$E(x_e) = x_e^n E_s \tag{17}$$

where $x_e \epsilon [0, 1]$ is the element design variable, ρ_s and E_s are the properties of the solid material, and n is the penalty factor.

The topology optimization is done by the BESO approach suggested in Ref. [15], which we summarize here. Elemental sensitivity numbers are defined as the gradient with opposite sign,

$$\alpha_e = -\frac{\partial \phi}{\partial x_e}, \tag{18}$$

and spatially filtered to ensure mesh independent designs. In order to stabilize the evolutionary process, the sensitivity history of each element is taken into account by averaging the obtained value with the sensitivity numbers of the previous iteration,

$$\alpha_e^k := \frac{\alpha_e + \alpha_e^{k-1}}{2}, \tag{19}$$

where k is the current iteration, and α_e^{k-1} contains information of all previous iterations since it was calculated in the same way.

To improve stability and convergence, the element updating routine between solid and air makes use of two control parameters: the evolutionary volume ratio, ER, and the maximum admission volume ratio, AR_{max}. The ER determines the percentage of volume reduction or increment allowed at each iteration, and the AR_{max} determines the percentage of elements that are allowed to change nature (solid to air or vice-versa) at each iteration. In the following, a detailed algorithm for the updating routine presented in Ref. [15] is given, assuming that all elements have the same volume:

1. Sort the sensitivity numbers in ascending order and store them into a vector, $\boldsymbol{\alpha}_{sorted}$.
2. Calculate the number of solid elements for the next iteration as $N_{k+1}^s = N_k^s(1 \pm ER)$, where N_k^s is the number of solid elements in the current iteration, k. The number will be increased (+) if the current volume is below the prescribed final volume, and decreased otherwise (-).
3. Set the elements corresponding to the last N_{k+1}^s values in $\boldsymbol{\alpha}_{sorted}$ to solid, and the rest to air.
4. Calculate AR as the ratio between the number of elements that have changed from solid to air and the total number of elements, N. If $AR > AR_{max}$, undo step 3 and follow (a) and (b). Otherwise, the updating step is finished.
   (a) Sort the sensitivity numbers corresponding to the air elements into a vector $\boldsymbol{\alpha}_{sorted}^a$, and set the elements corresponding to the last $N \cdot AR_{max}$ values to solid. The number of solid elements is now $N^* = N_k + N \cdot AR_{max}$.
   (b) Sort the sensitivity numbers corresponding to the solid elements into a vector $\boldsymbol{\alpha}_{sorted}^s$, and set the elements corresponding to the first $N_{k+1} - N^*$ values to air.

The optimization finishes when the prescribed volume requirement is reached and the following criterion is fulfilled,

$$\frac{\left|\sum_{i=1}^{N}(\phi_{k-i+1} - \phi_{k-N-i+1})\right|}{\sum_{i=1}^{N}\phi_{k-i+1}} < \tau, \tag{20}$$

where k is the current iteration, N is the number of iterations over which the error is calculated, and τ is the allowed error. The criterion evaluates the difference on the mean objective function value between the last N iterations and the previous N iterations, which does not necessarily indicate convergence, and is one of the main criticized points of the BESO method [13]. More rigorous convergence criteria are not directly applicable due to the discrete nature of the optimization variables; therefore, the engineer should look at the results carefully before trusting the final design. In this work, the procedure becomes extra prone to instabilities and convergence issues due to the error introduced in the sensitivity calculation, where the solid elements are assumed to become void instead of air; therefore, N is set to a relatively high value of 14, and the parameters ER and AR_{max} are set to a low value of 0.2%.

This method will be referred to as the "Segregated-BESO" method in the following.

3. Results

3.1. Problem statement

The aim of this work is to compare the applicability of two topology optimization methods for strongly structure-acoustic coupled problems in the context of hearing aid suspension design, and discuss their advantages and limitations. Since the purpose is not to come up with designs that can be used in reality, but to evaluate the methods, a simplified, yet relevant, 2D model is investigated. The model, shown in Figure 1, consists of two rigid masses connected by two stripes of solid material (representing the suspension) and an air canal, which is excited at one end with a prescribed pressure p_0. The two masses represent the loudspeaker (denominated receiver in the field of hearing aids) and the Hearing Instrument (HI) body. The air canal would in reality be connected to a tube that brings the sound from the receiver output into the impaired ear, but it is here terminated with a closed end for simplicity. In real hearing aids, the receiver excites the system both acoustically and structurally; however, the vibration forces applied by the receiver are not considered in this study, and the system is only excited by a prescribed pressure at the receiver output.

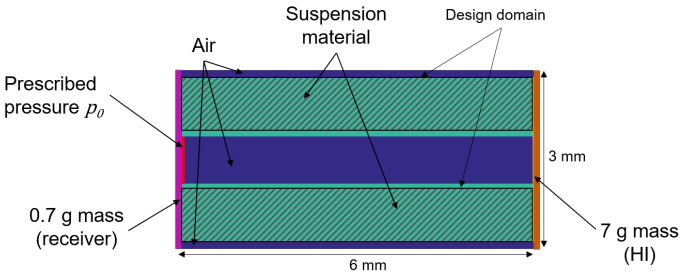

Figure 1: 2D suspension optimization problem set-up.

The topology optimization design domain consists of the two solid stripes of "suspension material" that connect the two masses, except for a layer around the tube that is not allowed to change. The aim of the optimization is to find a design that minimizes the vibration of the mass that represents the hearing aid, which can be formulated as a minimization of the objective function given in eq. (2) for a vector $\mathbf{l}$ that selects the displacement DOFs of the mass in both x and y directions.

Two different suspension materials are considered in order to vary the strength of the structure-acoustic coupling and study its effects on the performance of the methods and the results. A material that is commonly used in suspensions in hearing aids is chosen as a main study target, and one artificial materials (realistically not used in suspension design) is derived by increasing the Young's modulus and mass density proportionally, in order to maintain the structural resonances at the same frequencies. The varying material properties are stated in Table 3.1, and both materials have a Poisson's ratio of 0.49 and an internal material damping of 10%, implemented as an imaginary part of the Young's modulus, $E_c = (1 + j0.1)E$. When Material 2 is used, the mass of the suspension becomes close to that of the two masses connected at the extremes; therefore, those are also multiplied by a factor of 100 in order to preserve the same behavior of the system.

	Young's modulus (E) [MPa]	Mass density (ρ) [Kg/m^3]
Material 1	18	1100
Material 2	1800	110000

Table 1: Material properties

The results are divided in two sub-sections. Firstly, the degree of coupling between fluid and structure for the different materials is analysed using the segregated $\mathbf{u}/p$ formulation with and without coupling boundary condition. Secondly, the topology optimization problem is solved with the two suggested methods for the different materials.

3.2. Evaluating the degree of structure-acoustic coupling

The strength of the structure-acoustic interaction coupling depends on the geometry of the problem as well as the material properties. It is difficult to determine a "strength" indicator for an arbitrary geometry; therefore, the degree of coupling is evaluated here by solving the problem using the segregated $\mathbf{u}/p$ formulation with and without coupling, and analysing the differences in the obtained responses. The coupling is switched off when desired by setting matrix $\mathbf{S}$ to $\mathbf{0}$ in Eq. (15).

A structural force excitation is used, since the pressure will not set into motion the structural part when the coupling is off. The force acts perpendicularly on all the air cavity surfaces, which excites the structure in a similar way that the pressure excitation would do. In order to evaluate the influence of the coupling, the value of an objective function defined as in Eq. (2), with the domain comprising those degrees of freedom where the force is applied, is calculated with and without FSI. The resulting frequency responses are shown in Figure 2, where it can be seen that the first resonance is at around 3300 Hz for all uncoupled responses and for the coupled response of Material 2, while the resonance is shifted up in frequency for the coupled response of Material 1; this indicates that the coupling has a strong influence here.

The topology optimization problem will be solved at a frequency of 1 kHz, well below the first resonance. The values of the objective function at 1 kHz are shown in Table 2, where the ratio in the last column gives a measure of the strength of the coupling at that frequency. The ratio is close to 1 for Material 2 and approaches 0 for Material 1, confirming that the coupling has a strong influence for Material 1 at the quasi-static region too.

3.3. Topology optimization for suspension design

The topology optimization problem is solved for the two materials using the two different methods in the following. For the Segregated-BESO method, a symmetry condition with respect to the horizontal axis is imposed in order to improve stability and convergence to good designs. The initial point of the optimization is always the full design domain, and all objective function values given in this section are normalized with

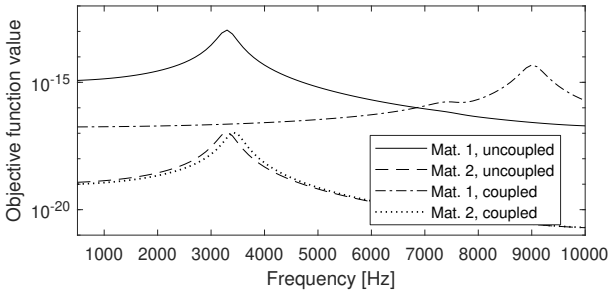

Figure 2: Objective function ϕ (eq.(2)) frequency responses for the 2 materials with and without FSI

	ϕ with FSI	ϕ no FSI	ϕ with FSI / ϕ no FSI
Material 1	$1.8 \cdot 10^{-11}$	$1.4 \cdot 10^{-9}$	0.01
Material 2	$1.1 \cdot 10^{-13}$	$1.3 \cdot 10^{-13}$	0.84

Table 2: Objective function ϕ (eq.(2)) values with and without FSI for the two different materials at 1 kHz, and ratio between the two values.

the objective function value at the initial point, so that the achieved improvement/worsening with respect to the full design domain is directly quantified.

The most classical application of topology optimization is structural compliance minimization; in that case, it is expected that the objective function will go up when material is removed, since less material directly means lower stiffness. The goal is usually to reduce the total mass of the structure, and the engineer seeks the best way to distribute the allowed amount of material given a volume constraint. In the case of HI suspension design, the final volume or mass of the structure is not a concern; instead, we are investigating here if there can be a positive effect from adding cavities that may reduce vibration at certain DOFs for a desired frequency. However, for the BESO technique, it is necessary to request a final structural volume as some percentage of the total design domain for the updating algorithm to work (while for MMA, the volume is a constraint that could in theory be eliminated). Therefore, the procedure applied in the following consists in setting an arbitrary volume constraint and monitoring the evolution of the objective function as material is gradually removed to determine if a decreasing trend is observed.

Since the goal is to find a design that minimizes the vibration of the HI mass, the objective function domain should be defined as all displacement DOFs of that mass (vertical and horizontal). However, when running the optimization, we observe that the algorithm is trying to disconnect the suspension from the masses; an example of that can be seen in Figure 3 (left) for Material 1 when using the Segregated-BESO method (grey indicates solid material in the figure, since black is used for the HI mass). This issue is often observed in topology optimization when the excitation and the objective domains are not directly connected. In order to improve the problem setup to obtain good designs, the objective domain is modified to also include the vertical displacement DOFs on the suspension surfaces that are in contact with the inner air cavity.

The optimization problem is analyzed firstly for Material 1, which has properties often used in hearing aid suspensions. Then, the case of Material 2, a heavy and stiff material not suitable for suspension design, is investigated for comparison to a weakly coupled system.

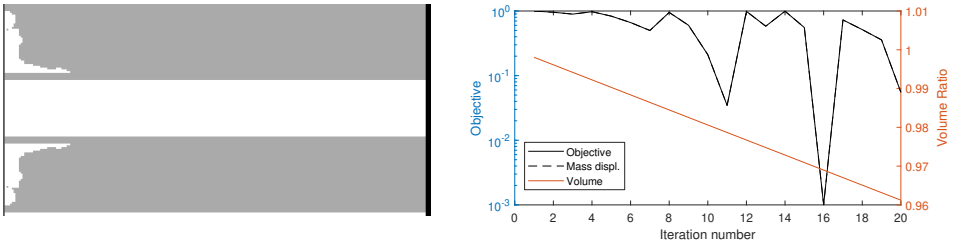

Figure 3: Result after a few iterations when only the DOFs in the HI mass are included in the objective domain. (left) Design. (right) Normalized objective function evolution.

3.3.1. Material 1

With the modified objective function, the resulting design for a volume requirement of 80% with the Segregated-BESO method can be seen in Figure 4 (left). The evolution of the volume ratio, the value of the objective function and the value of the original objective function which included only the mass DOFs in its domain (labeled as "Mass displ.") are shown in Figure 4 (right). The objective function shows a smooth, slightly decreasing trend up to the 40th iteration, after which it starts fluctuating and ends up with a value of 20.

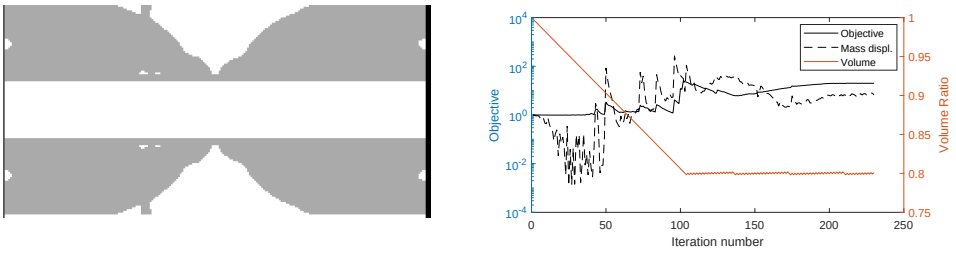

Figure 4: Result for Material 1 with the Segregated-BESO method with a 80% volume requirement. (left) Design. (right) Normalized objective function evolution.

Some sharp jumps are observed in the evolution of the objective function, which usually occur when the structure "breaks", meaning that a solid element between two air cavities is removed, uniting them, and this produces an abrupt increase of the objective function value. Since the sensitivity analysis is done with an interpolation scheme that assumes that the solid will become void instead of air, the sensitivity information does not account for the fact that the air cavities will be merged. The algorithm cannot "go back" to putting that element in place either, since the effect of that is not accounted for in the sensitivities either. Therefore, once the structure "breaks", the optimization continues and converges to the closer local minimum. Moreover, jumps in the objective function value make convergence more difficult, even though in this case a converged design (according to the stopping criterion in eq.(20)) is obtained.

Solving the same problem with the Mixed-MMA method yields the design shown in Figure 5 (left), which is completely different than that obtained with the Segregated-BESO method, and gives a much lower value of the objective function: 1.47 vs. 20. The design presents some intermediate elements that

the MMA algorithm has not managed to get rid of, even though a high value of the penalty parameter (8) is used. If the intermediate elements are projected to obtain a 0/1 design, and the objective function value is calculated with the segregated $\mathbf{u}/p$ formulation, a value of 6.5 is obtained, which is higher but still significantly better than 20. The Mixed-MMA method therefore converges to a more optimized result; moreover, looking at Figure 5 (right), it can be seen that the optimization converges in a smooth way.

The obtained fish-bone-like design in Figure 5 (left) may resemble a periodic structure; however, no bandgap behaviour is observed when looking at the frequency response around 1 kHz. Given that the optimization takes place at the quasi-static frequency range, it seems more possible that the structure results as a trade-off between maximizing the stiffness in both vertical and horizontal directions. The displacement and pressure fields for the projected black/white design are shown in Figure 7 (with the undeformed structure also shown in grey), where it can be seen that the displacement is lowest at the HI mass DOFs. Comparing to the response fields for the initial design shown in Figure 6, it can be seen that the overall displacement levels are higher for the fish-bone structure, and specially the horizontal deflection of the receiver mass is increased.

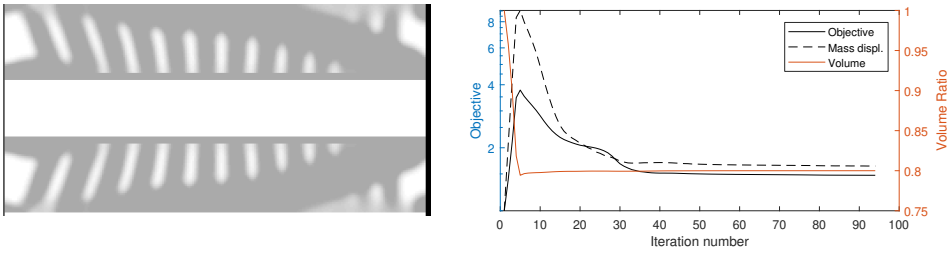

Figure 5: Result for Material 1 with the Mixed-MMA method with a 80% volume requirement. (left) Design. (right) Normalized objective function evolution.

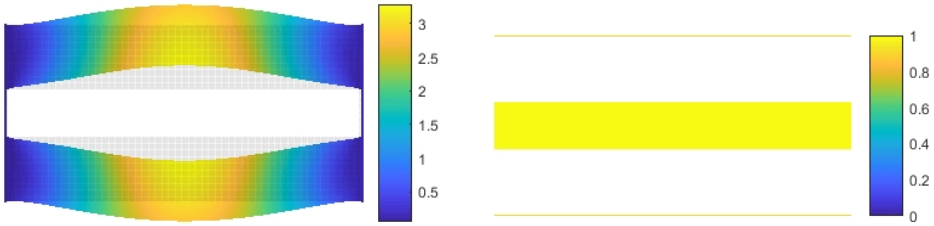

Figure 6: System response at initial point. (left) Total displacement [m] and undeformed structure in grey. (right) Pressure [Pa].

The "Mass displacement" curves shown in Figures 4 (right) and 5 (right) indicate that none of the obtained designs manages to decrease the displacement of the HI mass, though. Looking at the curve in Figure 4 (right), it can be seen that it decreases significantly in the first 40 iterations, and only starts taking values above 1 after that. Since we are not concerned with the final volume of the design, but only with reducing the vibration of the mass, a new optimization is run with a volume requirement of 95% (corresponding to the volume ratio at which the mass displacement is minimal), which yields the results shown in Figure 8. The final value of the mass displacement function is now 0.004, which means that the vibration of the HI

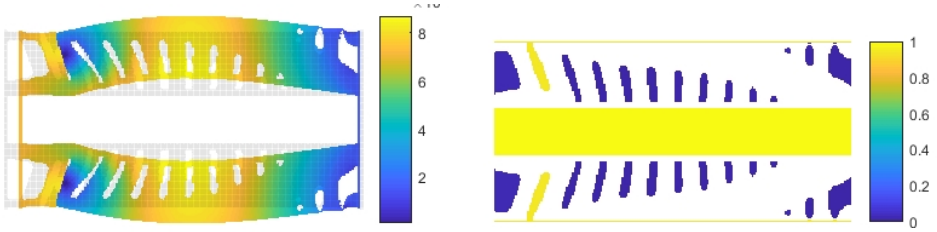

Figure 7: System response at final point for the design obtained with the Mixed-MMA method with an 80% volume constraint. (left) Total displacement [m] and undeformed structure in grey. (right) Pressure [Pa].

mass is reduced by 96%. Figure 9 shows the system response at 1 kHz for the final design, where it can be seen that the introduced cavities allow for a steeper bending at the sides of the suspension attached to the masses compared to the initial design in Figure 6. This results in the suspension transmitting a stronger structural excitation to the side masses, which acts in the opposite direction that the pressure excitation does, compensating for it and reducing the total vibration amplitude. The pressure build-up inside the new cavities is small and shows no resonances, which indicates that the achieved vibration reduction is a purely quasi-static effect.

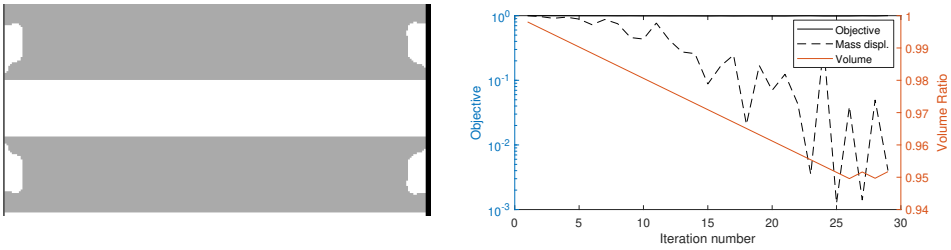

Figure 8: Result for Material 1 with the Segregated-BESO method with a 95% volume requirement. (left) Design. (right) Normalized objective function evolution.

Using the Mixed-MMA method and the same volume constraint, the results shown in Figure 10 are obtained. The design is now similar to the Segregated-BESO method one, and gives a similar final value of the "Mass displacement" function (0.002) after projection and evaluation with the Segregated $\mathbf{u}/p$ formulation. The final value obtained in the optimization was of 0.95; however, the values obtained at the final points when optimizing with the Mixed-MMA method vary in general when evaluated with the segregated formulation due to the projection of intermediate elements into 0/1 values.

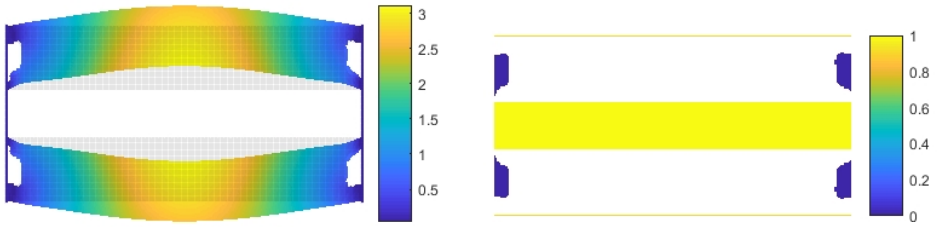

Figure 9: System response at final point for the design obtained with the Segregated-BESO with a 95% volume constraint. (left) Total displacement [m] and undeformed structure in grey. (right) Pressure [Pa].

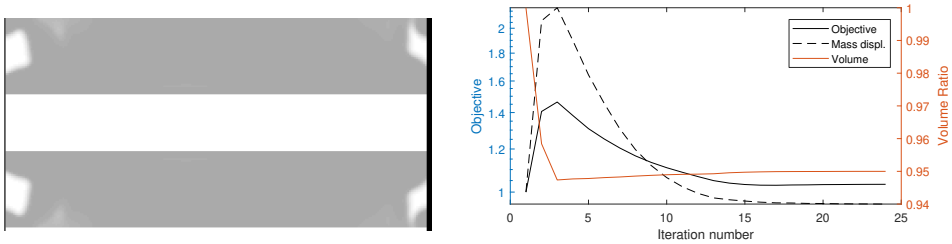

Figure 10: Result for Material 1 with the Mixed-MMA method with a 95% volume requirement. (left) Design. (right) Normalized objective function evolution.

3.3.2. Material 2

For Material 2, the design obtained with the Segregated-BESO method for a volume constraint of 80% and the objective function evolutions are shown in Figure 11. A noticeable difference with respect to the previous case is that the objective function evolves steadily and continuously throughout the optimization, until the volume constraint is fulfilled, without abrupt oscillations. The error introduced in the sensitivity analysis is smaller here, since the coupling is weak and the difference between an element becoming void or air has a less significant influence. This shows that the BESO algorithm is stable and converges smoothly when the sensitivities are correct.

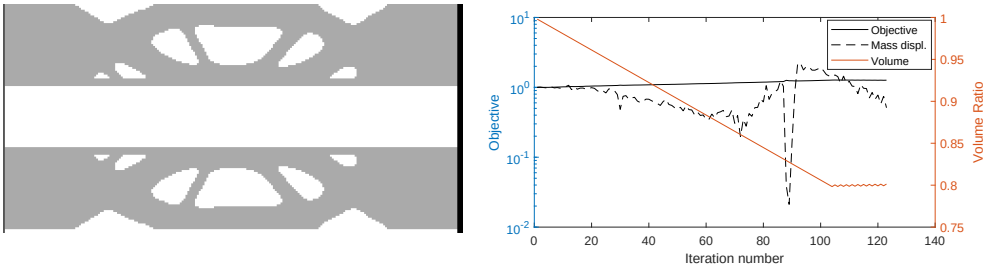

Figure 11: Result for Material 2 with the Segregated-BESO method with a 80% volume requirement. (left) Design. (right) Normalized objective function evolution.

Another difference is that the objective function value increases from the start of the optimization, while it decreased slightly in the first iterations for Material 1. This can be explained by the fact that the pressure built-up in the cavities has very little effect on the structural vibration due to the weak coupling, and therefore removing material translates directly into a less stiff structure that vibrates with more amplitude. However, the HI mass vibration is reduced in the first 80 iterations; this is a result of an increased vibration amplitude of the receiver mass, which compensates for the HI motion. If an optimization with a volume constraint of 87% (corresponding to the point where the mass displacement is minimal) is run, the results in Figure 12 are obtained, where the mass vibration has been reduced to 47%.

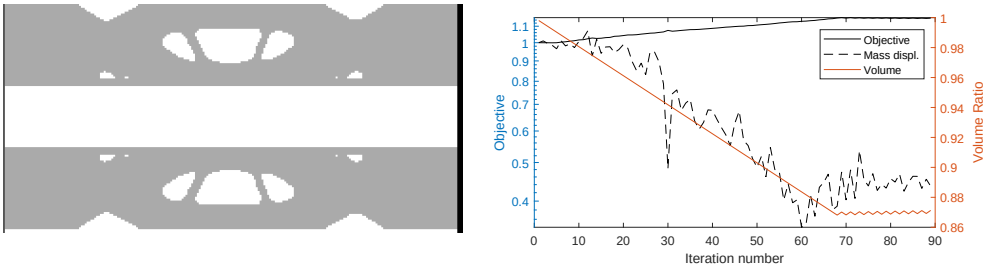

Figure 12: Result for Material 2 with the Segregated-BESO method with a 87% volume requirement. (left) Design. (right) Normalized objective function evolution.

The resulting designs for the same optimization problems using the Mixed-MMA method are shown in Figure 13. The designs are very similar to those obtained with the Segregated-BESO method, which confirms that the BESO routine has managed to converge to optimal minimums in this case. The design optimized for a volume constraint of 87% yields a mass vibration reduction of 55% after projection and evaluation with the Segregated-BESO method.

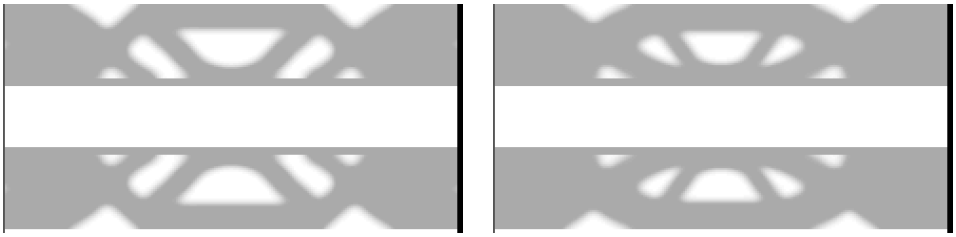

Figure 13: Resulting design for Material 2 with the Mixed-MMA method for a (left) 80% and (right) 87% volume constraint.

4. Discussion

Topology optimized designs that significantly reduce the displacement of the HI mass have been achieved for both materials and with both methods. However, the fact that extra DOFs had to be added to the original optimization domain (which contained the mass DOFs only) means that the obtained solutions do not necessarily correspond to minimums of the actual objective function of interest. The mass displacement

reduction is therefore obtained more as a side effect than as a result of a controlled process. Therefore, further investigation of the behaviour observed in Figure 3 is needed to determine the roots of the problem and improve the objective function definition.

Moreover, as a consequence of not using the actual objective function of interest, the fact that no volume constraint is required a priori for MMA cannot be exploited here to find the optimal design volume. When trying to run an unconstrained optimization with MMA, the algorithm makes no changes to the initial design, which indicates that a full design domain is a minimum of the used objective function. However, as we learn from the Segregated-BESO results, it is possible to reduce the mass vibration by introducing cavities. In this context, the BESO approach has turned out useful; since the elements are removed progressively, it is possible to determine the optimal volume target by monitoring the evolution of the objective function of interest in relation to the decreasing volume of the design.

It has also been observed that the Segregated-BESO method is challenged when optimizing Material 1 for an 80% volume constraint but not for Material 2, which shows that the error introduced in the sensitivities due to interpolating solid-to-void instead of solid-to-air has a significant influence for strongly coupled problems. This highlights the main weakness of the method, and also emphasizes the importance of considering coupling in topology optimization for hearing aid suspension design. Regarding the Mixed-MMA method, it should be noticed that the results for the obtained designs with intermediate elements vary significantly when they are converted to 0/1 designs by projection. It would therefore be interesting to apply additional techniques to force convergence to more binary designs.

Finally, it should be noticed that topology optimization for hearing aid parts should be done for more than one frequency in order to control performance in the whole frequency range of interest, typically from 100 Hz to 10 kHz. This poses other problems such as high frequency resonances giving rise to non-robust designs [4], and longer computational times. Further investigations on the high frequency optimization issues and model reduction techniques for coupled topology optimization problems are therefore needed in order to make it possible to consider an adequate frequency range.

5. Conclusions

The Segregated-BESO method has been shown to work well for optimization of problems with weak fluid-structure coupling; however, for strong coupling, the method has shown difficulties to converge to optimal designs due to the error introduced in the sensitivity information when the air domain is not accounted for. On the other hand, the Mixed-MMA method has been shown to converge smoothly to optimal designs for all cases. An advantage of the Segregated-BESO method is that the elements are removed progressively, which allows for monitoring the evolution of the objective function in relation to the decreasing volume of the design. This has proven useful in the studied problem, where there is no interest in reducing the mass of the structure but only in minimizing vibration, in order to determine the optimal structural volume constraint. When the right volume constraint is chosen, both the Segregated-BESO and the Mixed-MMA methods have produced highly optimized designs in the case under study.

6. Acknowledgments

The authors would like to thank the Innovation Fond Denmark and the Oticon Foundation for their financial support.

References

[1] M. P. Bendsøe, N. Kikuchi, Generating optimal topologies in structural design using a homogenization method, Computer Methods in Applied Mechanics and Engineering 71 (2) (1988) 197–224.

[2] M. B. Sondergaard, C. B. W. Pedersen, Applied topology optimization of vibro-acoustic hearing instrument models, Journal of Sound and Vibration 333 (3) (2014) 683–692. doi:10.1016/j.jsv.2013.09.029.

[3] J. Lee, S. Wang, A. Dikec, Topology optimization for the radiation and scattering of sound from thin-body using genetic algorithms, Journal of Sound and Vibration 276 (3-5) (2004) 899–918. doi:10.1016/j.jsv.2003.08.009.

[4] G. H. Yoon, J. S. Jensen, O. Sigmund, Topology optimization of acoustic-structure interaction problems using a mixed finite element formulation, International Journal for Numerical Methods in Engineering 70 (9) (2007) 1049–1075. doi:10.1002/nme.1900.

[5] M. B. Dühring, J. S. J. Jensen, O. Sigmund, Acoustic design by topology optimization, Journal of Sound and Vibration 317 (3-5) (2008) 557–575. doi:10.1016/j.jsv.2008.03.042.

[6] W. Akl, A. El-Sabbagh, K. Al-Mitani, A. Baz, Topology optimization of a plate coupled with acoustic cavity, International Journal of Solids and Structures 46 (10) (2009) 2060–2074. doi:10.1016/j.ijsolstr.2008.05.034.

[7] G. H. Yoon, Topology optimization for stationary fluid-structure interaction problems using a new monolithic formulation, International Journal for Numerical Methods in Engineering 82 (5) (2010) 591–616. doi:10.1002/nme.2777.

[8] L. Shu, M. Y. Wang, Z. Ma, Level set based topology optimization of vibrating structures for coupled acoustic-structural dynamics, Computers and Structures 132 (2014) 34–42. doi:10.1016/j.compstruc.2013.10.019.

[9] R. Picelli, W. M. Vicente, R. Pavanello, Y. M. Xie, Evolutionary topology optimization for natural frequency maximization problems considering acoustic-structure interaction, Finite Elements in Analysis and Design 106 (2015) 56–64. doi:10.1016/j.finel.2015.07.010.

[10] W. M. Vicente, R. Picelli, R. Pavanello, Y. M. Xie, Topology optimization of frequency responses of fluid-structure interaction systems, Finite Elements in Analysis and Design 98 (2015) 1–13. doi:10.1016/j.finel.2015.01.009.

[11] J. Kook, J. S. Jensen, Topology optimization of periodic microstructures for enhanced loss factor using acoustic-structure interaction, International Journal of Solids and Structures 122-123 (2017) 59–68. doi:10.1016/j.ijsolstr.2017.06.001.

[12] G. Everstine, Finite element formulations of structural acoustics problems, Computers and Structures 65 (3) (1997) 307–321. doi:10.1016/S0045-7949(96)00252-0.

[13] O. Sigmund, K. Maute, Topology optimization approaches, Structural and Multidisciplinary Optimization 48 (6) (2013) 1031–1055. doi:10.1007/s00158-013-0978-6.

[14] O. Sigmund, P. M. Clausen, Topology optimization using a mixed formulation: An alternative way to solve pressure load problems, Computer Methods in Applied Mechanics and Engineering 196 (13-16) (2007) 1874–1889. doi:10.1016/j.cma.2006.09.021.

[15] X. Huang, Y. M. Xie, Convergent and mesh-independent solutions for the bi-directional evolutionary structural optimization method, Finite Elements in Analysis and Design 43 (14) (2007) 1039–1049. doi:10.1016/j.finel.2007.06.006.

[16] M. P. Bendsøe, O. Sigmund, Topology Optimization - Theory, Methods, and Applications, Springer Verlag, 2003.

[17] O. Sigmund, On the usefulness of non-gradient approaches in topology optimization, Structural and Multidisciplinary Optimization 43 (5) (2011) 589–596. doi:10.1007/s00158-011-0638-7.

[18] K.-J. Bathe, Finite element procedures, Prentice-Hall, 1996.

[19] C. Greenshields, H. Weller, A unified formulation for continuum mechanics applied to fluid-structure interaction in flexible tubes, International Journal for Numerical Methods in Engineering 64 (12) (2005) 1575–1593. doi:10.1002/nme.1409.

[20] K. Svanberg, The method of moving asymptotes - a new method for structural optimization, International Journal for Numerical Methods in Engineering 24 (2) (1987) 359–373.

[21] O. Sigmund, On the design of compliant mechanisms using topology optimization, Mechanics of Structures and Machines 25 (4) (1997) 493–524. doi:10.1080/08905459708945415.

[22] G. Sandberg, R. Ohayon, Computational Aspects of Structural Acoustics and Vibration, Springer Vienna, 2009.

[23] N. L. Pedersen, Maximization of eigenvalues using topology optimization, Structural and Multidisciplinary Optimization 20 (1) (2000) 2–11. doi:10.1007/s001580050130.

[24] M. P. Bendsøe, Optimal shape design as a material distribution problem, Structural Optimization 1 (4) (1989) 193–202. doi:10.1007/BF01650949.